UNIVERSITÀ DEGLI STUDI DI BRESCIA

UNIVERSITÀ DEGLI STUDI DI BRESCIA

DOTTORATO DI RICERCA IN

INGEGNERIA CIVILE E AMBIENTALE

Curriculum: Analisi e gestione dei rischi naturali

Settore Scientifico Disciplinare: ICAR/02 Costruzioni idrauliche e marittime e Idrologia

XXXI CICLO

Sediment yield and transport: estimation and climate influence

Relatore e Tutor:

Prof. Giovanna Grossi

Tesi di Dottorato di:

Francesca Berteni

Coordinatore del Dottorato:

Prof. Paolo Secchi

Abstract

Erosion, transfer and deposition of soil particles due to water and the impact of climate change on these physical processes have acquired a great importance during the last decades. Indeed, it is the subject of focused research in several fields of the earth sciences (such as hydrology, hydraulics, ecology, agriculture, geology, civil and environmental engineering, etc.), as the result of the continuous increase in hydrogeological risk in different geographical areas around the world, including Italy. Knowledge of the sediment volumes generated and transported by streams is useful, for example, for the successful design of hydraulic infrastructures, dams or reservoirs, for changes to forest waterways and terrain, for the land management and environment, etc.

Sediment production at the catchment scale and solid transport in rivers can be assessed and quantified through mathematical and empirical models. Unfortunately, there is a shortage of gauged data regarding sediment fluxes and production at the catchment scale, because of topographical and pedological complexity and high spatial variability of all the hydrological characteristics. Another point that should be taken into account is the scarce availability of the appropriate equipment to make survey measurements. For these reasons, it is hard to implement monitoring techniques. However, in the absence of field data, major elements for land management, planning and protection include an estimate of soil loss and sediment yield and their comparison with other case studies.

In the first part of this thesis project, a detailed sediment transport analysis in a reach of the Mimico Creek, which is located in Southern Ontario (Canada), was conducted by making use of the sediment transport investigations. A hydraulic model was developed and calibrated through the HEC-RAS software, by using the Wilcock and Crowe transport function, to a series of discharge events where in-situ bedload sampling occurred. Bedload samplings used in calibrating the transport model were limited by the orifice of the Helley-Smith bedload sampler (ranging between 0.5 mm and 32 mm). Calibration curves, that determine bed material transport rates as a function of the dimensionless reference shear stress, were created considering both step-wise discharge and unsteady flow simulations. The results of the calibrated model were used to calculate the mean travel distance of bed material: the goal was to compare the simulation results achieved to field observations, derived through the bed material particle tracking (RFID technique). The values achieved showed that the Wilcock and Crowe equation under-predicts the transport of the coarsest fractions in the bed load and that the travel distances calculated considering the BSTEM option (which also considers the presence of fine material from bank erosion) are longer. Finally, the travel distances of different grain sizes were estimated using the calibrated model results. The obtained values showed that particles have a steep reduction in travel distance with an increase in their size. Furthermore, transport distance values are higher for the flood events with higher peak discharges, generally in accordance with field measurements. The fractional transport distances of different grain classes estimated by using simulation results are lower than tracer surveys because in the field only the mobile particles were considered,

while when using simulation results, both mobile and immobile particles were taken into account.
In the second part of this thesis project, a mean annual estimation of soil loss due to water erosion in the Guerna catchment, which is located in the Province of Bergamo (Northern Italy), was made in a GIS environment. Soil loss was estimated using the RUSLE and EPM models. Results showed that the mean annual value of soil loss computed through the RUSLE equation (302271 t/year) is about three times higher than its evaluation according to the EPM method (302634 m^3/year, which corresponds to 83225 t/year by considering a specific weight of 2.75 t/m^3). This estimate is coherent with the values obtained for other case studies and, in line with them, it can be said that the EPM approach is more suitable to water erosion assessment in mountain catchments. These estimations of mean annual value soil loss were evaluated also considering a spatial analysis of soil erosion trends in three different future climate scenarios, in line with the last IPCC Assessment Report. Results showed that, applying the RUSLE equation to different climate change scenarios, there are no relevant soil loss increases. The soil loss calculated using the EPM method for two of the three future scenarios is larger than the value estimated without considering climate change. Only rainfall and temperature regimes were considered to evaluate the effects of climate change on water erosion; the future variations of the land use were reasonably omitted. According to the EPM method and to the future scenarios, the annual average soil loss could change by 8-10% on a basin scale. Finally, the sediment yield for an analysed rainfall event was also estimated in the Guerna catchment, in order to create a combined sediment yield and solid transport system. Sediment yield was estimated in the Guerna catchment using the MUSLE equation in a GIS environment and the mean value achieved (32.5 t·ha^{-1}) is approximately one-third of the soil loss mean annual value obtained by the RUSLE model (97.7 t·ha^{-1}·$year^{-1}$). The sediment yield for the rainfall event analysed was also estimated, using the MUSLE equation, for the 7 sub-basins identified in the Guerna catchment. The found values were used as input sediment load in the HEC-RAS model, that was developed for the Guerna Creek in order to simulate sediment transport. Wilcock and Crowe is the transport function that was chosen and the "Time-Area method" was adopted to create runoff hydrographs. The mean value of sediment discharge achieved is 6632 t/d and 66810 t/d, respectively at the upstream cross section and downstream cross section of the study reach. The downstream cross section is the Guerna watershed outlet, with an area of 30.9 km^2. The upstream cross section is the outlet of its upstream sub-basin, with an area of 3 km^2. Results are comparable to the measured value in the Rio Cordon catchment, a small mountain basin (5 km^2) in the northeastern Italian Alps with similar characteristics to the Guerna catchment: during an intensive flood event the sediment discharge recorded is 8040 t/d.

Keywords: water erosion, soil loss, sediment yield, climate change, RUSLE, EPM, MUSLE, HEC-RAS, GIS

Sommario

L'erosione, il trasporto e il deposito di particelle solide dovuti all'azione dell'acqua e l'impatto del cambiamento climatico su questo fenomeno fisico ha acquisito grande importanza, in particolare durante gli ultimi decenni. Infatti è oggetto di ricerca in molti campi legati alle scienze della terra (ad esempio l'idrologia, l'idraulica, l'ecologia, le scienze agrarie, la geologia, l'ingegneria civile e ambientale, ecc.) a causa di un continuo aumento del rischio idrogeologico in diverse aree geografiche del mondo, non esclusa l'Italia. Conoscere il volume di sedimenti prodotti dall'erosione idrica e trasportati dai corpi idrici è utile, ad esempio, per la corretta progettazione di infrastrutture idrauliche, dighe o serbatoi di accumulo, per interventi di sistemazione idraulico-forestale, per la gestione del territorio e dell'ambiente, ecc.
La produzione di sedimenti a scala di versante e il trasporto solido nei fiumi possono essere valutati e quantificati servendosi di modelli matematici ed empirici. Purtroppo le misure di campo relativamente alla produzione e al trasporto di sedimenti a scala di bacino sono molto scarse e difficilmente applicabili in contesti geomorfologici diversi, a causa sia della complessità topografica e pedologica sia dell'alta variabilità spaziale delle caratteristiche idrologiche. Un altro elemento da tenere in considerazione è l'effettiva, spesso scarsa, disponibilità di una strumentazione adeguata per effettuare misure di campo. A fronte di queste ragioni, risulta difficile applicare tecniche di monitoraggio. Tuttavia, in assenza di dati di campo, una stima dell'ordine di grandezza della perdita di suolo e della produzione di sedimenti da confrontare con altri casi studio, sono elementi di non secondaria importanza nella pianificazione della gestione e protezione del territorio.
Nella prima parte del presente lavoro di tesi è stato svolto un accurato studio del trasporto solido su un tratto del torrente Mimico, sito nel sud del Canada (Ontario), servendosi dei dati di campo di portata solida disponibili. È stato costruito e calibrato un modello idraulico tramite il software HEC-RAS, calcolando la portata solida tramite la funzione di trasporto di Wilcock and Crowe e considerando una serie di eventi di piena durante i quali fosse stata effettuata la misura della portata solida. I campioni di terreno adoperati per la calibrazione avevano dimensione granulometrica limitata (da 0.5 mm a 32 mm) a causa delle caratteristiche del campionatore Helley-Smith usato. Le curve di calibrazione, che esprimono la portata solida in funzione dello sforzo tangenziale adimensionale di riferimento, sono state costruite considerando sia il regime di moto quasi-vario sia quello di moto vario. I risultati del modello calibrato sono stati utilizzati per calcolare la distanza media percorsa dal materiale solido di fondo alveo: l'obiettivo era quello di confrontare i risultati ottenuti dall'applicazione del modello con quelli di campo, ricavati grazie alla tecnica RFID. I valori ai quali si è pervenuti hanno mostrato che l'equazione di Wilcock and Crowe sottostima il trasporto delle particelle più grossolane e che, a causa della presenza di materiale a granulometria più fine, le distanze calcolate sono maggiori usando l'opzione BSTEM (che permette di considerare anche il materiale a granulometria molto fine proveniente dall'erosione delle sponde). Infine, i risultati del modello calibrato sono stati usati anche per

calcolare le distanze medie percorse dalle singole granulometrie del materiale che costituisce il fondo dell'alveo. I risultati hanno evidenziato una grossa riduzione della distanza percorsa dalle particelle con l'aumentare della loro dimensione. Inoltre, le distanze calcolate risultano maggiori per eventi di piena caratterizzati da un alto valore della portata di picco; quest'ultima considerazione è, in linea generale, in accordo con le misure di campo. Le distanze medie percorse dalle singole granulometrie che sono state calcolate partendo dai risultati della simulazione e che includono sia le particelle mobili che quelle immobili, risultano minori rispetto a quelle misurate in campo, dove vengono prese in considerazione solamente le particelle mobili.

Nella seconda parte del lavoro è stata analizzata in ambiente GIS la perdita di suolo media annua dovuta all'erosione idrica di versante del bacino del torrente Guerna, che ricade nella provincia di Bergamo (Nord Italia). La perdita di suolo è stata stimata utilizzando i modelli RUSLE e EPM. Dai risultati è emerso che il valore medio annuo di perdita di suolo calcolato con l'equazione RUSLE (302271 t/anno) è circa tre volte maggiore rispetto a quello ricavato con col metodo EPM (302634 m^3/anno che, considerando un peso specifico pari a 2.75 t/m^3, corrispondono a 83225 t/anno). Questa stima è coerente coi risultati di altri casi studio e, in accordo con questi ultimi, si può affermare che l'approccio EPM sia più adatto ad una valutazione dell'erosione idrica in bacini montani. La perdita di suolo media annua così stimata, è stata valutata considerando anche la variabilità spaziale dell'erosione idrica in tre diversi scenari climatici futuri costruiti in accordo con l'ultimo Rapporto IPCC. I risultati hanno mostrato che, applicando l'equazione RUSLE ai differenti scenari di cambiamento climatico, non si verificano grossi aumenti nella produzione di sedimenti. La perdita di suolo calcolata col metodo EPM risulta maggiore per due dei tre scenari futuri, rispetto al calcolo effettuato senza considerare l'impatto del cambiamento climatico. Solamente il regime di precipitazione e di temperatura sono stati presi in esame per valutare gli effetti del cambiamento climatico sull'erosione idrica; le possibili variazioni future dell'uso del suolo sono state ragionevolmente trascurate. Dall'applicazione del metodo EPM, considerando anche gli scenari futuri, è emerso che la perdita media annua di suolo può variare dal 8% al 10% a scala di bacino. Infine, è stata effettuata una stima della produzione di sedimenti che possono raggiungere la sezione di chiusura del bacino del Guerna, a seguito di un preciso evento meteorico che è stato studiato. L'obiettivo era quello di creare un sistema combinato di erosione idrica e trasporto solido nel torrente Guerna. Il quantitativo di sedimenti che può arrivare alla sezione di chiusura del bacino, in occasione dell'evento meteorico considerato, è stato stimato servendosi del modello MUSLE in ambiente GIS; il valore medio ottenuto (32.5 $t \cdot ha^{-1}$) è circa pari ad un terzo della perdita di suolo media annua calcolata col metodo RUSLE (97.7 $t \cdot ha^{-1} \cdot anno^{-1}$). L'equazione MUSLE è stata applicata anche a 7 sottobacini del torrente Guerna, per stabilire così la quantità di sedimenti che può raggiungere ciascuna sezione di chiusura dei sottobacini. I valori ottenuti sono stati adoperati come carico di sedimenti in ingresso nel modello HEC-RAS che è stato realizzato per il torrente Guerna, con lo scopo di simulare il suo trasporto solido. La funzione di trasporto che è stata scelta è quella di Wilcock and Crowe e gli idrogrammi in ingresso al modello sono stati costruiti usando il metodo della corrivazione. La portata solida media ottenuta è pari a 6632 t/d e 66810 t/d in corrispondenza, rispettivamente, della sezione a monte e di quella a valle del tratto di

torrente analizzato. La sezione di valle è quella di chiusura del bacino del torrente Guerna con area pari a 30.9 km^2, mentre quella di monte è la sezione di chiusura del suo sottobacino di monte con area di 3 km^2. I risultati ai quali si è pervenuti sono paragonabili con quelli misurati in campo, in occasione di un importante evento di piena, nel bacino di 5 km^2 del Rio Cordon (8041 t/d), sito nell'Italia nord-orientale (Veneto) e avente caratteristiche simili.

Parole-chiave: erosione idrica, perdita di suolo, produzione di sedimenti che raggiungono la sezione di chiusura del bacino, cambiamento climatico, RUSLE, EPM, MUSLE, HEC-RAS, GIS.

Index

1. Introduction

1.1. Background and goals

Sediment transport, sediment yield, soil loss due to water erosion and the effects of climate change at the catchment scale have acquired a great importance during the last decade. The climate change impacts on water erosion may not be negligible even by the middle of this century. The role of sediment transport and the quantity of sediment mobilized in river dynamics is essential to evaluating the impacts of large magnitude events. A common way to assess and quantify sediment production and transport is through a mathematical and empirical modelling approach. The importance of erosion, transfer and deposition of soil particles and the impact of climate change at the catchment scale has been acknowledged in several fields of the earth sciences (such as hydrology, hydraulics, ecology, agriculture, geology, civil engineering, environmental engineering, etc.). The most relevant goals of sediment estimation at the catchment scale are to quantify the sediment volumes generated and transported by a stream. The purposes are, for example, to support management and decision for land use, to design a reservoir and establish its operational rules, to support hydraulic infrastructure design, to sustain ecohydrological modelling for habitat evolution forecasting, etc.

In many scientific studies, the attention is directed towards the problems and uncertainties that attempt to link on-site rates of erosion and soil loss within a drainage basin to the sediment yield at the basin outlet, which is generated by sediment transport. A knowledge of this linkage is important in order to predict sediment yields from local erosion rates, to evaluate the impact of particular land use scenarios on sediment yields, to evaluate the movement of sediments associated with nutrients and contaminants from agricultural land and to use sediment load data for providing estimates of on-site rates of erosion or soil degradation [*Walling*, 1983].

The physical processes which govern the sediment cycle are complex and have not been totally understood yet. At the actual state of the art, the knowledge about soil erosion and sediment transport, at the laboratory or plot scale, and sediment cycle modelling at the scale of very small experimental basins is satisfactory. Nevertheless, the results of sediment cycle modelling at the catchment scale, with the exception of experimental sites, are often disappointing, due to scarce data availability, very high topographical and pedological complexity and high spatial variability of all hydrological characteristics. Therefore, errors on estimated erosion rates and sediment yield happen very easily.

One of the factors which most contribute to the lack of knowledge about erosion, transport and deposition processes at the catchment scale is the shortage of gauged data regarding sediment fluxes and production. This is due to the complexity of implementing monitoring techniques at a higher scale than a small plot or hillslope (up to a few square kilometres). Therefore, at the catchment scale, model parameter estimation, model calibration and validation is very difficult. The result is that model application to ungauged or poorly gauged catchments could provide disappointing performances. However, in the absence of field

data, models can provide provides an estimated value which is important for the management planning and for the protection of the territory; finally, the achieved estimation results can be compared to other case studies. In addition, there is a lack of sediment transport data available for rivers around the world.

This thesis project was partially implemented in Canada (at the University of Waterloo), and partially in Italy (at the University of Brescia).

The main goals of the first part of this PhD dissertation are:

- to develop a sediment transport HEC-RAS model for a reach of Mimico Creek, which is located in Ontario (Canada), where in situ bedload sampling occurred;
- to calibrate the HEC-RAS model using sediment discharges that were measured in the field;
- to use the results of the calibrated HEC-RAS model in order to calculate the mean travel distance of bed material and to compare the results achieved to travel distances measured in the field.

The main goals of the second part of this PhD dissertation are:

- to estimate mean annual soil loss value due to water erosion in the Guerna catchment, which is located in the province of Bergamo (Italy), implementing the RUSLE and the EPM empirical models in a Geographic Information System (GIS);
- to estimate mean annual soil loss value due to water erosion in the Guerna catchment, implementing the RUSLE and the EPM empirical models in a GIS environment and considering the impact of climate change through CORDEX data;
- to compare the results that were achieved applying the RUSLE and the EPM models to one another and to other case studies;
- to estimate sediment yield, due to water erosion, for a single rainfall-runoff event in the study area by implementing MUSLE empirical model in a GIS environment;
- to develop a sediment transport HEC-RAS model for the Guerna Creek by using, as sediment load input, the sediment yield estimated through the MUSLE model;
- to compare the results that were achieved by applying the MUSLE model and the combinated system of MUSLE and HEC-RAS model to another case study (the Rio Cordon catchment, Italy).

1.2. Outline of the document

This document was written following the structure showed below:

1. In chapter 2 and in chapter 4, a literature review is presented in the field of transport of sediment in rivers, water erosion and climate change. A few theoretical concepts are also underlined, in order to clarify the terms, the

models and the equations which are used along the document. Finally, many case study examples are presented.

2. In chapter 3, the first case study (Mimico Creek) is presented, describing the following points: introduction and goals;
    a. the case study: catchment characteristics;
    b. the data set: sediment transport measurements and flow hydrographs;
    c. construction of the HEC-RAS model;
    d. effects of flood wave propagation and of changes in lake water level and tides;
    e. transport function calibration;
    f. calculation of mean travel distance of bed material;
    g. results;
    h. conclusions.
3. In chapter 5, the second case study (Guerna catchment) is presented, describing the following points:
    a. introduction and goals;
    b. the case study: catchment characteristics;
    c. application of the RUSLE and EPM model;
    d. application of the RUSLE and EPM model considering the effects of climate change;
    e. application of the MUSLE model;
    f. construction of the HEC-RAS model;
    g. combinated system of MUSLE and HEC-RAS model;
    h. results;
    i. conclusions.
4. In chapter 6 the main conclusions are presented. The fundamental contributions, limitations and future research lines of this study are underlined.

1.3. Acknowledgments

- This research project would not have been possible without the guidance, support and mentorship of my supervisor, Prof. Giovanna Grossi (Associate Professor at the University of Brescia), that has been a mentor since I was an undergraduate student.
- The sediment transport analysis of the Mimico Creek and the opportunity to participate in an important international conference in order to present this work, it has been possible thanks to the support of Dr. William K. Annable (Associate Professor at the University of Waterloo).
- The Mimico Creek catchment and its maps were created using information provided by the “Land Information Ontario (LIO) Metadata Management Tool”

[*https://www.javacoeapp.lrc.gov.on.ca/geonetwork/srv/en/main.home*] and the "Government of Canada" [*https://open.canada.ca/en*].

- The hydrometeorological data in the Mimico catchment were provided by TRCA (Toronto and Region Conservation Authority).
- Water level variations in Lake Ontario were provided by the "Government of Canada" [*www.marinfo.gc.ca*].
- The following data on Mimico Creek were provided by the University of Waterloo (Ontario, Canada), in particular by Dr. Benjamin Douglas Plumb who started this work on sediment transport in the Mimico Creek:
  - the representative grain size distribution;
  - bedload sampling (sediment discharges);
  - sampling of the coarse particle transport (travel distance of bed material);
  - geometry and roughness parameters of the cross sections.
- The thematic maps of the Guerna catchment were created using infomation provided by "Geoportale della Lombardia" [*http://www.geoportale.regione.lombardia.it/*].
- The half an hour rainfall data in the Guerna catchment were provided by "Consorzio dell'Oglio" [*http://www.oglioconsorzio.it*].
- The daily amount of precipitation and temperature values in the Guerna catchment were provided by ARPA LOMBARDIA [*http://www.arpalombardia.it*].
- The precipitation and temperature data which were used in order to consider the impact of climate change in the future scenarios, were provided by CORDEX experiment [*http://www.cordex.org/*].
- The geometry of the cross sections in the Guerna Creek was provided in part by the "Comunità Montana del Basso Sebino e del Monte Bronzone" (in Province of Bergamo) and in part by surveys which were executed by the society "Gexcel s.r.l.", which is located in Brescia.
- The particle size analyses of the Guerna Creek riverbed and of the Guerna catchment slope were carried out in the Hydraulic and Hydrology Lab and in the Geotechnical Lab at the University of Brescia, with the support of Dr. Stefano Barontini.

1.4. Acronyms

In this PhD dissertation, many acronyms are used frequently. For each one, an explanation is provided at their first use in the document. In order to help the reader finding every acronym meaning easily, a further explanation is reported below for the most frequent ones.

AGEA = Agenzia per le Erogazioni in Agricoltura

AGI = Associazione Geotecnica Italiana

ASTM = American Society for Testing Materials

BMPs = Best Management Practices

BSTEM = Bank Stability and Toe Erosion Model

CORDEX = COordinated Regional Downscaling Experiment

DEM = Digital Elevation Model

DUSAF = Destinazione d'Uso dei Suoli Agricoli e Forestali

EPM = Erosion Potential Model

ERSAF = Ente Regionale per i Servizi all'Agricoltura e Foreste

ESDAC = European Soil Data Centre

ESGF = Earth System Grid Federation

GAI = Gruppo Aereo Rilevatore

GCM = Global Climate Models

GIS = Geographic Information System

HEC-RAS = Hydrologic Engineering Center River Analysis System

IPCC = Intergovernmental Panel on Climate Change

JRC = Joint Research Centre

MUSLE = Modified Universal Soil Loss Equation

RCD = Regional Climate Downscaling

RCM = Regional Climate Models

RCP = Representative Concentration Pathways

RFID = Radio-Frequency Identification

RUSLE = Revised Universal Soil Loss Equation

SCS-CN = Soil Conservation Service – Curve Number

SDR = Sediment Delivery Ratio

TRCA = Toronto and Region Conservation Authority

USACE = U.S. Army Corps of Engineers

USLE = Universal Soil Loss Equation

WCRP = World Climate Research Programme

WEPP = Water Erosion Prediction Project

2. Transport of sediments in rivers

2.1. Introduction

Many regions around the world have experienced an increased frequency of large magnitude flood events arising from changing climate patterns. Beyond the overt flooding issues which ensue, changes to river dynamics and rates of channel change can also be profoundly affected and they can lead to compromised infrastructure and changes in aquatic habitat niches. The role of sediment transport in river dynamics is essential to evaluating the impacts of large magnitude events. Indeed, the severity of an event is often the combined result of the flood wave and the ensuing sediment transport, particularly on the rising limb of the hydrograph [*Berteni et al.*, 2018]. The change of flow resistance over time produces variations in mean flow velocity along the river, that have important implications even for sediment transport [*Orlandini*, 2002]. A long-term analysis of a river's dynamics, is required to reasonably assess the quantity of sediment mobilized over the entire flow regime. However, there is a dearth of in-situ sediment transport data available for rivers around the world with even fewer studies obtaining observations during large magnitude events to authenticate the accuracy of event-based transport simulations [*Berteni et al.*, 2018]. Indeed, the quantification of the total sediment transport rate is still one of the most challenging tasks in river engineering, because both bedload and the total sediment load are often difficult to accurately determine [*Yang and Julien*, 2018].

The conventional methods of collecting data during extreme rainfall events and high river flows are expensive and dangerous, compared to water discharge measurements. Sediments in river are though usually transported in this type of events and therefore it is very important to measure the amount of sediment. This discharge can be measured using several methods, such as the direct methods that involve collectors and samplers (for example, estimation from data of past disasters or measurement of the weight of sediment accumulating in a collector). The main issues that are associated with the direct methods of sediment discharge measurement are: (a) troubles connected to the flow of water and the sediments, caused by the equipment, (b) the high costs of the equipment and its space requirement, (c) the impossibility of automatic and real-time operation, (d) the limited period available for measurements, (e) the high flow velocity, the wide range of grain size and the large quantities of sediment, (f) the dangerous field conditions in the field [*Tfwala and Wang*, 2016; *Taniguchi et al.*, 1992; *Miyamoto K. et al.*, 1992].

Due to the lack of sediment data and the problems associated with direct sediment measurements, several authors suggested other solutions. For example, Tfwala and Wang (2016) proposed the estimation of sediment discharge using sediment rating curves and artificial neural networks. Taniguchi et al. (1992) proposed that the amount of sediment discharge can be measured indirectly using a transducer; more specifically, they proposed a new acoustic sensor with signal processing for sediment discharge measurement. Due to the need for a continuous record of bedload movement in a gravel-bed stream, Reid at al. (1980) developed the birkbeck bedload sampler. It consists of a pit opening in the stream-bed into which bedload sediment falls.

Some basic concepts of sediment transport in rivers and travel distance of bed material are presented, as well as some concepts concerning mathematical modelling of the solid transport.

2.2. Sediment transport process and initiation of motion

Sediment transport in river dynamics is the movement of solid particles, called sediments, typically due to a combination of gravity acting on the sediment, and/or the movement of the water in which the sediment is entrained. Sediment transport occurs in natural systems where the particles are clastic rocks (sand, gravel, boulders, etc.), mud, or clay; the force of gravity acts to move the particles along the sloping surface on which they are resting.

There are three ways in which sediment is transported by rivers: bedload (rolling, sliding, saltation), suspended load (floating), and dissolved load (individual ions). The focus of this work is the bedload sediment transport, which concerns coarser-grained sediment (typically sand and gravel) transported on the bottom of the stream bed (Figure 2.1).

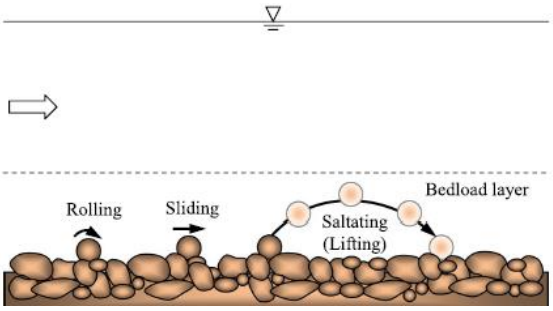

Figure 2.1 – Schematic of bedload transport **[Dei and Ali, 2017]**

Sediment transport is important in the fields of civil engineering and environmental engineering. Knowledge of sediment transport is most often used to determine whether erosion or deposition will occur, the magnitude of this erosion or deposition, and the time and distance over which it will occur. The *transport capacity* is defined as the maximum amount of sediments, in terms of mass or volume, that a flow can carry without deposition. It is the basic concept in determining erosion and deposition processes [*Huang et al.*, 1999; *Armanini*, 2018]: deposition of sediments occurs when the amount of sediments is higher than the transport capacity, otherwise erosion takes place. Then the amount of sediment passing through a river section depends on the erosion and deposition processes in the river network, upstream of the section. The *sediment load* is the total mass of sediment flowing through a river section. The velocity at which sediments pass through a section is called *sediment transport rate*. The *sediment discharge* is the product of the sediment transport rate and the cross-section area [*Doe and Harman*, 2001; *Bussi*, 2014].

Shields (1936) provided the first systematic approach to the problem of incipient motion of cohesionless loose particles on riverbed under under water flow. The initiation of motion of sediment particles in the bed depends on the hydraulic characteristics in the near-bed region. The beginning of motion can be analyzed by the balance at the equilibrium of the forces acting upon them: the gravity force, the hydrodynamic forces and the resisting forces. The main destabilizing forces are the gravity force and the hydrodynamic forces, which should become gradually greater with increasing slope. Particularly, the forces acting on each particle laying on the surface of a sediment bed and partially exposed to the water stream are: the hydrodynamic lift, hydrodynamic drag, gravity, buoyancy and seepage forces together with the friction due to contacts with the surrounding bed particles [*Armanini and Gregoretti*, 2005].

Therefore, flow characteristics in that region are of primary importance. Shear stress is the more prevalent, though not exclusive, way of determining the point of incipient motion.

Shear stress at the bed is represented by the following expression [*USACE,* 2016 (a)]:

$$\tau_b = \gamma \, R_H \, S \qquad \textbf{(2.1)}$$

where: τ_b = bed shea stress [Pa]

γ = unit weight of water [N/m^3]

R_H = hydraulic radius [m]

S = energy slope [-]

Another factor that plays an important role in the initiation of motion of particles is the turbulent fluctuations at the bed level, that can be represented by the current-related bed shear velocity:

$$u^* = \sqrt{\frac{\tau_b}{\rho}} \qquad \textbf{(2.2)}$$

where: u^* = current-related bed shear velocity [m/s]

ρ = density of water [kg/m^3]

There are other parameters that affect the rate of sediment transport in rivers such as the characteristics of the sediment particles (gradation, size, shape, roughness, fall velocity, density) the temperature of water, the depth of flow, the average channel velocity, the effective channel width as well as stream power [*Hossain and Rahman*, 1998].

Sediment grains in a non-choesive sediment bed begin rolling and sliding at isolated, random locations on the bed when the threshold condition is exceeded. The threshold condition can be described in terms of a critical shear stress or a critical velocity at which the forces or

moments resisting motion of an individual grain are overcome. Considering non-cohesive sediment, the forces resisting motion are due to the submerged weight of the grain. If the threshold motion is defined in terms of a critical shear stress (τ_c), it can be given as a function of the following variables [*Sturm*, 2001]:

$$\tau_c = f_1\big((\gamma_s - \gamma), d, \rho, \mu\big) \qquad \textbf{(2.3)}$$

where: $(\gamma_s-\gamma)$ = submerged specific weight of the sediment [N/m^3]

d = sediment grain size [m]

μ = dynamic viscosity of water [N s/m^2]

Dimensional analysis of Equation (2.3) leads to the following result:

$$\tau_c^* = \frac{\tau_c}{(\gamma_s - \gamma)d} = f_2\left(\frac{u_c^*\, d}{\nu}\right) \qquad \textbf{(2.4)}$$

where: $u_c^* = \sqrt{\tau_c/\rho}$ is the critical value of the shear velocity [m/s]

$\nu = \mu/\rho$ is the kinematic viscosity[m^2/s]

$Re^* = u_c^* \cdot d/\nu$

τ_c^* is the dimensional critical shear stress, which is called the Shield parameter

Equation (2.4) can also be expressed as follows:

$$\tau_c^* = \frac{(u_c^*)^2}{g\,\Delta\, d} = f_2\left(\frac{u_c^*\, d}{\nu}\right) \qquad \textbf{(2.5)}$$

where: g = acceleration of gravity [m/s^2]

$\Delta = (\rho_s - \rho)/\rho$ is the density of the submerged grain

Equation (2.4), as well as Equation (2.5), describes the trend of the curve in Figure 2.2. This graph is called “Shields diagram” [*Shields*, 1936].

The curve represents the initiation of motion and it separates mobility and immobility particle areas. Particles move when the point falls within the area above the curve.

It must not be forgotten that the assumptions underlying Shields diagram are: homogeneous particles, non-choesive particles and horizontal riverbed; then, in different conditions, have to be used correction factors [*Armanini and Scotton,* 1995].

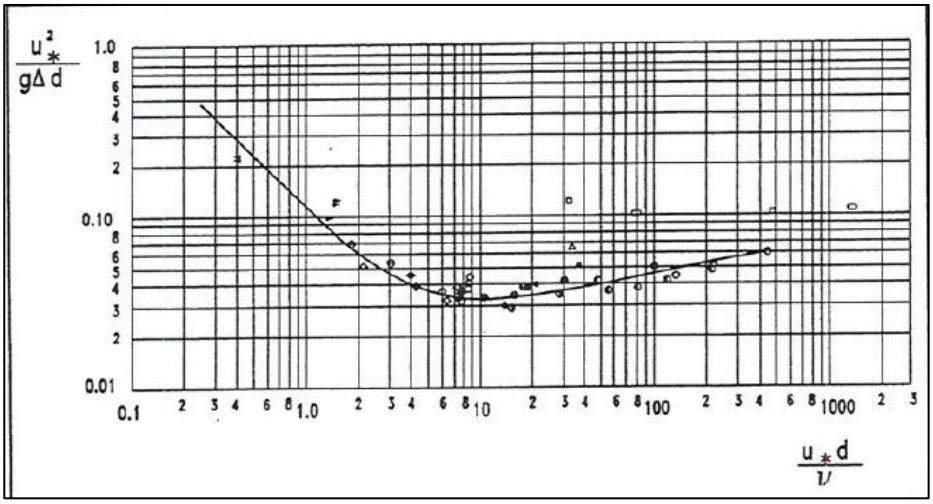

Figure 2.2 – Shields Diagram **[Armanini and Scotton, 1995]**

2.3. Sediment transport modelling

2.3.1. Sediment transport functions

It is very difficult to simultaneously incorporate all the variables mentioned at the end of the paragraph 2.2 in order to develop one sediment transport function. Not all of the transport equations to assess sediment discharge use all of these parameters. Tipically there are one or more correction factors that are used to adapt the basic formulae to transport measurements. In addition, there are many existing sediment transport equations and it is extremely complicated to choose the appropriate one since each situation is unique in its combination of physical phenomena [*Hossain and Rahman*, 1998]. Different sediment transport functions were developed under different conditions and so a wide range of results can be expected from one function to the other. For this reason, it is important to verify the accuracy of sediment prediction to an appreciable amount of measured data from either the study stream or a stream with similar characteristics. It is necessary to understand the procedures used in the development of the functions in order to be confident of its applicability to a given stream [*USACE,* 2016 (a)].

Some of the most used sediment transport functions in literature are described in Appendix *Meyer-Peter Müller* and *Wilcock and Crowe* transport functions are described below because they have been applied in this work. Table 2.1 resumes the function references.

Model	Reference
Ackers-White	*Ackers and White*, 1973
Engelund-Hansen	*Engelund and Hansen,* 1967
Laursen-Copeland	*Laursen and Emmett,* 1958 *Copeland et al.,* 1989
Toffaleti	*Toffaleti*, 1968
Yang	*Yang*, 1973 *Yang*, 1984
Meyer-Peter Müller	*Meyer-Peter and Müller*, 1948
Wilcock and Crowe	*Wilcock and Crowe*, 2003 *Wong and Parker*, 2006

Table 2.1 – Literature reference of the main sediment transport functions

Meyer-Peter Müller

The Meyer-Peter Müller is one of the earliest equations developed and it is still one of the most widely used. This bed load transport function is an empirical model based upon experimental flume data with particles ranging from very fine sands to gravels. The range of applicability is from 0.4 to 29 mm with a sediment specific gravity range of 1.25 to in excess of 4.0. The Meyer-Peter Müller equation development was mostly based upon relatively uniform gravel mixtures, making the transport equation largely applicable to streams with relatively unimodal grain size distributions. This equation tends to under predict transport of finer material.

The general transport equation for the Meyer-Peter Müller function is represented by:

$$(k_r/k_r')^{\frac{3}{2}}\gamma R_H S = 0.047(\gamma_s - \gamma)d_m + 0.25(\gamma/g)^{\frac{1}{3}}[(\gamma_s - \gamma)]^{\frac{2}{3}}q_b^{\frac{2}{3}} \qquad \textbf{(2.6)}$$

where: k_r = roughness coefficient [$m^{1/3}/s$]

k'_r = roughness coefficient based on grains [$m^{1/3}/s$]

γ = unit weight of water [N/m^3]

R_H = hydraulic radius [m]

S = energy gradient [-]

Υ_s = unit weight of the sediment [N/m^3]

d_m = median particle diameter [m]

g = acceleration of gravity [m/s^2]

q_b = volume bedload transport rate of sediment per unit width [$m^3/s/m$]

The dimensionless form of equation (2.6) is the following:

$$q^* = 8\left[\frac{q'_w}{q_w}\left(\frac{k_r}{k'_r}\right)^{\frac{3}{2}}\tau^* - 0.047\right]^{\frac{3}{2}} \quad \textbf{(2.7)}$$

$$q^* = \frac{q_b}{\sqrt{R_H\, g\, d_m}\, d_m} \quad \textbf{(2.8)}$$

$$\tau^* = \frac{\tau_0}{\rho\, R_H\, g\, d_m} = \frac{H\, S}{R_H\, d_m} \quad \textbf{(2.9)}$$

where: q^* = dimensionless volume bedload transport rate per unit channel width (Einstein number) [-]

q_w = volume discharge of water per unit channel width (without any sidewall correction) [$m^3/s/m$]

q'_w = volume discharge of water per unit channel width, including a correction for sidewall effects [$m^3/s/m$]

τ^* = dimensionless boundary shear stress (Shield number) [-]

d_m = arithmetic mean diameter of the sediment [m]

τ_o = boundary shear stress for a hydraulically wide-open channel flow [Pa]

ρ = density of water [kg/m^3]

H = water depth [m]

$(k_r/k'_r)^{3/2}$ is the form drag correction that isolates grain shear, computing transport based on the bed shear component acting only on the particles. The form drag correction is unnecessary in plane-bed conditions, as demonstrated by Wong and Parker (2006).

The Wong Parker correction changes the Meyer-Peter Müller equation in two ways. The first way is shown in Equation (2.10) and it sets the form drag correction to unity (k_r/k'_r=1), effectively removing it from the equation. The second way is shown in equation (2.11) and it consists in setting the Meyer-Peter Müller coefficients to those Wong and Parker (2006) computed using the plane-bed data sets from the original Meyer-Peter Müller analysis recasting.

$$q^* = 8(\tau^* - \tau_C^*)^{\frac{3}{2}} \qquad \tau_C^* = 0.047 \tag{2.10}$$

$$q^* = 3.97(\tau^* - \tau_C^*)^{\frac{3}{2}} \qquad \tau_C^* = 0.0495 \tag{2.11}$$

where τ_C^* is the "critical" Shields stress.

The Wong Parker correction is directly applicable only to lower-regime plane-bed conditions. Indeed, they based their work on the plane-bed data sets, without appreciable bed forms.

Wilcock and Crowe

Wilcock and Crowe is a surface-based transport model, developed and based on the surface gradations of flumes and rivers and used for sand and gravel bed material mixtures. This equation is based upon the theory that transport is primarily dependent on the material in direct contact with the flow and it uses the full size distribution of the bed surface (including sand). It accounts for the influence of the sand fraction on the mobility of the gravel fraction using a non-linear hiding function.

The transport equation for Wilcock and Crowe function is the following:

$$W_i^* = f(\tau/\tau_{ri}) \tag{2.12}$$

where τ is the bed shear stress, τ_{ri} is the reference value of τ (the reference shear stress of size fraction *i*) and W_i^* is the dimensionless transport rate of size fraction *i* defined by:

$$W_i^* = \frac{(s-1)\, g\, q_{bi}}{F_i\, u_*^3} \tag{2.13}$$

where: s = ratio of sediment to water density

g = gravitational acceleration [m/s^2]

q_{bi} = volumetric transport rate per unit width of size *i* [m^3/(m s)]

F_i = proportion of size *i* on the bed surface

u_* = shear velocity $\left(u_* = \sqrt{\tau/\rho}\right)$ [m/s]

The function fitted to the transport observations is as follows:

$$W_i^* = \begin{cases} 0.002\Phi^{7.5} & \text{for } \Phi < 1.35 \\ 14\left(1 - \frac{0.894}{\Phi^{0.5}}\right)^{4.5} & \text{for } \Phi \geq 1.35 \end{cases} \quad \textbf{(2.14)}$$

where $\phi = \tau/\tau_{ri}$

The model incorporates both a *hiding function* and a *nonlinear effect of sand content on the gravel transport rate*. The hiding function considers the influence of gravel and cobble on sand: sand nestles between larger gravel clasts; then the transport potential of smaller particles and the bed shear is reduced. The Wilcock and Crowe model also quantifies the effects of sand content on gravel transport rate: while coarse clasts reduce the shear and transport of fine particles, gravel transport increases with sand content which decreases the framework integrity of the bed and it deposits between interlocking on gravel contacts. Sand also allows bed shear to act on more of the gravel particles. Equation (2.15) and Equation (2.16) represent the hiding function:

$$\frac{\tau_{ri}}{\tau_{rm}} = \left(\frac{D_i}{D_{sm}}\right)^b \quad \textbf{(2.15)}$$

$$b = \frac{0.67}{1 + exp\left(1.5 - \frac{D_i}{D_{sm}}\right)} \quad \textbf{(2.16)}$$

where: τ_{rm} = reference shear stress of mean size of bed surface [Pa]

D_i = grain size of fraction *i* [m]

D_{sm} = mean grain of bed surface [m]

τ_{rm} value can be predicted using Equation (2.17) and Equation (2.18).

$$\tau_{rm}^* = \frac{\tau_{rm}}{(s-1)\,\rho\,g\,D_{sm}} \quad \textbf{(2.17)}$$

$$\tau_{rm}^* = 0.021 + 0.015\exp(-20F_s) \quad \textbf{(2.18)}$$

where: ρ = water density [kg/m^3]

τ^*_{rm} = dimensionaless Shield stress for size fraction *i*

F_s = proportion of sand in surface size distribution

2.3.2. Sediment transport functions calibration

Sediment loads can be computed using a sediment transport function, but the results have to be compared with those of the measured values. The discrepancy (ratio of calculated value to measured value) for each set of data must be considered for comparison of performance [*Hossain and Rahman*, 1998]. Indeed, the sediment transport functions are only the results of theoretical and empirical science. Even when an appropriate transport function is selected, the coefficients included in the equation will not always reflect the transport of a specific site precisely. Therefore, sediment models must be calibrated, changing the coefficient values, to provide reliable predictive results. Calibration parameters should be those that are most uncertain and most sensitive; they quantify the force or energy required to mobilize the particles.

The calibration parameter in the Laursen-Copeland model and in the Meyer-Peter Müller equation is the critical shear stress τ^*_c (also known as the Shields number), in the Ackers-White model it is the Threshold Mobility (A) and in the Wilcock and Crowe function it is the reference Shear Stress τ^*_{rm}. When calibrating a sediment transport function, these mobility factors (that are the calibration parameters) should be the main parameters adjusted, since they can be related to physical phenomena. Moreover, these variables should only be adjusted within reasonable ranges in response to a hypothesis based on observed physical processes. Changing coefficients no longer honors the form of the transport function [*USACE,* 2016 (b)].

2.4. Virtual rate of travel and mean bed material travel distances

The displacement of individual grains is the fundamental phenomenon that occurs during the transport of clastic particles by fluid flow. This phenomenon is complex and it is controlled by three categories of variables that interact with each other: sedimentological characteristics of the bed (e.g., texture, packing, armoring, bed forms), hydraulic conditions of the flow (e.g., discharge, velocity, duration) and characteristics of individual moving particles (e.g., size, shape, roundness) [*Hassan et al.*, 1991].

The mean distance of grains *L* during the interval of time *Δt* can be defined as [*Hassan et al.*, 1991]:

$$L = \Delta t \, V_v \qquad \textbf{(2.19)}$$

where V_v is the average or virtual rate of travel of the particles during a period of time Δt, which includes at least one rest period. In other words, virtual velocity can be defined as the total distance travelled (possibly incorporating multiple steps) by individual grains divided by the measurement interval, typically the total time of competent flow during a flood event [*Haschenburger and Church*, 1998]. Indeed, bedload transport is characterized by

intermittent motion, which means that particles move in a series of steps separated by rest periods.

Einstein (1937) introduced the concept of virtual rate of travel and, according to him, the mean distance (L) of movement during time (Δt) increases with an increase in the sediment discharge. However, considering constant flow, the mean virtual rate of travel (V_v) decreases with increasing time (Δt). This might be the result of the increase in the number of stationary particles, that is a consequence of the growth in the number of buried particles. Exchange of material with the bed reduces travel distance and material velocity [*Hassan et al.*, 1991].

The fundamental expression that relates the volumetric bed material transport rate (Q_b) with the virtual rate of travel (V_v), is the product of V_v and the active cross section of the bed [*Hassan et al.*, 1992]:

$$Q_b = V_v \, D_s \, W_s \, (1 - P) \qquad \textbf{(2.20)}$$

where: D_s = depth of the streambed active sediment layer [m]

W_s = width of the streambed active sediment layer [m]

P = bed material porosity [-]

The active sediment layer is the portion of the streambed that is mobilized during floods competent in order to transport sediments; its dimension can vary spatially and temporally with flow magnitude.

Bed material porosity (P) can be estimated using the porosity-particle size relation developed by Carling and Reader (1982) for poorly sorted, consolidated channel sediment [*Haschenburger and Church*, 1998]:

$$P = 0.4665 \, D_m^{-0.21} - 0.0333 \qquad \textbf{(2.21)}$$

where D_m is the median grain size (expressed in millimetres). In general, porosity remains a poorly characterized variable in sediment flux calculations. Its assigned value may be a source of bias because it is a constant in the calculations, but it is not a source of variability.

Excess stream power (ω-ω_0) can be used in order to estimate the time interval Δt when $\omega > \omega_0$. Specific stream power ω can be defined using Bagnold's equation (1966) [*Hassan et al.*, 1992]:

$$\omega = \rho \, g \, d \, S \, v = \tau \, v \qquad \textbf{(2.22)}$$

where: $\rho \, g$ = specific weight of water [N/m^3]

d = mean flow depth [m]

S = longitudinal slope [-]

v = mean velocity channel [m/s]

τ = reach averaged uniform estimate of the shear stress on the channel bed [N/m^2]

ω_0 is the stream power at the threshold of motion of bed material and it might be supposed to include an adjustment for the constraining effect of bed structure. It can be estimated using Bagnold's equation (1980) [*Hassan et al.*, 1992]:

$$\omega_0 \sim 290\ (D_m)^{1.5}\ log(12\ d/D_m) \qquad \textbf{(2.23)}$$

where D_m is the median grain size (expressed in metres).

2.5. Sediment transport in rivers: case study examples

Catchment of the Rio Cordon (northeastern Italian Alps)

Catchment of the Rio Cordon is a small mountain basin (5 km^2) of the Dolomites, where field observations on the movement of bed material particles were carried out and where long-term sediment load data obtained from measuring stations were analysed. The average elevation is 2200 m a.s.l., the mean hillslope gradient is 52% and the annual precipitation is 1100 mm. The Rio Cordon basin climatic conditions are typical of the Alpine environment: snow-related processes (i.e. snowpack accumulation and snowmelt runoff) dominate from November to May. The mean gradient and the mean width of the main channel are respectively 13.6% and 5.7 m. The mean diameter of the bed surface grain size distribution is D_m = 112 mm and the distribution of the particle-size in the active layer material is widely variable, ranging from silt to gravel. On 14th September 1994 an exceptional flash flood event occurred, presenting the maximum water discharge measured (10.4 m^3/s) and an hourly averaged bedload intensity much higher than all the other floods (up to 200 kg/s compared to 30 kg/s for the second highest event). A marked difference between the pre- and post-September 1994 flood was observed: this event represents a definite moment of change for the channel as to its morphology and sediment availability. From 1987 to 2003 (17 years) 21 floods involving bedload transport (grain size greater than 20 mm) were recorded at the measuring station [*Lenzi et al*., 2004; *Lenzi et al*., 2006].

Table 2.2 shows the most important hydrological and sediment load data for 17 of the 21 flood events, where hourly bed load transport rates are available.

These bedload rates were coupled to the mean water discharge corresponding to the relative time interval, and the best fit equation obtained is the following power relationship [*Lenzi et al*., 2006]:

$$Q_{sb} = 6.45 \cdot 10^{-3} \cdot Q^{5.368} \qquad \textbf{(2.24)}$$

where: Q_{sb} = bedload discharge [kg/s]

Q = liquid discharge [m^3/s]

***Table 2.2 – Most important hydrological and sediment load data for 17 flood events* [*Lenzi et al.*, 2004]**

Flood Event	Q_p [m^3/s]	BL [m^3]	T_{BL} [hours]	BL_R [m^3/h]
11 October 1987	5.2	54.8	8	6.9
3 July 1989	4.4	85	27	3.1
17 June 1991	4	39	20	2
5 October 1992	2.9	9.3	10	0.9
2 October 1993	4.3	13.7	6	2.3
18 May 1994	1.8	1	12	0.1
14 September 1994	*10.4*	*900*	*4*	*225*
13 August 1995	2.7	6.2	1	6.2
16 October 1996	3	57	15	3.8
7 October 1998	4.7	300	17	17.6
20 September 1999	3.7	19.2	6.4	3
12 October 2000	3.3	55.6	35	1.6
11 May 2001	1.5	80	13	6.2
20 July 2001	2	20.9	4.7	4.5
4 May 2002	2.3	27.4	20	1.4
16 November 2002	2.3	10.1	14.5	0.7
27 November 2002	2.8	69.1	30	2.3

Notes: Q_P = peak discharge, BL = bed load volume (bulk measure), T_{BL} = duration of bed load transport, BL_R = mean bed load intensity (bulk measure)

Displacement length of 860 marked pebbles, cobbles and boulders ($0.032 < D < 0.512$ m) were measured along the river bed during individual snowmelt and flood events in the periods 1993-1994 and 1996-1998. Of 860 tracers introduced in 1993, 560 were found in the final search in 1994. Between 860 tracers embedded in 1996, 447 were recovered in the last examination in 1998. After the inspection of each flow event, an average travel length was computed by averaging the relative single travel lengths (including those grains that did not move) weighted with their frequency of movements. Table 2.3 presents a summary of the flow events and related sediment movement observations in the Rio Cordon. Taking the flood events in Table 2.3 into account, only five of them are characterized by coarse bedload transport recorded at the instrumental station [*Lenzi*, 2004].

***Table 2.3 – Data of particle travel measurements on the Rio Cordon with corresponding peak discharge and main sediment load data* [*Lenzi*, 2004]**

Flood Event	Q_p [m^3/s]	T_{BL} [hours]	BL_R [m^3/h]	L [m]
2 October 1993	4.30	6	1.70	74.30 (38 mm)
30 October 1993	1.70	12	0.08	10.80 (38 mm)
12 September 1994	10.40	2.75	324	170 (38 mm)
19 May 1996	0.877	-	-	2.094 (38 mm)
15 October 1996	2.96	22	2.59	31.50 (54 mm)
12 September 1998	0.964	-	-	10.80 (38 mm)
7 October 1998	4.70	17	16.36	90.10 (54 mm)

Notes: Q_P = peak discharge, T_{BL} = duration of bed load transport, BL_R = mean bed load rate, L = maximum travel distance of particle size moved related to, in parentheses, the average class diameter

Carnation Creek (British Columbia, Canada)

Carnation Creek is located on the west coast of Vancouver Island, British Columbia (Canada). It is a small gravel-bed stream that drains about 11 km^2, where the mean annual precipitation is about 3200 mm and snow constitutes only 5% of the total precipitation. Bankfull width and depth average values are 15 m and 0.8 m, respectively. Surface and subsurface bed materials have a median diameter of 47 mm and 29 mm; D_{84} is 97 mm and 89 mm respectively for surface and subsurface bed materials. The mean bed gradient of the study reach is 0.96%.

An alternative approach from the traditional ones, was used to determine transport rates: the application of Equation (2.20), using information about virtual velocity of particle movement, dimensions (depth and width) of the active layer of the streambed and porosity and density of the bed material. Bed material porosity was estimated by using porosity-particle size relation developed by Carling and Reader (1982) for poorly, consolidated channel sediment. Two measurement techniques were used to find the dimensions of the active layer of the streambed: magnetically tagged stones (tracers) and scour indicators. Virtual velocity was determined by using measurements of travel distance of individual particles during flow events and either direct documentation or estimation of the total time particles might be in motion during floods. Measurements of travel distance were derived from knowing the positions of magnetically tagged stones before and after flood events. Approximately 1000 tracers were deployed in the study reach; tracer size fractions ranged from 16 to 180 mm [*Haschenburger and Church*, 1998].

Table 2.4 shows the mean travel distance, the number of mobile particles and the calculated transport rate (Equation (2.20)), using the two measurement techniques to determine the dimensions of the active layer, in three different subreaches of the Carnation Creek study reach.

***Table 2.4 – Data of particle travel measurements on the Carnation Creek with corresponding number of mobile particles and sediment discharge* [*Haschenburger and Church*, 1998]**

		FLOOD EVENT					
		A	**B**	**C**	**D**	**E**	**F**
SUBREACH 1st	**L [m]**	-	-	-	82.6	125.9	48.7
	N°	-	-	-	8	29	7
	(a) Q_g [kg/s]	-	-	-	1.10±1.37	3.74±0.79	0.66±0.70
	(a) Q_b [m³/h]	-	-	-	1.49±1.86	5.08±1.08	0.89±0.96
	(b) Q_g [kg/s]	-	-	-	0.76±0.97	9.72±1.96	0.62±0.67
	(b) Q_b [m³/h]	-	-	-	1.03±1.32	13.2±2.67	0.84±0.93
SUBREACH 2nd	**L [m]**	-	-	-	49.3	43.7	70.3
	N°	-	-	-	154	53	26
	(a) Q_g [kg/s]	-	-	-	0.28±0.031	0.47±0.053	0.41±0.17
	(a) Q_b [m³/h]	-	-	-	0.38±0.041	0.63±0.072	0.56±0.23
	(b) Q_g [kg/s]	-	-	-	0.29±0.050	1.61±0.27	0.60±0.29
	(b) Q_b [m³/h]	-	-	-	0.39±0.068	2.18±0.36	0.82±0.39
SUBREACH 3rd	**L [m]**	129.1	98.5	58.4	26.8	69.1	25.8
	N°	50	152	149	43	49	11
	(a) Q_g [kg/s]	0.32±0.047	0.84±0.059	0.24±0.037	0.21±0.041	1.14±0.15	0.16±0.12
	(a) Q_b [m³/h]	0.44±0.064	1.15±0.080	0.33±0.050	0.29±0.055	1.54±0.21	0.22±0.16
	(b) Q_g [kg/s]	-	0.88±0.19	0.20±0.044	0.28±0.069	0.99±0.18	0.090±0.063
	(b) Q_b [m³/h]	-	1.19±0.26	0.27±0.060	0.38±0.093	1.34±0.24	0.12±0.086

Notes: Flood events: A, 29/08/1991; B, 19/11/1991; C, 29/01/1992; D, 20/10/1992; E, 24/01/1993; F, 04/03/1993; L = mean travel distance; N°= number of mobile tracers (including only those tracers that moved a minimum distance of 1 m); Q_g and Q_b = total transport rate; (a) indicates total transport rate value calculated using magnetically tagged stoned (tracers) as measurement technique; (b) indicates total transport rate value calculated using scour indicators as measurement technique.

Ardennian rivers (Belgium)

The Ardennian rivers are found in the Ardenne Massif (Wallonia, Belgium). The bedload of these rivers is composed of gravel and their watersheds are located on impermeable rocks [*Houbrechts et al.*, 2012].

Characteristics of the rivers of interest are the following:

River	Location	Basin surface [km^2]	s [m/m]	D_{50} [mm]	D_{90} [mm]
Chavenne	Vaux-Chavenne	12	0.011	41	79
Eastern Ourthe	Houffalize	179	0.0036	66	101
Berwinne	Bombaye	123	0.0044	49	75
Aisne	Juzaine	186	0.0047	92	195

***Table 2.5 – Characteristics of the Ardennian rivers* [Houbrechts et al., 2012]**

Bedload discharge was evaluated by combining data obtained by using the scour chain technique and the distance covered by tracers (for elements greater than 20 mm). The following equation was used, which was initially proposed by Laronne et al. (1992) and subsequently adapted by Liébault and Laronne (2008):

$$Q_s = l_b d_s w_s \rho_a / A \qquad \textbf{(2.25)}$$

where: Q_s = specific bedload transport [kg/km^2 per hydrological event]

l_b = average distance travelled by the bedload estimated using pebbles marked with PIT-tags [m]

d_s = depth of the active layer obtained using scour chains [m]

w_s = width of the band of active transport in the channel obtained using scour chains [m]

ρ_a = 1600 kg/m^3 is the apparent density of the transported sediment

A = area of the watershed [km^2]

The scour chain technique was used in order to estimate the depth of the active layers, as well as the width of the band of active bedload transport. The distance travelled by the particles was calculated by using tracers that operated by means of RFID (radio-frequency identification).

Table 2.6 shows sedimentary transit of the bedload estimated by combining data obtained using scour chains and pebbles marked with PIT-tags:

River and location	Date of flood	Maximum discharge (Q_l) [m^3/s]	d_s [mm]	w_s [m]	l_b [m]	Q_s [t/km^2]
Aisne in Juzaine	17/02/2009	26.1	20	3	41.6	0.021
Aisne in Juzaine	12/05/2009	20.7	10	2.6	8.8	0.002
Aisne in Juzaine	23/02/2010	17	25	4.2	13	0.012
Aisne in Juzaine	09/01/2011	48	60	13.5	297	2.07
Berwinne in Bombaye	17/02/2009	19.1	30	3	17.9	0.021
Berwinne in Bombaye	17/01/2010	11.4	15	1.8	11.8	0.004
Berwinne in Bombaye	16/08/2010	6.6	20	2	4.2	0.002
Berwinne in Bombaye	13/11/2010	30.9	50	10	15.5	0.10
Eastern Ourthe in Houffalize	30/03/2008	16.8	27	5.9	29.9	0.04
Chavanne in Vaux-Chavanne	22/08/2007	2.7	9	3	4.9	0.02

***Table 2.6 – Sedimentary transit of the bedload estimated by combining data obtained using scour chains and pebbles marked with PIT-tags* [*Houbrechts et al.*, 2012]**

Berwinne river was selected in order to compare two different techniques to evaluate the solid discharge: the first one regards scour chains associated with tracing campaigns using PIT-tags (see Equation (2.25) and Table 2.6), the second one regards sampling using a Helley-Smith sampler. Bedload sampling using the Helley-Smith sampler allowed to establish the following relationship between the solid discharge and the liquid discharge, based on four mobilizing floods:

$$Q_s = 0.0079 \cdot Q_l^{3.9252} \qquad \textbf{(2.26)}$$

where: Q_s = bedload discharge [g/s]

Q_l = hourly liquid discharge [m^3/s]

It was noted that the solid transport quantified by using the Helley-Smith sampler is an underestimation because of the mesh of the sampling bag used, which allows a share of the fine sediment to pass through. Moreover, it was found that the combinated PIT-tag and scour chain technique also provide a clear underestimation of bedload transport when compared to the estimation provided by the Helley-Smith sampler (which has already been pointed out, understimates the solid discharge). Indeed, the PIT-tag and scour chain method

do not give information about the fine fraction which represented an important part of the load [*Houbrechts et al.*, 2012].

Simulation of sediment transport in the Southwest Kano underground canal using HEC-RAS (Kenya)

The canal in the Southwest Kano Irrigation Scheme (Kenya) was designed to convey water to rice fields through gravity flow. The water is abstracted from the Nyando river and therefore it reaches the canal. It is an underground circular concrete-lined canal having a diameter of 1500 mm, a length of 730 m and its slope is 0.002447 m/m. The aim is to ensure that water is conveyed with minimal erosion and sedimentation, but over time it was silted up and its conveyance capacity was significantly dropped: sediment concentration in the Nyando river is the main source of sediments in the underground canal in the Southwest Kano Irrigation Scheme.

The Ackers-White sediment transport equation was used to analyse sediment transport characteristics using the HEC-RAS model, that was calibrated in two steps. The first phase of calibration involved determination of Manning's roughness coefficient *n* for steady flow, which best fitted the observed water surface. The second phase of HEC-RAS model calibration for sediment transport was done using the *n* value derived after running the steady flow simulation and it consists of calibrating the sediment entrainment parameters, coefficients and exponents in HEC-RAS through their optimisation.

The output of the model was sediment discharge at different sections. The best fit curve of simulated against observed sediment discharge was based on the assumption that the flow entering the canal was at equilibrium sediment load [*Ochiere et al.*, 2015].

The following calibration curve was built after further optimisation simulation runs:

$$Q_{ss} = 1.3027 \cdot Q_{sm} - 174.21 \qquad \textbf{(2.27)}$$

where: Q_{ss} = cumulative simulated discharge [ton]

Q_{sm} = measured cumulative discharge [ton]

The calibrated HEC-RAS model was run considering different flow scenarios. The discharge for each scenario is shown in Table 2.7.

Flow discharge scenario [m³/s]	**Total cumulative sediment discharge at the canal inlet [kg/s]**	**Total cumulative sediment discharge at the canal outlet [kg/s]**
0.366	18.47	11.49
1.377	87.25	85.58
2.438	198.96	191.66
2.764	216.5	208.54

***Table 2.7 – Cumulative sediment discharge for different discharge scenario* [*Ochiere et al.*, 2015]**

3. The Mimico Creek case study

3.1. Introduction and goals

Channel morphological change is often evaluated by employing sediment transport models since field data during high magnitude low frequency events is rarely available. However, sediment transport rate estimates are heuristic at best to within 1 – 3 orders of magnitude. The study reach is a reach of Mimico Creek, an urban gravel-bed channel in Southern Ontario, Canada that has undergone intensive event-based sediment transport sampling and inter-event bed material particle tracking over a three-year period [*Berteni et al.,* 2018].

The selection of this study area arises from its critical hydraulic aspects and the availability of data needed to build and calibrate a HEC-RAS model. HEC-RAS is a computer program developed at the Hydrologic Engineering Center for the U.S. Army Corps of Engineers (USACE); it models the hydraulics of water flow through natural rivers and other channels. The Mimico Creek catchment is one of the TRCA (Toronto and Region Conservation Authority) watersheds affected by the July 8th, 2013 extreme rainfall event, that received the highest amount of rainfall: this precipitation event generated a flood exceeding the 100-year return period. According to the Insurance Bureau of Canada (IBC), this extreme event was the most expensive natural disaster in Ontario history [*AMEC,* 2014]. Pre and post erosion surveys along the 2.1 km reach combined with in-situ and inter-event sediment transport studies and a proximal hydrometric monitoring station afforded a unique opportunity to evaluate the performance of various sediment transport models applicable to gravel-bed rivers for flashy high magnitude events.

The objective of this chapter is to illustrate the developed representative sediment transport models of the study reach where intensive in-situ event based and inter-event sediment transport investigations have been conducted (including a large magnitude storm event) and compare the results to pre- and post-event observations, using HEC-RAS.

A HEC-RAS model was developed of the study reach and calibrated to a series of discharge events where in-situ bedload sampling occurred. Both step-wise discharge and unsteady flow simulations were evaluated to compare sediment transport rates for a range of transport models which included the *Meyer-Peter Müller* and the *Wilcock-Crowe* formulas (paragraph 2.3.1). Calibration curves were developed to estimate sediment discharge in Mimico Creek.

The results of the calibrated model were used to calculate the mean travel distance of bed material using the expression for the volumetric rate of bed material transport (Equation (2.19), (2.20)). Results from the modelling exercise found mean travel distances were similar and, in some cases, larger than those observed from field measurements, considering both mobile and immobile particles [*Berteni et al.,* 2018].

3.2. Catchment characteristics

Mimico Creek is a 89.7 km^2 catchment situated in Toronto, southern Ontario, Canada (Figure 3.1) [*https://www.javacoeapp.lrc.gov.on.ca/geonetwork/srv/en/main.home*]. Most of the upper watershed consists of glaciolacustrine deposits, which transition to Halton till, resulting from the late Wisconsinan period.

Figure 3.1 – Mimico Creek location

87% of the catchment is urbanized: the upper part is dominated by industrial and residential land-use, the midregion is dominated by industrial land-use and the lower portion of the watershed is dominated by residential use. Less than 30% of the urban area has at least one device for storm water management (SWM) control (e.g., SWM ponds) and only 10% having storm water controls pertaining to erosion control (e.g., specific volume capture and not just peak-flow shaving). Nonurban lands are well vegetated and they consist of golf courses, meadows, parklands, and riparian corridors, with little forest; these areas are not likely major sediment sources for the channel. The dominant sediment source is derived through bank erosion, which has been suggested as being the major contributor to long-term sediment yield in urban streams. Two in-line flood control structures (detention basins) located in the upper portion of the watershed (upstream of the study reach) are acting as sediment sinks, however the exact extent to which they disrupt the sediment continuity is unknown [*Plumb*, 2017].

Figure 3.2 shows the land use map for the Mimico Creek basin that was made using information taken from Government of Canada [*https://open.canada.ca/en*]. Table 3.1 provides the different land use classes with their respective definitions.

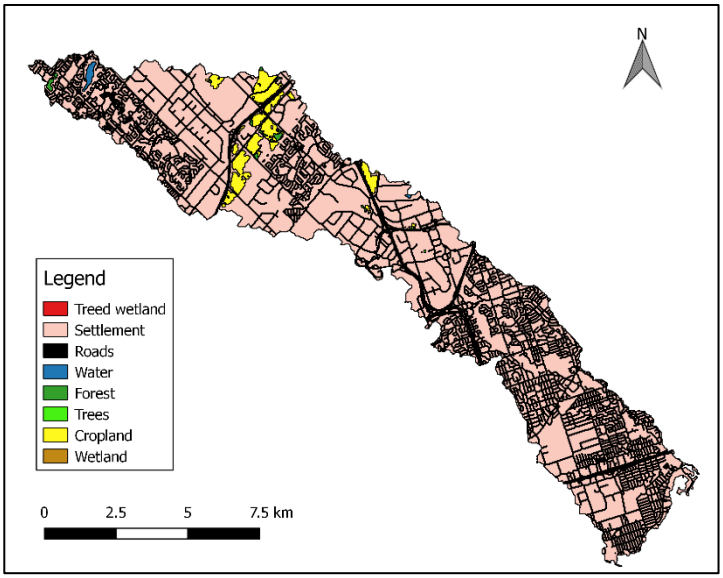

Figure 3.2 – Mimico Creek Land Use Map

Land Use Class	Definition
Treed Wetland	Wetland with tree cover
Settlement	Built-up and urban
Roads	Primary, secondary and tertiary
Water	Natural and human-made
Forest	Treed areas > 1 ha in size
Trees	Treed areas < 1 ha in size
Cropland	Annual and perennial
Wetland	Undifferentiated wetland

***Table 3.1 – Land Use Classes and their definitions* [https://open.canada.ca/en]**

Figure 3.3 shows the Digital Elevation Model (DEM) for the Mimico Creek catchment; the average altitude is 160 metres above mean sea level. This map was created starting from data made available by Government of Canada [*https://open.canada.ca/en*].

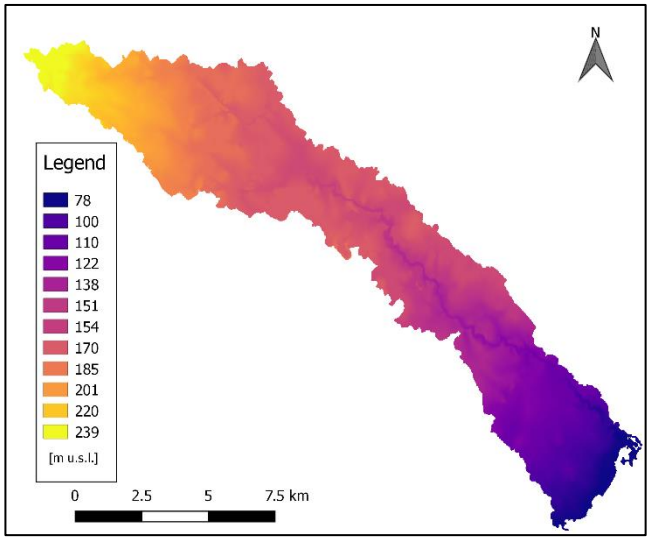

Figure 3.3 – Mimico Creek Digital Elevation Model (DEM)

The study reach is 1.8 km long and it is located in the lower portion of the basin (Figure 3.1) [*Plumb,* 2017]. Figure 3.4 shows the magnification of the study reach where the cross sections used to build the hydraulic model in HEC-RAS appear.

The dominant morphology of the reach is a single-thread riffle-pool morphology, with an average bankfull width of 13 m, gradient of 0.4%, and 25 riffle-pool sequences [*Plumb,* 2017]. Immediately upstream of the study reach, the channel flows within a concrete trapezoidal channel (0.5 km) before transitioning into a gravel-bed channel at the beginning of the study reach. Complete bed material routing is observed throughout the concrete channel section. Through the study reach, floodplain connectivity is relatively consistent above the approximate 2-year return period which also supports a relatively narrow but contiguous riparian corridor [*Berteni et al.,* 2018].

Figure 3.4 – Mimico Creek study reach

In the watershed there is a hydrometric gauge station (02HC033) with a 50 year record and operated by Environment Canada (Figure 3.1). This station is located a short distance downstream of the study reach, with no major tributaries entering the stream between the study reach and gauge such that continuity of flow can be assumed. It provides 15 min discharge data using the stage discharge rating curve method [*Plumb,* 2017].

The Mimico Creek study reach is a gravel bed river, exhibiting a bimodal distribution with a smaller secondary peak in the sand fraction. Figure 3.5 shows the bed material cumulative grain size distribution of subsurface, surface and bulk mixture. Bulk mixture is the combination of surface and subsurface [*Berteni et al.,* 2018].

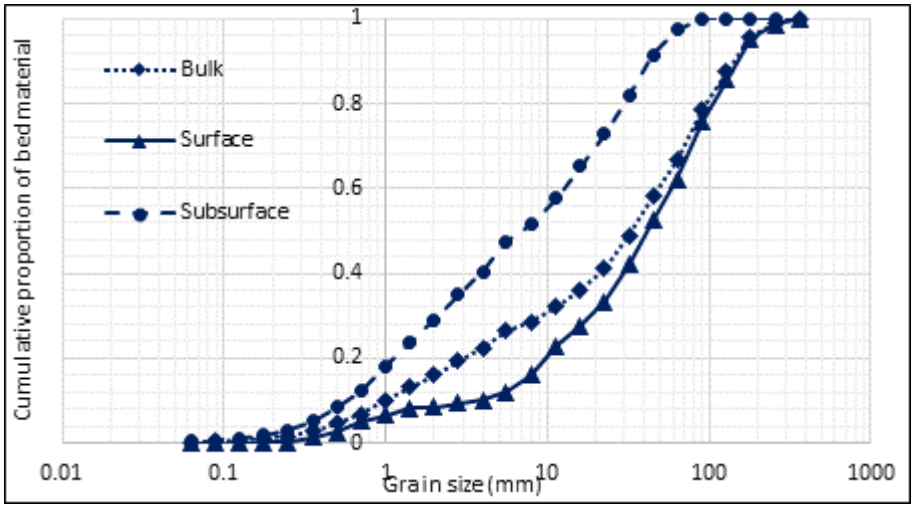

***Figure 3.5 – Representative grain size distributions for Mimico Creek* [*Plumb et al.*, 2017]**

3.3. July 8th, 2013: extreme rainfall event

The July 8th, 2013 rainfall event, which resulted in widespread flooding, was one of the most expensive natural disasters in Ontario history. Humber River, Don River, Etobicoke Creek and Mimico Creek are the four TRCA (Toronto and Region Conservation Authority) watersheds affected by this event, which received the highest amount of rainfall.

Rainfall data have been obtained and analyzed from 135 rain gauges operated by several municipalities, as well as provincial and federal agencies located in and around the TRCA jurisdiction. The maximum total rainfall during the storm occurred in the Mimico Creek watershed with an average of 94.6 mm of rain across the watershed.

Figure 3.6 shows the position of the rain gauges closest to the study reach. The extreme rainfall event had a duration of 10 hours and a total observed rainfall of 138 mm at rain gauge 1 (Figure 3.6), located east of Toronto Pearson International Airport. The maximum hourly rainfall was observed to be 79 mm also at rain gauge 1 [*AMEC*, 2014].

Figure 3.6 – Mimico Creek watershed: position of the rain gauges closest to the study reach

Figure 3.7 shows the hyetograph for the extreme rainfall event, considering the four rain gauges closest to the study reach [*AMEC*, 2014].

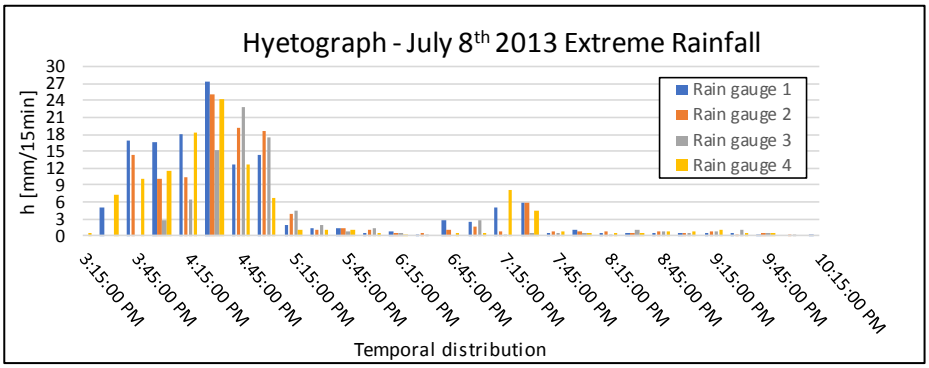

Figure 3.7 – Hyetograph - July 8th, 2013: extreme rainfall event

Water level and stream flow data from 58 stream gauges within TRCA watersheds (Humber River, Don River, Etobicoke Creek and Mimico Creek), which are operated by TRCA and Water Survey, were collected and analyzed. The stream flow gauge 02HC033 is the closest to the study reach (Figure 3.6). The observed water level at this stream flow gauge station is 115.23 mm on July 8th 2013, at 07:20 PM.

Figure 3.8 shows the stream discharge hydrograph at stream flow gauge 02HC033 for the July 8th, 2013 storm from the western TRCA Mimico Creek watershed [*AMEC*, 2014].

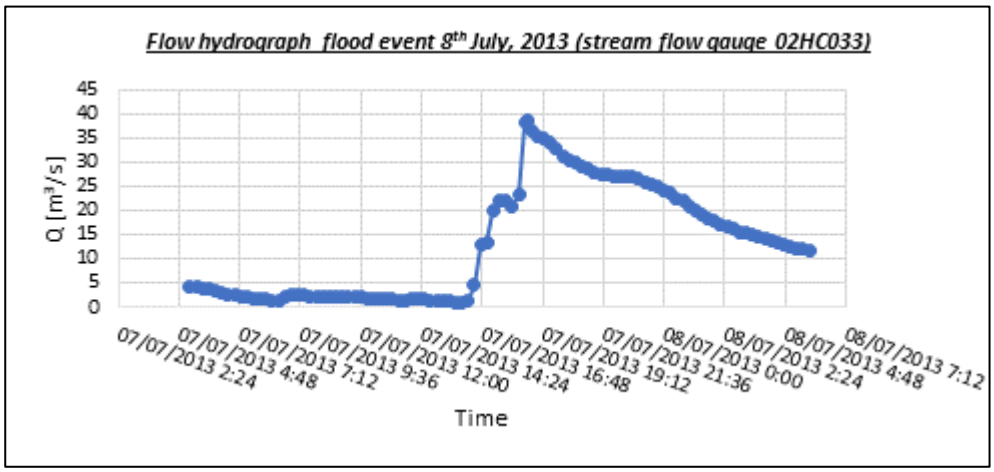

Figure 3.8 – Stream discharge hydrograph - July 8th, 2013: extreme rainfall event

It should noted that the flow hydrograph in Figure 3.8 was useful in investigating sediment transport and mean travel distance of bed material, as will be shown in the following paragraphs.

However, it was no generated by the hyetograph made available by TRCA (Figure 3.7), due to the difference of the time period. Indeed the recession limb of the hydrograph ends on July 8th 2013 at 07:12 AM, but the hyetograph starts on July 8th 2013 at 03:15 PM.

As seen in Figure 3.9, it was not possible to build the hydrograph generated by the hyetograph in Figure 3.7, because of missing data registered by the stream flow gauge 02HC033.

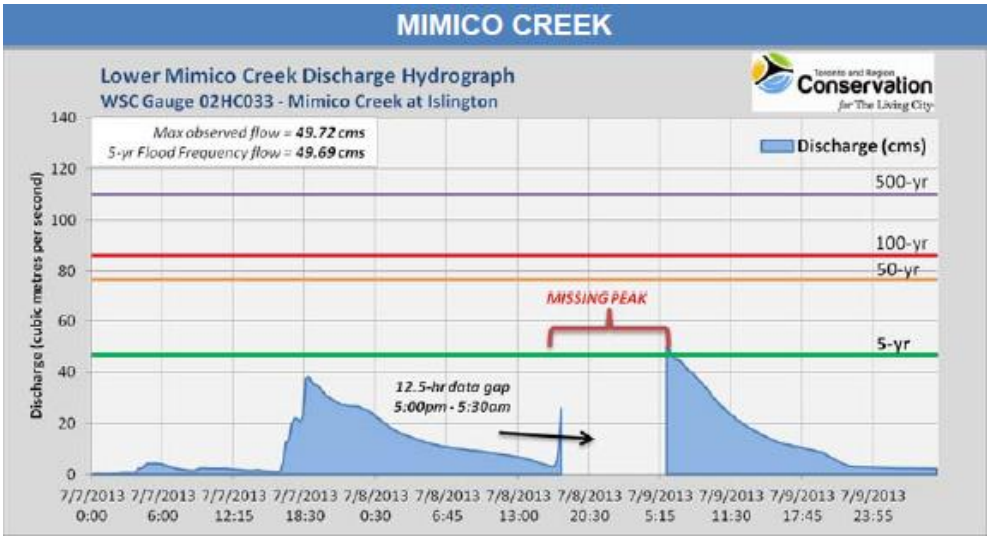

***Figure 3.9 – Stream discharge hydrograph for July 8th, 2013 storm from western TRCA watershed, including flood frequency flow in years.* [AMEC, 2014]**

3.4. Sediment transport measurements and flow hydrographs

Bedload sampling, necessary to calibrate a HEC-RAS model, was conducted during competent floods using the modified single width increment method with 0.076 m Helley-Smith samplers over a two-year period between 2012 and 2013 [*Plumb et al.*, 2017; *Berteni et al.,* 2017]. The Helley-Smith bedload sampler is a pressure-difference sampling device designed for use in natural streams carrying coarse sediments; it is a usable device which permits a direct measurement of coarse bedload in transport in relatively high-velocity flow regimes. The configuration of the sampler is shown in Figure 3.10 and in Figure 3.11. The torpedo shape is outlined by three curved aluminum tubes which connect the three entrance orifices to the stabilizing tail-fin assembly. The sample is caught in a mesh bag attached to the back of the orifice assembly. The expanded area provides the pressure difference, or velocity drop, necessary to trap the moving sediment. Material used for the collection bag is polyester monofilament mesh of 0.2 mm and meets ASTM (American Society for Testing Materials) standards for uniformity. It is rugged and extremely resistant to abrasion and wear and it does not absorb water [*Helley and Smith*, 1971].

***Figure 3.10 – The Helley-Smith bedload sampler* [*Erskine et al.,* 2011]**

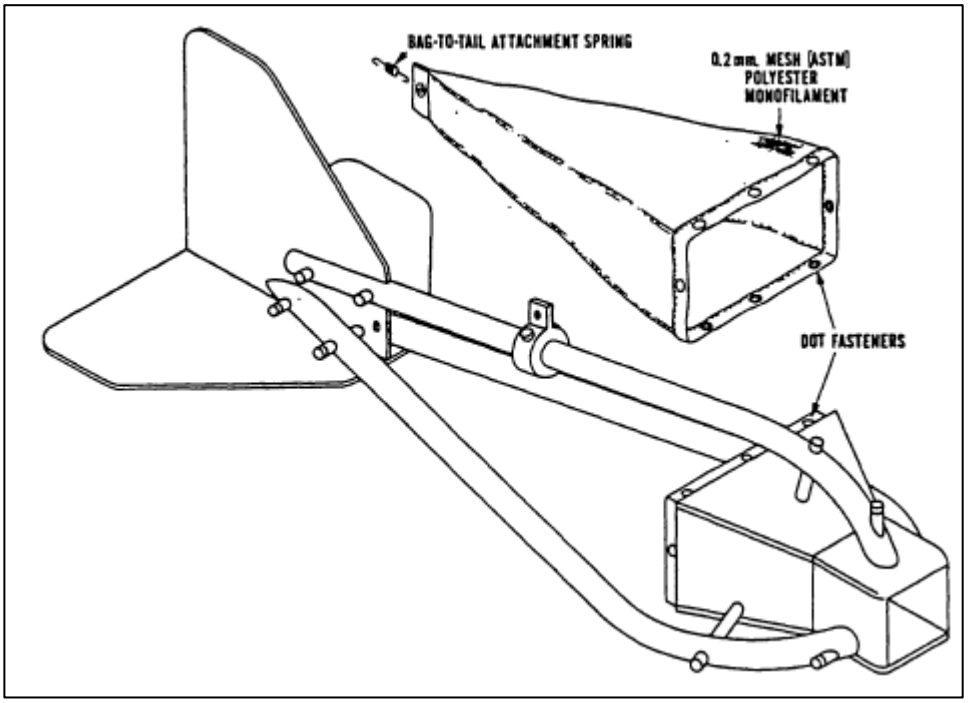

***Figure 3.11 – The Helley and Smith bedload sampler* [*Helley and Smith,* 1971]**

Table 3.2 shows sediment discharge measured in the field (Q_{b_field}) for each flood event and the corresponding peak flow (Q_{peak}) [*Berteni et al.*, 2018].

Flood Event	Date	Q_{peak} (m^3/s)	Q_{b_field} (t/day)
1	10/08/2012	15.6	**4.35**
2	04/09/2012	42.3	**5.68**
3	11/03/2013	15.7	**0.23**
4	09/04/2013	16.8	**0.17**
5	12/04/2013	21.4	**1.3**
6	29/05/2013	36.5	**1.99**
7	08/07/2013	38.7	**15.79**

Table 3.2 – Sediment discharge measured in the field

Figure 3.12 illustrates the results and the trend equation of the two-year (2012-2013) bedload field sampling campaign for flow events exceeding the cessation threshold of the bed material [*Berteni et al.,* 2018].

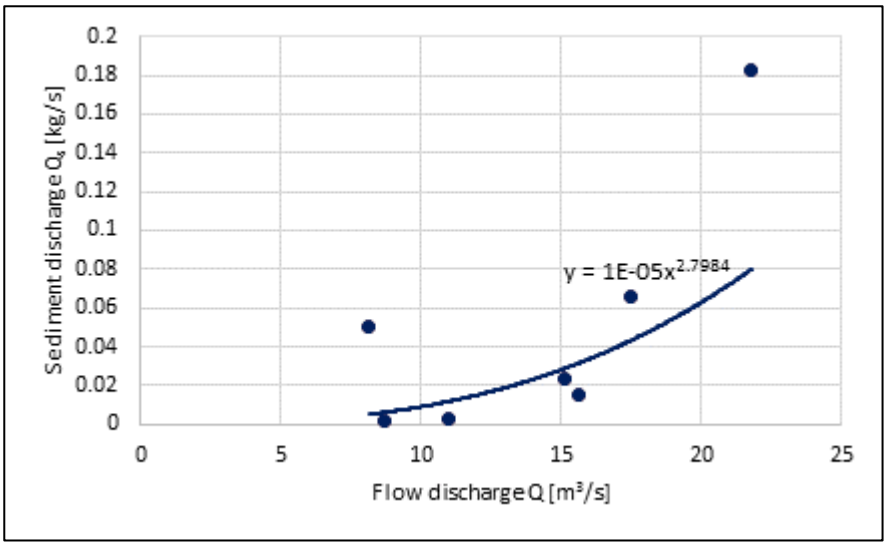

***Figure 3.12 – Field measured bed material transport rates through Mimico Creek* [*Berteni et al.,* 2018]**

The following illustration (from Figure 3.13 to Figure 3.19) contain flow hydrographs (in correspondence of the 02HC033 gauge station) for the seven flood events which were analysed. The red strokes on the horizontal axis indicate the time lags where sediment discharge measurement in the field (Table 3.2) occurred.

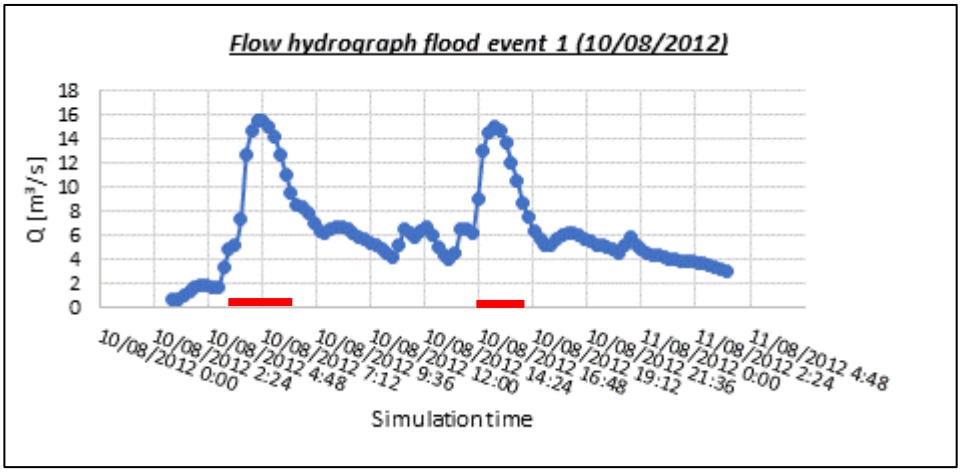

Figure 3.13 – Flow hydrograph flood event 1

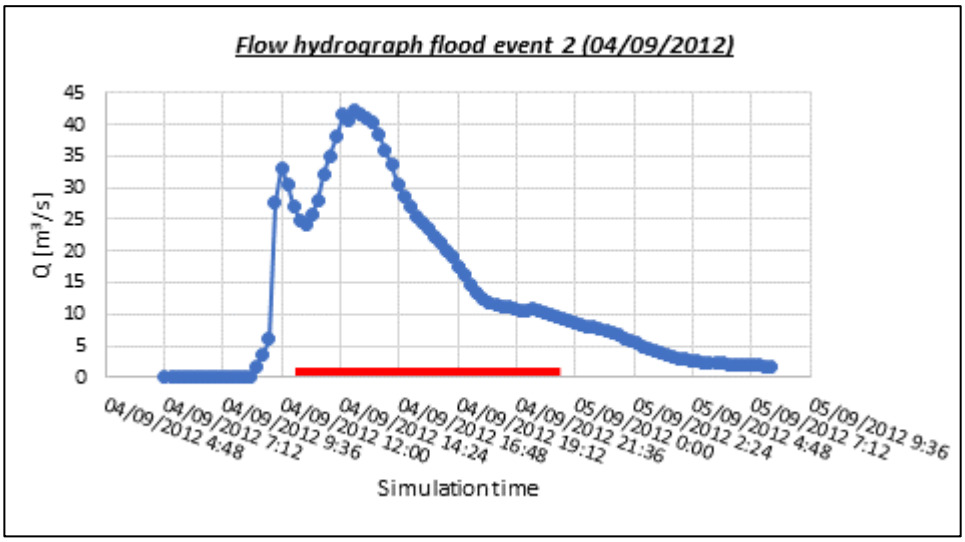

Figure 3.14 – Flow hydrograph flood event 2

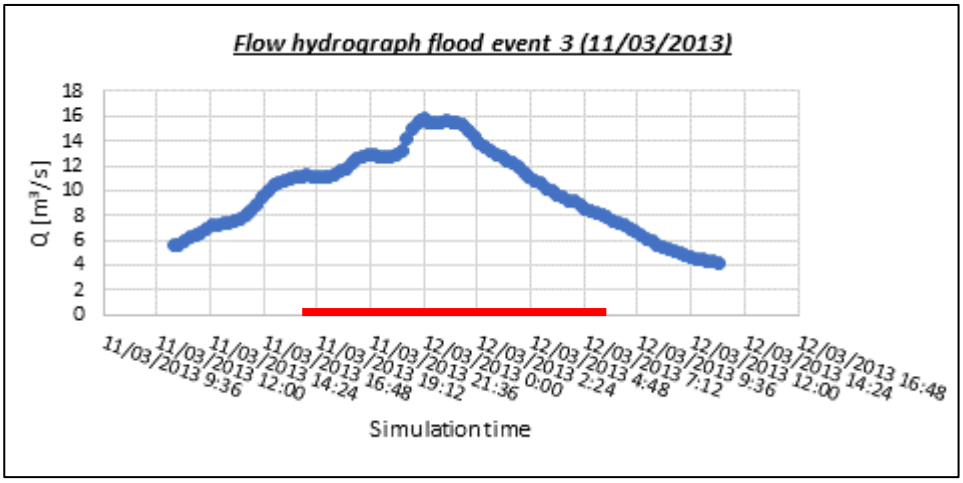

Figure 3.15 – Flow hydrograph flood event 3

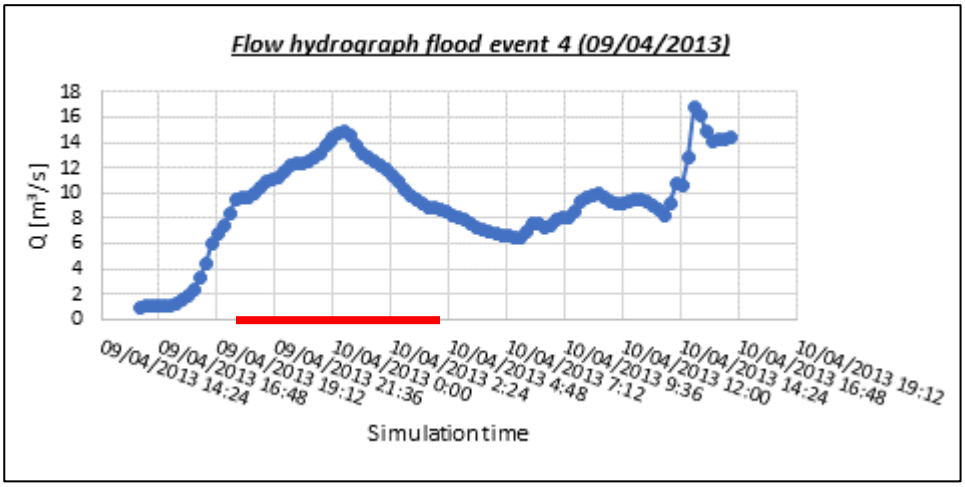

Figure 3.16 – Flow hydrograph flood event 4

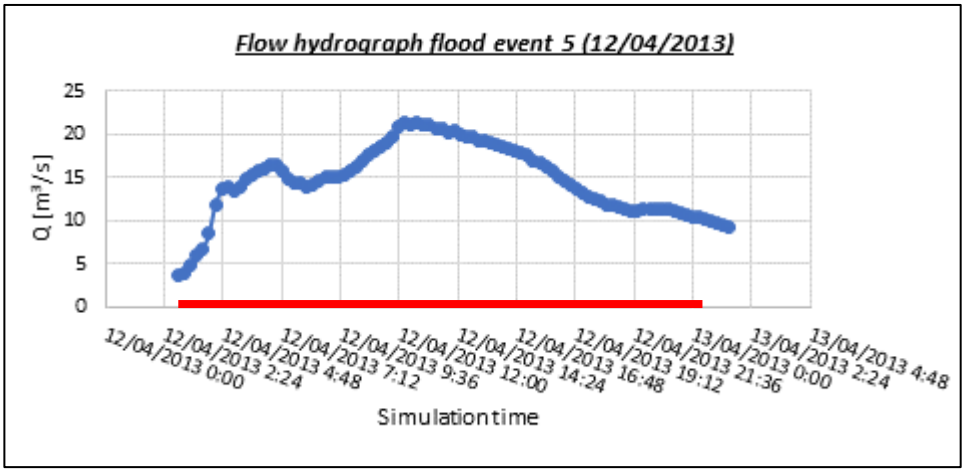

Figure 3.17 – Flow hydrograph flood event 5

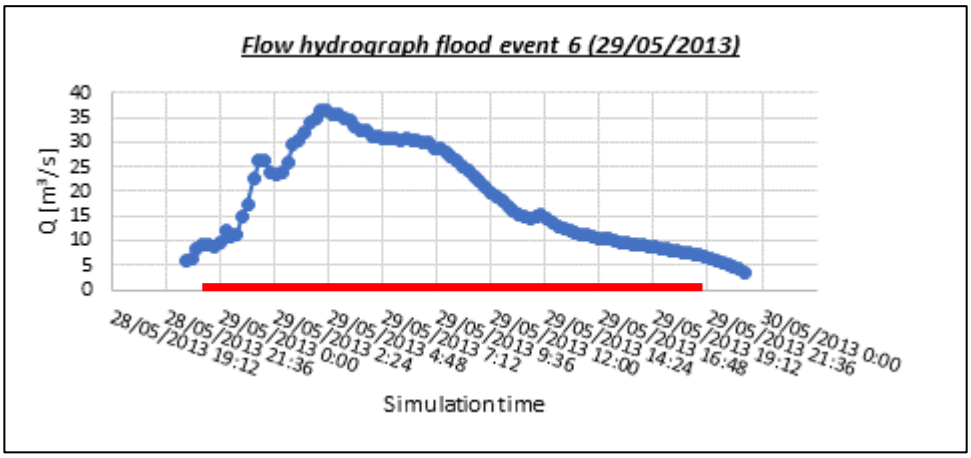

Figure 3.18 – Flow hydrograph flood event 6

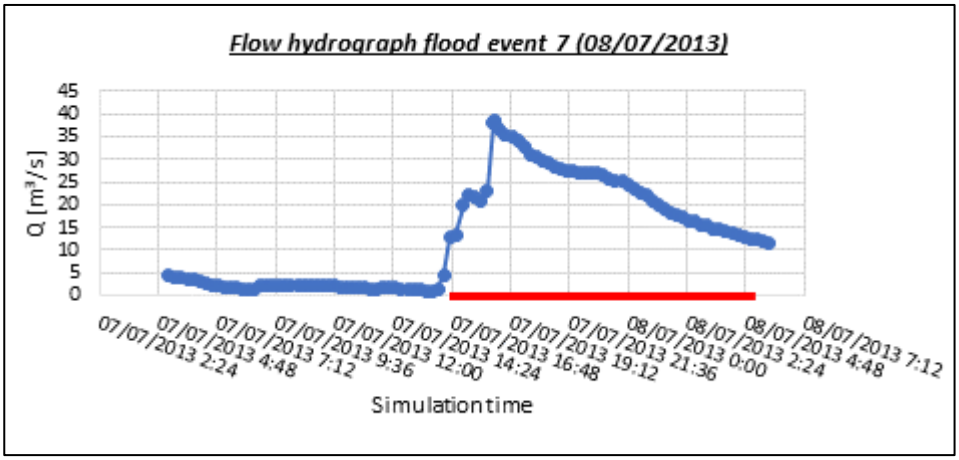

Figure 3.19 – Flow hydrograph flood event 7

Sampling of the coarse particle transport, necessary to compare the mean travel distances to the modelling results, were conducted using tracer particles embedded with RFID (radio-frequency identification) tags over a three-year period between 2011 and 2013. A total of 550 tracer particles were seeded in November 2011 throughout the study reach and their grain-size distribution spanned between D_{40surf} (40th percentile of particle sizes present on bed) and D_{max}, which is the largest grain class present on the bed (see Figure 3.5). D_{40surf} is the smallest tracer size set due to the physical limitations of drilling RFID tags into the particles. The event-based number and percentage of mobile particles is shown in Table 3.3 [*Plumb et al.*, 2017; *Nichols,* 2004; *Lamarre et al.,* 2005].

From the tracer surveys conducted between 2011 and 2013 (Table 3.3), the mean transport distance of event-based particles (L) ranged between 0.1 m < L < 3.5 m (which included tracking particles that did not move within any given discharge event) or ranged between 2.8 m < L < 16.2 m when immobile tracking particles were excluded [*Plumb et al.,* 2017].

The cells inverted in blue in Table 3.3 indicate the useful tracer surveys for comparison with HEC-RAS simulation results.

It is clear from the field observations (Table 3.3) that particles travel similar distances independent of the peak discharge. No relationships were found between mean tracer transport distance and peak discharge [*Plumb et al.,* 2017].

***Table 3.3 – Travel distances measured and number and percentage of mobile particles in the field* [*Plumb,* 2017]**

Tracer Survey Date	Q_{peak} (m^3/s)	L_{m_1} (m)	L_{m_2} (m)	N_{fevb} (-)	N_{mevb} (-)	P_{mevb} (%)
25/11/2011	12	0.1	2.8	500	9	2
02/12/2011	37	2.9	11.8	447	109	24
16/03/2012	11	0.4	9.2	439	20	5
09/05/2012	21	0.7	12.4	427	23	5
05/06/2012	18	0.4	4.8	435	32	7
02/08/2012	45	1.4	7.6	404	72	18
15/08/2012	**15**	**0.4**	**9.8**	**411**	**15**	**4**
06/09/2012	**42**	**1.4**	**8.5**	**403**	**67**	**17**
13/09/2012	36	1.8	16.2	399	44	11
24/09/2012	21	0.6	11.4	412	21	5
15/11/2012	15	0.3	3.2	340	28	8
04/04/2013	32	1.7	11.4	276	41	15
31/05/2013	**36**	**3.5**	**14.4**	**268**	**65**	**24**

Notes: tracer surveys were conducted after the recession of each hydrograph: L_{m_1} = mean transport distance of event-based particles (including immobile particles), L_{m_2} = mean transport distance of event-based particles (considering only mobile particles); N_{fevb} = number of particles found which were also found in the previous track event-based; N_{mevb} = event-based number of mobile particles; P_{mevb} = event-based percentage of mobile particles

Table 3.4 represents the fractional transport distances of different grain classes for events less than and greater than the bankfull discharge Q_{bf} ($Q_{bf} \approx 20$ m^3/s), conducted using RFID technology.

		Grain size [mm]					
		38.1	**53.8**	**76.1**	**107.6**	**152.2**	**215.3**
Events > Q_{bf}	**Moved particle number**	22	32	209	144	84	3
	Travel distance: mean value [m]	40.6	40.1	13.4	7.9	15.8	4.5
	Travel distance: maximum value [m]	159.8	342	258.2	226.3	225	7.7
	Travel distance: minimum value [m]	2.1	1.7	1.5	1.5	1.5	2.3
Events < Q_{bf}	**Moved particle number**	4	4	51	39	18	1
	Travel distance: mean value [m]	9.9	8.3	15.6	4.1	7.9	1.8
	Travel distance: maximum value [m]	22.2	24.2	177.3	54	64.7	1.8
	Travel distance: minimum value [m]	2.1	2.3	1.5	1.5	1.5	1.8

***Table 3.4 – Fractional transport distances of different grain sizes* [*Plumb,* 2017]**

Figure 3.20 shows the graph created using the mean values of fractional travel distance in Table 3.4.

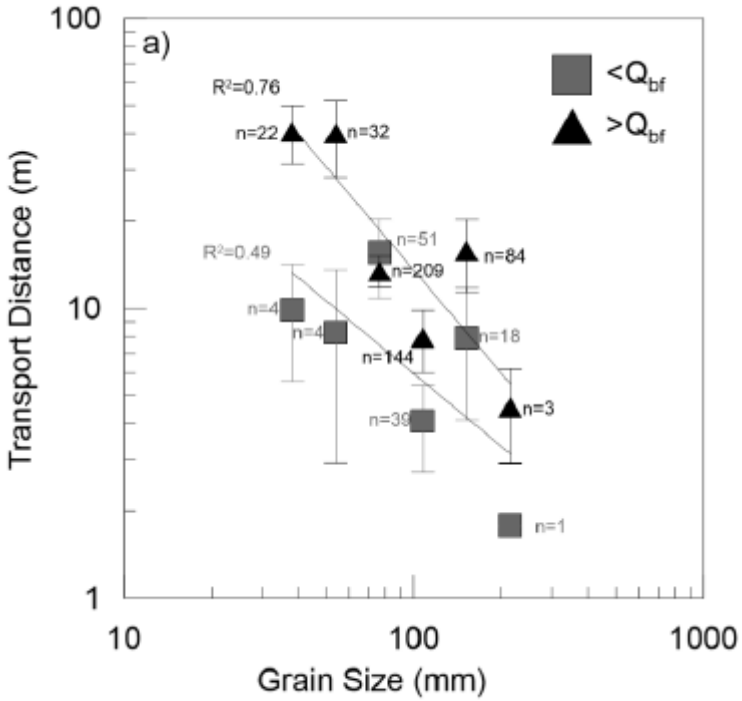

***Figure 3.20 – Fractional transport distances of different grain sizes* [*Plumb et al.,* 2017]**

3.5. Construction of the HEC-RAS model

3.5.1. Geometry data

Before adding sediment data and calibrating transport functions in HEC-RAS, it is important to calibrate the hydraulic model; this process depends on roughness parameters [*USACE,* 2016 (b)]. Estimates of Manning's roughness is an essential element in the accuracy of the results of computed water surface elevations [*Kuta et al.*, 2010]. In this case study, a HEC-RAS model was developed and calibrated to the study reach (by adjusting the roughness of the channel and the floodplain) against a series of discharge events where in-situ bedload sampling occurred over a range of competent bed mobilizing events (see paragraph 3.4) using the quasi-steady approximation. This calibration was made possible because of hydrometric gauge station (02HC033) shown in Figure 3.1 [*Plumb et al.,* 2017]. This approximation was employed to account for the non-linearity in the sediment transport processes as slight changes in hydraulic parameters (e.g. roughness) are known to have large impacts on estimated sediment transport rates [*USACE,* 2016 (b)].

Therefore, the geometry of the cross sections shown in Figure 3.4 and their roughness are known. Additional cross sections by interpolation were included to improve the geometry

model. The mean distance between the cross sections is 10 m, according to the transport distance mean value of mobile particles measured in the field.

3.5.2. Sediment Data

The following initial conditions and estimate options have to be specified in the HEC-RAS program:

- Transport Functions
- Bed Gradation
- Sediment Control Volumes
- Sorting Method
- Fall Velocity Method
- Boundary Condition
- Bank Stability and Toe Erosion Model (BSTEM)

Meyer-Peter Müller and *Wilcock and Crowe* are the **Transport Functions** used to simulate. The *Wilcock and Crowe* function was chosen because it is widely used to model sediment transport in heterogeneous sand-gravel mixtures, and it can be calibrated to the field measured sediment transport rate [*Wilcock,* 2001]. This function is a surface-based transport model and so the grain size distribution of the surface mixture was used to define **Bed Gradation** (see Figure 3.5). The *Meyer-Peter Müller* equation was chosen as it is one of the earliest equations developed and it is still one of the most widely used. However, it is mostly based upon relatively uniform gravel mixtures, making the transport equation largely applicable to streams with relatively unimodal grain size distributions. The *Meyer-Peter Müller* function tends to underpredict transport of finer material and then it was considered only for comparison purposes, using the grain size distribution of the bulk mixture as bed Gradation (see Figure 3.5) [*Berteni et al.,* 2018]. It must not be forgotten that "Bed gradation" (considering both the transport functions) was not defined for the first 0.5 km of the study reach because it is a concrete channel.

HEC-RAS **Sediment Control Volumes** contain the available erodible sediment and each one extends from the midpoint between the cross section and the next one upstream to the same midpoint downstream. Therefore, each volume is 'centered' around each cross section as shown in Figure 3.21 and characterized by its width and its vertical thickness. The width is defined by "Movable Bed Limits", coinciding with main channel bank stations. "Maximum Depth" value defines the vertical dimension of the sediment control volume and it indicates the bottom of the control volume to a distance below the original invert of the channel [*USACE,* 2016 (b)]. It was decided to assign to this value the grain size corresponding to 98% cumulative proportion of bed material (Figure 3.5).

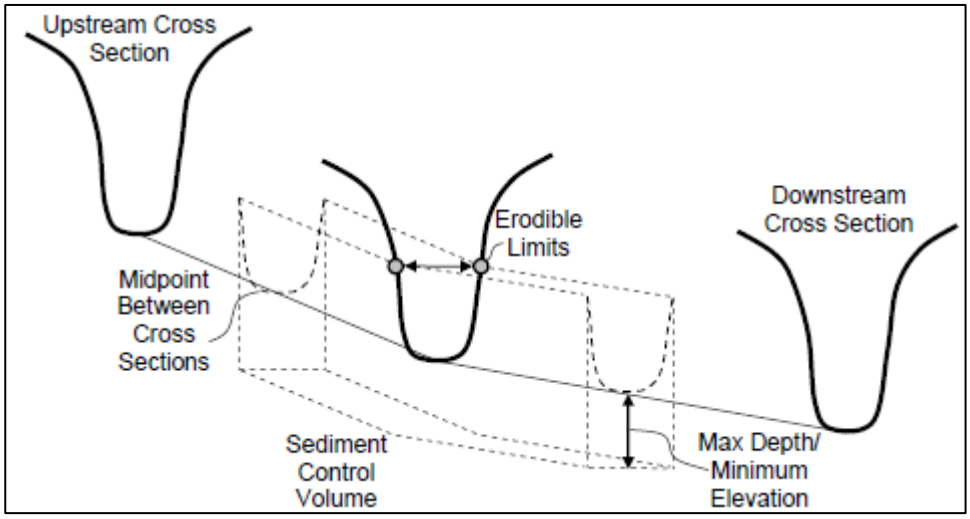

Figure 3.21 – Schematic of sediment control volume associated with each cross section **[USACE, 2016 (b)]**

The bed **Sorting Method** keeps track of the bed gradation which HEC-RAS uses to compute grain-class specific transport capacities and it can also simulate armoring processes which regulate supply [*USACE,* 2016 (b)]. In this case study the "Active Layer" sorting method was chosen, for both the *Meyer-Peter Müller* and the *Wilcock and Crowe* transport functions. This algorithm divides the bed into an active layer and an inactive layer. The active layer is a surface layer that represents actively transporting material or material that could be transported. The active layer gradation evolves independently and material is moved between it and the inactive layer below it. Transport capacity is based on the gradation of the active layer, not the entire bed [*USACE,* 2016 (a)].

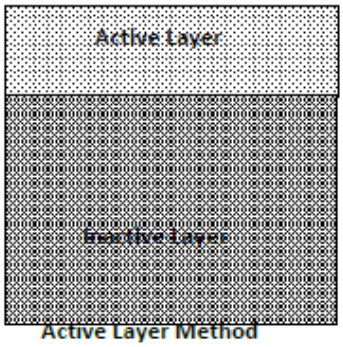

Figure 3.22 – Schematic of the mixing layers in HEC-RAS' Active Layer method **[USACE, 2016 (a)]**

Wilcock and Crowe is a surface based transport function and so it automatically accounts for dynamic armoring processes. It accounts for inter-particle interactions like hiding and sand-dependent gravel transport explicitly, but it builds the armor layer regulation in the equation

implicitly, by basing transport on armor layer gradations. For this reason the HEC-RAS manual suggests to use the "Active Layer" algorithm with this transport function. Using the other algorithms with a surface based transport equation double counts armoring effects [*USACE,* 2016 (a)]. It was decided to use this algorithm even with *Meyer-Peter Müller* because the other ones (Thomas and Copeland methods) are sophisticated and complicated and also to compare the results of different transport functions using the same bed sorting method. Moreover, this method is more intuitive and transparent, it can form a coarse or fine active layer and it is preferable in some cases for modeling armor systems [*Gibson and Piper,* 2007; *USACE,* 2016 (a)].

The "Rubey" **Fall Velocity Method** was used, considering both the *Meyer-Peter Müller* and the *Wilcock and Crowe* transport functions. Rubey (1933) developed an analytical relationship between the fluid, sediment properties and fall velocity that is adequate for silt, sand and gravel grains. The Mimico Creek study reach is a gravel bed river with a bimodal distribution (a smaller secondary peak in the sand fraction) and therefore this fall velocity method is well suited. In the Rubey method, the fall velocity is based on the combination of Stoke's law (for fine particles subject only to viscous resistance) and an impact formula (for large particles outside the Stoke's region) [*USACE,* 2016 (a)].

"Equilibrium Load" is the **Boundary Condition** used at the upstream cross section, considering both the *Meyer-Peter Müller* and the *Wilcock and Crowe* equation. This method computes the boundary sediment load from the bed gradation and the transport capacity. The load is set to transport capacity and then there is an equilibrium condition, without aggrade or degrade of the cross section [*USACE,* 2016 (b)]. The "Equilibrium Load" boundary condition is well suited to study reach because its upstream cross sections are made of concrete.

Fine-grain fractions were notably underestimated within the main channel of in-situ bedload sampling as floodplain storage of fine-grained sediments was observed in the field. Therefore, particle sizes used in evaluating transport models ranged between 0.5 mm (smaller sizes were observed in floodplain deposits) and 32 mm (limited by the orifice of the bedload sampler). Fractions finer than this range (< 0.5 mm) travel in suspension and then they are underrepresented in the bed load. Fractions larger than this range can be considered only partially mobile. [*Plumb et al.*, 2017]. All simulations (considering both *Meyer-Peter Müller* and the *Wilcock and Crowe* transport functions) prescribed that fine-grained fractions contributing to bed material supply originated from bank erosion, through the **Bank Stability and Toe Erosion Model (BSTEM)** that is integrated with the sediment transport methods in HEC-RAS. The BSTEM is a physically based bank-erosion model that accounts for hydraulic, toe erosion and bank failure processes in homogeneous or layered banks [*Gibson et al.,* 2015]. The bank stability model goes through a series of iterative computations to select potential failure planes, evaluate the factor of safety (FS) and converge to the failure plane most likely to fail. The computational approach used to compute the FS of a failure plane through the bank is the "Method of Slices", proposed by Langendoen (2008). This algorithm follows the classical geotechnical approach to planar

failure. The bank material selected for the study reach (where there is no concrete channel) is stiff clay, which has the following default material soil properties [*USACE,* 2015]:

- Saturated unit weight = 17.7 KN/m^3
- Fraction angle (ϕ') = 21.1°
- Cohesion = 12.6 KPa
- Angle representing the relationship between shear matrix suction and apparent cohesion (ϕ^b) = 15°
- Critical shear = 50 Pa
- Erodibility = $3.16 \cdot 10^{-7}$ m^3/(N-s)

The bank material properties employed where the channel is in concrete, are the following:

- Saturated unit weight = 24 KN/m^3
- Fraction angle (ϕ') = 42°
- Cohesion = 400 KPa
- Angle representing the relationship between shear matrix suction and apparent cohesion (ϕ^b) = 30°
- Critical shear = 21000 Pa
- Erodibility = 0.621 m^3/(N-s)

3.5.2.1. Sensitivity analysis: the effects of the BSTEM

Simulation results have shown that the sediment discharge values from bank-erosion are not insignificant compared to the global values of sediment discharge in the river bed, for the whole duration of the flood event. Therefore, the contribution from bank-erosion model BSTEM cannot be neglected.

A sensitivity analysis was conducted in order to understand the effects of BSTEM in HEC-RAS simulations. In the following paragraphs (3.8 and 3.9) the procedure adopted is described and the results obtained are shown.

In particular, HEC-RAS simulations considering and without considering the model BSTEM were carried out and the analysis revealed that the BSTEM option gives an important contribution to fine-grained fractions; therefore, it increases the total sediment discharge.

3.5.3. Flow Data

HEC-RAS includes two hydrodynamic approaches to Sediment Transport Analysis:

- Quasi-Unsteady Flow
- Unsteady Flow

The **Quasi-Unsteady Flow** approach is only used for sediment transport analysis. This hydrodynamic model simulates the flow series with a sequence of steady flow computations. Therefore, the hydrograph is approximated with a series of discrete steady flow profiles;

each profile lasts 15 minutes in all simulations (Figure 3.23). HEC-RAS computes water surface profile for steady gradually varied flow analysis by solving the energy equation with an iterative procedure (standard step method). Whenever a rapidly varying flow situation occurs, the energy equation is not considered to be applicable and so HEC-RAS uses the momentum equation. This hydrodynamic model is easier and more stable than the "Unsteady Flow" model, but it does not conserve flow and therefore it could introduce unacceptable errors [*USACE,* 2016 (a); *USACE,* 2016 (b)].

The **Unsteady Flow** approach with sediment data is new in HEC-RAS. This hydrodynamic model solves the De Saint-Venant equation implicitly and it conserves flow, but it is less stable and more complex [*USACE,* 2016 (b)].

Figure 3.23 and Figure 3.24 show an example (flood event 29/05/2013) of hydrograph modeled respectively with the quasi-unsteady flow model and the unsteady flow model. The hydrograph is the boundary condition at the upstream cross section in the study reach.

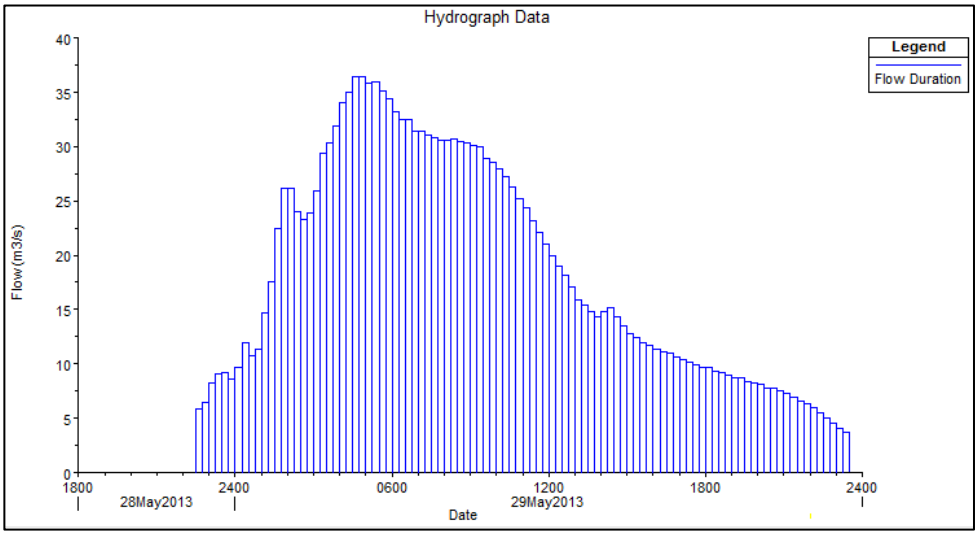

Figure 3.23 – Hydrograph modelled with the quasi- unsteady flow model

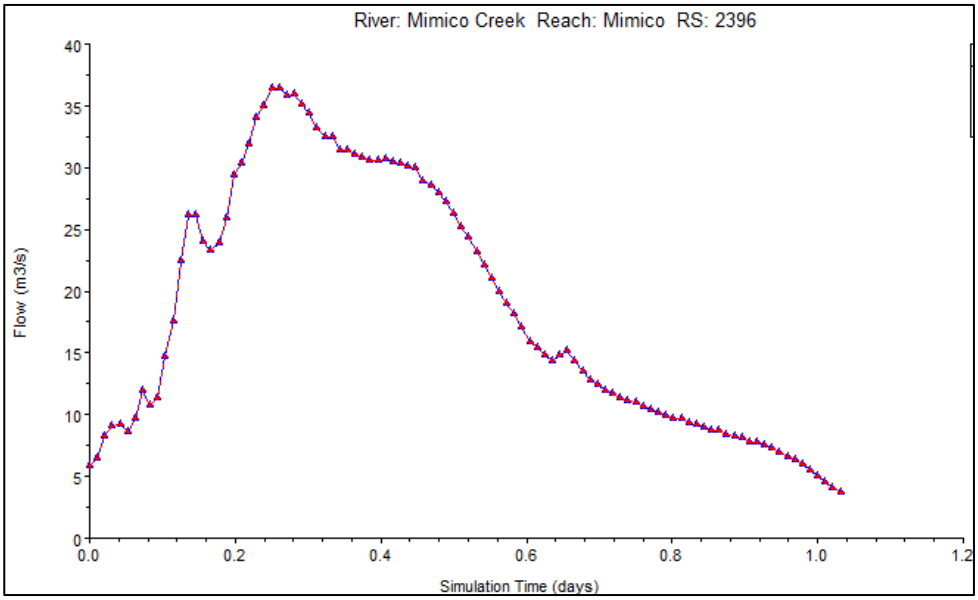

Figure 3.24 – Hydrograph modelled with the unsteady flow model

For the reasons given above, both step-wise discharge and unsteady flow simulations were evaluated.

3.6. Flood wave propagation in unsteady flow

In unsteady flow, velocities and depths change with time at any fixed spatial position in an open channel. Open channel flow in natural channels is almost always unsteady because of free surface. Mathematically, this means that the two dependent flow variables (e.g., velocity and depth or discharge and depth) are functions of both the distance along the channel and the time for one-dimensional applications. Problem formulation requires the solution of the governing equations called *De Saint-Venant equations*, which are two partial differential equations representing the continuity and momentum principles in the two unknown dependent variables. There are several numerical techniques to solve the partial differential equations of unsteady flow, with or without simplifications. HEC-RAS implements the implicit finite difference method to solve problems of flood routing and dam breaks [*Sturm,* 2010].

One or more terms of the governing equations are neglected in simplified methods, that are presented in the context of flow routing problems. Simplified methods incorporate the *kinematic wave routing* and the *diffusion routing*. In kinematic wave routing, the momentum equation is simplified by neglecting both the inertia terms and the pressure gradient term. The kinematic wave equation for constant wave celerity is linear with an analytical solution represented by a pure translation of the inflow hydrograph (Figure 3.25 (a)). In diffusion

routing, the momentum equation is simplified by neglecting only the inertia terms and it considers the lamination effect of the flood wave (Figure 3.25 (b)) [*Sturm,* 2010].

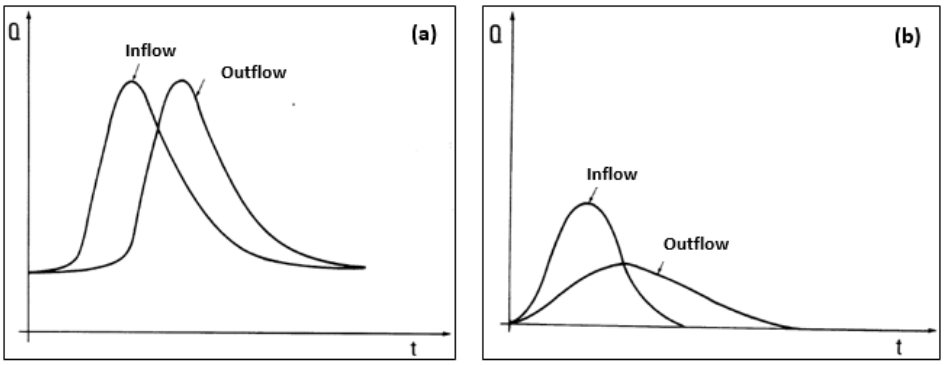

Figure 3.25 – Flood wave propagation: translation in kinematic wave (a), lamination in diffusion wave (b)

Figure 3.6 shows the position of the stream flow gauge 02HC033 where the flow hydrographs of the seven flood events analysed were recorded, even if each hydrograph is the boundary condition at the upstream cross section of the study reach for each flood event. This choice may be considered as acceptable for these reasons:

1) station 02HC033 is located a short distance downstream of the study reach, with no major tributaries entering the stream between the study reach and gauge such that continuity of flow can be assumed;
2) the flood wave propagation broadly follows the kinematic-wave model, without showing a significant lamination effect.

To demonstrate the second reason, considering each flood event analysed, different flow hydrgraphs at many points in the Mimico Creek over the same period were compared.

To carry out this operation, the geometry in the HEC-RAS model was amended (compared with Figure 3.4) to include one more segment from the end of the study reach to the position of the stream flow gauge 02HC033. The additional cross sections in the new segment were included by interpolation. Therefore, the "new study reach" in the HEC-RAS model extends from the beginning of the "old study reach" to the station 02HC033 location.

The following pictures (Figure 3.26, Figure 3.27, Figure 3.28) show three examples of the flow hydrographs obtained after HEC-RAS simulations, considering the "Unsteady Flow" approach, in three different cross sections:

- at the beginning of the "new study reach" (Cross section 1, which coincides with the beginning of the "old study reach");
- at the end of the "old study reach" (Cross section 2);
- at the stream flow gauge 02HC033 position (Cross section 3, which coincides with the ending of the "new study reach").

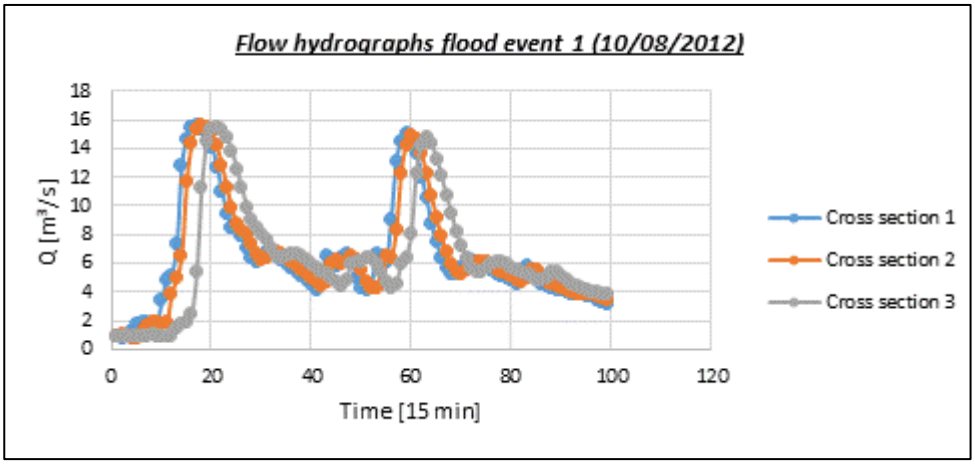

Figure 3.26 – Flow hydrographs flood event 1

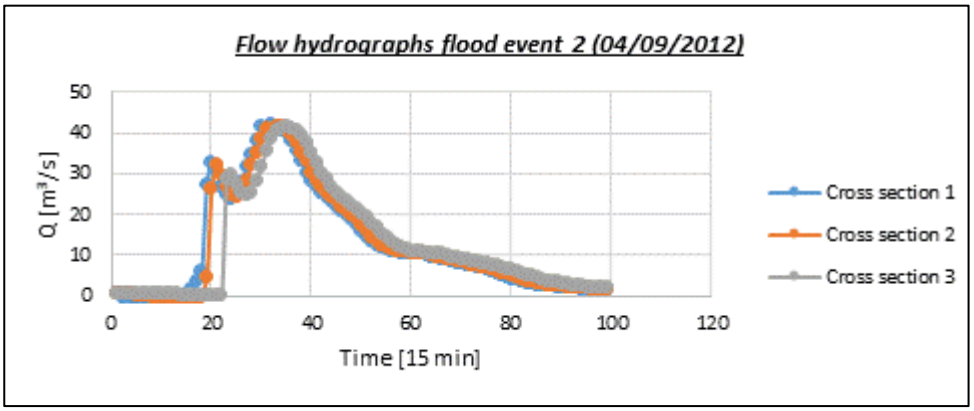

Figure 3.27 – Flow hydrographs flood event 2

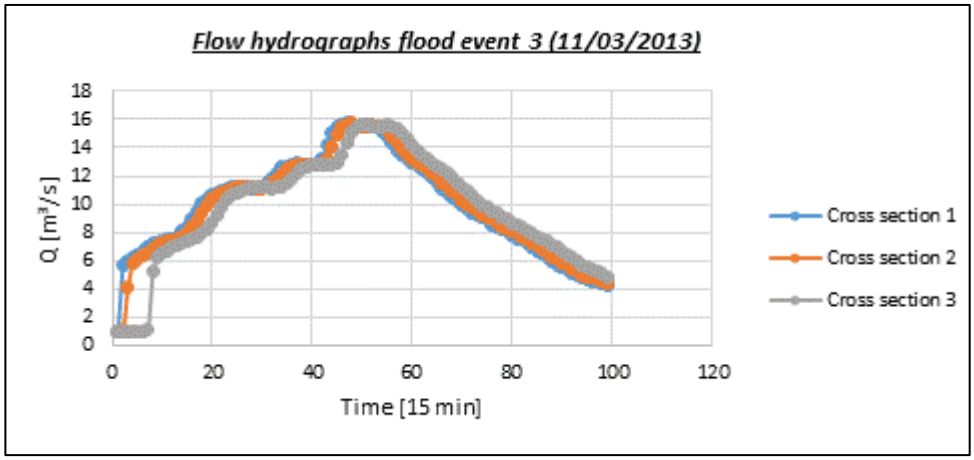

Figure 3.28 – Flow hydrographs flood event 3

Results obtained show that there is a translation of peak discharge in the flood wave within a 45-minute or 1-hour period. After the translation, peak discharge is substantially unchanged because it is reduced by no more than 1%, without visible effects of lamination. Consequently, the flood wave propagation broadly follows the kinematic-wave model.

3.7. Changes in water levels and tides

The Mimico Creek flows directly into Lake Ontario; therefore, lake water levels and tides have to be taken into account in evaluating flood events. True tides are variations in water level, up to 10-15 m, caused by the gravitational forces of the sun and moon.

Lake Ontario is one of the Great Lakes, where water levels change primarily because of meteorological effects. In these lakes, true tides occur in a semi-diurnal (twice daily) pattern. Studies indicate that the spring tides of the Great Lakes, being the largest tides caused by the combined forces of the sun and moon, are less than five centimeters in height. These minor variations are masked by the greater fluctuations in lake levels produced by wind and barometric pressure changes. Water levels in the Great Lakes have long-term, annual, and short-term variations. Long-term variations depend on precipitation and water storage over many years. Annual variations occur with the changing seasons. There is an annual high in the late spring and low in the winter. These changes occur at a rate that can be measured in centimetres per month. For these reasons the Great Lakes, and thus also Lake Ontario, are considered to be non-tidal [*https://oceanservice.noaa.gov/facts/gltides.html*].

Focusing attention on Lake Ontario, hourly water level variations were analysed. The values for the years 2012 and 2013 were considered, because in those years flood events of interest occurred. The data were provided by the Government of Canada [*www.marinfo.gc.ca*] and were registered at “Toronto Station” (station number 13320) shown in Figure 3.29. This

examination revealed that the difference of the observed water level from an hour to the next hour reaches, on average, 1.2 cm and the peak value achieved is 20 cm. The difference between the maximum and the minimum values recorded in the two years which were analysed is about 1 m.

Therefore, it can be argued that water levels and tides may be neglected in evaluating flood events that were examined. Indeed, the hydrographs included in the HEC-RAS models were not affected by tides, both due to the small change in water level observed and to the distance from the coast of the study reach.

Figure 3.29 – Position of the Toronto Station number 13320

3.8. Calibration of transport functions using HEC-RAS

In this case study, both step-wise discharge (quasi-unsteady flow simulations) and unsteady flow simulations were evaluated to calibrate the *Meyer-Peter Müller* and the *Wilcock and Crowe* transport models (see paragraph 2.3.2) [*Berteni et al.,* 2018].

As outlined below, in the case where the BSTEM was considered, the *Wilcock and Crowe* model was noted to more accurately portray the bulk in-situ sediment transport rates of field observations over the *Meyer-Peter Müller* equation.

A calibration curve was developed using the *Wilcock and Crowe* transport model to determine bed material transport rates as a function of reference shear stress and calibrated to observed transport rates utilizing the same flood events. The calibration parameter (reference shear stress) in the HEC-RAS model was modified to achieve, for each discrete flood event, comparable results between field observed and predicted transport rates [*Berteni et al.,* 2018].

The calibration process was conducted considering and without considering the BSTEM (Bank Stability and Toe Erosion Model) in HEC-RAS, as described in paragraphs 3.8.1 and 3.8.2

3.8.1. Calibration considering the BSTEM

The calibration process was initially carried out considering the BSTEM, which is described in paragraph 3.5.2, in the HEC-RAS model. This choice was made in order to consider fine-grained fractions contributing to bed material supply originated from bank erosion [*Berteni et al.,* 2018].

Figure 3.30 shows the calibration curve obtained.

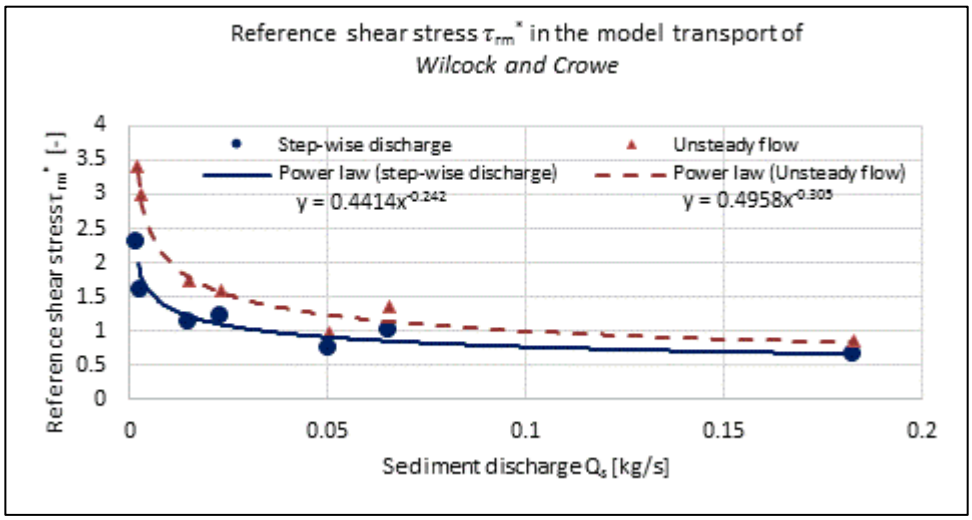

Figure 3.30 – Calibration curve for the Wilcock and Crowe transport model considering the BSTEM

In the case of the higher magnitude flood events, the *Wilcock and Crowe* model was noted to more accurately portray the bulk in-situ sediment transport rates of field observations over the *Meyer-Peter Müller* equation, which was applied without considering the Wong and Parker correction (see paragraph 2.3.1). The *Meyer-Peter Müller* equation is most applicable in streams with a tight unimodal bed material distribution, where particle sizes range from 0.4 to 29 mm (see paragraph 2.3.1). Mimico Creek is a gravel-bed river with heterogeneous bed material distribution containing both sand and gravel fractions where more than 50% of

the bed material is larger than 29 mm (Figure 3.5). To achieve a calibration with the field measurements using the *Meyer-Peter Müller* equation, critical shear stress (τ_C^*) values (used as a calibration parameter) would have had to be set to values beyond the valid parameter range (50 $\leq \tau_C^* \leq$ 570) [*Berteni et al.,* 2018]. Table 3.5 lists the comparison of discharge events between field observations and results of the *Wilcock and Crowe* model simulations; Figure 3.31 shows its linear trend.

Flood Event	Date	Q_{peak} (m^3/s)	Q_{b_field} (t/day)	Q_{b_model} (step-wise discharge) (t/day)	Q_{b_model} (unsteady flow) (t/day)
1	10/08/2012	15.6	4.35	4.66	4.33
2	04/09/2012	42.3	5.68	5.25	5.73
3	11/03/2013	15.7	0.23	0.31	0.25
4	09/04/2013	16.8	0.17	0.18	0.19
5	12/04/2013	21.4	1.3	1.33	1.28
6	29/05/2013	36.5	1.99	2.02	2.03
7	08/07/2013	38.7	15.79	15.9	15.80

***Table 3.5 – Comparison between sediment discharge measured in the field (Q_{b_field}) and calibrated modelling results (Q_{b_model}) using the Wilcock and Crowe equation and considering the BSTEM* [Berteni et al., 2018]**

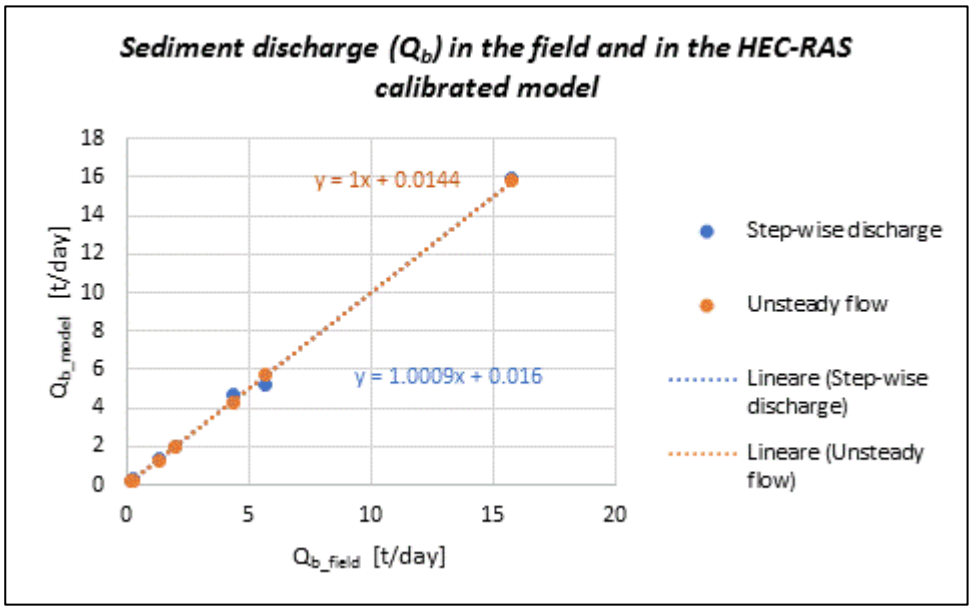

Figure 3.31 – Linear trend: sediment discharge measured in the field (Q_{b_field}) and calibrated modelling results (Q_{b_model}) using the Wilcock and Crowe equation considering the BSTEM

3.8.2. Calibration without considering the BSTEM

It was finally decided to calibrate the HEC-RAS model using the *Wilcock and Crowe* transport function also without considering the BSTEM. This choice was made because simulation results showed that the sediment discharge values from bank-erosion are significant compared to the global values of sediment discharge in the river bed (see paragraph 3.5.2.1).

In the calibration process, field observed and predicted transport rates have to be comparable. By using the BSTEM, the calibration parameter in the HEC-RAS model could appear altered because field observed rates do not include fine-grained material, whereas predicted transport rates in the model include it.

Furthermore, also the use of the *Wilcock and Crowe* transport function can be altered. Indeed, *Wilcock and Crowe* is a surface-based transport model, developed for sand and gravel bed material mixtures. By using the BSTEM, there is the need to take into account the significant fine-grained fractions.

Figure 3.32 shows the calibration curve obtained without considering the BSTEM.

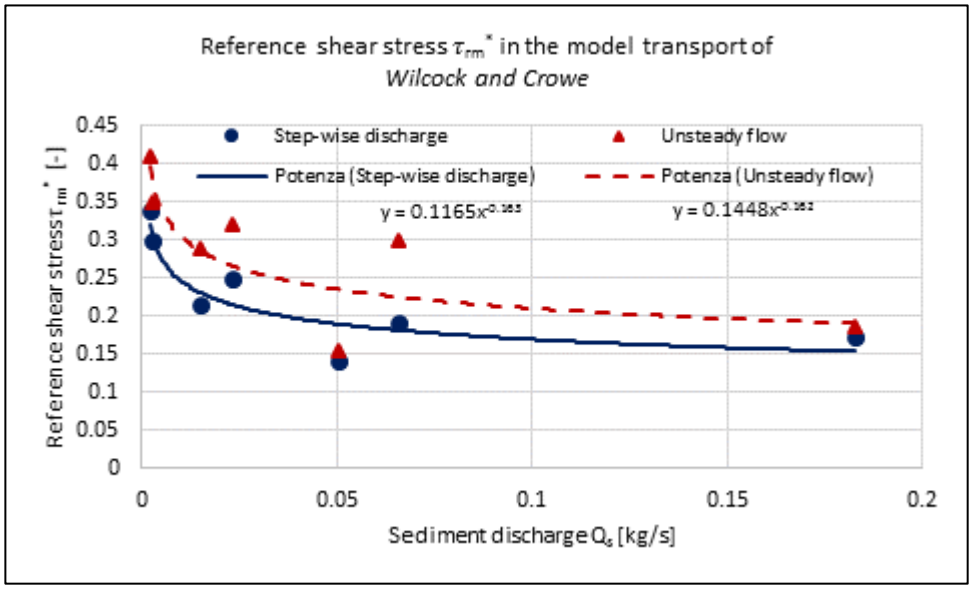

Figure 3.32 – Calibration curve for the Wilcock and Crowe transport model without considering the BSTEM in HEC-RAS

Table 3.6 lists the comparison of discharge events between field observations and results of the *Wilcock and Crowe* model simulations without considering the BSTEM. Figure 3.33 shows its linear trend.

Flood Event	Date	Q_{peak} (m^3/s)	Q_{b_field} (t/day)	Q_{b_model} (step-wise discharge) (t/day)	Q_{b_model} (unsteady flow) (t/day)
1	10/08/2012	15.6	4.35	4.16	4.33
2	04/09/2012	42.3	5.68	5.38	5.78
3	11/03/2013	15.7	0.23	0.22	0.24
4	09/04/2013	16.8	0.17	0.17	0.17
5	12/04/2013	21.4	1.3	1.30	1.39
6	29/05/2013	36.5	1.99	2.16	1.97
7	08/07/2013	38.7	15.79	15.83	15.40

Table 3.6 – Comparison between sediment discharge measured in the field (Q_{b_field}) and calibrated modelling results (Q_{b_model}) using the Wilcock and Crowe equation and without considering the BSTEM

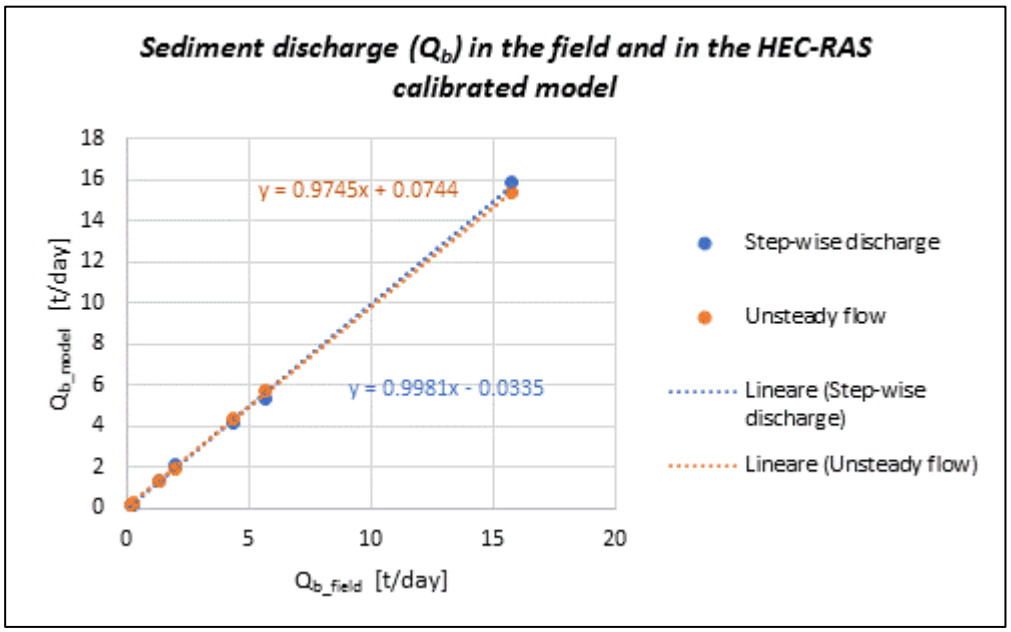

Figure 3.33 – Linear trend: sediment discharge measured in the field (Q_{b_field}) and calibrated modelling results (Q_{b_model}) using the Wilcock and Crowe equation without considering the BSTEM

3.8.3. Comparison between calibration with and without the BSTEM

The examination in paragraphs 3.8.1 and 3.8.2 had shown that values of τ_{rm}^* are larger than those predicted with the *Wilcock and Crowe* equation (Eq. (2.18)), which are between 0.021 and 0.036. The τ_{rm}^* default value proposed by HEC-RAS is 0.04. Nevertheless, as shown in

Figure 3.34 and in Figure 3.35, the calibration without the BSTEM allows an estimation of τ_{rm}^* that is closer to the range of values predicted with Equation (2.18).

The reason for these high values may be that, considering the BSTEM, there is the need to take into account the significant fine-grained fractions not provided for the *Wilcock and Crowe* model; indeed, this transport equation was developed for sand and gravel bed material mixtures.

However, high values of τ_{rm}^* remain also without considering the BSTEM. It seems reasonable to accept the deviations of the empirical values of the calibration parameter (τ_{rm}^*) from the *Wilcock and Crowe* equation (Equation (2.18)). It is clear that value of τ_{rm}^* for a sediment mixture with a given mean particle size is influenced by a number of additional factors, including differences in the particle size distribution of the mixture, differences in the arrangement of particles on the streambed and other hydraulic factors. None of these additional factors is captured in Equation (2.18), where τ_{rm}^* is a function of the fraction of sand (F_s) on the bed surface only. Therefore, F_s alone could provide an incomplete description of the bed surface condition [*Gaeuman et al.*, 2009].

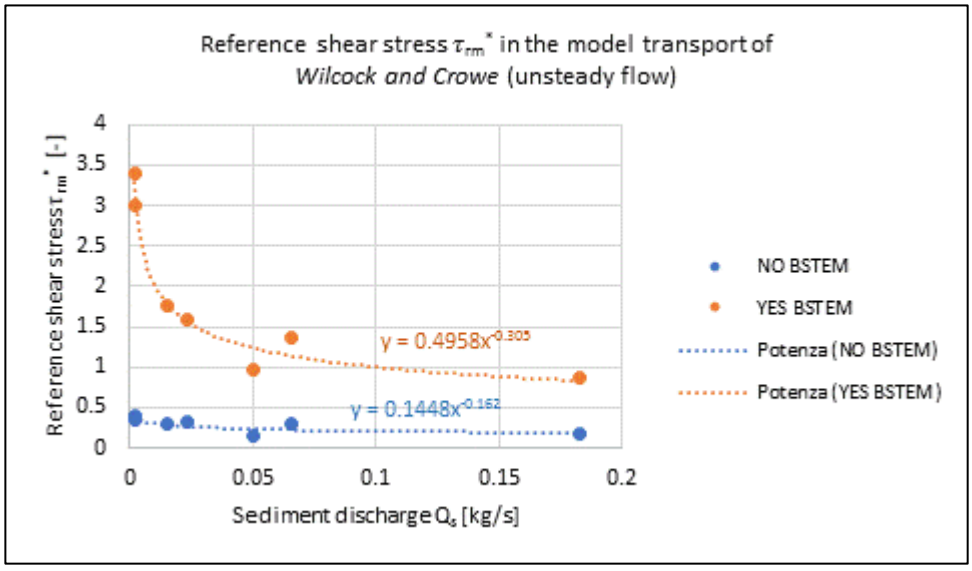

Figure 3.34 – Calibration curve for the Wilcock and Crowe transport model (unsteady flow) considering and not the BSTEM in HEC-RAS

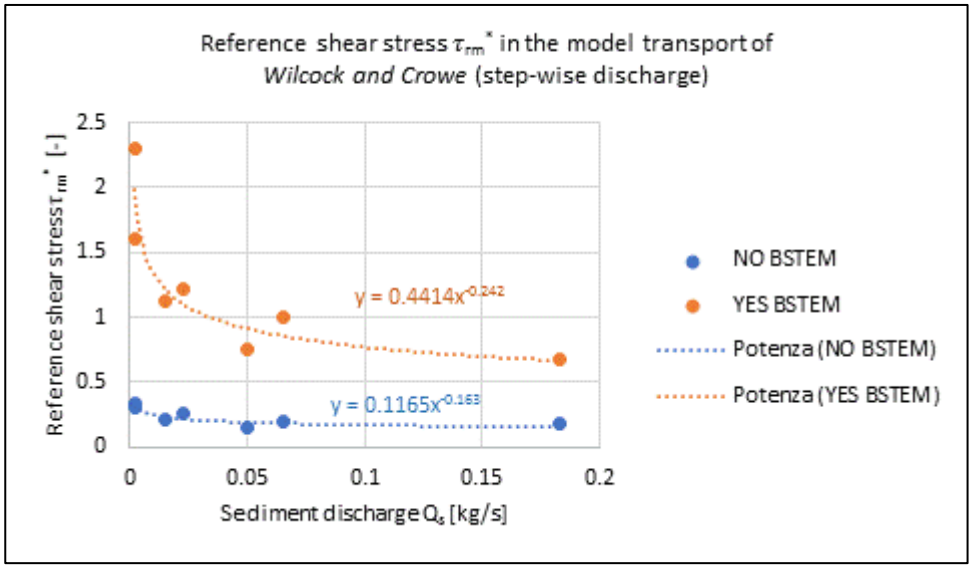

Figure 3.35 – Calibration curve for the Wilcock and Crowe transport model (step-wise discharge) considering and not the BSTEM in HEC-RAS

Considering Trinity River, which is another case study, Gaeuman et al. (2009) say that the larger dimensionless reference shear stresses (τ_{rm}^*) found are likely related to differences in bed surface organization caused by sediment supply limitations and the preferential entrainment of unstable particles.

This analysis showed that calibration without the BSTEM results better than the one that considers the BSTEM for several reasons: (1) the values of the calibration parameter τ_{rm}^* are closer to those predicted with the *Wilcock and Crowe* equation (Equation (2.18)), (2) field observed rates used to calibrate the model do not include fine-grained material and (3) *Wilcock and Crowe* is a transport function that does not take into account fine-grained fractions.

The comparison of the sediment discharge rate for each size fraction, considering field observed and predicted transport rates, is another reason in support of this argument. Table 3.7 shows this comparison for the July 8th, 2013 extreme rainfall event. The simulation results were estimated considering the calibrated *Wilcock and Crowe* transport function with the unsteady flow approach. In accordance with Emmett (1980), Lisle (1995) and Whiting and King (2003), the particle diameters considered in Table 3.7 are between 0.5 and 32 mm because particles smaller than 0.5 mm and larger than 32 mm are not suitable due to sampling biases associated with the Helley-Smith [*Plumb et al.*, 2017]. Simulation results, without considering the BSTEM, are closer to the sediment discharge for each size fraction measured in the field.

Particle diameter **(mm)**	***$Q_{sediment-i}$ for each size fraction-i*** **(ton/s)**		
	Field observations [*Plumb*, 2017]	***Simulation results (YES BSTEM)***	***Simulation results (NO BSTEM)***
32	$6.30\ 10^{-6}$	$2.96\ 10^{-12}$	$1.09\ 10^{-7}$
16	$9.46\ 10^{-6}$	$1.12\ 10^{-10}$	$1.46\ 10^{-6}$
8	$1.43\ 10^{-5}$	$2.95\ 10^{-9}$	$2.61\ 10^{-6}$
5.6	$1.04\ 10^{-5}$	$9.65\ 10^{-8}$	$5.75\ 10^{-6}$
2.8	$1.71\ 10^{-5}$	$5.70\ 10^{-7}$	$1.07\ 10^{-5}$
2	$1.75\ 10^{-5}$	$9.75\ 10^{-7}$	$1.47\ 10^{-5}$
1	$1.32\ 10^{-5}$	$1.28\ 10^{-6}$	$1.86\ 10^{-5}$
0.707	$1.13\ 10^{-5}$	$1.66\ 10^{-6}$	$2.19\ 10^{-5}$
0.5	$6.10\ 10^{-6}$	$2.11\ 10^{-6}$	$2.42\ 10^{-5}$

Table 3.7 – Comparison of sediment discharge for each size fraction-i ($Q_{sediment-i}$) between field observations and simulation results using calibrated Wilcock and Crowe equation, without considering the BSTEM and using the unsteady flow approach (Flood event: July 8th, 2013)

3.9. Mean travel distance of bed material using HEC-RAS results

For each of the seven flood events analyzed, the results of the calibrated HEC-RAS model were used to estimate the mean travel distance (L) of bed material using Equation (2.19) and Equation (2.20).

Mean values of volumetric bed material transport rates (Q_b), average active layer streambed depths (D_s) and widths (W_s) were estimated over the time interval Δt when $\omega > \omega_0$. The active thickness (D_s) was considered here to be the thickness of the active layer at the beginning of each computational time step, whereas the effective width (W_s) was considered to be the bottom width at the end of the computational time step [*USACE,* 2016 (b)]. The specific stream power ω was calculated using results from the HEC-RAS model.

An average porosity of P = 0.18 (see Equation (2.21)) was used for all *Wilcock and Crowe* simulations, where a grain size distribution from the surface mixture was used [*Berteni et al.,* 2018].

The median grain size D_m used, is 45.3 mm and it corresponds to 52% of the cumulative proportion of bed material from the surface particle size distribution. This value was used to calculate both the bed material porosity P and the stream power at the threshold of motion of bed material ω_0 (see Equation (2.23)).

The mean travel distance of bed material was calculated using the simulation results of the calibrated HEC-RAS model considering and without considering the BSTEM, as described in paragraphs 3.9.1 and 3.9.2.

3.9.1. Mean travel distance considering the BSTEM

The mean travel distance of bed material was initially estimated using the simulation results of the calibrated HEC-RAS model which considers the BSTEM (see paragraph 3.8.1). The BSTEM is described in paragraph 3.5.2.

Table 3.8 shows the comparison between simulation results (using the *Wilcock and Crowe* equation for Q_b) and field observations.

From the tracer surveys conducted between 2011 and 2013, the mean transport distance of event-based particles (L) ranged between 0.1 m < L_{m_1} < 3.5 m (which included tracking particles that did not move within any given discharge event) or ranged between 2.8 m < L_{m_2} < 16.2 m when immobile tracking particles were excluded [*Plumb,* 2017]. Mean travel distances determined from the *Wilcock and Crowe* equation simulations were found to range between 0.12 m < L < 5.7 m and between 0.11 m < L < 6 m, considering respectively step-wise discharge and unsteady flow simulations. Modelling results found that mean travel distances varied widely (above and below mean observed transport distances) compared to calculated mean field distances (Table 3.8). For the second flood event (Table 3.8), the simulated (step-wise discharge) mean travel distance is similar to the observed one when immobile tracer particles are included (L_{m_1}).

***Table 3.8 – Comparison between simulation results (using the Wilcock and Crowe equation and considering the BSTEM) and field observations* [Berteni et al., 2018]**

Field Observations [*Plumb,* 2017]					***Simulation Results*** ***(step-wise discharge)***		***Simulation Results*** ***(unsteady flow)***	
Flood event	**Date**	Q_{peak} **(m^3/s)**	L_{m_1} **(m)**	L_{m_2} **(m)**	Q_b **(m^3/s)**	L **(m)**	Q_b **(m^3/s)**	L **(m)**
1	10/08/2012	15.6	0.4	9.8	$1.3\ 10^{-5}$	1.12	$1.0\ 10^{-5}$	0.92
2	04/09/2012	42.3	1.4	8.5	$2.7\ 10^{-5}$	2.00	$6.2\ 10^{-5}$	4.82
3	11/03/2013	15.7			$1.8\ 10^{-6}$	0.16	$1.2\ 10^{-6}$	0.11
4	09/04/2013	16.8			$1.4\ 10^{-6}$	0.12	$1.4\ 10^{-6}$	0.12
5	12/04/2013	21.4			$9.9\ 10^{-6}$	0.80	$9.4\ 10^{-6}$	0.80
6	29/05/2013	36.5	3.5	14.4	$1.4\ 10^{-5}$	1.10	$1.8\ 10^{-5}$	1.51
7	08/07/2013	38.7			$6.9\ 10^{-5}$	5.70	$6.9\ 10^{-5}$	6.00

Notes: tracer surveys were conducted after the recession of each hydrograph: L_{m_1} = mean transport distance of event-based particles (including immobile particles), L_{m_2} = mean transport distance of event-based particles (considering only mobile particles)

It is clear from the field observations (Table 3.8) that particles travel similar distances independent of the peak discharge. No relationships were found between mean tracer

transport distance and peak discharge [*Plumb et al.,* 2017]. The same situation is visible in simulation results, where there is not a monotone function relating peak discharge (Q_{peak}) and mean travel distance (Table 3.8). Indeed, the mean travel distance *L* depends upon many factors (Q_b, Δt, D_s, W_s), not necessarily related to the peak discharge.

Considering tracer mobility, the event-based percentage of mobile particles (P_{mevb}) for the 1st, the 2nd and the 6th flood events is shown in Table 3.9. A general trend was found between L_{m_1} (and L_{m_2}) and P_{mevb}: higher values of L_{m_1} (and L_{m_2}) corresponded to higher values of P_{mevb}.

Flood event	Date	P_{mevb} (%)	L_{m_1} (m)	L_{m_2} (m)
1	10/08/2012	4	0.4	9.8
2	04/09/2012	17	1.4	8.5
6	29/05/2013	24	3.5	14.4

Table 3.9 – Event-based percentage of mobile particles and mean transport distance of event-based particles. [Plumb, 2017]

Concerning simulation results, it was not possible to estimate P_{mevb}, but the volume of bed material (*V*) could be evaluated as the product of the mean values of volumetric bed material transport rates (Q_b) and the time interval Δt, when $\omega > \omega_0$ (Table 3.10) [*Berteni et al.,* 2018].

		Simulations Results ***(step-wise discharge)***			***Simulation Results*** ***(unsteady flow)***		
Flood event	**Date**	Q_b (m^3/s)	Δt (s)	$V = Q_b \times \Delta t$ (m^3)	Q_b (m^3/s)	Δt (s)	$V = Q_b \times \Delta t$ (m^3)
1	10/08/2012	$1.3\ 10^{-5}$	84600	**1.10**	$1.0\ 10^{-5}$	84600	**0.87**
2	04/09/2012	$2.7\ 10^{-5}$	75600	**2.01**	$6.2\ 10^{-5}$	75600	**4.71**
3	11/03/2013	$1.8\ 10^{-6}$	89100	**0.16**	$1.2\ 10^{-6}$	89100	**0.11**
4	09/04/2013	$1.4\ 10^{-6}$	83700	**0.11**	$1.4\ 10^{-6}$	82800	**0.11**
5	12/04/2013	$9.9\ 10^{-6}$	89100	**0.88**	$9.4\ 10^{-6}$	89100	**0.84**
6	29/05/2013	$1.4\ 10^{-5}$	89100	**1.20**	$1.8\ 10^{-5}$	89100	**1.59**
7	08/07/2013	$6.9\ 10^{-5}$	88200	**6.06**	$6.9\ 10^{-5}$	88200	**6.10**

Table 3.10 – Determination of the volume of bed material using Wilcock and Crowe simulation results and considering the BSTEM

A correlation between *L* and the volume of bed material was observed such that higher values of *L* corresponded to higher values of volumetric bed material transport rates [*Berteni et al.,* 2018].

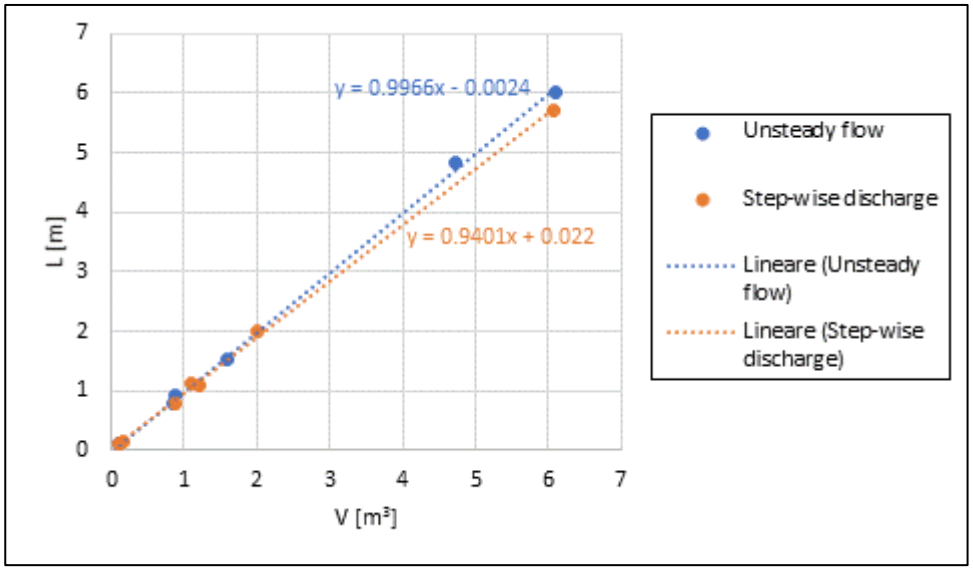

Figure 3.36 – Mean travel distance (L) from simulation results (using Wilcock and Crowe) as a function of the volume of bed material (V) calculated using simulation results with the Wilcock and Crowe transport function considering the BSTEM

3.9.2. Mean travel distance without considering the BSTEM

The analysis in chapter 3.8 above shows that calibration without the BSTEM results better than the one that considers the BSTEM. For this reason, the mean travel distance of bed material was also estimated without considering the BSTEM.

Table 3.11 shows the comparison between simulation results (using the *Wilcock and Crowe* equation for Q_b) and field observations.

As already indicated in paragraph 3.9.1, from the tracer surveys conducted between 2011 and 2013, the mean transport distance of event-based particles ranged between 0.1 m < L_{m_1} < 3.5 m or ranged between 2.8 m < L_{m_2} < 16.2 m [*Plumb,* 2017]. Mean travel distances determined from simulation were found to range between 0.06 m < L < 3.3 m and between 0.04 m < L < 4.44 m, considering respectively step-wise discharge and unsteady flow simulations. Modelling results found that mean travel distances varied widely (above and below mean observed transport distances) compared to calculated mean field distances (Table 3.11). For the first flood event (Table 3.11), the simulated (step-wise discharge and unsteady flow) mean travel distance is similar to the observed one when immobile tracer particles are included (L_{m_1}). For the second flood event (Table 3.11), the simulated (unsteady flow) mean travel distance is similar to the observed one when immobile tracer particles are included (L_{m_1}).

As is the case for field observations and for simulations considering the BSTEM in paragraph 3.9.1, the mean travel distance *L* depends upon many factors (Q_b, Δt, D_s, W_s) and therefore it is not necessarily related to the peak discharge. Indeed, no relationships were found between mean tracer transport distance and peak discharge.

Table 3.11 – Comparison between simulation results (using the Wilcock and Crowe equation and without considering the BSTEM) and field observations

Field Observations [*Plumb,* 2017]					***Simulation Results*** ***(step-wise discharge)***		***Simulation Results*** ***(unsteady flow)***	
Flood event	**Date**	Q_{peak} **(m³/s)**	L_{m_1} **(m)**	L_{m_2} **(m)**	Q_b **(m³/s)**	***L*** **(m)**	Q_b **(m³/s)**	***L*** **(m)**
1	10/08/2012	15.6	0.4	9.8	$1.1\ 10^{-5}$	0.67	$9.8\ 10^{-6}$	0.64
2	04/09/2012	42.3	1.4	8.5	$4.9\ 10^{-5}$	2.40	$3.0\ 10^{-5}$	1.76
3	11/03/2013	15.7			$1.0\ 10^{-6}$	0.08	$9.2\ 10^{-7}$	0.07
4	09/04/2013	16.8			$8.7\ 10^{-7}$	0.06	$6.4\ 10^{-7}$	0.04
5	12/04/2013	21.4			$1.1\ 10^{-5}$	0.70	$5.1\ 10^{-6}$	0.35
6	29/05/2013	36.5	3.5	14.4	$1.9\ 10^{-5}$	1.14	$9.5\ 10^{-6}$	0.62
7	08/07/2013	38.7			$5.3\ 10^{-5}$	3.30	$7.0\ 10^{-5}$	4.44

Notes: tracer surveys were conducted after the recession of each hydrograph: L_{m_1} = mean transport distance of event-based particles (including immobile particles), L_{m_2} = mean transport distance of event-based particles (considering only mobile particles)

Where the BSTEM was considered (paragraph 3.9.1), a correlation between *L* and the volume of bed material was observed. Also in this paragraph, where the BSTEM was not considered, higher values of *L* corresponded to higher values of volumetric bed material transport rates (Table 3.12 and Figure 3.37).

		Simulations Results ***(step-wise discharge)***			***Simulation Results*** ***(unsteady flow)***		
Flood event	**Date**	Q_b **(m³/s)**	Δt **(s)**	$V = Q_b \times \Delta t$ **(m³)**	Q_b **(m³/s)**	Δt **(s)**	$V = Q_b \times \Delta t$ **(m³)**
1	10/08/2012	$1.1\ 10^{-5}$	84600	**0.93**	$9.8\ 10^{-6}$	84600	**0.83**
2	04/09/2012	$4.9\ 10^{-5}$	75600	**3.70**	$3.0\ 10^{-5}$	75600	**2.27**
3	11/03/2013	$1.0\ 10^{-6}$	89100	**0.09**	$9.2\ 10^{-7}$	89100	**0.08**
4	09/04/2013	$8.7\ 10^{-7}$	83700	**0.07**	$6.4\ 10^{-7}$	82800	**0.05**
5	12/04/2013	$1.1\ 10^{-5}$	89100	**0.98**	$5.1\ 10^{-6}$	89100	**0.45**
6	29/05/2013	$1.9\ 10^{-5}$	89100	**1.69**	$9.5\ 10^{-6}$	89100	**0.85**
7	08/07/2013	$5.3\ 10^{-5}$	88200	**4.67**	$7.0\ 10^{-5}$	88200	**6.17**

Table 3.12 – Determination of the volume of bed material using Wilcock and Crowe simulation results and without considering the BSTEM

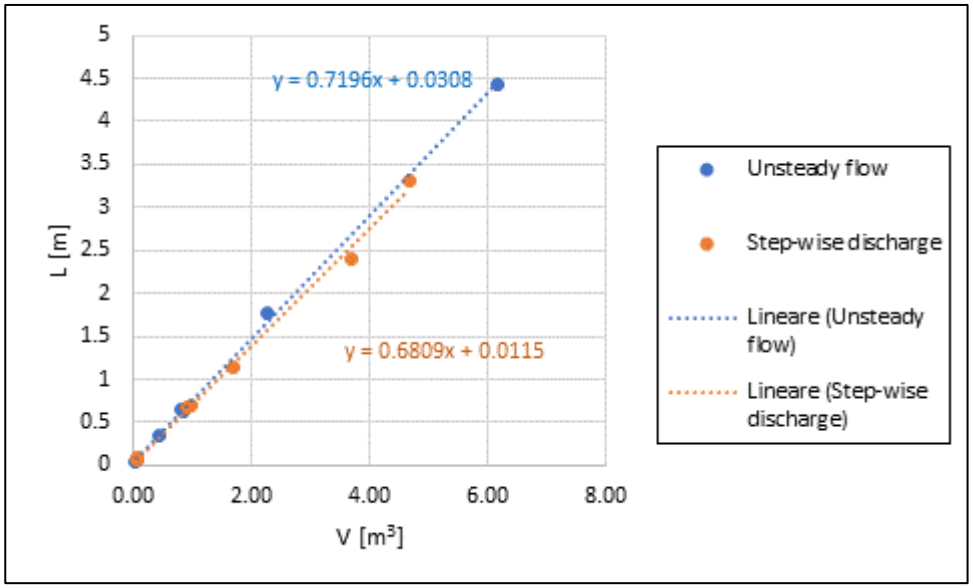

Figure 3.37 – Mean travel distance (L) from simulation results (using Wilcock and Crowe) as a function of the volume of bed material (V) calculated using simulation results with the Wilcock and Crowe transport function without considering the BSTEM

3.9.3. Comparison between mean travel distances estimated by considering and without considering the BSTEM

The analysis in paragraphs 3.9.1 and 3.9.2 had shown that mean travel distances of bed material calculated using modelling results, varied widely (above and below mean observed transport distances) compared to mean travel distances observed in the field. Table 3.13 summarises the results achieved (Q_{peak} is the peak discharge, Q_b is the volumetric bed material transport rate, L_{m_1} and L_{m_2} is the mean transport distance of event-based particles measured in the field including and not including immobile particles, L is the mean transport distance estimated using simulation results):

Field Observations [*Plumb,* 2017]				***Simulation results (YES BSTEM) (step-wise discharge)***		***Simulation results (YES BSTEM) (unsteady flow)***		***Simulation results (NO BSTEM) (step-wise discharge)***		***Simulation results (NO BSTEM) (unsteady flow)***	
Flood event	Q_{peak} (m^3/s)	L_{m_1} (m)	L_{m_2} (m)	Q_b (m^3/s)	L (m)	Q_b (m^3/s)	L (m)	Q_b (m^3/s)	L (m)	Q_b (m^3/s)	L (m)
1	15.6	0.4	9.8	$1.3\ 10^{-5}$	1.12	$1.0\ 10^{-5}$	0.92	$1.07\ 10^{-5}$	0.67	$9.8\ 10^{-6}$	0.64
2	42.3	1.4	8.5	$2.7\ 10^{-5}$	2.00	$6.2\ 10^{-5}$	4.82	$4.9\ 10^{-5}$	2.41	$3.03\ 10^{-5}$	1.76
3	15.7			$1.8\ 10^{-6}$	0.16	$1.2\ 10^{-6}$	0.11	$1.03\ 10^{-6}$	0.075	$9.2\ 10^{-7}$	0.067
4	16.8			$1.4\ 10^{-6}$	0.12	$1.4\ 10^{-6}$	0.12	$8.7\ 10^{-7}$	0.06	$6.4\ 10^{-7}$	0.045
5	21.4			$9.9\ 10^{-6}$	0.80	$9.4\ 10^{-6}$	0.80	$1.07\ 10^{-5}$	0.70	$5.08\ 10^{-6}$	0.35
6	36.5	3.5	14.4	$1.4\ 10^{-5}$	1.10	$1.8\ 10^{-5}$	1.51	$1.9\ 10^{-5}$	1.14	$9.5\ 10^{-6}$	0.62
7	38.7			$6.9\ 10^{-5}$	5.70	$6.9\ 10^{-5}$	6.00	$5.3\ 10^{-5}$	3.34	$7.04\ 10^{-5}$	4.45

Table 3.13 – Summary of the results

The main reason why mean travel distance is different considering simulation results and field observations (L_{m_2}), is that the minimum grain-size distribution of tracer particles in the field is 30 mm while concerning simulation results, finer particles were also considered.

However, L and L_{m_1} present the same order of magnitude; indeed, from the tracer surveys conducted between 2011 and 2013, L_{m_1} ranged between 0.1 m and 3.5 m. It is more reasonable to compare the L value with L_{m_1} because travel distance L was calculated considering mean values of Q_b in the time period Δt in the study reach; therefore both mobile and immobile particles were involved.

The comparison between the simulation results (L), both considering and not considering the BSTEM (Table 3.13), shows that the latter provide lower values. The reason is that the mean travel distances estimated without considering the BSTEM overlook the presence of fine material, that travel longer distances. Only sand and gravel are involved. It should be kept in mind that the *Wilcock and Crowe* equation systematically under-predicts the transport of the coarsest fractions in the bed load [*Gaeuman et al.*, 2009].

3.10. Mean travel distance of different grain sizes of bed material using HEC-RAS results

The goal in this paragraph is to compare the travel distance of different grain sizes, calculated using the HEC-RAS results, to the field measurements in Figure 3.20. Two of the seven flood events analysed were chosen to estimate travel distances of different grain sizes: flood event 1 (10/08/2012) and flood event 7 (08/07/2013), characterised by a low and a high value of

peak discharge respectively. The simulation results, using the *Wilcock and Crowe* sediment function, which were adopted for the analysis, (1) neglect the contribution of the BSTEM and (2) consider the unsteady flow approach. These two elements allow the model to best describe the reality.

For both the considered flood events, the results of the calibrated HEC-RAS model were used to estimate the mean travel distance of different grain sizes (L_i) in bed material using Equation (2.19) and Equation (2.20). Mean values of volumetric bed material transport rates ($Q_{b\text{-}i}$), average active layer streambed depths ($D_{s\text{-}i}$) and widths ($W_{s\text{-}i}$) were estimated over the time interval Δt_i; each of these parameters was calculated for all grain sizes.

The mean values of volumetric bed material transport rates ($Q_{b\text{-}i}$) and the effective width ($W_{s\text{-}i}$), for each grain size, were directly returned by simulation process; the latter was considered to be the bottom width at the end of the computational time step, as in the case of estimating the mean travel distance of bed material in paragraph 3.9. The average active layer streambed depths ($D_{s\text{-}i}$) for each grain size was not directly returned by simulation process, which only provides the "Active thickness" (expressed in metres), the total volume of the active layer (expressed in cubic metres) and the volume of each grain size in the active layer (expressed in cubic metres). The "Active thickness" is defined as the thickness of the active layer at the start of each computational time increment, the "total volume of the active layer" is the total volume of material in the active layer at the end of each computational time increment and the "volume of each grain size in the active layer" is referred to as the volume of a specific grain size in the active layer at the end of each computational time increment [*USACE,* 2016 (b)]. Therefore, the average active layer streambed depth ($D_{s\text{-}i}$) for each grain size, which is the value at the beginning of each computational time step, was calculated using the following ratio:

$$D_{s-i} = \frac{(Active\ thickness) \cdot (Vol.of\ grain\ size - i\ in\ the\ active\ layer)}{(Total\ volume\ of\ the\ active\ layer)} \qquad \textbf{(3.1)}$$

A similar interpretation was given by Wilcock (1997), in order to estimate the fractional exchange depth of the bed material.

The time interval Δt_i was calculated considering the time where $\tau^* > \tau^*_c$ in the study reach, through the use of Shields diagram (Figure 2.2). τ^*_c is the dimensionless critical shear stress, which is also called Shields number (Equation (2.5)) and τ^* is the non-critical value. The bed shear velocity u^*, that is used for calculating the particle Reynolds number $Re^* = u^* d/v$ (see paragraph 2.2), was returned by the HEC-RAS model.

In Equation (2.20), P is the porosity bed material and in paragraph 3.9 it was calculated through Equation (2.21) for poorly sorted, consolidated channel sediment. Nevertheless, the mean travel distance of different grain sizes cannot be estimated using the same equation because the bed material of the individual grain size is well sorted. Therefore, in this case, it was decided to neglect the P value. Porosity is, in general, a poorly characterized variable in

sediment flux calculations because it is a constant; therefore, its assigned value may be a source of bias, but not of variability [*Haschenburger and Church*, 1998].

Table 3.14 and Figure 3.38 show the results achieved by the calculation described. The results of the analysis of the two flood events investigated yield the regression equations in Figure 3.38.

The relationships between distance travelled and particle size in Figure 3.38, show a steep reduction in travel distance with an increase in particle size. These results are in line with Wilcock (1997) and Parsons and Stromberg (1998). The total displacement length decreases rapidly with grain size for larger fractions in a state of partial transport (which uses both mobile and immobile grains) [*Wilcock*, 1997].

The travel distance of different grain sizes, calculated by using the HEC-RAS results, may be defined in a state of partial transport. Wilcock (1997) defines it as the condition in which only a portion of the surface grains of a given size are mobilized over the duration of the transport event. Values of ($D_{s\text{-}i}$-D_{90}) < 1 indicate a state of partial transport, where D_{90} provides an appropriate estimate of the thickness of the bed surface layer [*Wilcock*, 1997]. A similar interpretation can be given to the values of (D_s/"*Maximum Depth*") < 1, where "$Maximum\ Depth$" defines the vertical dimension of the sediment control volume (see paragraph 3.5.2) and D_s is the depth of the streambed active sediment layer (see paragraph 2.4). In both flood events analysed, this ratio is less than 1((D_s/"*Maximum Depth*")≈0.6) and considering each grain size, the ratio ($D_{s\text{-}i}$/"*Maximum Depth*") is lower than 1 and lower than 0.6. Consequently, these elements indicate a state of partial transport.

The findings indicate that the mean travel distance increase as the grain classes decrease and that transport distance values are higher for the flood event with higher peak discharge (08/07/2013). These elements are generally consistent with field measurements (Table 3.4 and Figure 3.20).

The strong dependence of travel distance on particle size is characteristic of partial transport, whereas the weaker dependence is indicative of fully mobilized transport [*Parsons and Stromberg*, 1998]. This is also validated by field measurements in Table 3.4, where the fractional transport distances of different grain classes consider only mobile particles and, therefore, they are characterised by being fully mobile. In Table 3.4, although generally the mean travel distance increases as the grain sizes decrease, there are some cases where the bigger the grain class is, the longer the travel distance was. On the other hand, considering mean travel distances from simulation results (Table 3.14) characterised by partial transport, the strong dependence on the travel distance of particle class is clear because when the former increases, the latter continues to decrease.

Grain size [mm]	*Particle mean transport distance [m]*	
	Flood event 08/07/2013	**Flood event 10/08/2012**
0.177	26.7	4.3
0.354	15.5	2.3
0.5	12.4	1.7
0.707	10.7	1.4
1	10	1.1
2	8.2	0.9
2.8	7.0	0.7
5.6	4.4	0.5
8	2.5	0.3
16	0.9	0.09
32	0.07	0.01
64	0.008	0.0006
90.5	0.004	0.00003
181	0	0
362	0	0

Table 3.14 – Fractional transport distances of different grain classes for two flood events, calculated using unsteady flow simulation results with the calibrated Wilcock and Crowe transport function (without considering the BSTEM)

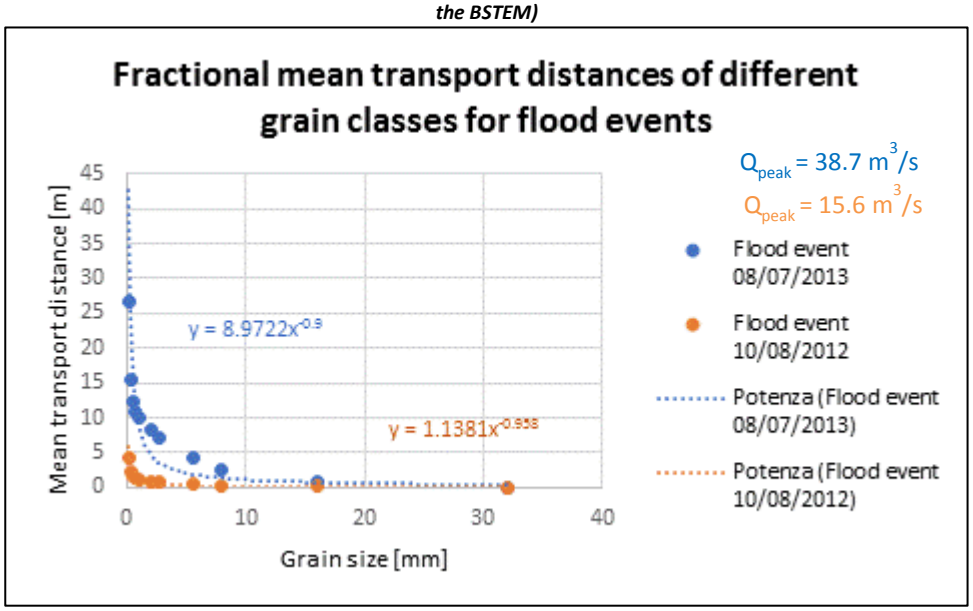

Figure 3.38 – Fractional transport distances of different grain classes for two flood events, calculated using unsteady flow simulation results with the calibrated Wilcock and Crowe transport function (without considering the BSTEM)

The fractional transport distances of different grain classes estimated by using simulation results (Table 3.14), are lower than field measurements (Table 3.4 and Figure 3.20). Indeed, in the field only the mobile particles with a diameter greater than 30 mm were considered, while when using simulation results, both mobile and immobile particles were taken into account. This situation is in accordance with Wilcock (1997); he argues that the value of displacement length calculated in a state of partial transport, is smaller than the value calculated using only mobile grains. This element is also confirmed by tracer surveys that were conducted in the field (Table 3.3), where it is clear that mean transport distance of event-based particles L_{m_1} (including immobile particles) may be more than ten times smaller than the mean transport distance of event-based particles L_{m_2} (considering only mobile particles).

It should also be kept in mind that the *Wilcock and Crowe* equation consistently under-predicts the transport of particles larger than 128 mm. Furthermore, in line with Gaeuman et al. (2009), the underestimation of the coarsest particles is of little significance in the context of total loads, because they represent a small portion of the sediment transported [*Gaeuman et al.*, 2009].

3.11. Concluding remarks

This study employed the *Meyer-Peter Müller* and *Wilcock and Crowe* models within the HEC-RAS modelling framework to evaluate the representativeness of event-based estimates of sediment transport and bed material transport distances. Results were compared to a three-year (2011-2013) field sampling campaign where in-situ bedload and inter-event particle tracking had occurred. Results showed that the *Wilcock and Crowe* transport model represented poorly graded gravel bed channel conditions over the range of flows inventoried; this model was noted to more accurately portray the bulk in-situ sediment transport rates of field observations over the *Meyer-Peter Müller* equation. Findings from this study reinforce the importance of accounting for clast interactions in transport estimates. The *Wilcock and Crowe* model accounts for bulk inter-particle interactions (e.g. hiding and sand-dependent gravel transport) and also the armor layering effects [*USACE,* 2016 (a)]. These could not be accounted for using the *Meyer-Peter Müller* equation, which could not be correlated to the field conditions and bed material gradation [*Berteni et al.,* 2018].

Through the observed transport rates for different flood events, a calibration curve was developed using the *Wilcock and Crowe* transport model (considering both step-wise discharge and unsteady flow simulations) to determine bed material transport rates as a function of reference shear stress (τ^*_{rm}). The calibration process was conducted both implementing and not implementing the BSTEM (Bank Stability and Toe Erosion Model) in HEC-RAS. The analysis showed that calibration without the BSTEM looks better than the one which considers the BSTEM for several reasons: (1) the values of the calibration parameter τ^*_{rm} are closer to those predicted with the *Wilcock and Crowe* equation, (2) field observed

rates used to calibrate the model do not include fine-grained material, (3) *Wilcock and Crowe* is a transport function that does not take into account fine-grained fractions and finally, (4) considering the sediment discharge rate for each size fraction, simulation results without the BSTEM are closer to the field measurements.

Mean bed material transport distances using the *Wilcock and Crowe* calibrated model and the BSTEM (0.12 m < L < 5.7 m and 0.11 m < L < 6 m, considering respectively step-wise discharge and unsteady flow simulations) compared relatively well against field observations L_{m_1} (0.1 m < L_{m_1} < 3.5 m) which include mobile and immobile particles larger than 30 mm, and in some instances overestimated travel distances. Also without implementing the BSTEM in the same model, the results (0.06 m < L < 3.34 m and 0.045 m < L < 4.45 m, considering respectively step-wise discharge and unsteady flow simulations) hold the same order of magnitude. However, the calculated mean travel distance is different when it is compared to field observations L_{m_2} (2.8 m < L_{m_2} < 16.2 m), because only mobile particles larger than 30 mm were involved. The *Wilcock and Crowe* equation under-predicts the transport of the coarsest fractions in the bed load and the BSTEM overlooks the presence of fine material; for these reasons the travel distances calculated considering the BSTEM are longer.

Finally, the travel distances of different grain sizes were estimated using the *Wilcock and Crowe* calibrated model, neglecting the contribution of the BSTEM and considering the unsteady flow approach. The relationships between the calculated distance travelled of different grain classes (which may be defined in a state of partial transport) and particle size show a steep reduction in travel distance with increase in particle size. The findings indicate that transport distance values are higher for the flood event with higher peak discharge, generally in accordance with field measurements. Considering mean travel distances from simulation results characterised by partial transport, the strong dependence of travel distance on particle class is clear because when the former increases, the latter continues to decrease. Regarding field measurements that consider only mobile particles, although the mean travel distance increases as the grain sizes decrease, there are some cases where the bigger the grain class is, the longer the travel distance was. The fractional transport distances of different grain classes estimated by using simulation results are lower than tracer surveys because in the field only the mobile particles with a diameter greater than 30 mm were considered, while using simulation results, both mobile and immobile particles were taken into account.

The comparison of simulated transport distances against available field observations also provides another mechanism to validate appropriate transport equations; particularly where in-situ bedload sampling may not be available [*Berteni et al.,* 2018].

4. Water erosion and climate change

4.1. Introduction

The evaluation of the water erosion and the knowledge of climate change impacts on this phenomenon in a basin is fundamental to ensure a good management of the territory and to identify potential hydrogeological risk areas. A change in the mean and variability of some variables of the climate system is expected to affect the sediment yield of mountainous areas in several ways: for example, through soil temperature and precipitation peak intensity change, permafrost thawing, snow- and ice-melt time shifting [*Berteni and Grossi*, 2017].

Water erosion, the evaluation of the soil loss and the effects of climate change on these physical phenomena are the focus of this chapter. Water erosion produces damage on-site and off-site. The damage on-site occurs in the same place where water erosion happens; it includes soil loss, fertility reduction and a decline in biodiversity. The damage off-site takes place distant from where water erosion happens; it consists in the increase of solid transport in the rivers and problems to infrastructures. In addition, the volume of eroded material might accumulate in irrigation basins or in hydroelectric reservoirs and it may cause severe related problems such as the reduction of the storage capacity. Finally, sediments may be a dominant source of pollution in water bodies, due to transport of fertilizers and pesticides, in agricultural areas.

Soil erosion by water is particularly difficult to measure directly. Systematic and harmonised data on trends in soil erosion across Europe are lacking [*Jones et al*., 2012]. Using experimental plots, soil erosion markers (e.g. Cesium 137) or sampling river sediment load in large areas is technically and logistically difficult and financially expensive. Also the use of remote sensed data on large areas present some cost and availability limitations [*Bosco et al.*, 2015]. Therefore, it is often necessary to use models that predict soil loss from causal parameters that exist for areas where no measurements of soil loss have been made or are feasible [*Panagos et al.*, 2014 (f)].

The sensitivity of soil loss estimates to a change of condition of the climate system may be investigated through the application of different models, each characterized by its own features and limits [*Berteni and Grossi*, 2017]. The main issue relating to the erosion models is the validation of their estimates, because the field data for comparing the calculations of the models with actual soil losses are often missing [*Gitas et al.*, 2009]. For example, many reported applications of the MUSLE model, that is described in paragraph 4.3.1.2, have assumed fixed values for its parameters; this is largely due to the lack of data available for calibration, for many practical applications at the basin scale [*Gwapedza et al.*, 2018]. Moreover, it is widely recognized that the RUSLE model, which is described in paragraph 4.3.1.1, is prone to overestimate soil losses [*Keizer et al.*, 2016].

Some basic concepts of water erosion and climate change are presented, as well as some concepts concerning mathematical models to calculate eroded material.

4.2. Water erosion, transfer and deposition processes

Soil erosion by water is the result of rain *detaching* and *transporting* vulnerable soil. It can be originated by natural phenomena, such as rainfall or snow melting, or by human-induced phenomena, such as irrigation [*Bussi*, 2014]. The main factors affecting water erosion are precipitation, run-off, soil type, topography, land use and land management [*Panagos et al.*, 2015 (a)].

Soil erosion by water is characterised by different phases. **Splash erosion** (Figure 4.1) is the first stage of the erosion process and it occurs when raindrops hit the soil surface. The explosive impact breaks up soil aggregates so that individual soil particles are 'splashed' onto the soil surface. The particles block the spaces between soil aggregates and then the soil forms a crust that reduces infiltration and increases runoff. As long as the precipitation effect continues, water infiltrates in the soil, depending on the infiltration capacity on the soil and on the rainfall amount. Exceeding water (i.e. the water which does not infiltrate) accumulates in small depressions (ponds). When the water depth is high enough, generation of *overland flow* takes place along the steepest slope, entraining soil particles. Soil particles can be dissolved, in suspension, or entrained on the soil surface, originating sediment transport. **Sheet (or interrill) erosion** (Figure 4.1 and Figure 4.2) is the uniform removal of soil in thin layers by the forces of raindrops and *overland flow*. If left unattended, this type of erosion will gradually remove most of the available nutrients and organic matter in the soil, which are important to agriculture and it could lead to unproductive soil. Early signs of sheet erosion include bare areas, water puddling as soon as rain falls, visible grass roots, exposed tree roots, and exposed subsoil or stony soils. Vegetation cover is important to prevent sheet erosion because it protects the soil, it impedes waterflow and it encourages water to infiltrate into the soil. The surface water flows that cause sheet erosion rarely flow for more than a few metres before concentrating into rills (small channels). Rills are shallow drainage lines less than 30 cm deep. They develop when surface water concentrates in depressions and it erodes the soil. **Rill erosion** (Figure 4.1 and Figure 4.2) is common in bare agricultural land, particularly overgrazed land, and in freshly cultivated soil where the soil structure has been loosened. The rills can usually be removed with farm machinery. Rill erosion can be reduced by reducing the volume and speed of surface water with grassed waterways and filter strips. Rill erosion is often described as the intermediate stage between sheet erosion and gully erosion. **Gully erosion** (Figure 4.1 and Figure 4.2) is the advanced stage of channel erosion. Gullies are channels deeper than 30 cm that cannot be removed by normal cultivation. Gullies occur when smaller water flows concentrate and cut a channel through the soil. Most gullies extend.

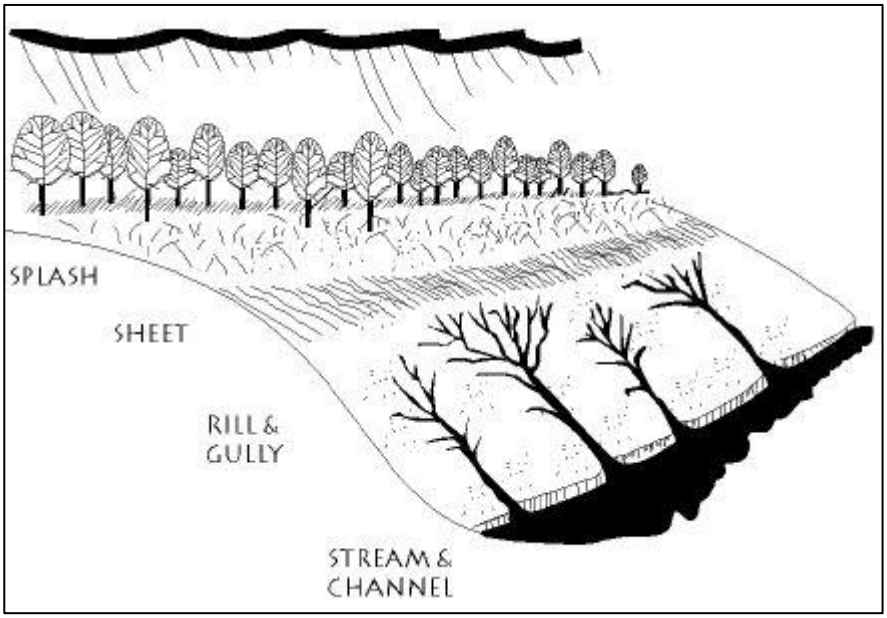

***Figure 4.1 – Types of erosion* [*https://www.dpi.nsw.gov.au/__data/assets/pdf_file/0003/255153/fact-sheet-1-types-of-erosion.pdf*]**

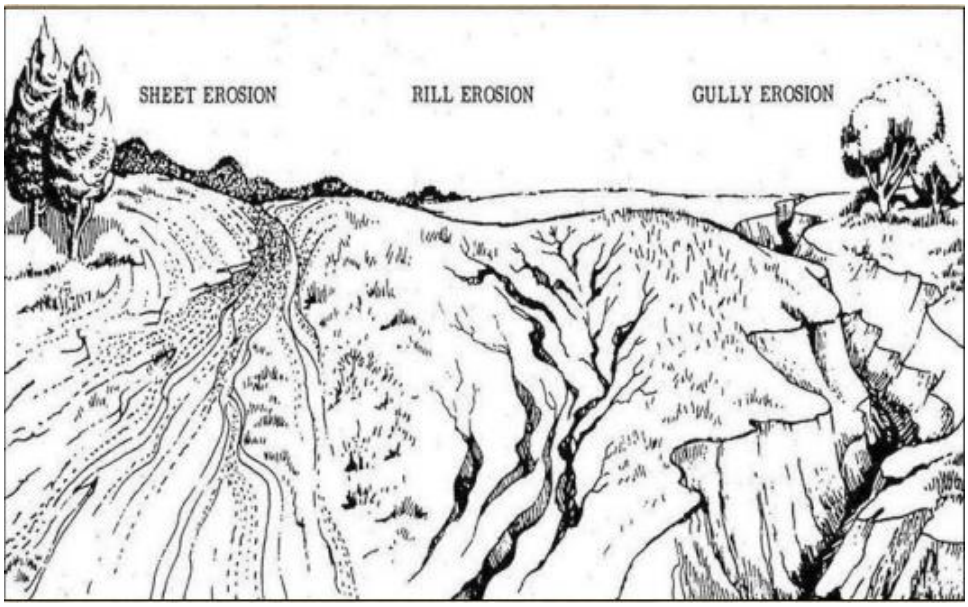

Figure 4.2 – Sheet rill and gully erosion (from Berteni,* [2012]*)

Generally, only a fraction of the sediment eroded within a drainage watershed finds its way to the basin outlet and it is represented in the sediment yield. Deposition and temporary or permanent sediment storage may occur on the slope, particularly in swales, on the flood plain, where the slope is low and in the channel itself. A simple way to estimate the total volume passing through a section is to calculate the **Sediment Delivery Ratio (SDR)**, which is the ratio of sediment passing through the catchment outlet to total eroded material within the basin:

$$SDR = VOL / EROS \quad (4.1)$$

where *VOL* is the total sediment volume passing through a given section in time and *EROS* is the total gross erosion in the whole catchment drained by that given cross section, in the same time [*Walling*, 1983; *Bussi*, 2014].

Therefore, the SDR can be defined as a scaling factor that relates sediment availability and deposition at different spatial and time scale. This ratio has usually a value between 0 and 1, due to sediment deposition caused by change of flow regime, loss of flood plains and storage of reservoirs [*Lane et al.*, 1997; *Lu et al.*, 2006]. The main factors affecting SDR are hydrological inputs (mainly rainfall), landscape properties (for example vegetation, topography and soil properties) and their complex interactions [*Walling*, 1983; *Richards*, 1993; *Lu et al.*, 2006]. However, considering the time scale of the single rainfall-runoff event, SDR is deeply connected to the soil water content before the event, the period of the year when the event occurs and the storm kinetic energy. Evaluating the time scale of the single rainfall-runoff event, the sediment delivery ratio could result equal to or greater than 1. The reason for this value is that sediments already formed and arrested in previous period on the slopes or within the hydrographic network, may be transported together with the eroded material during the time window considered. In general, considering different time scales, the SDR increases with decreasing the catchment area [*Piest et al.*, 1975; *Bagarello and Ferro*, 2006].

4.3. Mathematical sediment models

The prevision of soil erosion by water can follow different approaches, using mathematical sediment models. Literature suggests physically-based models, conceptual models and empirical models.

- A physically-based model (or “process-oriented”) is able to describe the individual physical processes occurring in the catchment, up to its outlet. Considering an assigned value of input precipitation, it uses the fundamental equations of hydraulics, hydrology and soil and sediment transport. The WEPP (Water Erosion Prediction Project) model (Nearing et al., 1989) is one of the most used. It was developed in order to estimate soil erosion by water on hillslopes for use in new

USDA erosion prediction technology. This model represents detachment, transport and deposition processes of soil during the single rainfall event and it takes into account the spatial variability in topography, surface roughness, soil properties, hydrology and land use conditions on hillslopes [*Ferro*, 2002; *Nearing et al.*, 1989].

- A conceptual model describes the process of soil water erosion by simulating the subprocesses of this physical phenomenon. This model uses analytical relationships and it has a "process-oriented" pattern. Nevertheless, it differs from the physically-based model due to the use of empirical equations that include numerical constants. Specific measures are required in order to define the numerical constants. Meyer and Wischmeier's model (1969) is the best known and it considers four individual subprocesses (detachment by rainfall, detachment by runoff, transportation capacity of rainfall and transportation capacity of runoff) which are separated, but interrelated phases of the process of soil erosion by water [*Ferro*, 2002; *Meyer and Wischmeier*, 1969].
- An empirical model finds its source in laboratory investigations and field trials, which make it possible to assess soil loss by water through the estimation of some factors influencing this physical phenomenon. The USLE model (Wischmeier and Smith, 1961) is among the most widely used, even in territories different from those for which it was originally deducted [*Ferro*, 2002]. The USLE equation and its different versions that were later developed are described in paragraph 4.3.1.

The "ideal model" would be the physically-based model because it can describe the physical processes in the catchment by using the fundamental equations of hydraulics, hydrology and soil and sediment transport. However, also this model (even the most complex available) is an extreme simplification of the real world. Beven (1988) states that the descriptive equations at the base of this type of models are good descriptors of processes occurring in well defined, spatially homogeneous, structurally stationary model catchments and hillslopes in the laboratory. But we are not sure that those equations may describe the complex three-dimensional spatially heterogeneous and time-varying system that characterises a real catchment. There are also other limitations associated with the physically-based models: the level of uncertainty in estimation of boundary conditions and the spatial distribution of parameter values on the discretized watershed, the lack of observed data to calibrate parameter values and the absence of a programme of field measurements that ensures consistency between model predictions and real world processes [*Beven*, 1989; *Ferro*, 2002; *Bagarello and Ferro*, 2006; *Orlandini*, 2002].

Also the conceptual model shows troubles and limitations; the main one is the difficulty in assessing erosion and transport numerical constants [*Ferro*, 2002].

Engineering applications showed that USLE is the best compromise between the reliability and the applicability (in terms of input data required). The reliability increases when the time period of soil loss assessment goes up [*Ferro*, 2002]. Therefore, because of uncertainties and difficulties of "process oriented" models, the USLE equation remains an important tool in

practical applications [*Bagarello and Ferro*, 2006]. In this regard, for example, Zhang et al. (2001) compared results of the physically-based model WEPP with the results of the empirical models RUSLE and USLE in order to test the WEPP model, also considering different agricultural land use [*Zhang et al.*, 2001; *Bagarello and Ferro*, 2006].

Despite many models were proposed to that describe soil erosion by water, there is not yet a best unique solution that is accepted by the scientific community. Therefore, further studies are needed [*Bagarello and Ferro*, 2006].

4.3.1. Empirical sediment models

In this paragraph, empirical models used to evaluate erosion by water are described.

Among the empirical models, the most known and used is the Universal Soil Loss Equation – **USLE**, developed by Wischmeier and Smith (1961) and others with the U.S. Department of Agriculture (USDA), Agricultural Research Services (ARS), Soil Conservation Service (SCS) and Purdue University in the late 1950s. This is an erosion model designed to predict the longtime average soil losses in runoff from specific field areas in specific cropping and management systems. It resulted from an empirical analysis of a great amount of data derived from experimental plots spread over more than 40 study sites in the USA. During the 1970s, USLE equation was widely used to calculate sediment production and different versions were developed, such as **RUSLE** (Revised Universal Soil Loss Equation) [*Renard et al,* 1991], which maintains the same mathematical structure but it includes improvements and updates, concerning for example the rainfall erosivity. Williams (1975) proposed to evaluate sediment yield using the modified USLE (**MUSLE**), in order to predict soil erosion for a water erosion event and to consider the runoff effect.

Another empirical instrument to estimate the quantity of eroded material by water is the **EPM** (Erosion Potential Model) method [*Gavrilovic*, 1988]. This is an empirical semi-distributed model to estimate the mean annual volumes of soil erosion and sediment yield at the basin scale. Water erosion of soil particles is the result of an interaction between lithological, topographic, climatic and land use elements. EPM combines in a simple structure all the most statistically significant parameters controlling soil particles detachment and transport. In this method, temperature coefficient and mean annual rainfall are connected with climate changes and they influence the erosive phenomenon. This model is a result of experimental research on a station that was located in Serbia, but it was also applied elsewhere such as in Switzerland and in Italy [*Auddino et al.*, 2015].

4.3.1.1. RUSLE model

In both the USLE and the RUSLE, the fundamental equation is the following [*Renard et al.*, 1991]:

$$A = R \cdot K \cdot LS \cdot C \cdot P \qquad \textbf{(4.2)}$$

where: A = computed soil loss [t·ha^{-1}· yr^{-1}]
R = rainfall-runoff erosivity factor [MJ·mm·ha^{-1}·h^{-1}·yr^{-1}]
K = soil erodibility factor [t·ha·h·ha^{-1}·MJ^{-1}·mm^{-1}]
LS = topographic factor combining slope length L and slope steepness S [-]
C = cover-management factor [-]
P = supporting practices factor [-]

R factor

The *R* factor represents the climate erosivity because it defines the total annual erosive potential that is due to climatic effects; it represents the driving force of the sheet and rill erosion.

In the RUSLE equation, the R factor can be calculated using EI (Erosivity Index) parameter [*Wischmeier and Smith*, 1978] and the updating suggested by Brown and Foster (1987). In the study area, different rainfall events are considered, which are separated by dry periods lasting 6 hours or more. Every rainstorm is considered an erosive event. For each erosive event, the erosivity index, R_e [MJ·mm·h^{-1}·ha^{-1}], equals the product between the specific total storm energy, E [MJ·ha^{-1}], and the maximum amount of rainfall 30-min intensity, I_{30} [mm·h^{-1}]. If the rainy period lasts less than 30 minutes, a fictitious 30-min duration is assumed. According to Wischmeier and Smith (1978), 63.5 mm·h^{-1} represents the upper limit of I_{30} [*Wischmeier and Smith*, 1978]:

$$R_e = E \cdot I_{30} \qquad \textbf{(4.3)}$$

Each erosive rain event can be divided into n "elementary rains" with constant intensity I_i [mm·h^{-1}] of *i-th* "elementary rain" [*Bagarello and Ferro*, 2006]:

$$I_i = \frac{h_i}{t_i} \qquad \textbf{(4.4)}$$

where: h_i = rain amount [mm]
t_i = rain duration [h]

According to Wischmeier and Smith (1978), 76 mm·h^{-1} represents the upper limit of I_i.

For each "elementary rain", the corresponding specific (per unit area) and unitary (per unit of rain amount) energy, e'_i [MJ·ha^{-1}·mm^{-1}] is [*Brown and Foster*, 1987]:

$$e'_i = 0.29[1 - 0.72exp(-0.05I_i)] \qquad \textbf{(4.5)}$$

The specific energy, e_i [MJ·ha^{-1}], is obtained by multiplying the specific and unitary energy (e'_i) by the rain amount of *i-th* "elementary rain" (h_i) [*Bagarello and Ferro*, 2006]:

$$e_i = e_i' \cdot h_i \qquad \textbf{(4.6)}$$

The specific total storm energy (*E*) is the following [*Bagarello and Ferro*, 2006]:

$$E = \sum_{i=1}^{n} e_i \qquad \textbf{(4.7)}$$

The climatic factor (R_{aj}) is the sum of $R_{e,i}$ values, calculated for each rain erosive event $N_{e,j}$ during the year *j* [*Bagarello and Ferro*, 2006]:

$$R_{aj} = \sum_{i=1}^{N_{e,j}} R_{e,i} \qquad \textbf{(4.8)}$$

The rainfall-runoff erosivity factor *R* is the annual average R_{aj} [*Bagarello and Ferro*, 2006]:

$$R = \frac{1}{N} \sum_{j=1}^{N} R_{aj} \qquad \textbf{(4.9)}$$

K factor

K factor describes soil erodibility under a set of standard conditions and it is defined as the unit erosion index for the *R* factor in relation to a standard fallow parcel (22.13 m length and 9% slope). On this basis, the value of the other RUSLE factors (*LS* factor, *C* factor and *P* factor) become unitary.

K factor is usually estimated using the normograph and formulae which are published in Wischmeier and Smith (1978). However, these equations are suitable for large areas of USA, but they are not ideally suited for European conditions. Romkens et al. (1986) performed for this reason a regression analysis on a world-wide dataset of all measured K-values, which yielded the following equation [*Renard et al.*, 1997]:

$$K = 0.0034 + 0.0405 exp\left[-0.5\left(\frac{log D_g + 1.659}{0.7101}\right)^2\right] \qquad \textbf{(4.10)}$$

where D_g [mm] is the geometric mean weight diameter of the primary soil particles [*Bosco and Oliveri*, 2007]:

$$D_g = exp\left(\sum f_i \cdot ln\left(\frac{d_i + d_{i-1}}{2}\right)\right) \qquad \textbf{(4.11)}$$

For each particle size class (clay, silt and sand), d_i [mm] is the maximum diameter, d_{i-1} [mm] is the minimum diameter and f_i is the corresponding mass fraction.

LS factor

The *LS* factor represents the effects of topography on erosion and then it accounts for slope length and slope steepness on soil loss. This factor is the main innovation of the RUSLE model, in comparison with the original model (USLE): it considers the flow convergence and it is the result of the combination of the slope (*S*) and the length (*L*) [*Bosco and Oliveri*, 2007].

The *L* factor and the *S* factor in USLE equation are the following [*Wischmeier and Smith*, 1978]:

$$L = \left(\frac{\lambda}{22.13}\right)^m \qquad \textbf{(4.12)}$$

$$S = (65.41sen^2\alpha + 4.56sen\alpha + 0.065) \qquad \textbf{(4.13)}$$

where: λ = slope length [m]
α = angle of slope
m = 0.5 if the slope is 5% or more, 0.4 on slopes of 3% to 5%, 0.3 on slope of 1% to 3% and 0.2 on uniform gradient of less than 1%

The calculation of the topographic factor may reach high accuracy thanks to the implementation of GIS systems and to the terrain digital models (DEM). Therefore, the *LS* factor was expressed as a function of the "Upslope Contributing Area" (UCA) [*Moore and Burch*, 1986; *Mitasova et al.*, 1996; *Desmet and Govers*, 1996] in order to consider the convergence and divergence of the superficial runoff. The UCA area is where water flows in a given cell of the grid.

The *LS* factor can be determined through GIS procedures using the following relation of Moore and Burch (1986):

$$LS = \left(\frac{Area}{22.13}\right)^m \cdot \left(\frac{\sin\alpha}{0.0896}\right)^n \qquad \textbf{(4.14)}$$

where: *Area* = drainage area of a point belonging to a certain cell of the grid (it is the UCA)
α = slope (degrees)
m = 0.4 (as suggested by many researchers)
n = 1.3 (as suggested by many researchers)

The *LS* factor calculation in complex hillslopes can be problematic, in particular when slope morphology presents great spatial variability [*Moore and Burch*, 1986; *Mitasova and Brown*,

2002; *Engel and Mohtar*, 1999]. The topographic complexity of the alpine territory, shows significant challenges in estimating the *S* factor. Therefore, as suggested by Bosco and Oliveri (2007), it is preferable to modify Moore and Burch's equation and to evaluate the *S* factor using Nearing's formula (1997), which provides more reliable results for a higher degree slope (more than 50%):

$$S = -1.5 + \frac{17}{(1 + e^{(2.3 - 6.1 sin\alpha)})} \qquad \textbf{(4.15)}$$

The formula that can be applied in a GIS environment, substituting "*Area*" with the result of flow accumulation ("*Flowacc*") multiplied by the pixel dimension ("*Cell_size*") is the following:

$$LS = \left(\frac{Flowacc \cdot Cell\_size}{22.13}\right)^{0.4} \cdot \left(-1.5 + \frac{17}{(1 + e^{(2.3 - 6.1 sin\alpha)})}\right) \qquad \textbf{(4.16)}$$

Flow accumulation consists of the number of cells bringing runoff water to each pixel in the grid.

In GIS applications to long mountain slopes, it is usually considered that above a flow accumulation value, corresponding to about 300 m of slope length, water starts flowing in channels, which are not considered by the RUSLE. Then this flow accumulation value is the upper limit of "*Flowacc*" parameter [*Pregnolato and D'Amico*, 2011].

C factor

The *C* factor describes the effects of cover and land use on average annual soil loss. It represents the relation between the soil loss in certain agricultural or cover conditions and the erosion that would be obtained from a standard fallow parcel (bare soil). This factor is very important in soil loss estimation because it represents conditions that can be modified most easily to reduce erosion. The *C* factor depends on changes (in terms of environment cultivations, agricultural activities, residual management and on the morphology of the plants during the year) and certain soil cover typologies may have different values. For these reasons, together with the lack of detailed information and with the difficulties in processing all factors on a large scale, it is hard to use RUSLE guidelines to estimate the *C* factor. Therefore, average values in the literature can be used. Table 4.1 shows *C* factor values proposed by Angeli (2004):

Description	*C* factor [-]
Continuous and discontinuous urban fabric	0.003
Industrial and business units	0.003
Networks of streets, rail tracks and associated territories	0.003
Port areas and airports	0.003
Places of minerals extraction, landfills and building places	0.36
Urban green areas, sport facilities and leisure facilities	0.003
Paddies	0
Grasslands	0.1
Annual crops associated to permanents crops and elaborate cultivation	0.5
Agricultural soil mainly	0.04
Coniferous forest	0.001
Mixed forest	0.002
Natural grasslands, heath and moorland, sclerophyll vegetation, transition from forest to shrubs	0.04
Beaches, dunes, sandy slope, bare rock, poorly vegetated areas and burnt areas	0.36
Marshes, water courses, water bodies and coastal lagoons	0
Simple arable crops and horticultural crops in areas not served by irrigation systems	0.4
Canopied vineyards or per row	0.451
Orchards and olive groves	0.296
Deciduous oaks forest, primarily evergreen oaks forest and mixed thermophilic forest	0.003

***Table 4.1 – Soil cover value (C factor)* [*Angeli*, 2004]**

P factor

The *P* factor reflects the impact of support practices on the average annual erosion rate. This factor is the soil protection factor and it primarily represents how surface conditions affect flow paths and flow hydraulics. The *P* factor expresses soil protection from erosion regarding human practices and it is usually set to 1 when these practices are not applied. Table 4.2 shows the *P* factor suggested by Wischmeier and Smith (1978), considering crops in alternating stripes or terracing:

s [%]	Working according to height profiles	*P* factor [-]
1.1 – 2.0	0.60	0.30
2.1 – 7.0	0.50	0.25
7.1 – 12.0	0.60	0.30
12.1 – 18.0	0.80	0.40
18.1 – 24.0	0.90	0.45

***Table 4.2 – Human practices aimed at erosion control (P factor)* [*Wischmeier and Smith*, 1978]**

4.3.1.2. MUSLE model

Williams (1975) used data collected from 18 small US watersheds to evaluate the MUSLE equation, a Modified Universal Soil Loss Equation which is used to calculate sediment yield. Sediment yield is defined as the amount of sediment that, in a certain interval of time, crosses the outlet basin. He showed that runoff is highly correlated to sediment yield and therefore the rainfall factor *R* in Equation (4.2) was replaced by a runoff factor (R_d), that takes into account both the climate effects and the solid transport mitigation effects along the slope. He evaluated sediment yield (Y_s) for a single storm (in t·ha^{-1}) using the following equations (Equation (4.17) and Equation (4.18)), where *K* is the soil erodibility factor in t·ha·h·ha^{-1}·MJ^{-1}·mm^{-1} and *LS*, *C* and *P* are the other RUSLE factors (see paragraph 4.3.1.1) [*Bagarello and Ferro*, 2006]:

$$Y_S = R_d \cdot K \cdot LS \cdot C \cdot P \qquad \textbf{(4.17)}$$

$$R_d = \frac{89.6}{A_w}(Q \cdot V)^{0.56} \qquad \textbf{(4.18)}$$

where: R_d = event runoff factor [t·ha^{-1}·(unit of *K*)$^{-1}$]
A_w = watershed area [ha]
Q = peak flow rate of the flood event at outlet of the watershed [m^3/s]
V = volume of runoff event at outlet of the watershed [m^3]

Sadeghi used a particular MUSLE model, that was calibrated on experimental results. The runoff factor has the following expression, where *K* is the soil erodibility factor in t·ha·h·ha^{-1}·MJ^{-1}·mm^{-1} and the sediment yield is in t [*Sadeghi*, 2004; *Sadeghi et al.*, 2013]:

$$R_d = 11.8(Q \cdot V)^{0.56} \qquad \textbf{(4.19)}$$

where: R_d = event runoff factor [t·(unit of *K*)$^{-1}$]
Q = peak flow rate of the flood event at outlet of the watershed [m^3/s]
V = volume of runoff event at outlet of the watershed [m^3]

4.3.1.3. EPM model

The EPM (Empirical Potential Model) combines in the following simple structure all the most statistically significant parameters controlling soil particle detachment and transport [*Gavrilovic*, 1988]:

$$W_{sp} = T \cdot H \cdot \pi \cdot \sqrt{Z^3} \qquad \textbf{(4.20)}$$

where: W_{sp} = average annual specific production of sediments [m^3·km^{-2}· yr^{-1}]
T = temperature coefficient [-]
H = mean annual amount of precipitations [mm · yr^{-1}]
Z = coefficient of erosion [-]

The temperature coefficient *T* is calculated as:

$$T = \sqrt{\frac{t}{10} + 0.1} \qquad \textbf{(4.21)}$$

where *t* represents the mean annual temperature in degrees Celsius [°C].

The coefficient of erosion *Z* is defined as:

$$Z = X_a \cdot Y \cdot (\varphi + \sqrt{i}) \qquad \textbf{(4.22)}$$

where: X_a = land use coefficient [-]
Y = coefficient of soil resistance to erosion [-]
φ = coefficient value for the observed erosion processes [-]
i = average land slope [m/m]

The average annual production of erosional sediments in the catchment area W_g [m^3/y] is the product between surface area *A* in km^2 and the weighted averaged annual specific sediment production W_{sp}:

$$W_g = A \cdot W_{sp} \qquad \textbf{(4.23)}$$

4.4. Water erosion: case study examples

Application of EPM: Sfalassà Fiumara catchment (Calabria, Italy)

The Sfalassà Fiumara catchment is located in the southwestern slope of Aspromonte Massif (southern Calabria). It has an area of 24.2 km^2, the altitudine ranges from 0 to 1174 m a.s.l and has an elongated shape. The climate is sub-humid with average annual precipitation and temperature strongly controlled by elevation. Along the coast the average annual precipitation and temperature is respectively 1004 mm/y and 18°C while in the mountains 1550mm/y and 13°C. In this watershed, the Gavrilovic EPM model was applied by the use of spatially distributed input data on geology, soils, and land use in a geographic information system environment. Three evaluations of the Sfalassà Fiumara catchment erosion were carried out, changing coefficient X_a, Y and φ. In the first evaluation X_a and Y factors came from geological map of Calabria and Corine 2000. The second evaluation was integrated by to definition of the grade weathering and RMR (Rock mass Rating) related to the values of Zemljic's table (1971). In the third evaluation the basin was divided in three smaller, more homogeneous, sub-basins and the Sfalassà Fiumara catchment showed a strong spatial variability in *T*, *H* and *Z*; an intersection of different dataset (X_a, Y and φ) was operated in a GIS environment. Results obtained by the three evaluations are W_g^{1st} *= 37699 m^3/year*, W_g^{2nd} *= 45075 m^3/year*, W_g^{3rd} *= 48062.5 m^3/year* [*Auddino et al.,* 2015].
The computed soil loss obtained under the RUSLE model application is around 3 times higher than the value estimated using EPM equation [*Dominici et al.,* 2015].

Application of EPM: Stilaro Fiumara catchment (Calabria, Italy)

The Stilaro Fiumara catchment is located in Calabria, on the Ionian side of the Serre massif (south-east Calabria). It has an area of 95.17 km^2, a perimeter of about 59.8 km from 0 m a.s.l. to 1420 m and an average elevation of 585 m a.s.l. By applying Gavrilovic EPM model, different results were obtained using meteoclimatic parameter data from the years characterized by heavy rainfall (e.g. 2004), low rainfall (e.g. 1998) and average rainfall calculated in the period 1996-2005: $W_g^{2004} = 126082.95\ m^3/year$, $W_g^{1998} = 52493.53\ m^3/year$, $W_g^{1996\text{-}2005} = 86789.63\ m^3/year$ [*Vacca and Dominici*, 2015].

Application of EPM: Frodolfo and Cedec catchment (Lombardia, Italy)

The EPM was implemented in a distributed form for the Frodolfo and Cedec catchment, which is located in Alta Valtellina (Northern Italy). Frodolfo basin has an area of 29.1 km^2, the maximum and the minimum altitude amounted to respectively 3755 m a.s.l. and 2171 m a.s.l.; its average yearly temperature at the mean altitude (3014 m a.s.l.) is -1.7°C. The Cedec basin has an area of 17.8 km^2, the maximum and the minimum altitude amounted to respectively 3851 m a.s.l. and 2182 m a.s.l.; its average yearly temperature at the mean altitude (2909 m a.s.l.) is -1.3°C. Considering both these catchments, the result of the application of EPM is $W_g = 49631\ m^3/year$ [*Milanesi et al.*, 2015].

Application of EPM and RUSLE: Venetikos River catchment (Western Macedonia, Greece)

The catchment of the Venetikos River, the major tributary of the Aliakmonas River, is located in Western Macedonia, Northern Greece. The basin is mountainous (the average slope is 23.64%), with an almost circular shape covering an area of 855.23 km^2. The elevation ranges from 437.76 to 2240 m a.s.l. and the mean elevation is 1008.71 m a.s.l. For the time period from 1965 to 1982 mean annual values of rainfall and temperature were estimated equal to 1015.1 mm and 10.0°C, respectively. In this watershed, both the EPM and the RUSLE model were applied to evaluate soil erosion and investigate its spatial distribution. The volume of detached soil due to surface erosion (W) was calculated (using the EPM model) equal to *687,377.47 m^3/year*. The result is multiplied to the soil's specific weight value (ranging between 2.65~2.75 t/m³), in order to be expressed in the same units as the RUSLE ones (t/year) and to compare the results. Mean annual soil loss is estimated equal to *2,145.97 t/(km^2·year)*. Concerning the implementation of the RUSLE model, mean annual soil loss was calculated equal to *2,349.07 t/(km^2·year).* The Gavrilovic model, slightly underestimated the final results in comparison to the RUSLE method [*Efthimiou et al.*, 2016].

Application of RUSLE: Rio Centonara catchment (Emilia Romagna, Italy)

The Rio Centonara catchment is located in the Apennines in northern Italy, about 20 km from Bologna, and it covers an area of 273 ha. The watershed is characterized by a Mediterranean climate and the altitude ranges between 84 and 50 m a.s.l. The mean total annual rainfall is 749 mm/year and the mean air temperature is 15°C (period 2000-2010). Slope values range from less than 10% (more than 13% of area) to more than 50% (almost 14% of area), with the intermediate classes, 20-30% and 30-35%, as predominant. By spatial application of RUSLE, the mean value obtained is *35 t/(ha·year)* [*Mezzini et al.*, 2015].

By considering a specific weight of 2.75 t/m^3 [*Efthimiou et al.,* 2016], soil loss computed for different case study examples by the RUSLE and/or EPM method, are shown in Table 4.3:

Catchment	***Location***	***Model used***	***Computed soil loss [m³/yr]***	***Computed soil loss [t/yr]***
Sfalassà Fiumara	Calabria, Italy	EPM	1st evaluation: 37699	1st evaluation: 103672.3
			2nd evaluation: 45075	2nd evaluation: 123956.3
			3rd evaluation: 48062.5	3rd evaluation: 132171.9
Stilaro Fiumara	Calabria, Italy	EPM	Year 2004: 126083	Year 2004: 45848.4
			Year 1998: 52493.5	Year 1998: 19088.6
			Years 1996-2005: 86789.6	Years 1996-2005: 31559.9
Frodolfo and Cedec	Lombardia, Italy	EPM	49631	136485.3
Venetikos River	Western Macedonia, Greece	EPM	687377.5	1890288
		RUSLE	667390.4	1835324
Rio Centonara	Emilia Romagna, Italy	RUSLE	25454.6	70000

Table 4.3 – Overview table of case study examples of evaluation water erosion

Application of MUSLE: Kengir watershed (Iyvan City, Ilam Province, Iran)

The Kengir watershed is located in western Iran and its geographical area is approximately 41368 ha (elevation ranging from 995 to 2555 m a.s.l.). The mean annual precipitation of the watershed is 674 mm; the minimum and maximum temperatures vary from -3.1 to 32.4°C. The basin is mainly covered by agricultural areas in mid- and downstream and by forests and rangeland in the upstream areas. In order to apply the MUSLE model in this watershed, six storm events were considered. The MUSLE model adopted is the following [*Arekhi et al.*, 2011] (see paragraph 4.3.1.2):

$$S_y = 11.8(Q \cdot V)^{0.56} \cdot K \cdot LS \cdot C \cdot P \qquad \textbf{(4.24)}$$

where S_y is the sediment yield (in t) on a storm basis and for the entire study watershed, V is the volume of runoff (in m^3), Q is the peak flow rate (in m^3·s^{-1}) and K, LS, C and P are,

respectively, the soil erodibility (in $t \cdot ha \cdot h \cdot ha^{-1} \cdot MJ^{-1} \cdot mm^{-1}$), length and slope steepness, crop management and soil erosion control practice factors (see paragraphs 4.3.1.1 and 4.3.1.2). The results of application of the MUSLE model for the storms are shown in Table 4.4:

Storm date	Duration [h]	Peak flow [m^3/s]	Runoff volume [m^3]	Sediment yield (MUSLE) [t]
07/01/2000	13	13.61	325283	364.97
06/03/2000	5	1.24	13536	16.57
13/05/2000	6	4.33	68976	82.77
07/09/2000	12	49.19	835956	1310.29
29/03/2000	20	96.30	2079576	3179.73
16/02/2000	7	4.93	70848	90.71

Table 4.4 – Characteristics of selected storms and sediment yield in Kengir watershed **[Arekhi et al., 2011]**

Application of MUSLE: watershed in Black Hawk County (Iowa, USA)

The study area is a watershed located in Black Hawk County, Iowa, with an area of 24.2 km^2. This study integrated the MUSLE model in a Geographic Information System (GIS) framework in the form of a tool (ArcMUSLE), which is an extension of ArcGIS software. In this tool, the MUSLE equation is expressed as follows [*Williams*, 1975]:

$$S_y = 95(Q \cdot V)^{0.56} \cdot K \cdot LS \cdot C \cdot P \qquad \textbf{(4.25)}$$

where S_y is the sediment yield (in t) on a storm basis and for the entire study watershed, V is the volume of runoff (in acre·feet) and Q is the peak flow rate (in $feet^3 \cdot s^{-1}$). The runoff was calculated based on the widely used Soil Conservation Service (SCS) curve number method [*SCS*, 1972]. The time of concentration was required for the calculation of peak discharge Q; it was developed by calculating a travel time for sheet flow and a travel time for shallow concentrated flow. The *LS* factor was estimated in a GIS environment and it was derived from the DEM, using the relation of Moore and Burch (1986). The soil erodibility factor *K* and the cover management factor *C* were derived, respectively, from Soil Survey Geographic (SSURGO) data and land cover data. The erosion control practice factor *P* was associated with a field specific value. MUSLE was finally applied to calculate the soil erosion amount for a typical 24-hour rainfall event for a 2-year return period, that is 80.3 mm. After running the model, the total amount of predicted sediment delivered to waterbodies was *6669 t* and the total runoff volume was *765370 m^3* for the whole watershed [*Zhang et al.*, 2009].

Application of the MUSLE: Amameh catchment (Iran)

The Amameh catchment falls in the Tehran province (Iran) and it has an area of 3712 ha, which is mainly covered by mountainous rangelands. The mean elevation is 2620 m a.s.l., the average slope is 2.5% and the length of the main river is 13.5 km. The annual mean depth of precipitation is 848.8 mm and the annual mean temperature in the area is 8.6°C (minimum

value: -24°C, maximum vale: 35°C). The MUSLE model was applied on the catchment using Equation (4.25) and the results are presented in Table 4.5.
It was found that Equation (4.25) significantly overestimated the sediment yield as compared with the measured values. Therefore, a calibration was made to obtain an accurate sediment yield prediction and the following equation was developed [*Sadeghi*, 2004]:

$$S_y = 11.8(Q \cdot V)^{0.081} \cdot K \cdot LS \cdot C \cdot P \qquad \textbf{(4.26)}$$

Storm date	Duration [h]	Peak flow [m³/s]	Runoff volume [m³]	Sediment yield (MUSLE) [t]
23/04/1970	3.00	0.86	13680	1303.95
14/04/1971	6.50	8.55	95580	14045.78
02/08/1972	2.00	0.89	11466	899.58
03/11/1972	2.25	3.40	64350	6581.30
18/07/1974	1.75	4.00	27540	3221.94
23/04/1975	5.00	6.80	66600	10090.97
22/07/1976	5.00	10.44	64440	9414.72
29/04/1980	4.00	4.15	97065	9447.73
25/04/1983	6.50	3.43	68634	6997.63
05/05/1984	2.50	1.38	8712	1322.99
25/07/1988	2.00	2.15	32040	2626.93
18/11/1988	4.00	0.82	16353	1374.22
13/03/1989	2.50	1.80	80064	7919.09
28/10/1990	1.50	0.91	7578	948.36
06/04/1997	7.25	2.01	35656	3588.91

Table 4.5 – Characteristics of selected storms and sediment yield in Amameh catchment **[Sadeghi, 2004]**

4.5. Impact of climate change

BOX 1: What is climate change?

According to the World Meteorological Organization (WMO), climate change refers to a statistically significant variation in either the mean state of the climate or in its variability, persisting for an extended period (typically decades or longer).
[*http://www.wmo.int/pages/prog/wcp/ccl/faqs.php*].
The Intergovernmental Panel on Climate Change (IPCC) relates their definition to the one of the United Nations Framework Convention on Climate Change (UNFCCC). Climate change in IPCC usage refers to a change in the state of the climate that can be identified (e.g. using statistical tests) by changes in the mean and/or the variability of its properties, that persist for an extended period, typically decades or longer. It refers to any change in climate over time, whether due to natural variability or as a result of human activity. This usage differs from that in the UNFCCC, where climate change refers to a change of climate that is attributed directly or indirectly to human activity that alters the composition of the global atmosphere and that is in addition to natural climate variability observed over comparable time periods.
[*http://www.ipcc.ch/publications_and_data/ar4/syr/en/mains1.html*]

Different climate change scenarios can be considered in order to tentatively assess the impact on the water erosion and sediment yield at the small basin scale [*Berteni and Grossi*, 2017].

The most important variables in RUSLE and EPM equations affecting climate system are the annual amount of precipitation and the annual temperature.

4.5.1. CORDEX experiment

In this work CORDEX data were used in order to consider the impact of climate change in the future. CORDEX is the Coordinated Regional Downscaling Experiment that was initiated by the World Climate Research Programme (WCRP) in response to the need for a coordinated framework for evaluating and improving Regional Climate Downscaling (RCD) techniques and producing a new generation of RCD-based fine-scale climate projections for identified regions worldwide. Global Climate Models (GCM) can provide projections of how the earth's climate may change in the future, on scales of around 1000 by 1000 km; then the GCM covers a vastly differing landscape (from very mountainous to flat coastal plains for example) with greatly varying potential for floods, droughts and other extreme events. GCM are built on mathematical descriptions of the governing physical processes of the climate system (e.g. momentum, mass and energy conservation, etc.). Numerical solutions of the underlying equations are then obtained based on numerical algorithms. However, the impacts of climate change occur on more regional and national scales; for this reason RCD are necessary to provide projections with much greater detail and more accurate representation of

localized extreme events. Regional Climate Models (RCM) and Empirical Statistical Downscaling (ESD), applied over a limited area and driven by GCMs, can provide information on much smaller scales. CORDEX data were calculated using Regional Climate Models (RCM) together with a technique called *dynamical downscaling*. A GCM, the *driving model*, is used to embed the domain in a simulated global climate, i.e. data from a global climate simulation is used as input for a RCM [*http://www.cordex.org/*].

In this work, the selected driving model (GCM) was the **ICHEC-EC-EARTH**. EC-Earth was developed as part of a Europe-wide consortium thus promoting international cooperation and access to knowledge and a wide data base. Its main object is to develop and apply an Earth System Model (ESM) based on a seasonal forecasting system to provide trustworthy climate information. EC-Earth has become a prominent state-of-the-art model within the European landscape of Earth System Models and it has been essential to the success of the Coupled Model Intercomparison Project Phase 5 (CMIP5) [*http://www.ec-earth.org/*]. CMIP5 organizes all climate modeling groups in a coordinated effort to simulate the recent past and the future climate and its protocol defines the experiment guidelines that all models are expected to follow, for example the change of greenhouse gas concentrations over time. ICHEC (Irish Centre for High-End Computing) is the Irish partner in EC-Earth that organizes the CMIP5 archive for all contributions from the EC-EARTH community [*https://www.smhi.se/en/*].

In this work the selected RCM was **RCA4 (The surface processes of the Rossby Centre regional atmospheric climate model)**, described by the report of Samuelsson et al., 2015.

There are 14 different CORDEX domains: a "domain" is a region where the regional downscaling takes place. For example the European "domain" (EURO) covers the whole of the European continent [*http://www.cordex.org/*].

In this work, the domain used was **EUR-11i**: the number "11" behind the domain abbreviation "EUR" is the grid resolution in the native CORDEX simulation of 0.11 degrees and rotated poles. The letter "i" was added to the domain name because the poles have been rotated back and the grid resolution has been slightly modified by interpolation. Therefore EUR-11i data have a resolution of 0.125 degrees, latitude and longitude [*https://portal.enes.org/*].

There are different climate scenarios (or climate projections) that are the representations of various possible future states of the climate system, based on numerical model simulations. These models describe the complex processes and interactions affecting the climate system, but they also use information about anthropogenic climate forcing. Different factors of anthropogenic activity (socio-economic, technological, demographic factors and environmental development) are characterized in climate models as equivalent changes in greenhouse gas concentrations. Since the future evaluation of anthropogenic factors cannot be known in advance, their potential effects are explored through different scenarios describing several possible emission (greenhouse gas concentration) pathways. When performing a climate simulation, the chosen emission scenario provides forcing data for the

climate model; these data represent the particular future anthropogenic forcing in the physical reaction of the climate system. Due to this forcing-dependent character, climate model outcomes are not interpreted as *forecasts* (known as an initial value problem in mathematics), but as *projections* based on a specific emission scenario (a boundary value in mathematics). The EURO-CORDEX ensemble is based on the Representative Concentration Pathways (RCP) scenarios, which are the most recent climate modelling and impact modelling developed for the last IPCC Assessment Report (AR5). RCP scenarios define pathways of the additional radiative forcing caused by anthropogenic activity till the end of the 21st century (the value in 1750 is considered as a reference). The reason behind the conceptual change is the fact that a single radiative forcing pathway can result from a range of socio-economic and technological development scenarios. A set of scenarios were created, named after their total radiative forcing (in W/m^2) in year 2100 relative to 1750: RCP 8.5, RCP 6.0, RCP 4.5 and RCP 2.6. RCP 8.5 represents very high greenhouse gas emission radiative forcing (8.5 W/m^2), which continues to rise even after 2100. RCP 4.5 (radiative forcing value of 4.5 W/m^2) and RCP 6.0 (radiative forcing value of 6.0 W/m^2) are stabilization scenarios, because forcing will stabilize at their given value around the end of the century. RCP 2.6 (radiative forcing value of 2.6 W/m^2) represents an aggressive mitigation scenario with a considerable negative future emission [*Benestad R. et al.*, 2017].

In this work **RCP 2.6**, **RCP 4.5** and **RCP 8.5** (from 2041 to 2060) and the **historical scenario** (from 1986 to 2005) were considered. The historical simulation had to be investigated since this type of experiment is not synchronised with the observed climate. By comparing historical and future simulations a correction factor can be derived which can be applied to actual (observed) climate date in order to evaluate climate change.

BOX 2: How to access CORDEX data?

There is no central CORDEX archive and CORDEX output can be accessed using ESGF infrastructure, Impact Portals, Regional Data Portals or services provided by institutions. In this work **ESGF** infrastructure was used to access data. The Earth System Grid Federation (ESGF) is an up-to-date scientific infrastructure for distributing climate data [*http://www.cordex.org/*].
CORDEX simulations are visible on all ESGF index nodes worldwide and it does not matter which of the ESGF nodes is used because all of them provide links to the same files. The node used in this work was **SMHI-NSC, Sweden**. This ESGF datanode at the National Supercomputer Centre, Linköping, is Sweden's first datanode in the ESGF framework. It is a joint activity of NSC, an independent organization within the Linköping University, and the Swedish Meteorological and Hydrological Institute (SMHI) [*https://esg-dn1.nsc.liu.se/projects/esgf-liu/*].

5. The Guerna catchment case study

5.1. Introduction and goals

Water erosion, sediment transport and yield and the effects of climate change on these physical phenomena are the focus of this work.

There are three different groups of models to calculate eroded material: physically-based models, conceptual models and empirical models. In this analysis, the RUSLE [*Renard et al*., 1991], the EPM [*Gavrilovic*, 1988] and the MUSLE [*Williams*, 1975] method are the three empirical models used that are based on formulas generated by laboratory investigations and by field observations and experiments (paragraph 4.3). They have been applied to the study area: a small mountain basin, the Guerna creek watershed, located in the Central Southern Alps (Lombardy, Southern Alps, Bergamo). These models are implemented in a Geographical Information System (GIS) supporting the management of the territorial database used to estimate relevant geomorphological parameters and to create different thematic maps. On one hand the geographical and geomorphological information is required (land use, slope and hydrogeological instability, resistance to erosion, lithological characterization and granulometric composition). On the other hand knowledge of the weather-climate parameters (precipitation and temperature data) is fundamental as well to evaluate the intensity and variability of the erosive processes and estimate the sediment yield at the basin outlet. Therefore, different future climate scenarios were considered in order to tentatively assess the impact of climate change on the water erosion and sediment yield on a small basin scale [*Berteni and Grossi*, 2017].

Interest in the Guerna catchment arises from its geographical location and from the need to evaluate sediment transport and yield, manifested by the authority managing the body of Iseo lake and the Oglio river (Consorzio dell'Oglio). The Guerna creek was affected in the past by flooding and erosion events which stressed the hydraulic weaknesses of the study area. Therefore, this watershed is exposed to hydrogeological risk because of, for example, poor cleaning of the water courses, abandonment of the territory, or disuse of agricultural practices [*Berteni*, 2012].

The aim of the RUSLE methodology is to estimate water erosion in agricultural areas, therefore the approach is not perfectly suitable to erosion assessment in mountain catchments. The EPM method is accounting for a more complete description of the meteorological forcing, since both precipitation and air temperature are included in the evaluation of procedure. Soil loss computed for the Guerna watershed in the years 2005-2016 by RUSLE equation is about 3 times higher than its evaluation according to the EPM method. This overestimate is coherent with the results obtained for another case study (Fiumara Sfalassa, South Italy), with a similar topography [*Dominici et al.*, 2015; *Auddino et al.*, 2015].

The climate change impacts on water erosion may not be negligible even by the mid century and they can be direct and indirect. The direct impacts are mainly caused by changes in

rainfall and the indirect impacts are related to rising temperatures. Many studies suggest that rainfall is the most direct influencing factor. The influencing mechanisms of both rising temperatures and changing rainfall patterns are very complex because both factors can cause positive and negative impacts [*Li and Fang*, 2016]. Rainfall varies in different parts of the world; precipitation patterns in different regions of the same continent or country can either increase or decrease. This also accords with the prediction of IPCC for the various precipitation changes around the globe. Therefore, soil erosion rates may increase or decrease under climate change, depending on geographic locations, climate scenarios, precipitation patterns, topographic conditions and land use management. Soil erosion is likely to increase with increased rainfall, but it is not only dependent on the amount of rainfall; also rainfall intensity and precipitation variability affect soil loss greatly. Therefore, soil erosion does not necessarily increase with increased the amount of rainfall. In quite a few studies, despite the predicted decline of precipitation, increased soil loss was projected due to increased frequency of intense rainfall events. Prusky and Nearing (2002) found that impacts of precipitation intensity were greater than those of storm frequency (the number of wet days). Nearing et al. (2005) concluded that the combined changes in rainfall amount and rainfall instensity are likely to have a greater influence than changes in any single factor [*Li and Fang*, 2016]. According to the EPM method and to RCP2.6, RCP4.5 and RCP8.5 (paragraph 4.5.1) the annual average soil loss in the Guerna catchment can change by 8-10% at the basin scale [*Berteni and Grossi*, 2017].

Finally, the sediment yield for a single rainfall event was estimated through the MUSLE equation. This value was used as the input material for the HEC-RAS model in order to simulate sediment transport in the Guerna Creek.

5.2. Catchment characteristics

5.2.1. Location and thematic maps

The Guerna watershed is located in the Province of Bergamo (Northern Italy). The Guerna creek springs from Monte Foppa at 1024 m a.s.l. and it is a right tributary of the Oglio river; its difference in level and its average slope are, respectively, 834 m and 0.06 m/m. It flows for approximately 10.6 km before joining the Oglio river, a few meters downstream of the Sarnico dam controlling the water level in Iseo lake. Most of the watershed surface belongs to the municipalities of Adrara S. Rocco, Adrara S. Martino and Viadanica. The area of the basin is 30.9 km^2 wide, the average slope is about 27° (0.5 m/m) and the average elevation is around 649 m a.s.l.. The maximum difference in altitude is 1147 m: the maximum elevation is 1332 m a.s.l. and the minimum is 185 m a.s.l. [*Berteni and Grossi*, 2017].

Figure 5.1 and Figure 5.2 show the location of the study area:

Figure 5.1 – Guerna catchment location (a)

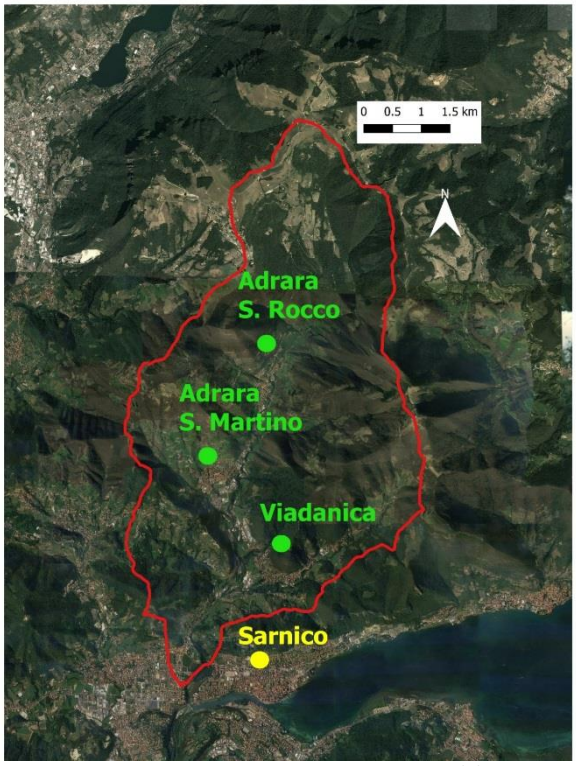

Figure 5.2 – Guerna catchment location (b)

Thematic maps of the Guerna watershed (Figure 5.3, Figure 5.4, Figure 5.5 and Figure 5.6) were created in QGIS [*https://www.qgis.org/it/site/*]: a free and open-source (cross-platform) desktop Geographic Information System (GIS) application which supports viewing, editing and analysis of geospatial data. Geoportale della Regione Lombardia (Regione Lombardia geo-portal) [*http://www.geoportale.regione.lombardia.it/*] contains the territorial database which has been used for creating these maps.

Figure 5.3 (a) shows the Digital Elevation Model (DEM) for the Guerna creek catchment. DEM resolution is 5x5m.

Figure 5.3 (b) shows the slope map for the study area that was created by applying a QGIS function on DEM.

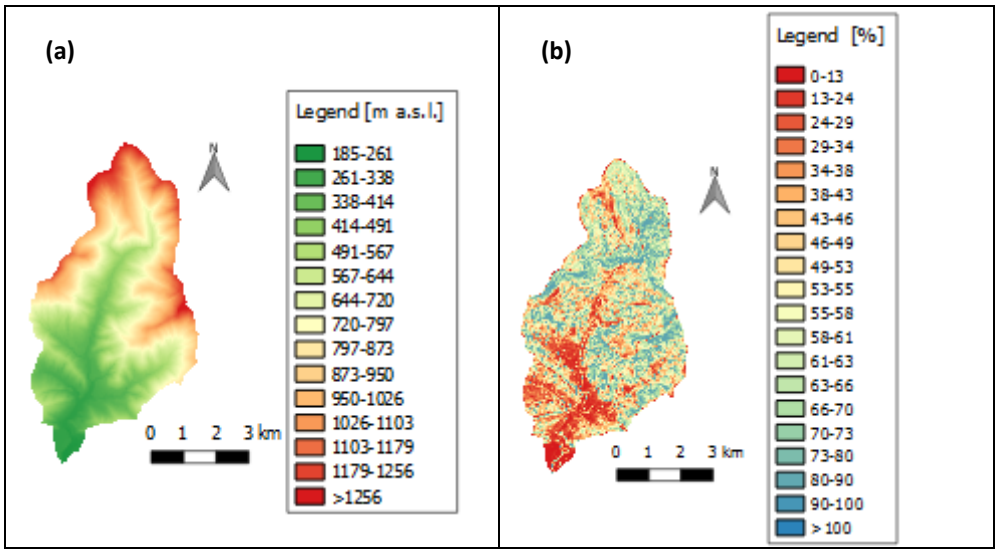

Figure 5.3 –Digital Elevation Model (DEM)* (a) *and slope map* (b) *of the Guerna catchment

Figure 5.4 shows the Guerna catchment lithological map: limestones, marly limestones and flint limestones are present in most of the part of the territory. In correspondence of Guerna mouth there are gravel, sand, blocks and ferritization silt.

Figure 5.5 shows the study area hydrogeological instability map. There are different sites characterized by landslides, alluvial cone, debris or terrigenous cover, rill erosion and gully erosion.

Figure 5.6 shows the Guerna watershed land use map. It displays that most of the soil is covered by woods, reforestations and forests. Urban areas represent a small part of territory and they are concentrated along the Guerna torrent.

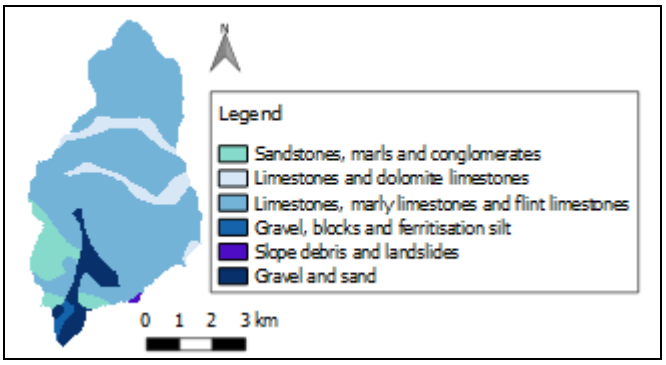

Figure 5.4 – Guerna catchment lithological map

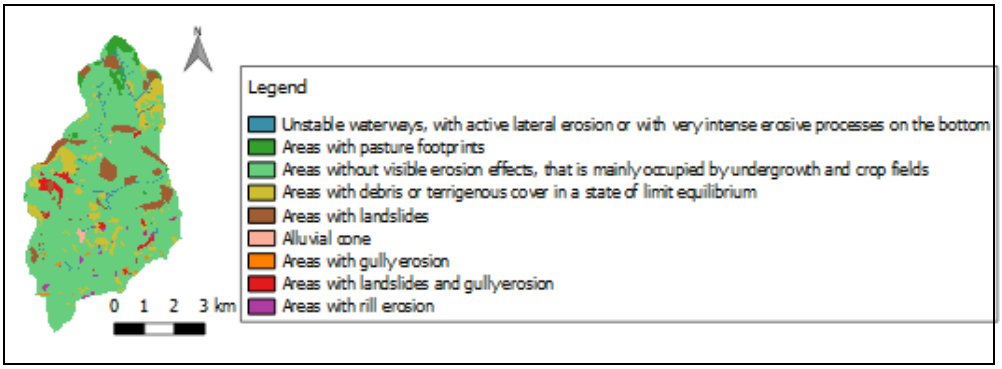

Figure 5.5 – Guerna catchment hydrogeological instability map

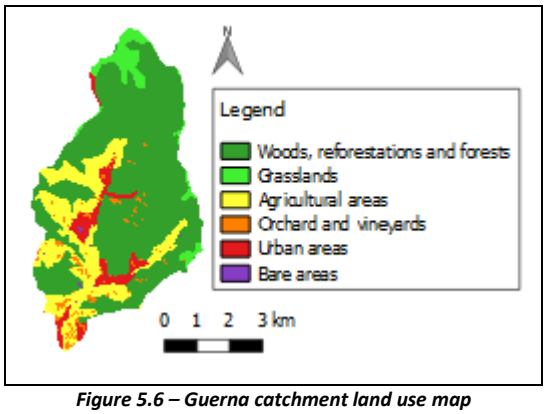

Figure 5.6 – Guerna catchment land use map

5.2.2. Hypsographic and hypsometric curve

Figure 5.7 and Figure 5.8 show the hypsographic and the hypsometric curves for the Guerna catchment that were made using DEM and GIS tools.

The hypsographic curve is (Figure 5.7) a graphic representation of the elevation of points on the Earth's surface (or a part of the Earth's surface) with reference to the Earth's sea level. Therefore, the hypsographic curve is a graph with an x-axis (horizontal) and a y-axis (vertical). In this case study, the x-axis contains the value of the Guerna watershed area above the corresponding elevation on the y-axis.

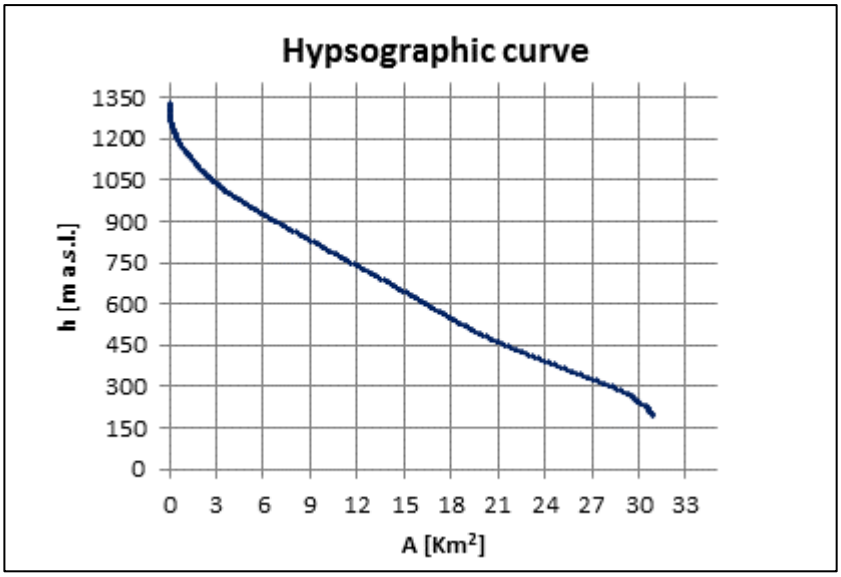

Figure 5.7 – Hypsographic curve of the Guerna catchment

The hypsometric curve (Figure 5.8) is similar to the hypsographic curve, but it is presented in a non-dimensional form by scaling elevation and area by the maximum values. The hypsometric curve is very useful in assessing the similarity of watersheds.

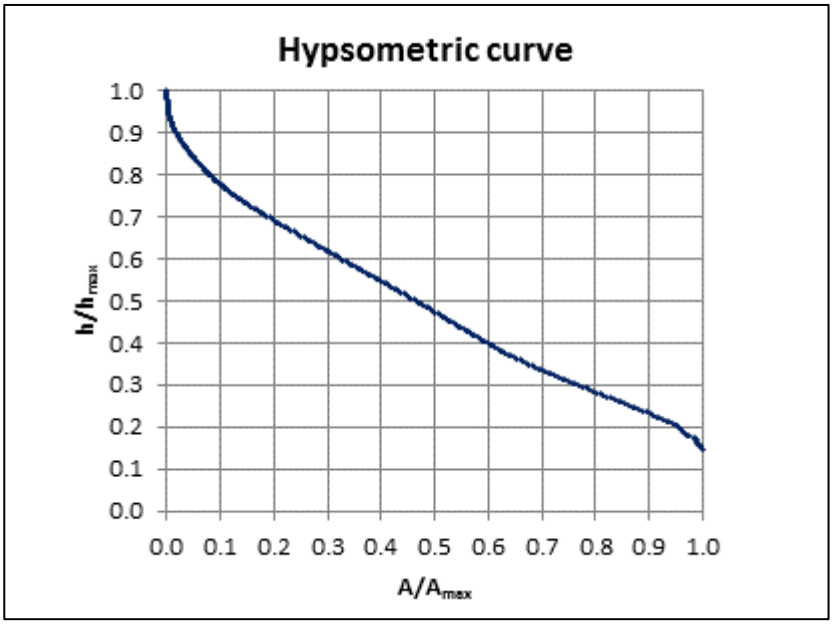

Figure 5.8 – Hypsometric curve of the Guerna catchment

The hypsometric curve can also be related to the concept on erosion cycle and to the stage of watershed evolution. Curve a), b) and c) in Figure 5.9 represent, respectively, the "youthful stage" (catchment in the process of erosion), the "mature stage" (catchment in the position of equilibrium) and "old age stage" or "monadnock stage" (catchment characterized by isolated hills, which are the remains of a surface subject to erosion). The integral of the hypsometric curve returns a value *V* which is used to assess the volume of the watershed compared to the one that was initially (and theoretically) present, as follows [*Ferro*, 2002]:

- $V > 0.6$ these values indicate the "youthful stage" of the catchment
- $0.4 \leq V \leq 0.6$ these values indicate the "mature stage" of the catchment
- $V < 0.4$ these values indicate the "old age stage" of the catchment

The *V* value in the Guerna catchment is around 0.5 and, therefore, it is within the "mature stage".

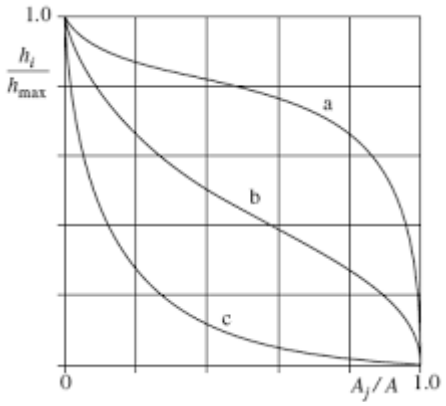

Figure 5.9 – Interpretation of the hypsometric curve **[Puglisi, 1986]**

5.2.3. Time of concentration and time-area function

The travel time of surface runoff or time of concentration measures the time response of a watershed to a rain event. It is the time needed for water to flow from the farthest point in a watershed to the watershed outlet. It is a function of land use, topography and geology within the basin.

In the technical literature there are many empirical formulas that find ample application, due to the limited amount of information they require in estimating the time of concentration on a basin scale in ungauged conditions. Giandotti (1934) proposed the dominant formula in Italy, which can be used for basins with drainage areas between 170 and 70000 km^2:

$$t_c = \frac{4\sqrt{A} + 1.5L}{0.8\sqrt{H_m}} \qquad \textbf{(5.1)}$$

where t_c is the time of concentration [h], A the watershed area [km^2], L the length of the main channel [km] and H_m the difference between the mean basin elevation and the outlet elevation [m].

However, the Giandotti formula is not very suited for the Guerna catchment because of its size. The most appropriate formulas for the study area are Tournon [*Merlo*, 1973] and Fattorelli and Marchi (1988) formulas. The Tournon formula was deduced from observations in Piedmontese mountain catchments with drainage areas between 30 and 170 km^2:

$$t_c = 0.396\frac{L}{\sqrt{i_a}}\left(\frac{A\sqrt{i_a}}{L^2\sqrt{i_m}}\right)^{0.72} \qquad \textbf{(5.2)}$$

where t_c is the time of concentration [h], A the watershed area [km^2], L the length of the main channel [km], i_m the basin average slope [m/m] and i_a the main channel average slope

[m/m], which is composed of *n*-stretches of river (each stretch has an average slope i_{ai} [m/m] and length L_i [m]):

$$\sqrt{i_a} = \frac{L}{\sum_{i=1}^{n} \frac{L_i}{\sqrt{i_{ai}}}} \qquad \textbf{(5.3)}$$

The Fattorelli and Marchi formula was deducted from observations in alpine basins with drainage areas between 7 and 200 km^2:

$$t_c = 6\frac{L^{2/3}}{d^{1/3}} \qquad \textbf{(5.4)}$$

where t_c is the time of concentration [h], *L* the length of the main channel [km] and *d* is the difference in level of the main channel [m].

Table 5.1 shows the results achieved for the Guerna catchment, by applying the different empirical formulas:

Empirical formula	Time of concentration [h]
Giandotti	2.21
Tournon	3.15
Fattorelli e Marchi	3.07

Table 5.1 – Time of concentration achieved in the Guerna catchment by applying different empirical formulas

The time of concentration map was made for the Guerna catchment in a GIS environment; the GIS software GRASS was used [*https://grass.osgeo.org/*]. Although GRASS GIS has both raster and vector capabilities, raster data structures were used because of their analytical power. Raster data structures allow mathematical combinations of data from multiple images. The raster map resolution adopted to calculate the travel time is 20x20 m.

The GRASS GIS function used is "r.traveltime", which makes it possible to compute the travel time of surface and channel runoff to an outlet. The raster GIS functions were used to calculate the travel time from each point in the watershed to the outlet by determining the flow path and the travel time through each cell along the path. The program starts at the basin outlet and calculates the travel time for each raster cell recursively. Therefore, the travel time through each individual cell along the flow path was summed to estimate the cumulative travel time to the outlet.
A drainage area related threshold considers either surface runoff (with overland velocity) or channel runoff (with channel velocity). The watershed channels were delineated based on the upstream area above each cell. It was assumed that any upstream area smaller than the threshold value did not produce enough runoff to support a channel. Any cells that were not determined to be part of the stream network were assumed to be controlled by overland flow. Cells that did not have any other cells flowing into them were considered to be ridge cells. It should be born in mind that it is very difficult to decide the channel flow threshold because there is no good way to quantify the threshold where overland flow becomes

channel flow. For this watershed, a channel flow threshold of 12 cells (0.48 ha) was chosen. This choice is in line with the discussion in paragraph 4.3.1.1 to estimate the LS factor. All cells with less upstream area were assumed to be dominated by overland flow.
In order to calculate the travel time through each cell, the runoff velocity is required. The GRASS function considers the following elements in determining flow velocities: watershed position, slope, land use, channel characteristics and rainfall excess intensity. In accordance with Muzik (1996), the excess rainfall is the total rainfall minus infiltration and other abstractions. The runoff velocity for areas with overland flow were derived by assuming kinematic wave approximation: the depth of flow at equilibrium (Overton and Meadows, 1976) was used in Manning's equation to calculate the equilibrium overland runoff velocity. In order to derive channel flow velocities, an equilibrium discharge (Ajward, 1996) for each cell was calculated (Q=Area*Specific discharge), and was combined with Manning's equation. For this study area, the specific discharge used is 5555 $l/(s \cdot km^2)$, which corresponds to approximately 19 mm/h intensity of rainfall excess. This decision arises out of the observations of rainfall amount at the Sarnico station. Considering the data available, the latest and maximum rainfall value registered is 28.8 mm/h, which represents the rainfall event that happened in 2011 (04/09/2011). Anyway, there is a good deal of uncertainty in the estimate of the rainfall excess intensity. The travel time through each grid cell was calculated as flow distance divided by flow velocity.
For both surface and channel flow, the flow distance was determined based on the flow direction. The flowdirection map was made for the Guerna catchment in a GIS environment, using the DEM and the "r.watershed" GRASS function.
There is a good deal of uncertainty also in the channel width estimates. Considering the watershed structure, it was decided to set a value of around 2 m.
The Manning's roughness coefficient adopted, respectively for channels and overland, is 0.025 $s \cdot m^{1/3}$ and 0.035 $s \cdot m^{1/3}$.
In accordance with the GRASS manual, the minimum slope for flat areas that was assumed is 0.001 m/m. Indeed, for smaller gradients, the program uses this value.
[*Kilgore*, 1997; *https://grass.osgeo.org/grass74/manuals/addons/r.traveltime.html*]

Figure 5.10 shows the time of concentration map for the Guerna catchment.

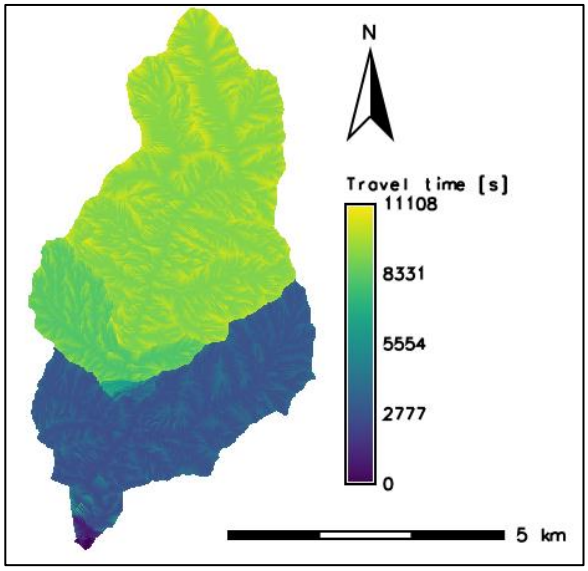

Figure 5.10 – Time of concentration map for the Guerna catchment

The cumulative time of concentration of the entire watershed is 3.08 h, in line with the Tournon and Fattorelli e Marchi empirical formulas in Table 5.1.

The cumulative travel time map (Figure 5.10) is divided into isochrones which are used to generate the following time-area curve.

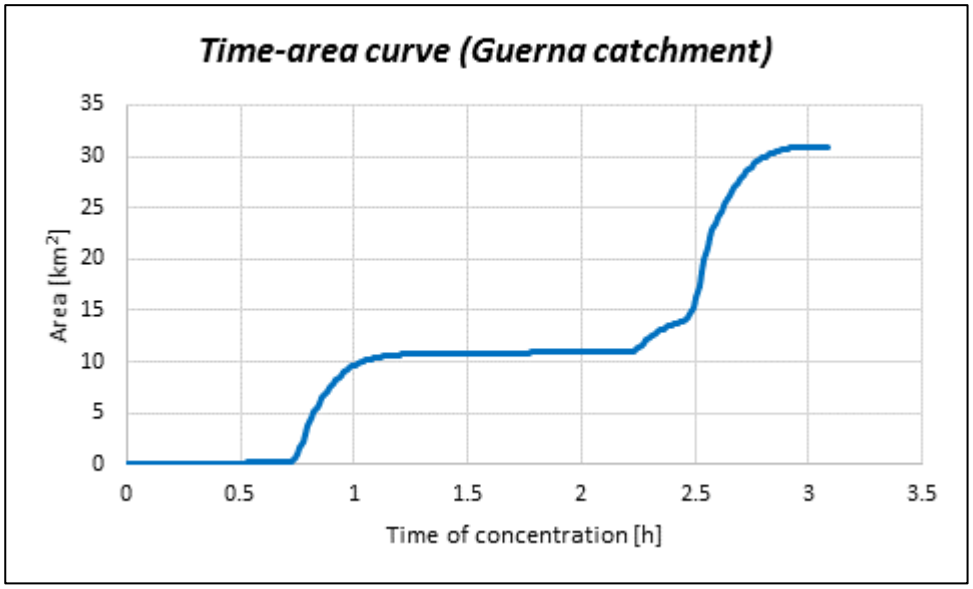

Figure 5.11 – Time-area curve (Guerna catchment)

The clear abrupt jump (green-blue) both in Figure 5.10 and in Figure 5.11 is related to the watershed morphology and to the imposed threshold in "r.traveltime" function to produce runoff channels. From the analysis of the DEM raster map, it was noted that in correspondence of the abrupt jump there is a significant elevation increase. Indeed, the line of the abrupt jump coincides with the boundary of other sub-basins. A sensitivity analysis revealed that the time of concentration map, created without considering channel runoff and just taking into account the surface runoff (Figure 5.12), is different. The abrupt jump is less apparent, but the cumulative time of concentration of the entire watershed is 66.8 h. This value is unacceptable.

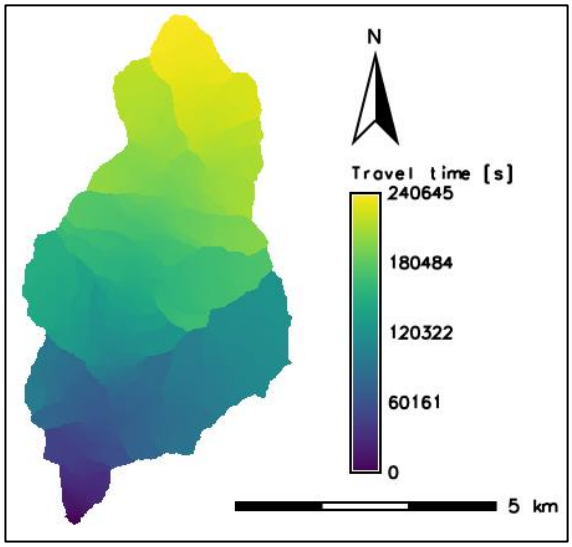

Figure 5.12 – Time of concentration map for the Guerna catchment without considering channel runoff

The time of concentration map and the time-area curve were made for 7 sub-basins in the Guerna catchment. The GRASS GIS function "r.traveltime" was used to create the maps, in a similar way to the Guerna watershed in Figure 5.10 and in Figure 5.11.

The following images (from Figure 5.13 and Figure 5.19) contain the results obtained.

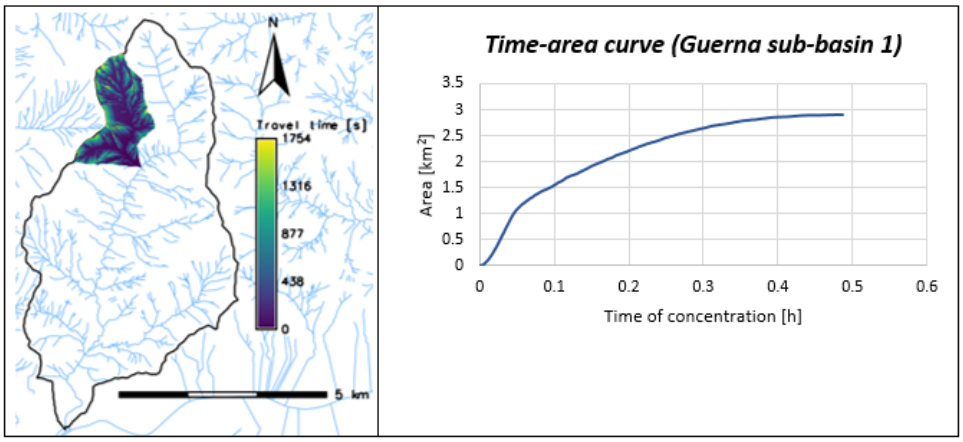

Figure 5.13 – Time of concentration map and time-area curve for the Guerna sub-basin 1

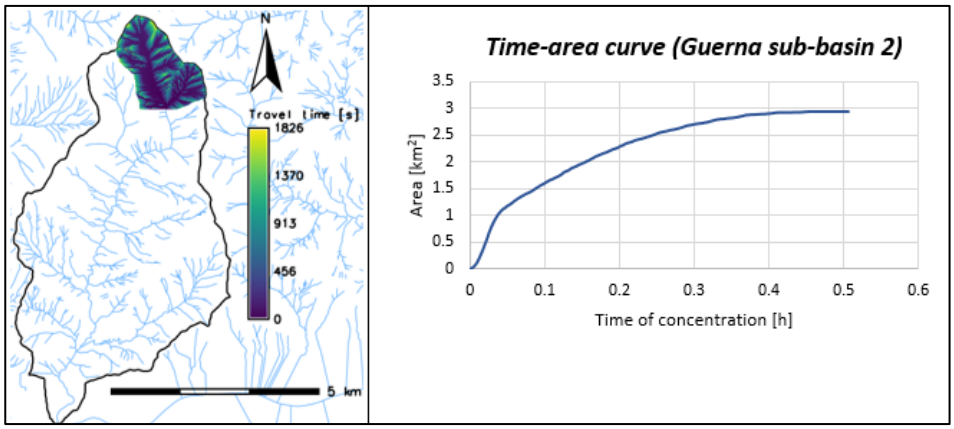

Figure 5.14 – Time of concentration map and time-area curve for the Guerna sub-basin 2

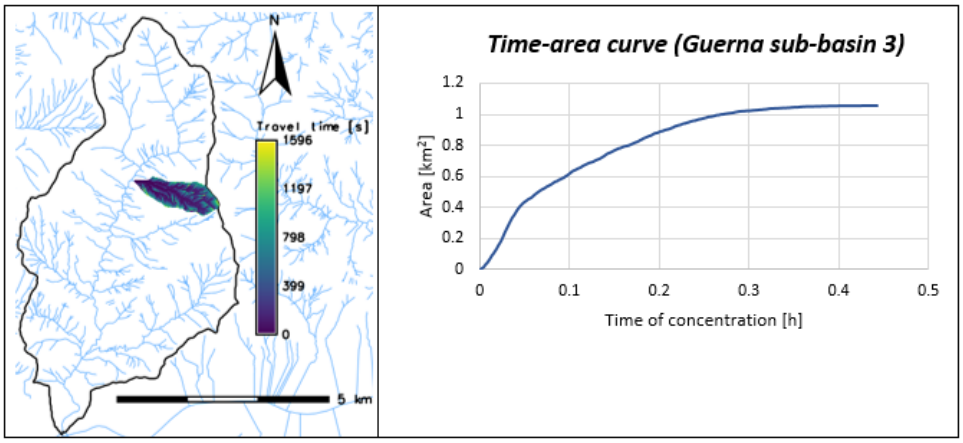

Figure 5.15 – Time of concentration map and time-area curve for the Guerna sub-basin 3

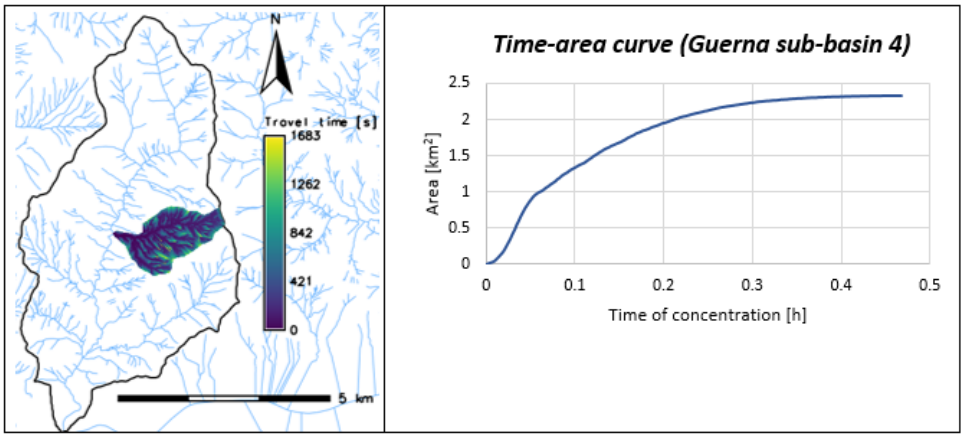

Figure 5.16 – Time of concentration map and time-area curve for the Guerna sub-basin 4

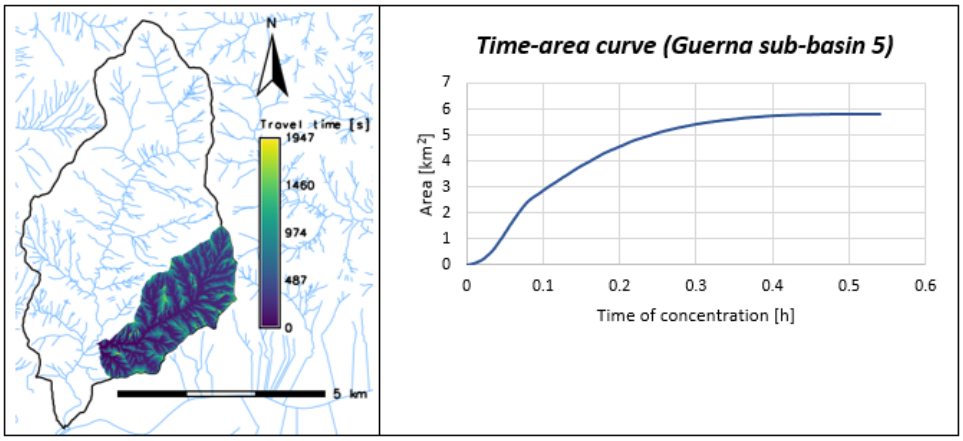

Figure 5.17 – Time of concentration map and time-area curve for the Guerna sub-basin 5

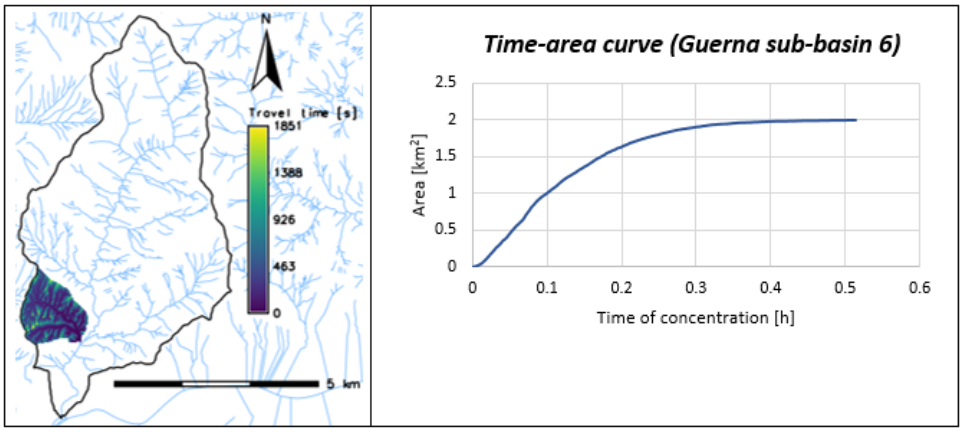

Figure 5.18 – Time of concentration map and time-area curve for the Guerna sub-basin 6

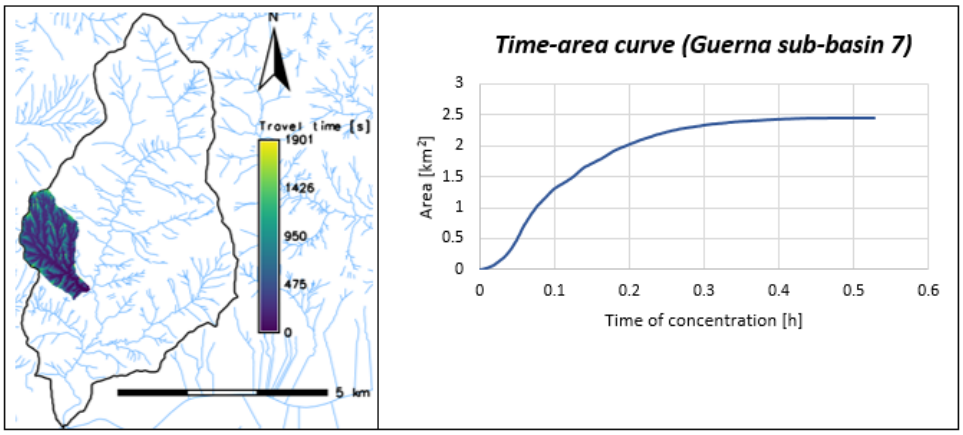

Figure 5.19 – Time of concentration map and time-area curve for the Guerna sub-basin 7

5.3. Application of the RUSLE model

The RUSLE (Revised Universal Soil Loss Equation) model [*Renard et al.*, 1991] is an erosion prediction and conservation planning tool based in large part on the USLE (Universal Soil Loss Equation) and its supporting data, but also including major improvements and updates. The USLE is an erosion model designed to predict the longtime average soil losses in runoff from specific field areas in a specific cropping and management system. A revision of this model transformed it into the RUSLE. The detailed description of the RUSLE method is in paragraph 4.3.1.1.

The first step in implementing the RUSLE model is to estimate the **R factor** (which was considered uniform in the Guerna catchment) using the procedure defined in paragraph 4.3.1.1.

In the study area, rainfall events from 2008 to 2011 are considered; they are separated by non-rainy periods lasting 6 hours or more and every rainstorm is considered an erosive event. Rainfall at the Sarnico station for each half an hour is known. These data were provided by "Consorzio dell'Oglio" [*http://www.oglioconsorzio.it*].

The R factor obtained from elaboration is *R = 2620 MJ·mm/(ha·h·year)*.

Also the **K factor** was considered uniform in the study area and it was calculated using Equation (4.10) and Equation (4.11).

The grain size distribution curve of the samples was determined by wet-sieving (according to ASTM standards number D 422/72 and E 11/81) and sedimentation (according to ASTM standards number E 100/86, D 1140/71), in the Hydraulic and Hydrology Lab and in the Geotechnical Lab at the University of Brescia. Two soil samples were taken in two different points of the study area: in Adrara S. Rocco (BG) and in Adrara S. Martino (BG). The samples

were dried and washed with a sieve capable of containing material larger than 75 µm. Material larger than 75 µm, after drying, was subjected to particle sedimentation analysis. Material larger than 75 µm, after drying, was subjected to particle sieving analysis, using sieves with slotted perforations ranging from 75 mm to 0.075 mm [*Berteni*, 2012].

The grain size distribution curves were classified according to AGI (Associazione Geotecnica Italiana, 1990) classification, with the following references:

- clay: d_i = 0.002 mm
  d_{i-1} = 0.000001 mm
- silt: d_i = 0.06 mm
  d_{i-1} = 0.002 mm
- sand: d_i = 2 mm
  d_{i-1} = 0.06 mm

For each particle size class (clay, silt and sand), the corresponding mass fraction f_i were determined.
Table 5.2 shows the useful results of the particle analysis and the K factor for each soil sample:

	f_i **clay [%]**	f_i **silt [%]**	f_i **sand [%]**	D_g	***K factor*** $\left[\frac{t \cdot ha \cdot h}{ha \cdot MJ \cdot mm}\right]$
Adrara S. Martino sample	22.9	38.48	38.62	0.0546	*0.038054*
Adrara S. Rocco sample	24.52	36.18	39.31	0.0529	*0.038426*

***Table 5.2 – Results of the particle analysis and K factor* [*Berteni*, 2012]**

For simplification, one K value factor was used for the study area: *K = 0.038 t·ha·h/(ha·MJ·mm)*.

The **LS factor** map (Figure 5.20) has a spatial variability in the Guerna catchment and it was created through Equation (4.16) using the GIS system. The *Senα* raster map was built on the basis of the slope map (Figure 5.3 (b)). The *Flowaccumulation* map was created using the "r.watershed" GRASS application. Flow accumulation consists in the number of cells bringing runoff water to each pixel in the grid and, in accordance with Pregnolato and D'Amico (2011), an upper limit of the "Flowaccumulation" parameter was imposed (see paragraph 4.3.1.1). This limit corresponds to about 300 m of slope length and therefore, taking into account the pixel dimension (5 x 5m), the maximum value of this parameter is equal to 60 cells.

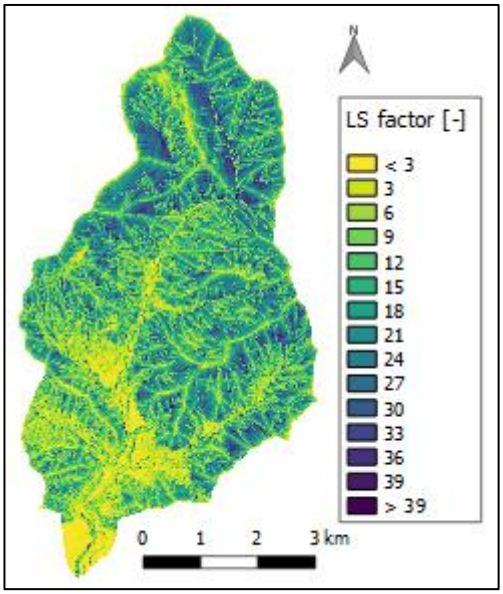

Figure 5.20 – Guerna catchment LS factor

The **C factor** was also built for the Guerna watershed. Table 5.3 shows *C factor* values that were associated with each area in the land use map (Figure 5.6), according to the indications in Table 4.1 by Angeli, 2004:

Description	***Area*** **[km²]**	***C*** **factor** **[-]**
Wood, reforestation and forest	20.5	0.002
Grassland	1.64	0.07
Agricultural areas	6.00	0.45
Orchard and vineyard	1.07	0.37
Urban areas	1.83	0.003
Bare areas	0.05	0.36

Table 5.3 – C factor values used in the Guerna catchment

The **P factor** has a spatial variability in the Guerna watershed. Table 5.4 shows *P factor* values that were associated with each area in the land use map (Figure 5.6), according to the indications in Table 4.2 by Wischmeier and Smith, 1978:

Description	*Area* [km²]	*P* factor [-]
Wood, reforestation and forest	20.5	1
Grassland	1.64	1
Agricultural areas	6.00	1
Orchard and vineyard	1.07	0.45
Urban areas	1.83	1
Bare areas	0.05	1

Table 5.4 – P factor values used in the Guerna catchment

In the present case, the P value was considered to be different from 1 only in areas occupied by orchards and vineyards because they are terrace cultivations. These areas have an average slope greater than 24%, which is the upper limit reported in Table 4.2. Therefore, a P value corresponding to the maximum value reported in Table 4.2 was associated to them.

The computed soil loss A (Figure 5.21) was calculated by solving Equation (4.2) in a GIS environment.

The **mean value ($A_{\_mean}$)** and the **total value ($A_{\_tot}$)** in the Guerna catchment of computed soil loss are the following:

- $A_{\_mean}$ = 97.7 t/(ha·year) or $A_{\_mean}$ = 0.25 t/(cell·year)
- $A_{\_tot}$ = 302271.1 t/year

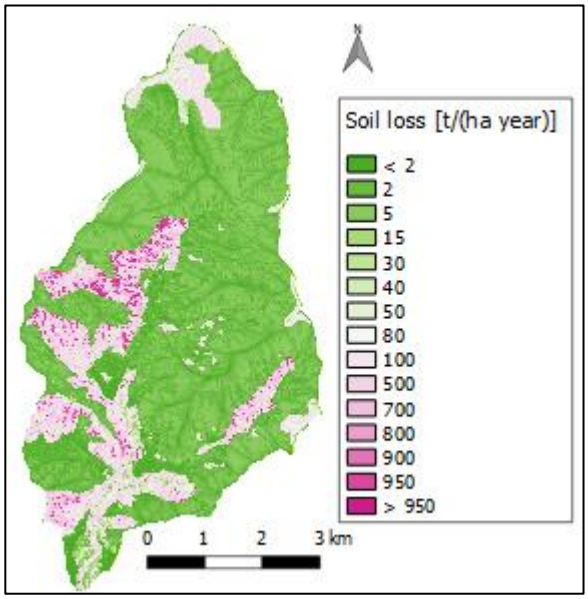

Figure 5.21 – Guerna catchment: map of computed soil loss (A)

5.3.1. Comparison with the European Soil Data Centre (ESDAC)

The **European Soil Data Centre (ESDAC)** is the thematic centre for soil related data in Europe and it is hosted by the Joint Research centre (JRC) of the European Commission. Its ambition is to be the single reference point for and to host all relevant soil data and information at the European level. It contains different resources that are organized and presented in various ways (datasets, services, applications, maps, documents, events, projects and external links) [*https://esdac.jrc.ec.europa.eu/*].

With the use of the GIS system, it was possible to find the mean value of each RUSLE factor provided by the ESDAC maps in the Guerna catchment. These values were compared with the values found in paragraph 5.3.

The mean value of the rainfall erosivity R-factor in the Guerna catchment and provided by the ESDAC is 2290 MJ·mm/(ha·h·year), considering a spatial resolution of 500 m. The ESDAC calculated the R-factor as the product of kinetic energy of a rainfall event (E) and its maximum 30-min intensity (I_{30}), as suggested by Brown and Foster (1987) (see paragraph 4.3.1.1) [*Panagos et al.*, 2015 (b)]. This value was evaluated by using the same procedure described in paragraph 4.3.1.1 and it has the same order of magnitude as that computed in paragraph 5.3 (2620 MJ·mm/(ha·h·year)). Figure 5.22 shows the mean R-factor value in the north of Italy provided by the ESDAC.

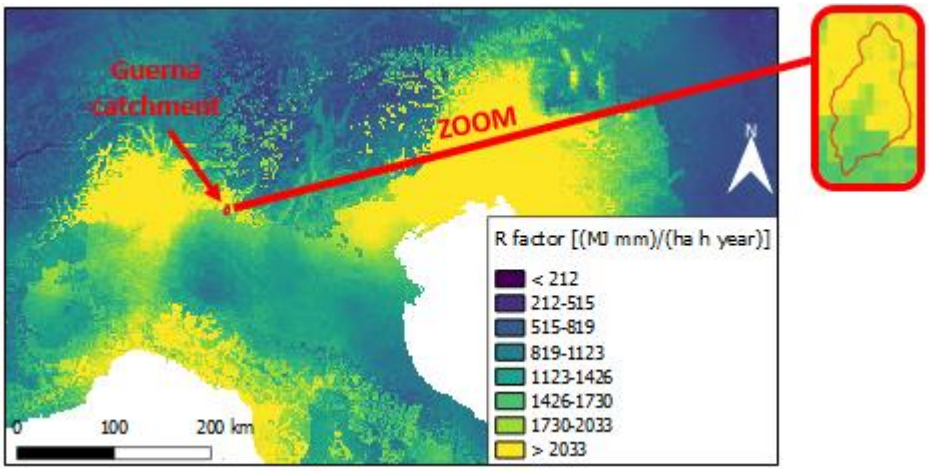

Figure 5.22 – High-resolution map of rainfall erosivity in Europe Union (north of Italy). [https://esdac.jrc.ec.europa.eu/]

The ESDAC estimated the P-factor considering a spatial resolution of 100 m and it assigned a value of 1 for the Guerna catchment area as a whole. This value is in accordance with the mean value adopted in paragraph 5.3 (P-factor = 0.98). At European level, the P-factor was proposed as a product of 3 sub-factors: contour farming, maintenance of stone walls and

grass margins [*Panagos et al.*, 2015 (c)]. Figure 5.23 shows the support practice P-factor value in the north of Italy provided by the ESDAC.

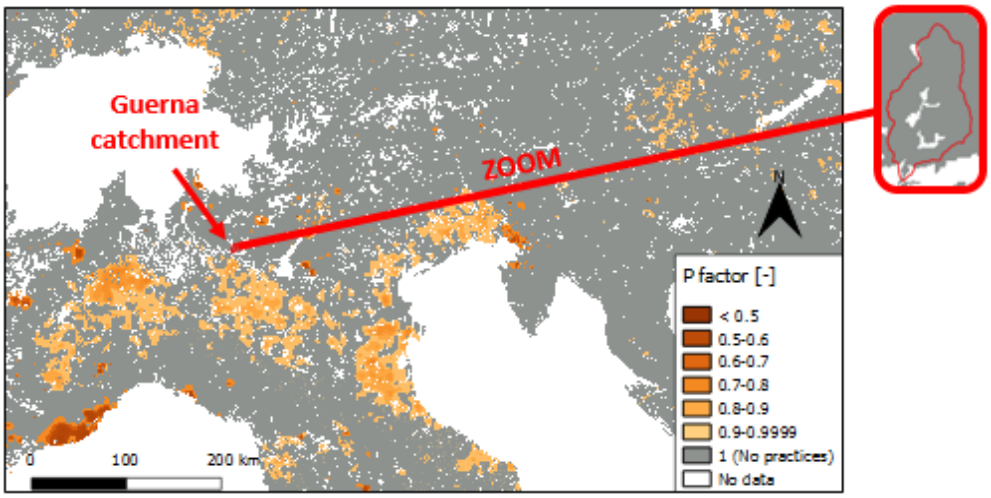

Figure 5.23 – Support practice P-factor in the European Union (north of Italy). [https://esdac.jrc.ec.europa.eu/]

The mean value of the cover-management C-factor estimated by the ESDAC in the Guerna catchment, using a spatial resolution of 100 m, is 0.028. This value is almost 4 times lower than the mean one used in paragraph 5.3 (C-factor = 0.105). The reason relates to the higher level of detail and to the different method used for its evaluation in paragraph 5.3. Most of the basin (20.5 km^2) is wooded area (C-factor = 0.002), but the C-factor associated to agricultural area (6 km^2) is 0.45; for this reason the mean value of the C-factor is higher than the value provided by the ESDAC. The estimation of the C-factor in the European Union considered a hybrid C-factor land use and management (LANDUM) model, developed for the European-scale study. It is based on a literature review, remote sensing data at high spatial resolution and statistical data on agricultural and management practices. The LANDUM model for C-factor estimation was differentiated between arable lands and all other land uses (non-arable), considering the combination of different sub-factors. Finally, a mosaic layer of the C-factor for arable lands and for non-arable lands was proposed as the annual C-factor in Europe [*Panagos et al.*, 2015 (d)]. Figure 5.24 shows the mean C-factor value in the north of Italy provided by the ESDAC.

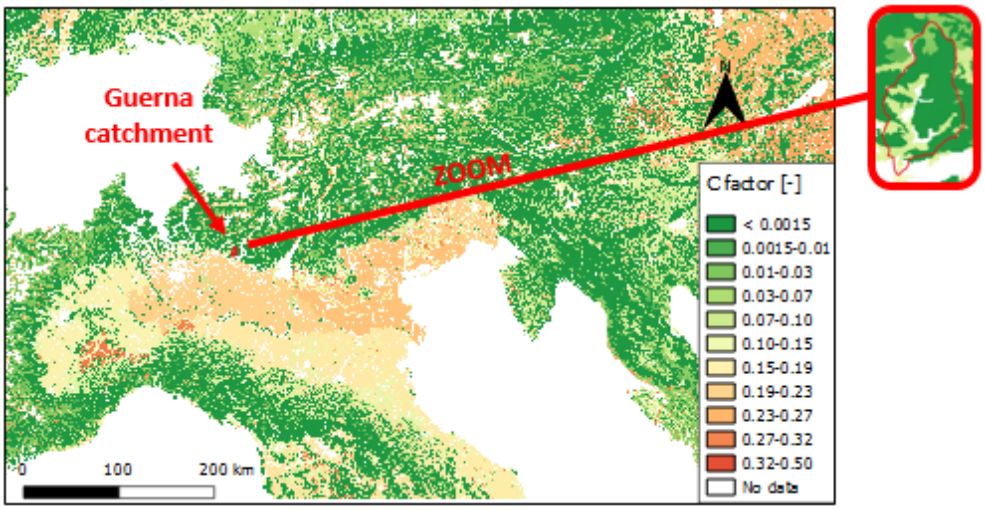

Figure 5.24 – C-factor map of the European Union (north of Italy). [https://esdac.jrc.ec.europa.eu/]

The mean value of the K-factor provided by the ESDAC in the Guerna catchment is 0.027 t·ha·h/(ha·MJ·mm), considering a spatial resolution of 500 m. This value is similar to the value calculated and adopted in paragraph 5.3 (K-factor = 0.038 t·ha·h/(ha·MJ·mm)). At European level, with the Land Use/Cover Area frame Survey (LUCAS) topsoil data [*Toth et al.*, 2013], the K-factor was calculated using an algebric approximation of the nomograph [*Wischmeier and Smith*, 1978]. This equation includes five soil parameters (texture, organic matter, coarse fragments, structure and permeability). A regression model was applied to correlate spatial data such as latitude, longitude, remotely sensed and terrain features in order to develop a high resolution soil erodibility map in Europe. Then the K-factor value of each LUCAS point sample was interpolated to derive a continuous map for Europe [*Panagos et al.*, 2014]. Figure 5.25 shows the map of Soil Erodibility estimated as the K-factor in the north of Italy and provided by the ESDAC.

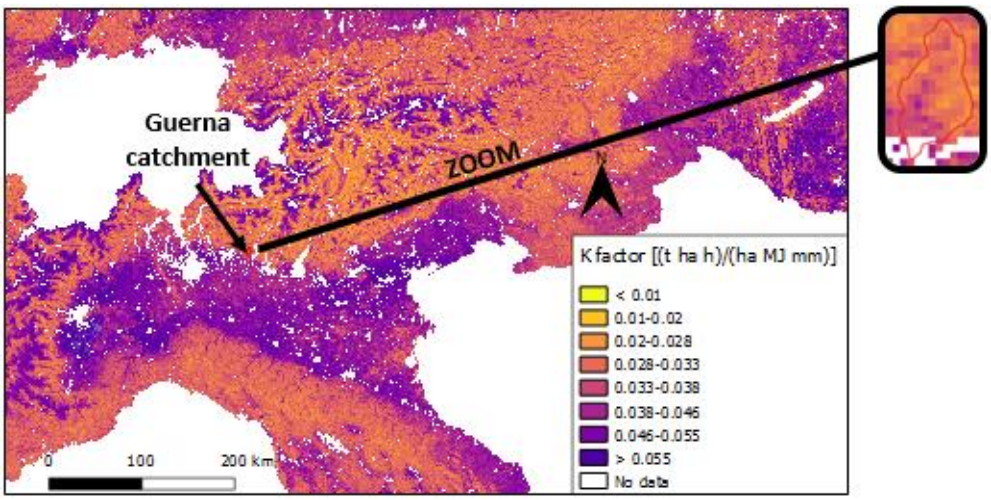

Figure 5.25 – High-resolution (500 m grid cell size) map of Soil Erodibility estimated as K-factor in the Europe Union (north of Italy). [https://esdac.jrc.ec.europa.eu/]

The mean value of the slope length and steepness factor (LS-factor) estimated by the ESDAC in the Guerna basin is 7.73. This value is half of the mean value calculated in paragraph 5.3 (LS-factor = 14.09). The reason relates to the higher level of detail and to the different method used for its evaluation in paragraph 5.3, where the equation suggested by Bosco and Oliveri (2007) was used, the resolution of the Digital Elevation Model (DEM) adopted is 5 m and a surface runoff concentration in less than 300 m was assumed. The grid-cell size is very important for the S-factor, since the slope decreases as the cell size increases [*Molnar and Julien*, 1998]. When DEM resolution and accuracy increase, the landscape is more accurately described, the soil erosion topographic factor is calculated precisely and erosion estimates approach actual values. Then DEM resolution has profound consequences on the spatial pattern of the LS-factor. At European level, the LS-factor was calculated using GIS software tools with high-resolution (25 m) Digital Elevation Model (DEM); the methodology applied is the Desmet and Govers (1996) algorithm and the estimation of this factor is limited to a maximum slope angle of 50% (26.6°) [*Panagos et al.*, 2015 (e)]. Figure 5.26 shows the slope length and steepness factor (LS-factor) in the north of Italy provided by the ESDAC.

It follows from this analysis in particular that the RUSLE factors estimated in paragraph 5.3 are similar to the factors proposed by the ESDAC in the Guerna catchment; they have the same order of magnitude, despite the formers are always higher than the latters. Higher differences are especially visible in C-factor and LS-factor values. This result makes sense because of the DEM higher resolution adopted, a more accurate creation of the land use map and the more specific analysis of the soil properties in paragraph 5.3.

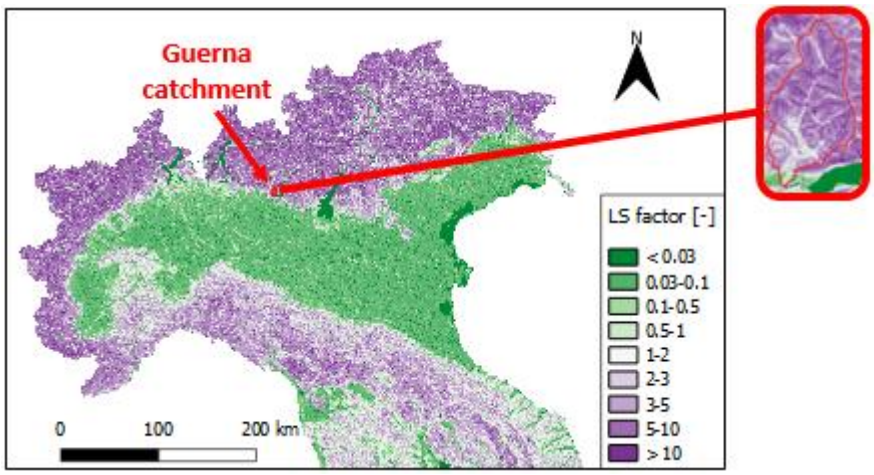

***Figure 5.26 – Slope length and steepness factor (LS-factor) in the Europe Union (north of Italy*). [*https://esdac.jrc.ec.europa.eu/*]**

5.4. Application of the EPM method

The EPM (Erosion Potential Model) method [*Gavrilovic*, 1988] is an empirical semi-distributed model to estimate the mean annual volumes of soil erosion and sediment yield at the basin scale. This method is described in paragraph 4.3.1.3.

The first step in implementing the EPM method is to create a map of the coefficient of erosion *Z*, using Equation (4.22). This coefficient has a spatial variability in the study area because it was calculated using QGIS and considering spatial variability of the terms in Equation (4.22).

Land use coefficient X_a was achieved by associating a value to each area in the land use map (Figure 5.6), as shown in Table 5.5:

Land use description	***Land use coefficient X_a [-]***
Woods, reforestations and forests	0.125
Grasslands	0.40
Agricultural areas	0.70
Orchards and vineyards	0.70
Urban areas	0.50
Bare areas	0.90

***Table 5.5 – Land use coefficient X_a* [*Milanesi et al.*, 2015]**

Coefficient of soil resistance to erosion *Y* was obtained by associating a value to each area in the lithological map (Figure 5.4), as shown in Table 5.6:

Lithological description	***Coefficient of soil resistance to erosion Y [-]***
Slope debris and landslides	1.30
Sandstones, marls and conglomerates	1.10
Gravel and sand	2.00
Limestones, marly limestones and flint limestones	1.20
Gravel blocks and ferritisation silt	1.40
Limestones and dolomite limestones	0.90

***Table 5.6 – Coefficient of soil resistance to erosion Y* [*Milanesi et al.,* 2015]**

The **coefficient value for the observed erosion process φ** was obtained by associating a value to each area in the hydrogeological instability map (Figure 5.5), as shown in Table 5.7:

Hydrogeological instability description	***Coefficient value for the observed erosion process φ [-]***
Unstable waterway, with active lateral erosion or with very intense erosive processes on the bottom	0.80
Area with pasture footprints footprints	0.80
Area without visible erosion effects, that is mainly occupied by undergrowth and crop fields	0.15
Area with debris or terrigenous cover in a state of limit equilibrium	0.70
Area with landslide	0.80
Alluvial cone	0.70
Area with gully erosion	0.90
Area with landslides and gully erosion	0.90
Area with rill erosion	0.80

***Table 5.7 –Coefficient value for the observed erosion process φ* [*Milanesi et al.,* 2015]**

In Figure 5.27 the **coefficient of erosion (*Z*)** map obtained by applying Equation (4.22) in a GIS environment is illustrated:

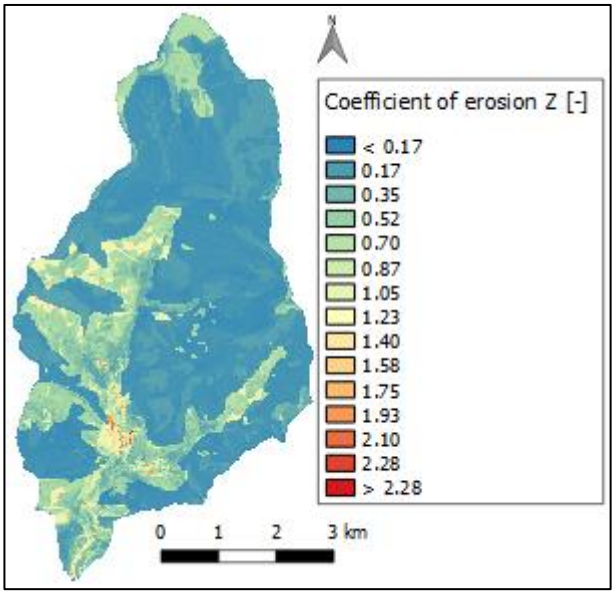

Figure 5.27 – Guerna catchment coefficient of erosion (Z) map

The mean annual amount of precipitation *H* and the temperature coefficient *T* are needed in order to solve Equation (4.20) and to find the average annual specific production of sediments (W_{sp}).

The **mean annual amount of precipitation (*H*)** was considered constant over the entire study area and it has a value of 1100.63 mm/year. This value was calculated using daily precipitation data from year 2005 to year 2016, recorded by the monitoring station located at Sarnico (BG) and managed by ARPA LOMBARDIA.
[*http://www.arpalombardia.it/Pages/ARPA_Home_Page.aspx*]

Figure 5.28 shows the mean monthly amount of precipitations at Sarnico station:

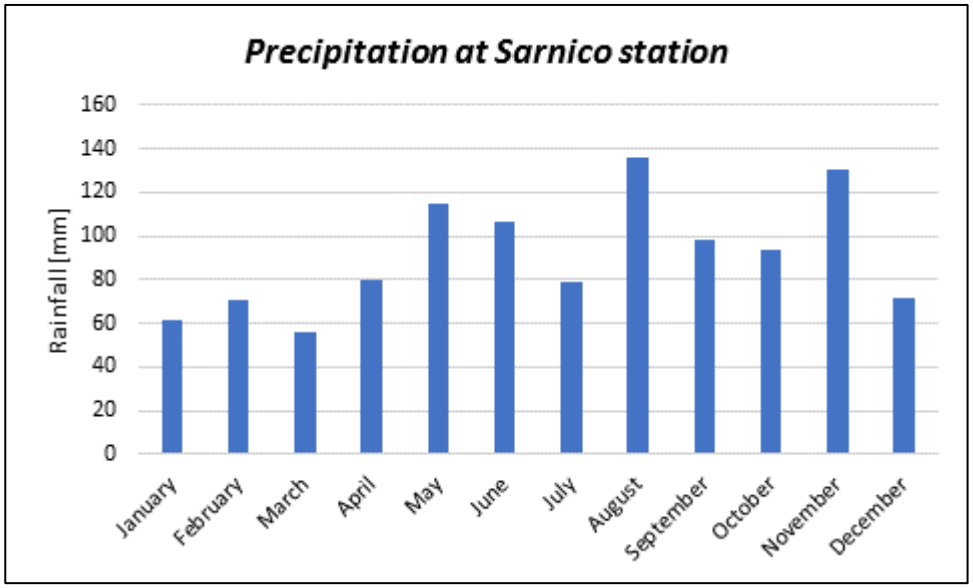

Figure 5.28 – Mean monthly amount of precipitations at Sarnico station (2005-2016) **[ARPA LOMBARDIA]**

The **temperature coefficient (*T*)** was calculated by Equation (4.21), taking into account its spatial variability. A linear trend of temperature as a function of altitude was assumed by the use of the DEM (Figure 5.3 (a)). Using daily temperature data from year 2005 to year 2016 provided by ARPA LOMBARDIA at Sarnico station ($h_{Sarn.}$ = 197 m a.s.l.) and at Ranzanico station ($h_{Ranz.}$ = 512 m a.p.s.), it was possible to find monthly temperatures in Sarnico (BG) and Ranzanico (BG) (Figure 5.30) and then to use them in order to calculate the slope of the straight line equation for each month, where *t* is the mean monthly temperature (Equation (5.5)). Figure 5.29 shows the location of the Sarnico and Ranzanico station.

Figure 5.29 – Location of Sarnico (BG) and Ranzanico (BG) monitoring stations

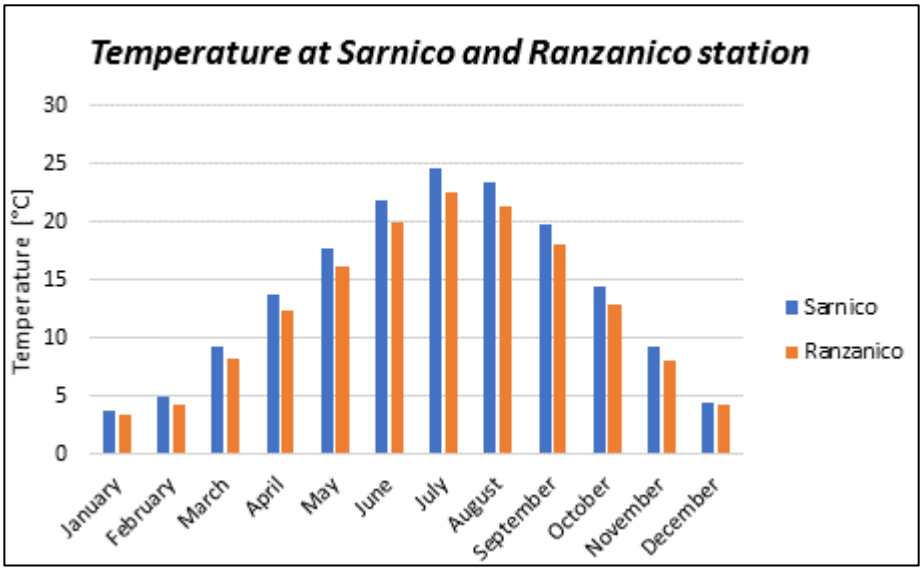

Figure 5.30 – Mean monthly temperature at the Sarnico (BG) and Ranzanico (BG) stations

$$Slope_{ith-month} = \frac{(t_{Sarn.})_{ith-month} - (t_{Ranz.})_{ith-month}}{(h_{Sarn.}) - (h_{Ranz.})} \quad \textbf{(5.5)}$$

The slope of the straight line equation for each month was used to create a monthly temperature map (t_{MAP}) with a spatial variability for each month. The following equation was solved in a GIS environment:

$$(t_{MAP})_{ith-month} = (Slope_{ith-month})(DEM - h_{Sarn.}) + (t_{Sarn.})_{ith-month} \quad \textbf{(5.6)}$$

where *DEM* is the Digital Elevation Model (Figure 5.3 (a)).

The 12 monthly temperature maps were used to create the mean annual temperature map $(t_{MAP})_{mean\ anuual}$ with a spatial variability, solving the following equation in QGIS:

$$(t_{MAP})_{mean\ annual} = \frac{1}{12}\sum_{ith=1}^{12}(t_{MAP})_{ith-month} \quad \textbf{(5.7)}$$

The mean annual temperature map was used in order to solve Equation (4.21) in the GIS environment and to create the map of temperature coefficient (Figure 5.31), which has a spatial variability.

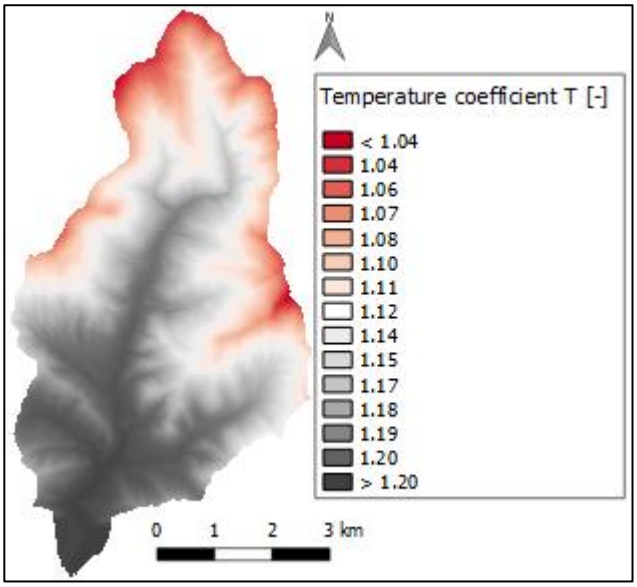

Figure 5.31 – Guerna catchment temperature coefficient (T) map

The temperature coefficient map was used in order to solve Equation (4.20) and Equation (4.23) in a GIS environment and to create the map of average annual production of erosional

sediment (Figure 5.32), which has a spatial variability. In Equation (4.23), *A* is the DEM cell area (*A* = 0.000025 km^2).

The **mean value (W_{g_mean})** and the **total value (W_{g_tot})** in the Guerna catchment of computed soil loss are the following:

- W_{g_mean} = 0.024 m^3/(cell·year)
- W_{g_tot} = 30263.6 m^3/year

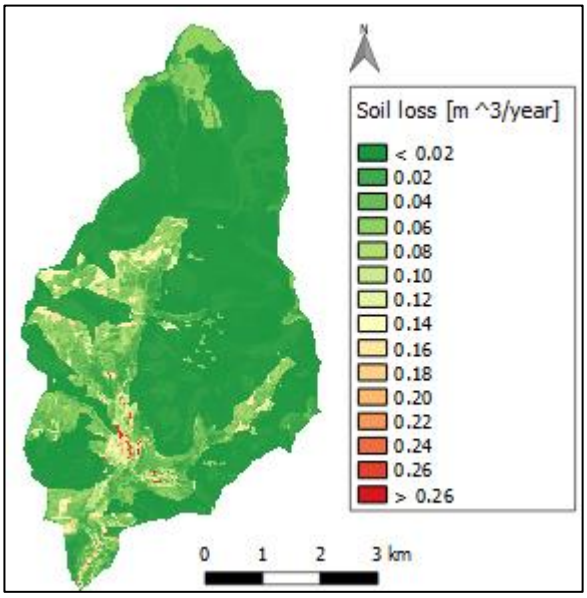

Figure 5.32 – Guerna catchment: map of average annual production of erosional sediment (W_g)

5.5. Application of the RUSLE model considering the impact of climate change

Different climate change scenarios were considered in order to tentatively assess the impact on water erosion on a small basin scale. The most important variable in the RUSLE model affecting the climate system is the annual amount of precipitation.

In this paragraph the computed soil loss (*A*) was estimated by solving in a GIS environment Equation (4.2), as in paragraph 5.3, but changing the rainfall-erosivity factor (*R* factor) according to climate change. The *R* factor represents the climate erosivity because it defines the total annual erosive potential that is due to climatic effects.

CORDEX data were used in order to consider the impact of climate change in the future and the following elements were chosen:

- access data: *ESGF infrastructure*
- node: *SMHI-NSC, Sweden*
- driving model (GCM): *ICHEC-EC-EARTH*
- Regional Climate Model (RCM): *RCA4*
- domain: *EUR-11i*
- climate scenarios or climate projections: *RCP 2.6* (from 2041 to 2060)*, RCP 4.5* (from 2041 to 2060)*, RCP 8.5* (from 2041 to 2060) and *historical scenario* (from 1986 to 2005)

For more details on CORDEX experiments and on the elements that were chosen, refer to paragraph 4.5.1.

CORDEX delivers dataset about different parameters (precipitation, temperature, moisture, etc.) in specific points, which are organised in a grid. In this case, precipitation is the relevant parameter: monthly rainfall from 2041 to 2060 (considering different climate scenarios) is known in each point of the grid.

Figure 5.33 shows the "RCM grid point" (the yellow points) and the green arrow indicates the relevant point belonging to the Guerna watershed in the grid: precipitation data for different climate scenarios, corresponding to this point, were considered to evaluate climate change.

The historical simulation has to be investigated since this type of experiment is not synchronised with the observed climate. By the comparison with historical and future simulation (RCP 2.6, RCP 4.5, RCP 8.5) shown in Figure 5.34, a coefficient (*J*) was derived, which was then applied to actual (observed) climate data in order to evaluate climate change. Actual data was provided by "Consorzio dell'Oglio" and they were used in paragraph 5.3 to estimate the *R* factor (without considering climate change).

Figure 5.33 – RCM grid points

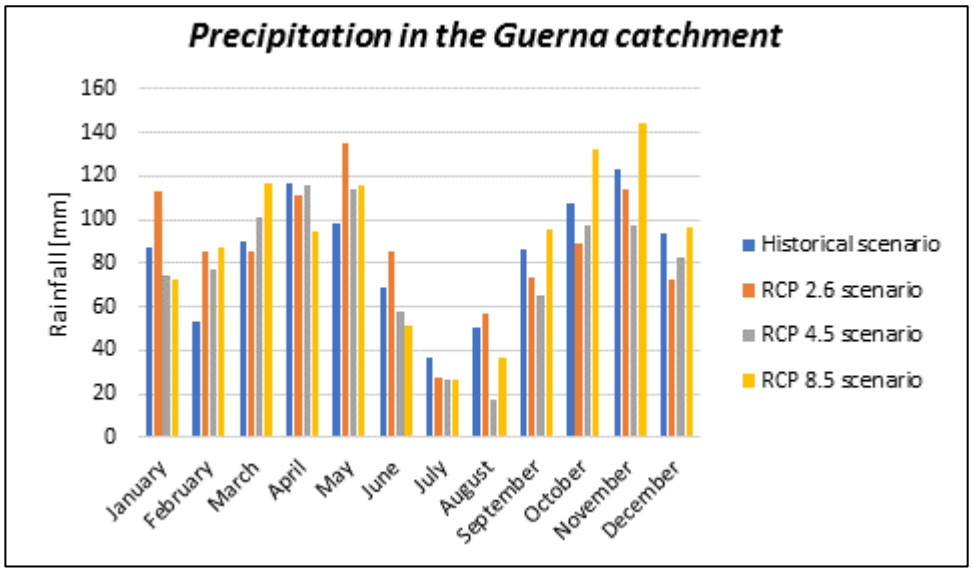

Figure 5.34– Results of historical and future simulations (mean monthly precipitation)

J coefficient was determined by the following equation:

$$J_{ith-month} = \frac{(h_{future\_scenario})_{ith-month}}{(h_{historical\_scenario})_{ith-month}} \quad \textbf{(5.8)}$$

where *h* is the mean monthly precipitation shown in Figure 5.34 for different scenarios.

J coefficient [-]			
Month	**RCP 2.6 scenario**	**RCP 4.5 scenario**	**RCP 8.5 scenario**
January	1.29	0.85	0.83
February	1.59	1.44	1.64
March	0.95	1.12	1.29
April	0.96	0.99	0.81
May	1.37	1.16	1.18
June	1.23	0.84	0.74
July	0.74	0.73	0.72
August	1.12	0.34	0.72
September	0.85	0.76	1.11
October	0.82	0.90	1.23
November	0.92	0.79	1.17
December	0.78	0.88	1.03

Table 5.8 – J coefficients

J is the multiplicative coefficient, which was applied to the observed rainfall data from year 2008 to year 2011 and provided by "Consorzio dell'Oglio": the aim is to consider climate change. These are the same rainfall data that were used in paragraph 5.3 in order to calculate the *R* factor without considering climate change.

After projecting precipitation data in the future climate, a new **R factor** value for each scenario was estimated, using the same procedure applied in paragraph 5.3, as defined in paragraph 4.3.1.1:

- *RCP 2.6 scenario:* *R factor = 2681 MJ·mm/(ha·h·year)*
- *RCP 4.5 scenario:* *R factor = 1616 MJ·mm/(ha·h·year)*
- *RCP 8.5 scenario:* *R factor = 2510 MJ·mm/(ha·h·year)*

The evaluation of the other factors (**K factor**, **LS factor**, **C factor** and **P factor**) required for the implementation of the RUSLE model did not account for climate change. Therefore, the values reported in paragraph 5.3 were used.

Computed soil loss *A* was calculated by solving in a GIS environment Equation (4.2) and considering 3 different future scenarios (Figure 5.35).

The **mean value ($A_{\_mean}$)** and the **total value ($A_{\_tot}$)** in the Guerna catchment of computed soil loss in future scenarios are shown in Table 5.9, where "cell" is the cell of the DEM (resolution: 5x5 m):

Future scenario	$A_{\_mean}$ *[t/(ha·year)]*	$A_{\_mean}$ *[t/(cell·year)]*	$A_{\_tot}$ *[t/(year)]*
RCP 2.6	99.9	0.25	308889.9
RCP 4.5	60.3	0.15	186186.5
RCP 8.5	93.6	0.23	289188.2

Table 5.9 – Computed soil loss considering different future scenarios

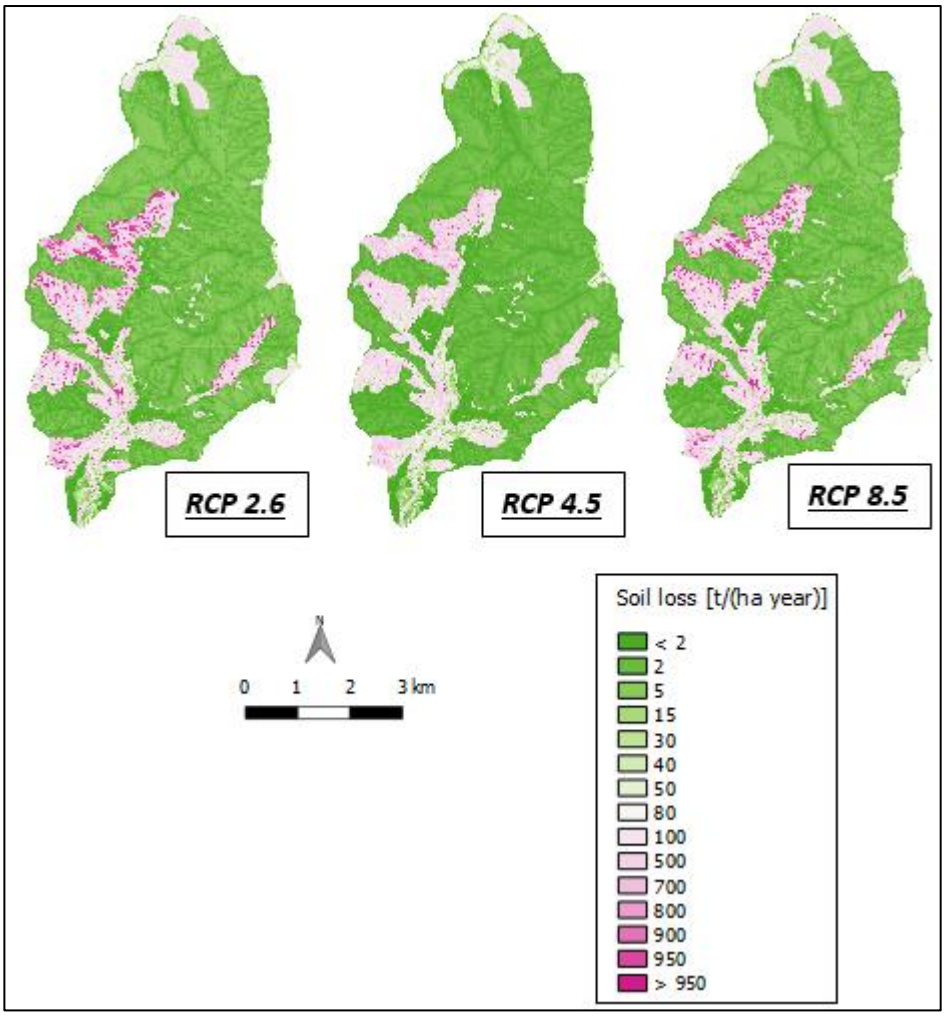

Figure 5.35 – Guerna catchment: map of computed soil loss (A) considering future scenario RCP 2.6, RCP 4.5 and RCP 8.5

5.6. Application of the EPM method considering the impact of climate change

Different climate change scenarios were considered in order to tentatively assess the impact on water erosion on a small basin scale. The most important variables in the EPM method affecting the climate system are the annual amount of precipitation and the mean annual temperature.

In this paragraph the average annual production of erosional sediment (W_g) was estimated by solving in a GIS environment Equation (4.20) and Equation (4.23), as in paragraph 5.4, but changing the mean annual amount of precipitation (H) and the temperature coefficient (T) according to climate change.

Just as in the case of the RUSLE model application (paragraph 5.5), CORDEX data were used in order to consider the impact of climate change in the future and the following elements were chosen:

- access data: *ESGF infrastructure*
- node: *SMHI-NSC, Sweden*
- driving model (GCM): *ICHEC-EC-EARTH*
- Regional Climate Model (RCM): *RCA4*
- domain: *EUR-11i*
- climate scenarios or climate projections: *RCP 2.6* (from 2041 to 2060)*, RCP 4.5* (from 2041 to 2060)*, RCP 8.5* (from 2041 to 2060) and *historical scenario* (from 1986 to 2005)

For more details on CORDEX experiments and on the elements that have been chosen, refer to paragraph 4.5.1.

CORDEX delivers dataset about different parameters (precipitation, temperature, moisture, etc.) in specific points, which are organised in a grid. In this model, both precipitation and temperature information are relevant: monthly rainfall and monthly temperature from 2041 to 2060 (considering different climate scenarios) are known in each point of the RCM grid.

Figure 5.36 shows the "RCM grid points" (the yellow points) and the green arrow indicates the relevant point (point 1.1) belonging to the Guerna watershed in the grid: precipitation data for different climate scenarios, corresponding to point 1.1, were considered to evaluate climate change. Data corresponding to grid point 2.1 (indicated by the orange arrow) were useful to estimate temperature coefficient (T) in future simulations considering climate change, as it is further explained.

Just as in the case of the RUSLE model application (paragraph 5.5), the historical simulation has to be investigated since this type of experiment is not synchronised with the observed climate. By the comparison with historical and future simulation (RCP 2.6, RCP 4.5, RCP 8.5) shown in Figure 5.34, a coefficient (J) was derived shown in Table 5.8. The J coefficient was

applied to actual (observed) climate data in order to evaluate climate change. Actual data were provided by ARPA LOMBARDIA and they were used in paragraph 5.4 to estimate the mean annual amount of precipitation *H* (without considering climate change).

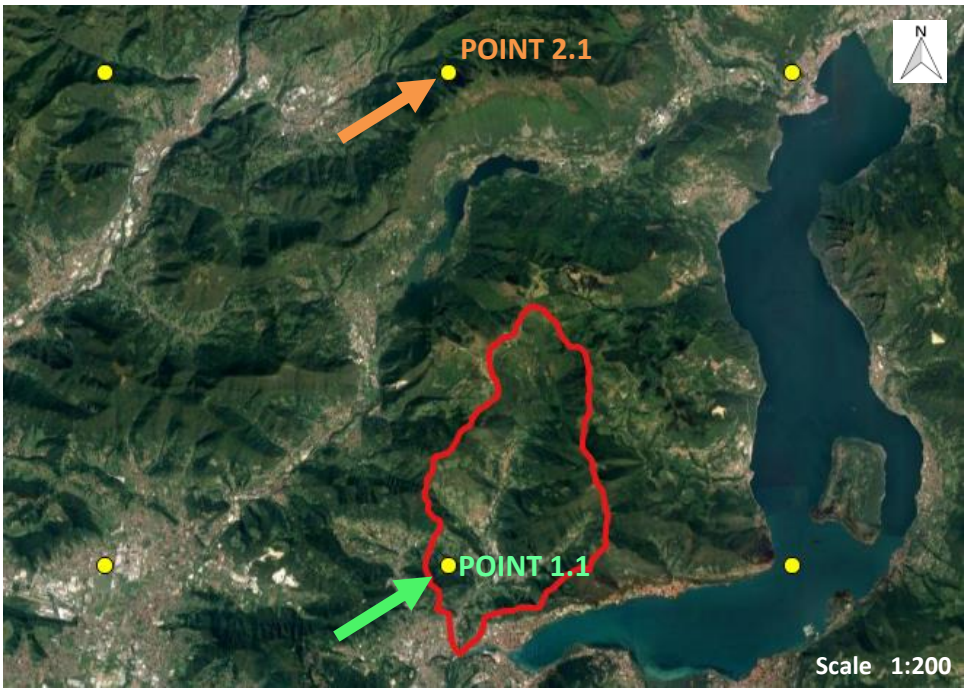

Figure 5.36 – RCM grid points

J is the multiplicative coefficient, which was applied to the observed rainfall data from year 2005 to year 2016 and provided by ARPA LOMBARDIA (Figure 5.28): the aim is to consider climate change. These are the same rainfall data that were used in paragraph 5.4 in order to calculate the mean annual amount of precipitation *H* without considering climate change.

After having found the new monthly rainfall data (applying the *J* coefficient in order to consider climate change), a new **mean amount of precipitation H** for each scenario was estimated, using the same procedure applied in paragraph 5.4. The results are shown below and in Figure 5.37.

- *RCP 2.6 scenario:* *H = 1161 mm/(year)*
- *RCP 4.5 scenario:* *H = 951 mm/(year)*
- *RCP 8.5 scenario:* *H = 1125 mm/(year)*

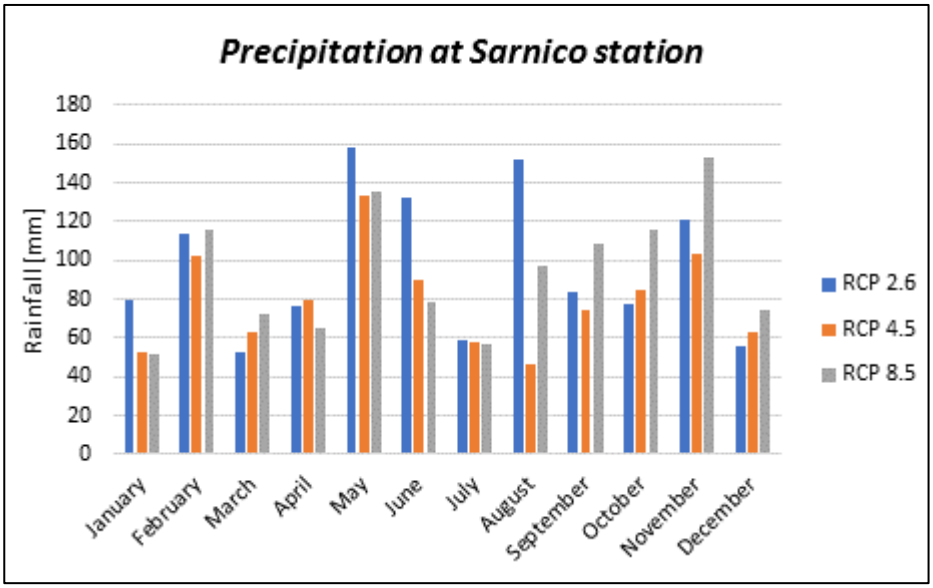

Figure 5.37 – Mean monthly amount of precipitation considering the impact of climate change for different scenarios (EPM method)

Another important variable in the EPM method affecting climate change is the mean annual temperature, and then the temperature coefficient (*T*).

The **temperature coefficient (*T*)** was calculated by Equation (4.21), taking into account its spatial variability, likewise the previous case without climate change (paragraph 5.4). A linear trend of temperature as a function of altitude was assumed; the altitude value at each catchment point is known through the DEM (Figure 5.3 (a)).

The first step is to calculate the temperature difference $\overline{\Delta t}$, which is essential to evaluate climate change. Using daily temperature data from year 2041 to year 2061 (for RCP 2.6, RCP 4.5, RCP 8.5 scenarios) and from 1986 to 2005 (for the historical scenario) provided by CORDEX experiment at point 1.1 ($h_{1.1.}$ = 433.8 m a.s.l.) (see Figure 5.36), it was possible to find monthly temperatures at point 1.1 (Figure 5.38). These values were used to calculate the temperature difference $\overline{\Delta t}$ (Table 5.10):

$$\overline{\Delta t}_{ith-month} = (\bar{t}_{ith-month})_{RCP\ scenario} - (\bar{t}_{ith-month})_{historical\ scenario} \qquad \textbf{(5.9)}$$

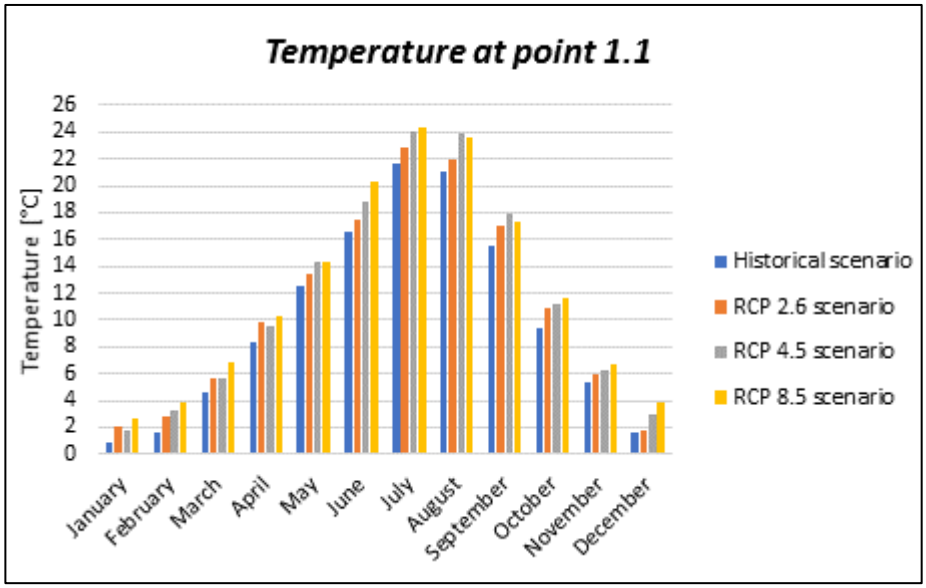

Figure 5.39 – Mean monthly temperature ($\bar{t}$) at point 1.1 provided by the CORDEX experiment for future and historical scenarios

Month	***Temperature difference $\overline{\Delta t}$ [°C] at point 1.1***		
	RCP 2.6 scenario	**RCP 4.5 scenario**	**RCP 8.5 scenario**
January	1.36	1.00	1.91
February	1.16	1.62	2.30
March	1.13	1.07	2.37
April	1.43	1.20	1.90
May	0.78	1.70	1.72
June	0.84	2.22	3.71
July	1.22	2.48	2.71
August	0.97	2.99	2.61
September	1.48	2.37	1.79
October	1.49	1.74	2.15
November	0.65	0.91	1.38
December	0.19	1.32	2.24

Table 5.10 – Temperature difference between future and historical scenarios

Due to the linear trend of temperature (as a function of altitude), the second step is to calculate the slope of the straight line equation for each month, where $\bar{t}$ is the mean monthly temperature at point 1.1 and at point 2.1:

$$\overline{Slope}_{ith-month} = \frac{(\bar{t}_{point\ 1.1.})_{ith-month} - (\bar{t}_{point\ 2.1.})_{ith-month}}{(h_{1.1.}) - (h_{2.1})} \quad \textbf{(5.10)}$$

The grid point 2.1 location is indicated in Figure 5.36 ($h_{2.1.}$ = 796.6 m a.s.l.). The mean monthly temperatures at point 1.1 ($\bar{t}_{point\ 1.1.}$) are shown in Figure 5.39 and the mean monthly temperatures at point 2.1 ($\bar{t}_{point\ 2.1.}$), provided by the CORDEX experiment, are shown in Figure 5.40:

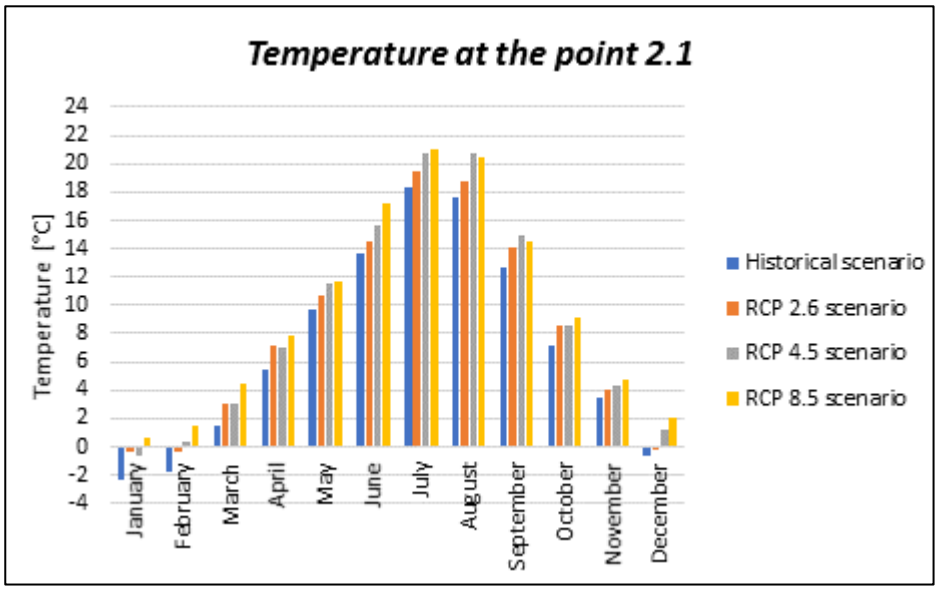

Figure 5.40 – Mean monthly temperature ($\bar{t}$) at point 2.1 provided by the CORDEX experiment for future and historical scenarios

The third step is to use Equation (5.6), in order to find the monthly "actual" temperature *t* at point 1.1 (not in the study area as a whole). Therefore, *t* values are not provided by CORDEX experiment:

$$(t_{point\ 1.1})_{ith-month} = (Slope_{ith-month})(h_{1.1} - h_{Sarn.}) + (t_{Sarn.})_{ith-month} \quad \textbf{(5.11)}$$

The results are shown in the following histogram:

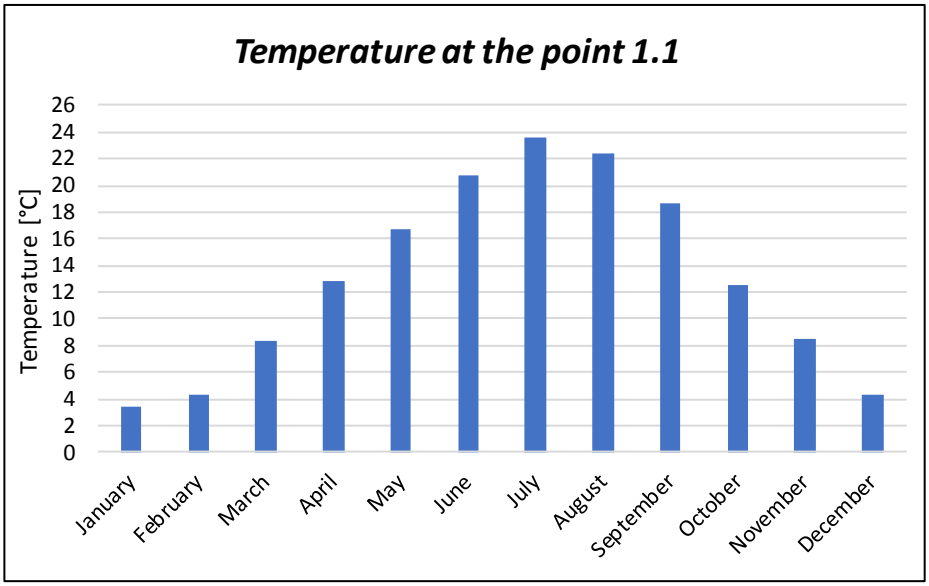

Figure 5.41 – Mean monthly temperatures (t) at point 1.1 produced by the solution of linear equation

Information obtained from previous steps (the temperature difference $\overline{\Delta t}$, the slope of the straight line equation for each month $\overline{Slope}_{ith-month}$ and the monthly "actual" temperature *t* at point 1.1) were used to create a monthly temperature map $(t_{MAP\_CC})_{ith\text{-}month}$ with a spatial variability for each month. The following equation was solved in a GIS environment:

$$(t_{MAP\_CC})_{ith-month} = (\overline{Slope}_{ith-month})(DEM - h_{1.1}) + \left(t_{point\ 1.1} + \overline{\Delta t}\right)_{ith-month} \quad \textbf{(5.12)}$$

where *DEM* is the Digital Elevation Model (Figure 5.3 (a)).

The 12 monthly temperature maps were used to create a mean annual temperature map $(t_{MAP\_CC})_{mean\ anuual}$ (with a spatial variability and considering climate change) solving the following equation in QGIS:

$$(t_{MAP\_CC})_{mean\ annual} = \frac{1}{12}\sum_{ith=1}^{12}(t_{MAP\_CC})_{ith-month} \quad \textbf{(5.13)}$$

The mean annual temperature map $(t_{MAP\_CC})_{mean\ annual}$ was determined by considering each of the future scenarios (RCP 2.6, RCP 4.5, RCP 8.5); it was used in order to solve Equation (4.21) in a GIS environment and to create a map of temperature coefficient (Figure 5.42), which has a spatial variability.

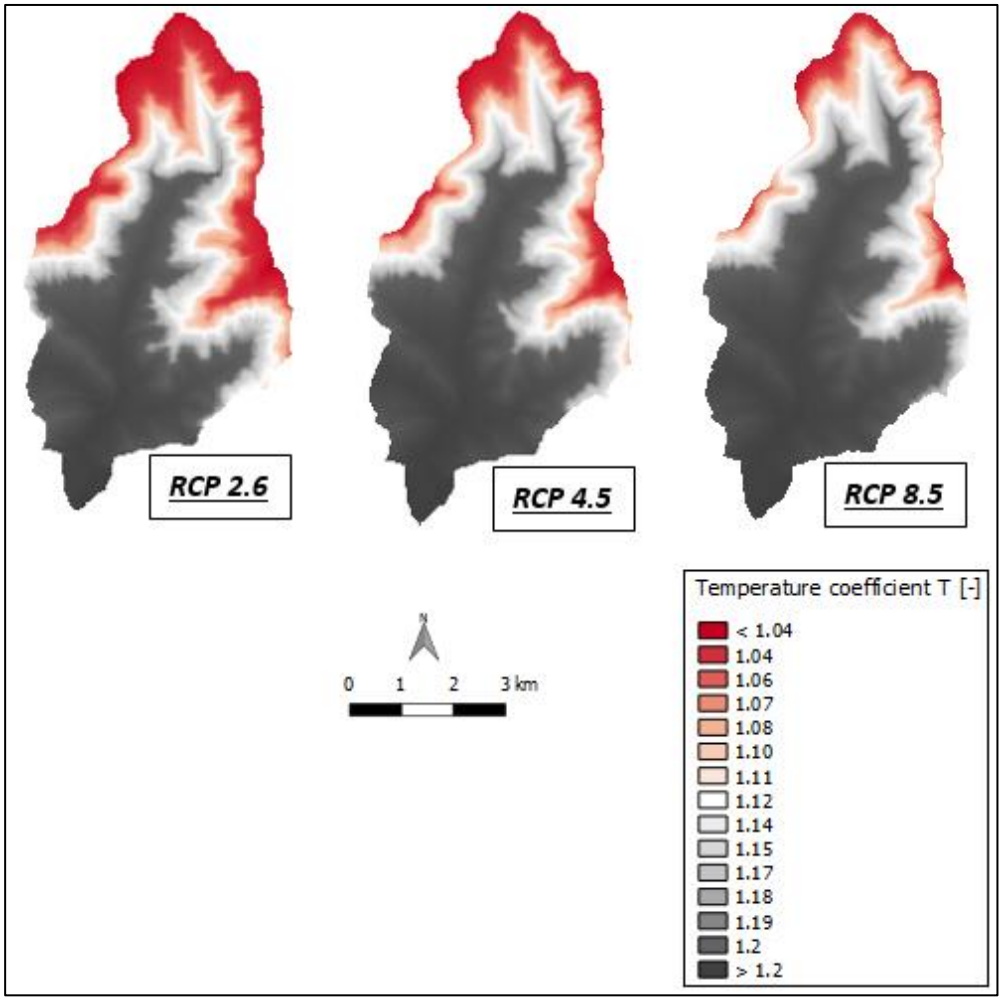

Figure 5.42 – Guerna catchment temperature coefficient (T) map considering future scenario RCP 2.6, RCP 4.5 and RCP 8.5

The **coefficient of erosion Z** implementing the EPM method has no changes, compared with the case without climate change in paragraph 5.4.

The map of average annual production of erosional sediment W_g was calculated by solving in a GIS environment Equation (4.20) and Equation (4.23), considering 3 different future scenarios (Figure 5.43). In Equation (4.23), A is the DEM cell area (A = 0.000025 km^2).

The **mean value (W_{g_mean})** and the **total value (W_{g_tot})** in the Guerna catchment of computed soil loss in future scenarios, are shown in Table 5.11:

Future scenario	***W_{g_mean} [m³/(cell·year)]***	***W_{g_tot} [m³/(year)]***
RCP 2.6	0.026	32581.7
RCP 4.5	0.022	27305.7
RCP 8.5	0.027	32913.3

Table 5.11 – Production of erosional sediment considering different future scenarios

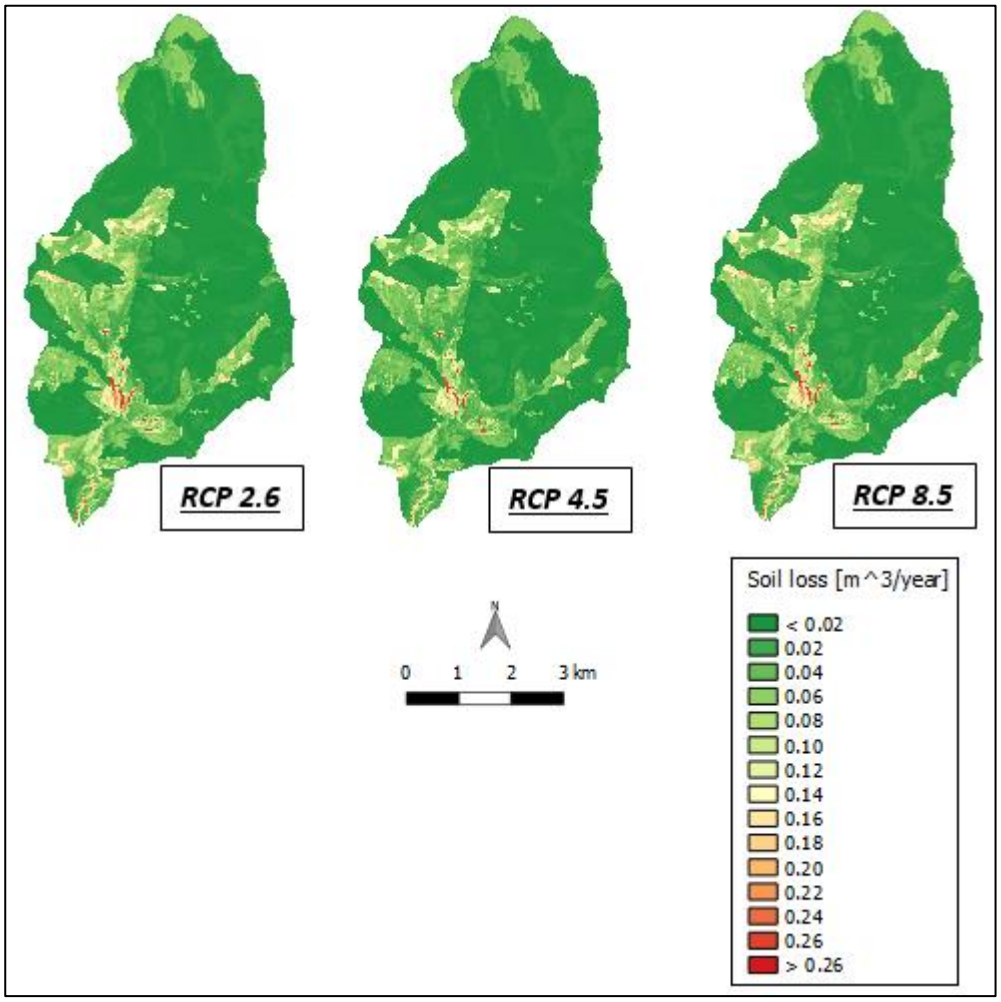

Figure 5.43 – Guerna catchment: map of average annual production of erosional sediment (W_g) considering future scenario RCP 2.6, RCP 4.5 and RCP 8.5

5.7. The effect of climate change on land use

In paragraphs 5.5 and 5.6, the computed soil loss considering the effects of climate change was estimated by solving in a GIS environment Equation (4.2) and Equation (4.23), respectively for the RUSLE (paragraph 5.5) and EPM method (paragraph 5.6).

As regards the RUSLE method, the computed soil loss (*A*) was calculated by changing only the rainfall-erosivity factor (*R* factor) according to climate change. On the other hand, considering the EPM equation, the average annual production of erosional sediment (W_g) was estimated by changing only the mean annual amount of precipitation (*H*) and the temperature coefficient (*T*) considering the impact of climate change. Therefore, in both cases, the future variations of the cover management factor were omitted.

Bosco et al. (2008) conducted a study to estimate actual erosion using the RUSLE method over the whole alpine space. They analysed soil erosion trends in different IPCC scenarios. Even in this study, the factor *K*, *LS* and *C* coincided with the ones used for actual erosion estimation (without considering climate change). In that regard, they claimed, first, that soil erosion trends in the alpine region are mainly attributable to changes in rainfall regimes; only a better estimation of soil losses in climate change scenarios could be assured by evaluating future variations of the cover management factor [*Bosco et al.*, 2008]. In Vietnam, for example, the rainfall factor is the most important among the factors affecting soil erosion [*Le et al.*, 2009]. The Guerna basin is located in an alpine region and then, in accordance with Bosco et al. (2008), only rainfall and temperature regime were considered to evaluate the effects of climate change on water erosion.

The land use over time in the Guerna catchment was analysed in order to understand the changes which have taken place over the past years. This operation was implemented by the comparison between the land use map in 1954 and the land use map in 2015; both maps were made available by "Geoportale della Lombardia".
[*http://www.geoportale.regione.lombardia.it/*]

The name of the shapefile that describes the land use map in 1954 is "Uso del suolo storico (1954)" and it was made by using photo-interpretation of the GAI (Gruppo Aereo Rilevatore) flight. The information content was produced by ERSAF (Ente Regionale per i Servizi all'Agricoltura e Foreste) in the context of a project supported and financed by "Direzioni Generali Territorio e Urbanistica, Agricoltura e Sistemi Verdi e Paesaggio di Regione Lombardia". The name of the shapefile that describes the land use map in 2015 is "DUSAF (Destinazione d'Uso dei Suoli Agricoli e Forestali) 5.0 – Uso del suolo 2015" and it was made by using aerophotogrammetry AGEA (AGenzia per le Erogazioni in Agricoltura) 2015. The update of the map, compared to the previous versions of DUSAF, was developed by ERSAF (Ente Regionale per I Servizi all'Agricoltura e Foreste) in the context of the implementation project financed by "Direzione generale Agricoltura" in 2015-2016.
[*http://www.geoportale.regione.lombardia.it/*]

The analysis established that most of the Guerna catchment area is covered by forest (broadleaved forests, coniferous forests, mixed forests dominated by coppice formations, riparian forests) and bushes (with the significative presence of high and arboreal shrub species), both in 1954 and in 2015 (Figure 5.44). In particular, the most recurrent type of tree that remains in the forest in time, is the broadleaved tree.

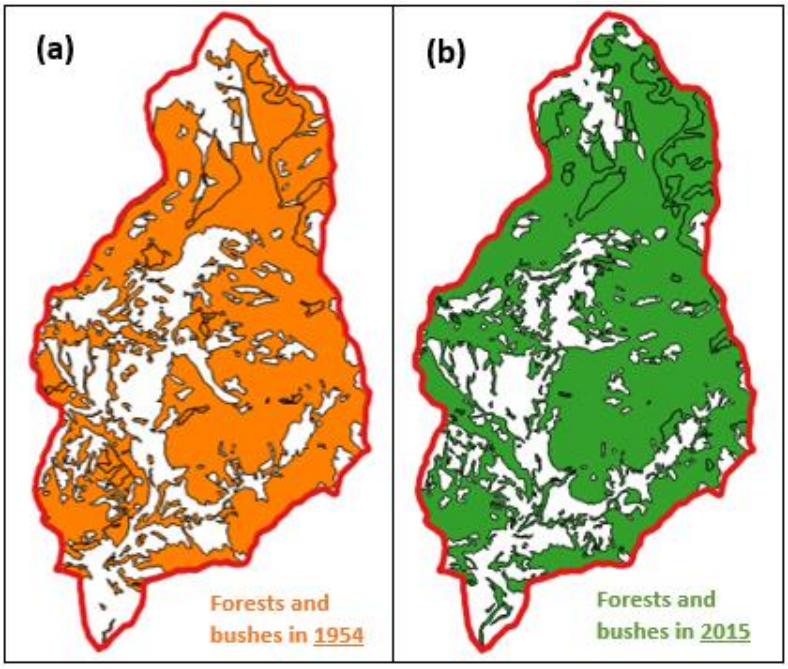

Figure 5.44 – Forests and bushes in the Guerna catchment, in year 1954 (a) and in year 2015 (b)

Figure 5.45 shows that the areas occupied by forests and bushes are very similar considering the year 1954 and the year 2015.

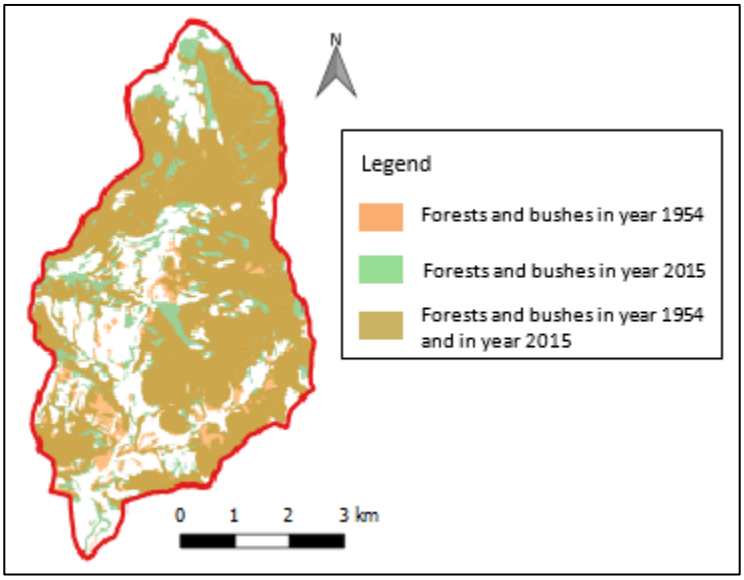

Figure 5.45 – Overlapping of forests and bushes in year 1954 and in year 2015 in the Guerna catchment

The green areas ("Forests and bushes in year 2015") in Figure 5.45 are the areas covered by forests and bushes only in year 2015. From the analysis of the land use map ("Uso del suolo storico (1954)"), it emerged that in year 1954 those areas were primarily occupied by grasslands and by sparse vegetation arable lands, vineyards and chestnut trees. The orange areas ("Forests and bushes in year 1954") in Figure 5.45 are the areas covered by forests and bushes only in year 1954. From the analysis of the land use map (DUSAF 5.0 – Uso del suolo 2015), it was found that in year 2015 those areas were occupied by farms, residential areas, industrial establishments, road networks and sport facilities and by a minor part of grasslands, vineyards, olive trees and arable lands. The green areas and the orange areas in Figure 5.45 cover respectively about 3.4 km^2 and 1.5 km^2. It can thereby be stated that there was an increase of around 1.9 km^2 of forests and bushes in year 2015, compared with year 1954. The brown areas ("Forests and bushes in year 1954 and in year 2015") in Figure 5.45, that cover most of the Guerna catchment, show the places covered by forests and bushes both in year 1954 and in year 2015.

As resulting from Table 5.3 and Table 5.5, the presence of forests and bushes mitigates water erosion more than grasslands, agricultural areas, orchards and vineyards; the water erosion in urban area (residential areas, industrial establishments, road networks, etc.) is instead highly similar to that occupied by forests and bushes. However, also orchards and vineyards can reduce water erosion because of their *P* factor value (see Table 5.4).

One example of assessment of land use change scenarios was made in the Lo river basin (Vietnam). In this catchment, major land use classes correspond to agriculture, forest, urban areas and water. Vegetation cover has changed in the last decades, due to deforestation for

agriculture development and forest fires. The land use change that was investigated in this area, assumed the conversion of 20% of forest area into rice and agricultural crops and 15% of forest area into bushed, shrubs and meadows. These cover soil variations showed a 28% increase of sediment load and then it produced a severe impact on sediment production in the Lo basin [*Ranzi et al.*, 2012; *Le et al.*, 2009]. Concerning the Guerna watershed, the land use map analysis showed an approximate 6% increase in forests in the last decades, that protect the soil from water erosion.

Another example of land use consequences on water erosion is given by Nunes et al (2013), which analyzed the changes of runoff and soil erosion in two catchments in Portugal during 2071-2100. They found that erosion rates in one watershed would increase on croplands whereas they would decrease on forest and vineyard lands. Therefore, afforestation is believed to be an efficient way to cambact soil loss under global change [*Li and Fang*, 2016].

The last example, worth to be mentioned, is the Carapelle watershed in Puglia (Southern Italy). Four different BMPs (Best management Practices) scenarios were implemented in the study area; the aim is to quantify soil erosion and to identify specific BMPs for reducing erosion. The investigation established that the reforestation BMP provides the highest specific sediment reduction (ranging from 50% to 99%) and that winter wheat, which corresponds to contour planting BMP, is the higher producer of sediment yield (between 0 and 63.8 $t \cdot ha^{-1} \cdot year^{-1}$] [*Ricci et al.*, 2018].

The above considerations lead to the conclusion that, considering the effects of climate changes, the future variations of the cover management factor in the Guerna watershed can be omitted. Indeed, in the last 60 years there have not been significant transformations in land use, except for a small increase in forests and bushes that slightly reduced water erosion. Therefore, keeping the same cover management factor in future scenarios, improves security.

5.8. Application of the MUSLE model

5.8.1. Guerna catchment

The MUSLE (Modified Universal Soil Loss Equation) model [*Williams*, 1975] is a modified USLE model that can evaluate sediment yield for a single runoff event. This model takes into account runoff which is highly correlated to sediment yield.

In this paragraph the MUSLE model was implemented by solving in a GIS environment Equation (4.2), as in paragraph 5.3, but replacing the rainfall-erosivity factor (*R* factor) with the R_d factor. Therefore, *K* factor, *LS* factor, *C* factor and *P* factor in the MUSLE model were not subjecte to changes, compared to the values obtained in paragraph 5.3, that were used both for the actual and the future climate. The R_d factor was calculated following the outlines in paragraph 4.3.1.2 and it was considered uniform in the Guerna catchment.

The sediment yield was estimated for the 04/09/2011 rainfall event at the Sarnico station, that presents the highest rainfall intensity in year 2011. The rainfall amount of precipitation for each half an hour was provided by "Consorzio dell'Oglio". These data were used to create the hydrograph at the outlet of the Guerna watershed, in order to find the volume of runoff and the peak flow rate and to calculate the R_d factor.

The first step in making the hydrograph, is to estimate the direct runoff depth from storm rainfall depth; to achieve this aim, it was decided to use the Soil Conservation Service-Curve Number (SCS-CN) method [*SCS*, 1972]. This method has several positive characteristics and it has already been used to solve the MUSLE equation, for example in Black Hawk County, USA (see paragraph 4.4). The most important advantages of the method are its simplicity and predictability, its stability and reliance on only one parameter and finally its responsiveness to major-runoff producing watershed properties (soil type, land use, surface condition, etc.) [*Ponce and Hawkins*, 1996].

The **SCS-CN method** assumes a proportionality between soil retention and surface runoff that, after a few mathematical passages, leads to the following expression:

$$\begin{cases} R = \dfrac{(P - I_a)^2}{(P - I_a + S)} & if\ P > I_a \\ R = 0 & if\ P \leq I_a \end{cases} \qquad \textbf{(5.14)}$$

where R is the actual runoff [mm], P is the potential runoff (and therefore it is the precipitation) [mm], I_a is the initial abstraction [mm] and S is the potential maximum retention [mm]:

$$I_a = 0.2 \cdot S \qquad \textbf{(5.15)}$$

$$S = 254\left(\frac{100}{CN} - 1\right) \qquad \textbf{(5.16)}$$

where *CN* is the runoff curve number.

The Antecedent Moisture Condition (AMC) was determined in order to calculate *CN*. There are three levels of AMC (AMC I, AMC II and AMC III). The limits of these three AMC classes are based on the rainfall magnitude of the previous five days and on the season (dormant season and growing season). AMC for determination of curve number is given in Table 5.12.

AMC	**Total Rain in Previous 5 days**	
	Dormant Season	*Growing Season*
I	Less than 13 mm	Less than 36 mm
II	13 to 28 mm	36 to 53 mm
III	More than 28 mm	More than 53 mm

***Table 5.12 – AMC for determination of CN value* [SCS, 1972]**

As regards the 04/09/2011 rainfall event in the Guerna catchment, the rainfall magnitude of the previous five days is 19 mm and, in favour of security, it was decided to take the AMC II class.

A table with different *CN* values for AMC II is given in SCS (1972). In this table, various *CN* values under AMC II are presented on the basis of the land use and the Hydrological Soil Group (HSG). There are four HSG groups, which are identified as A, B, C, and D according to their minimum infiltration rate and runoff potential.

Table 5.13 shows the *CN* values attributed to the different land use areas in the Guerna catchment:

Description	***Area*** **[km²]**	***CN*** **[-]**
Wood, reforestation and forest	20.5	74
Grassland	1.64	71
Agricultural area	6.00	83
Orchard and vineyard	1.07	83
Urban area	1.83	90
Bare area	0.05	90

Table 5.13 – CN values in the Guerna catchment

Using values in Table 5.13, the average weigh on the area of *CN* values was calculated and the result obtained is *CN = 76.8*. This value was used in Equation (5.16) (and therefore in Equation (5.14)) in order to estimate the actual runoff R_d.

Figure 5.46 compares the intensity of the actual runoff, that was calculated using the SCS-CN method, and the intensity of precipitation (or potential runoff) recorded at the Sarnico station for the 04/09/2011 rainfall event.

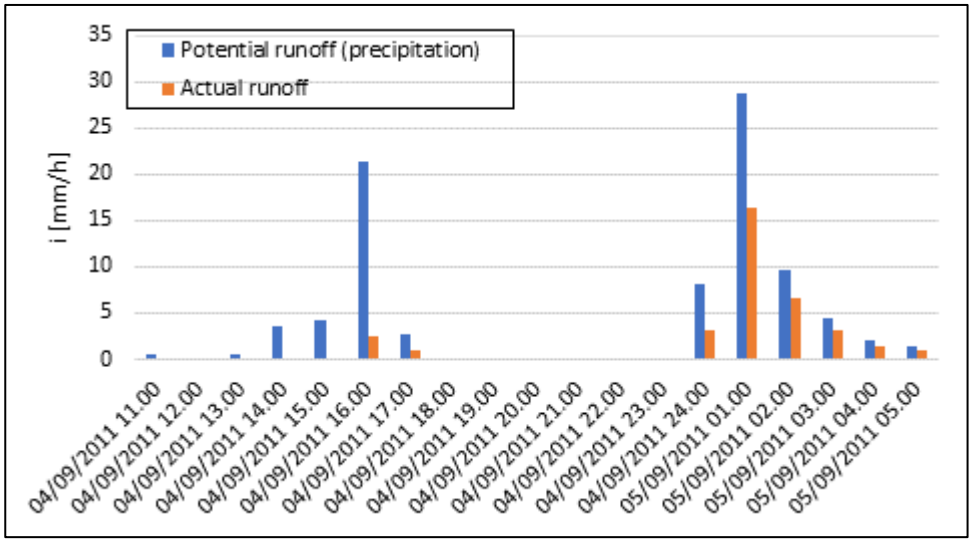

Figure 5.46 – Potential and actual runoff at Sarnico station (04/09/2011 rainfall event)

The intensity of actual runoff values in Figure 5.46 and the time-area curve described in paragraph 5.2.3 were used to create the **runoff hydrograph at the outlet** of the Guerna watershed. The "Time-Area method" was used; this method utilises a convolution of rainfall excess (or actual runoff) hyetograph with a time-area curve representing the progressive area contributions within the catchment in set time increments. Pure translation of the direct runoff (or actual runoff) to the outlet is described using the concept of travel time and it results in an outflow hydrograph that ignores storage effects. Using the time-area curve, the translated inflow hydrograph ordinates (Q_j) for any selected design hyetograph (that is the intensity of actual runoff in Figure 5.46) were determined. Each "block" of actual runoff intensity was applied to the entire Guerna catchment. The simultaneous arrival of the runoff (Q_j) from area A_1, A_2,… for actual runoff intensity I_1, I_2,… was determined by properly lagging and adding contributions. Therefore, Q_j can be generally expressed as:

$$Q_j = I_j \cdot A_1 + I_{j-1} \cdot A_2 + \ldots + I_1 \cdot A_j \qquad \textbf{(5.17)}$$

where Q_j is the flow hydrograph ordinate [m^3/s], I_j is the rainfall excess (or actual runoff) hyetograph ordinates [m/s], A_j is the time-area curve ordinate [m^2] and j is the number of the isochrones contributing to the outlet [*Government of Malaysia*, 2012; *Moisello*, 2003].

Figure 5.47 shows the simulated hydrograph at the Guerna catchment outlet and the hyetograph that caused it.

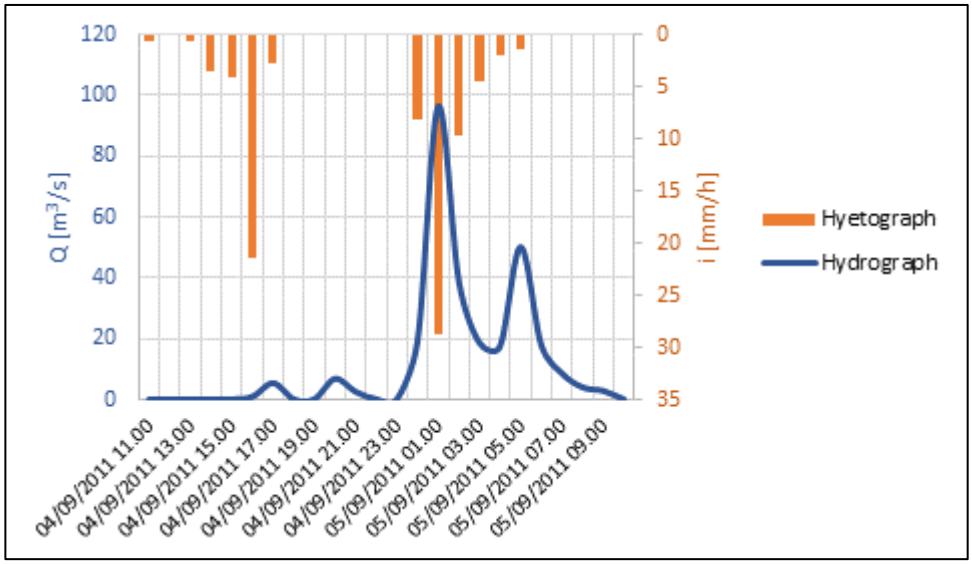

Figure 5.47 – Recorded hyetograph in Sarnico and simulated hydrograph at the outlet (04/09/2011 rainfall event)

The peak flow rate (Q = 96 m^3/s) and the volume of runoff (V = 1036606 m^3) of this flood event in Figure 5.47, were used to calculate the **event runoff factor R_d**. The R_d factor obtained by applying Williams' equation (Equations (4.18)) is R_d = 873 t/(unit K·ha).

It was decided to use Williams' equation (Equations (4.18)) instead of Sadeghi's equation (Equation (4.19)) because Williams made the original form of the equation. Sadeghi used a particular MUSLE model, in order to predict sediment yield in Iranian conditions.

The sediment yield Y_s (Figure 5.48) was calculated by solving Equation (4.17) in a GIS environment.

The **mean value (Y_{s_mean})** and the **total value (Y_{s_tot})** in the Guerna catchment of computed sediment yield, for the flood event that was analysed, are the following:

- Y_{s_mean} = 32.5 t/ha
- Y_{s_tot} = 98880 t

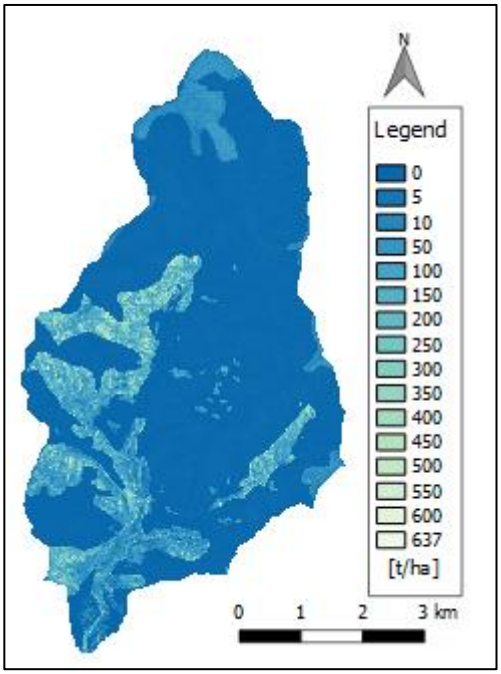

Figure 5.48 – Guerna catchment: map of computed sediment yield (Y_s) applying MUSLE model (04/09/2011 flood event)

5.8.2. Sub-basins identified in the Guerna catchment

The sediment yield for the 04/09/2011 rainfall event was also estimated, using the MUSLE equation, for the 7 sub-basins identified in the Guerna catchment. The sub-basins are shown in paragraph 5.2.3.

The MUSLE model was implemented by solving in a GIS environment Equation (4.17), as in paragraph 5.8.1. Therefore, *K* factor, *LS* factor, *C* factor and *P* factor in the MUSLE model were not subjected to changes, compared to the values obtained in paragraph 5.3. The R_d factor was calculated following the outlines in paragraph 5.8.1 and it was considered uniform in each sub-basin. The hyetograph of actual runoff shown in Figure 5.46 and the time-area curves in paragraph 5.2.3 were used in order to simulate the hydrograph at the outlet of each sub-basin.

The following images (from Figure 5.49 to Figure 5.55) contain the results obtained, where Q_{peak} is the peak flow rate, *V* is the volume of runoff, R_d is the event runoff factor. Y_{s_mean} and Y_{s_tot} are, respectively, the mean value and the total value in the sub-basin of the computed sediment yield calculated by applying the MUSLE model for the flood event analysed.

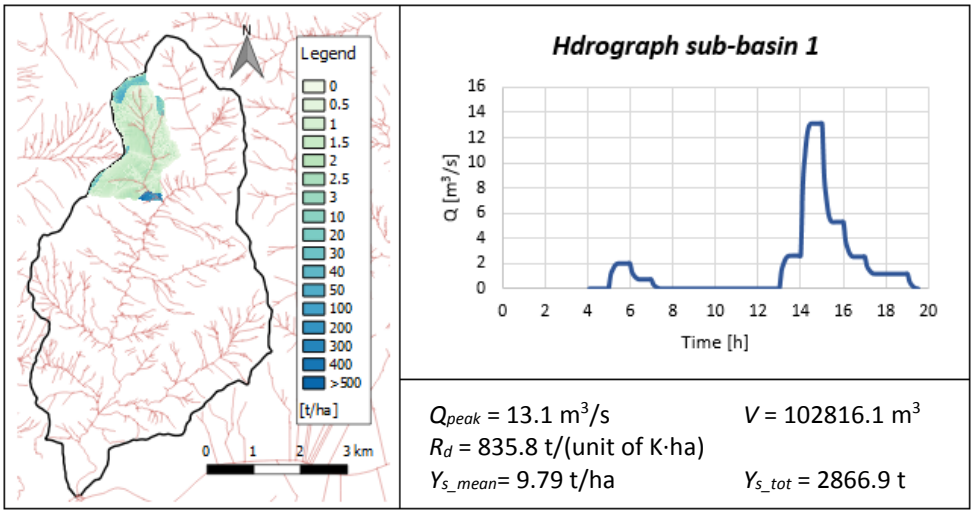

Figure 5.49 – Sub-basin 1 of the Guerna catchment: map of computed sediment yield (Y_s) applying the MUSLE model and hydrograph (04/09/2011 flood event)

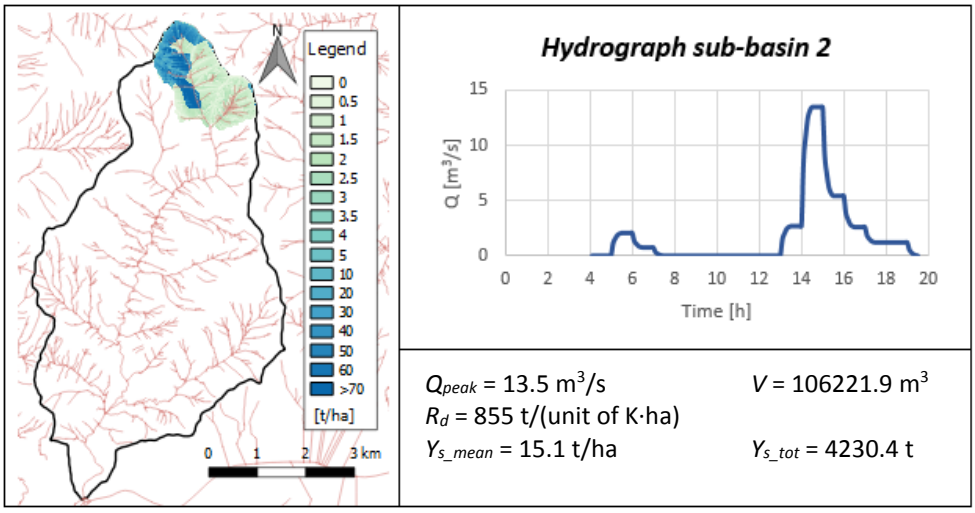

Figure 5.50 – Sub-basin 2 of the Guerna catchment: map of computed sediment yield (Y_s) applying the MUSLE model and hydrograph (04/09/2011 flood event)

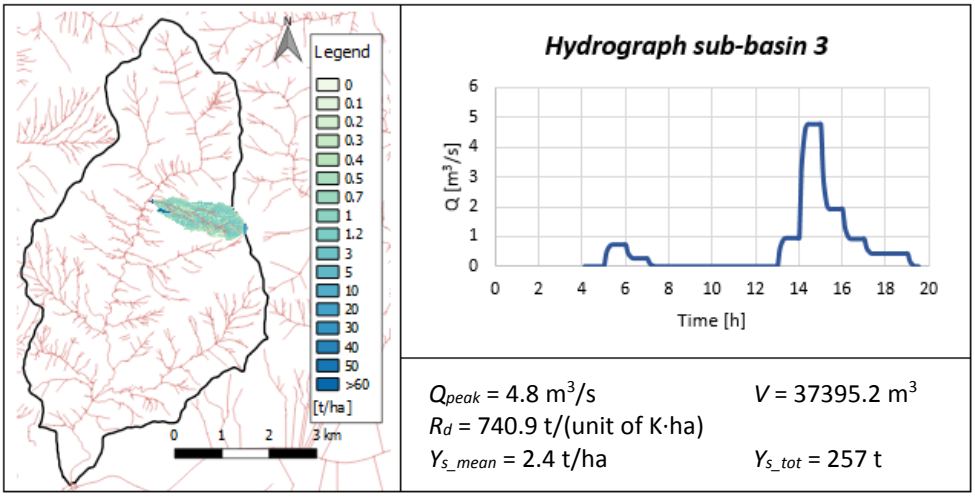

Figure 5.51 – Sub-basin 3 of the Guerna catchment: map of computed sediment yield (Y_s) applying the MUSLE model and hydrograph (04/09/2011 flood event)

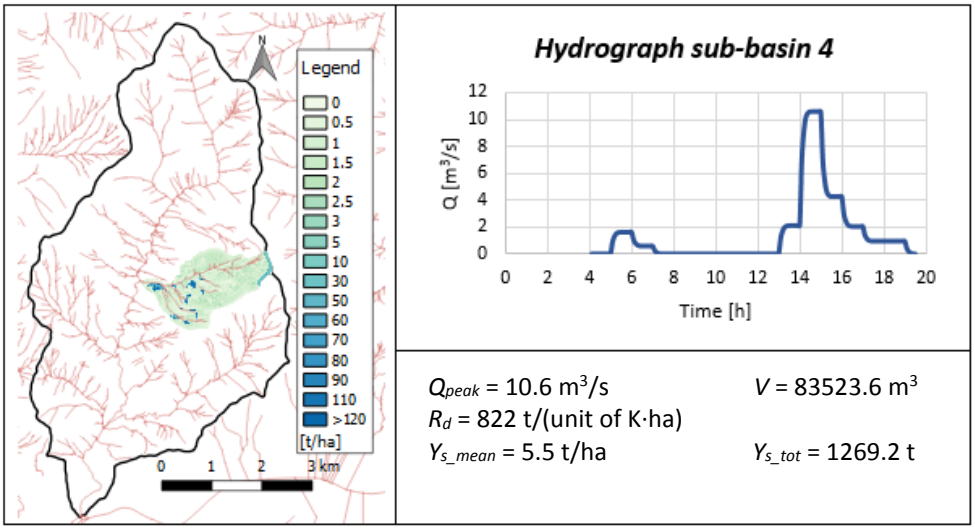

Figure 5.52 – Sub-basin 4 of the Guerna catchment: map of computed sediment yield (Y_s) applying the MUSLE model and hydrograph (04/09/2011 flood event)

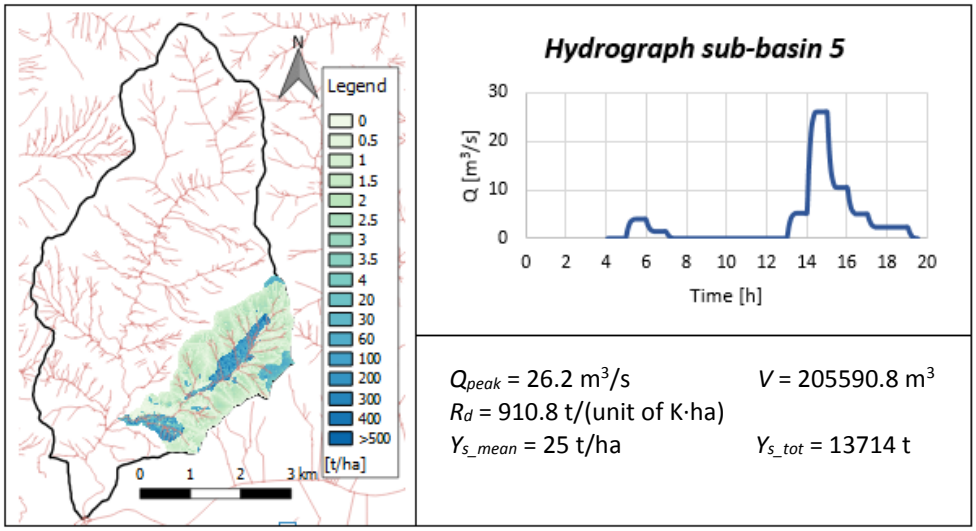

Figure 5.53 – Sub-basin 5 of the Guerna catchment: map of computed sediment yield (Y_s) applying the MUSLE model and hydrograph (04/09/2011 flood event)

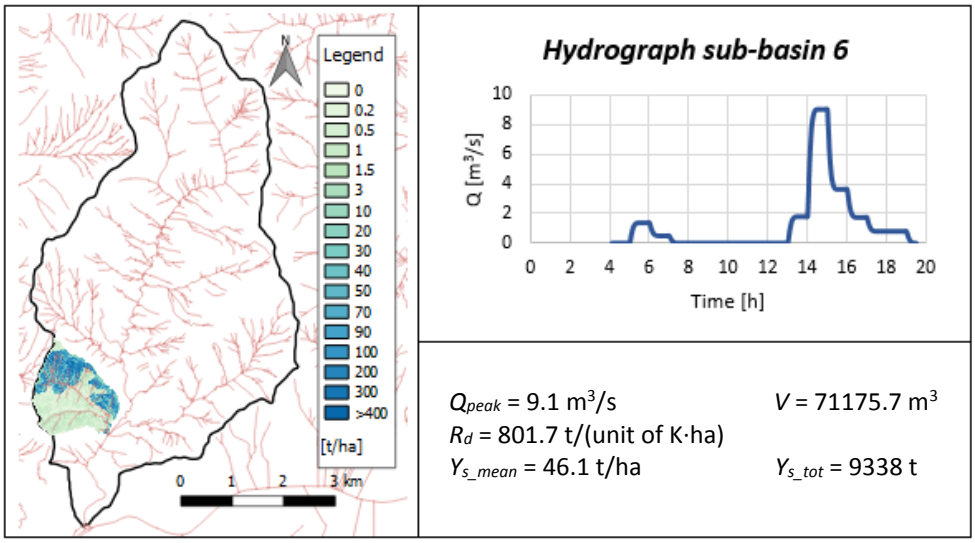

Figure 5.54 – Sub-basin 6 of the Guerna catchment: map of computed sediment yield (Y_s) applying the MUSLE model and hydrograph (04/09/2011 flood event)

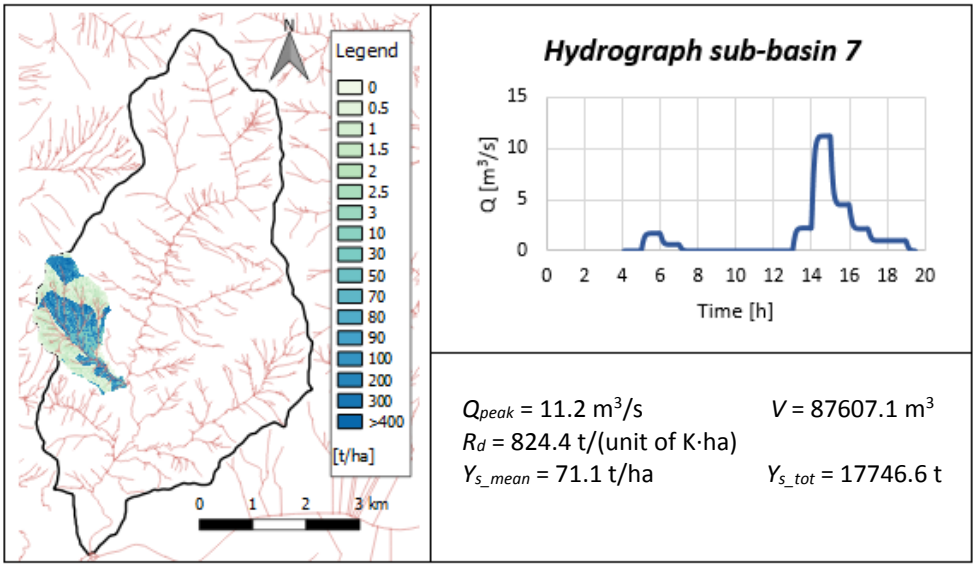

Figure 5.55 – Sub-basin 7 of the Guerna catchment: map of computed sediment yield (Y_s) applying the MUSLE model and hydrograph (04/09/2011 flood event)

5.9. The HEC-RAS model

5.9.1. Geometry data

A HEC-RAS model was developed for the Guerna creek. Figure 5.56 shows the scheme of the watercourse and its cross sections, which was built in HEC-RAS. Both the watercourse and the cross sections were georeferenced. The geometry of the cross sections was provided in part by the "Comunità Montana del Basso Sebino e del Monte Bronzone" (in the Province of Bergamo) and in part by surveys which were executed by the society "Gexcel s.r.l." (plant in Brescia). Additional cross sections by interpolation were included to improve the geometry model. The distance between the cross sections is always lower than 50 m.

Manning's coefficient values for the main channel, the left overbank and the right overbank were established by using photographs taken during the on-site investigation and by using the values proposed by Chow (1959). Manning's coefficient values used for the overbank and for the main channel are, respectively, n = 0.07 s/m$^{1/3}$ and 0.03 < n < 0.05 s/m$^{1/3}$.

Due to the lack of flow discharges measured in the field, it was not possible to calibrate the hydraulic model by adjusting the roughness of the channel and the floodplain, nevertheless these values are in line with the photographs and the Manning's values proposed in literature.

Figure 5.56 – Guerna creek in the HEC-RAS model

5.9.2. Sediment data and particle size analyses

Wilcock and Crowe is the **Transport Functions** that was chosen to simulate sediment transport, because it is widely used to model sediment transport in heterogeneous sand-gravel mixtures and it is a surface-based transport model (see paragraph 2.3.1). The dimensionless reference shear stress τ_{rm}^{*} used for the *Wilcock and Crowe* transport function is 0.021. This value value was calculated using equation (2.18) and it is a function of the sand content of the bed surface. Therefore, τ_{rm}^{*} value was estimated through the surface and subsurface grain size distributions (Figure 5.58, Figure 5.59 and Figure 5.60) and the same value was used for both surface and subsurface bed gradation of the different samples (as explained below).

The grain size distribution of the surface and subsurface mixture was also used to define **Bed Gradation** in HEC-RAS. The grain size distribution was determined in three different points of Guerna creek considering, for each point, both the surface and subsurface samples. The three sampling points fall within the municipality of Adrara S. Rocco (BG), Adrara S. Martino (BG) and Villongo (BG), as shown in Figure 5.57.

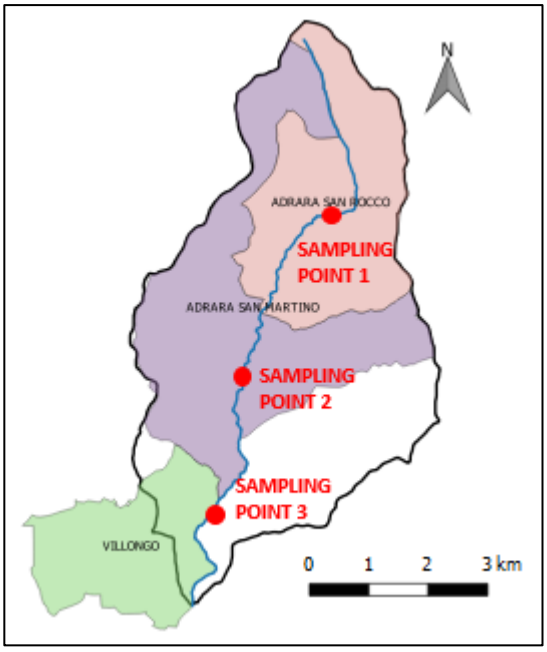

Figure 5.57 – Sampling points in the Guerna creek

The grain size distribution was determined over loose soil samples collected in the field, by means of dry-sieving according with ASTM standards number D 422/72 and number E 11/81. Thirteen sieves were used, with a mesh size ranging from 75 mm to 0.075 mm. Table 5.14, Table 5.15 and Table 5.16 show the grain size distributions obtained and the corresponding grading curves (Figure 5.58, Figure 5.59 and Figure 5.60).

The grain size distribution for sampling point 1, point 2 and point 3 were used to describe the bed gradation in HEC-RAS for the river-reaches that fall, respectively, within the municipality of Adrara S. Rocco, Adrara S. Martino and Villongo.

Adrara S. Rocco sample (point 1) (surface mixture)			**Adrara S. Rocco sample (point 1) (subsurface mixture)**		
Total weight = 2504.5 g			**Total weight = 1963.7 g**		
Mesh size of the sieve (or grain ø) [mm]	**Retained weight [g]**	**Cumulative proportion of bed material [%]**	**Mesh size of the sieve (or grain ø) [mm]**	**Retained weight [g]**	**Cumulative proportion of bed material [%]**
75	-	100	75	-	100
50	242.83	90.30	50	-	100
37.5	549.8	68.35	37.5	-	100
25	505.7	48.16	25	38.04	98.06
19	254.76	37.99	19	706.7	62.07
9.5	424.9	21.02	9.5	283.54	47.64
4.75	235.68	11.61	4.75	280.09	33.37
2	164.81	5.03	2	330.43	16.54
0.85	86.78	1.57	0,85	225.40	5.07
0.425	27.83	0.46	0.425	75.86	1.20
0.250	7.36	0.16	0.250	16.15	0.38
0.15	2.28	0.07	0.15	3.94	0.18
0.075	1.43	0.01	0.075	2.53	0.05

Table 5.14 – Particle size analysis results (Adrara S. Rocco sample)

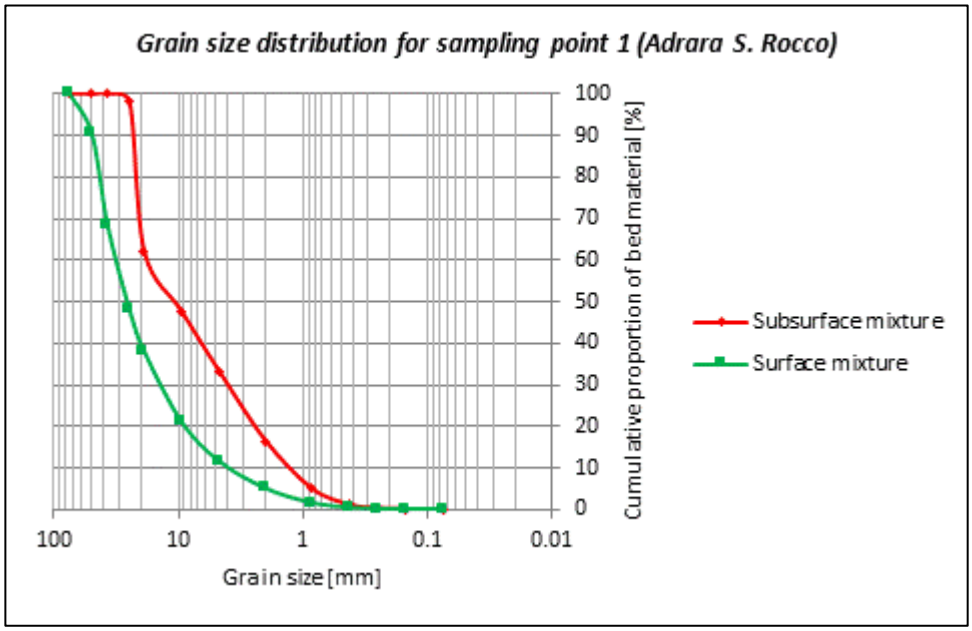

Figure 5.58 – Grain size distribution for sampling point 1 (Adrara S. Rocco)

Adrara S. Martino sample (point 2) (surface mixture)			Adrara S. Martino sample (point 2) (subsurface mixture)		
Total weight = 2775.6 g			Total weight = 926.9 g		
Mesh size of the sieve (or grain ø) [mm]	**Retained weight [g]**	**Cumulative proportion of bed material [%]**	**Mesh size of the sieve (or grain ø) [mm]**	**Retained weight [g]**	**Cumulative proportion of bed material [%]**
75	-	100	75	-	100
50	188.26	93.22	50	-	100
37.5	858.4	62.29	37.5	-	100
25	1341.2	13.97	25	30.12	96.75
19	150	8.57	19	74.80	88.68
9.5	151.5	3.11	9.5	264.59	60.13
4.75	40.92	1.63	4.75	202.30	38.31
2	31.01	0.52	2	214.83	15.13
0.85	11	0.12	0,85	110.22	3.24
0.425	2.44	0.03	0.425	26.21	0.41
0.250	0.37	0.02	0.250	2.75	0.12
0.15	0.10	0.01	0.15	0.42	0.07
0.075	0.05	0.01	0.075	0.33	0.04

Table 5.15 – Particle size analysis results (Adrara S. Martino sample)

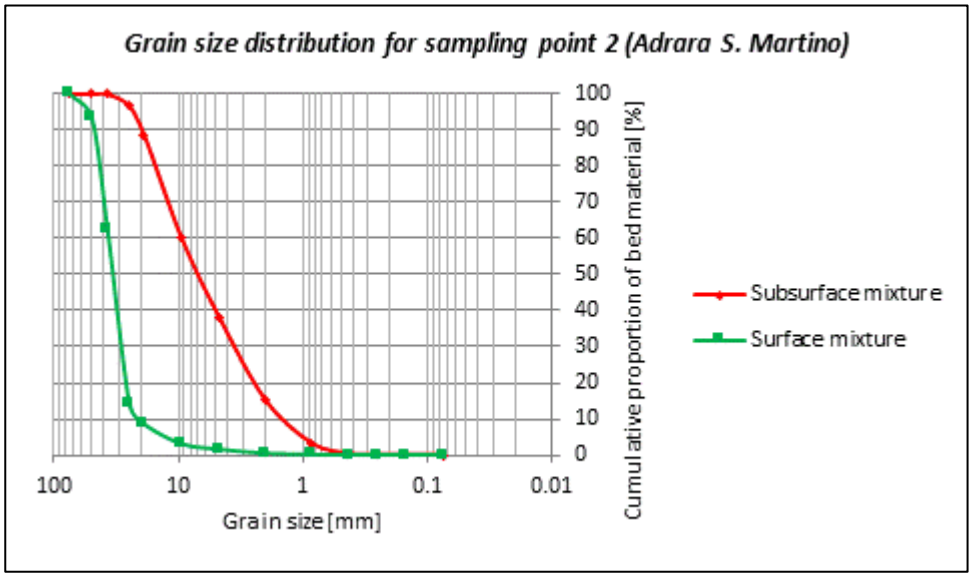

Figure 5.59 – Grain size distribution for sampling point 2 (Adrara S. Martino)

Villongo sample (point 3) (surface mixture)			Villongo sample (point 3) (subsurface mixture)		
Total weight = 8151.1 g			Total weight = 449.3 g		
Mesh size of the sieve (or grain ø) [mm]	Retained weight [g]	Cumulative proportion of bed material [%]	Mesh size of the sieve (or grain ø) [mm]	Retained weight [g]	Cumulative proportion of bed material [%]
75	-	100	75	-	100.00
50	1582.10	80.59	50	0.00	100.00
37.5	914.90	69.37	37.5	0.00	100.00
25	1878.20	46.32	25	156.30	96.52
19	792.70	36.60	19	246.00	91.05
9.5	1170.80	22.24	9.5	836.90	72.44
4.75	610.70	14.74	4.75	910.30	52.19
2	649.60	6.77	2	1183.20	25.88
0.85	436.10	1.42	0,85	847.70	7.03
0.425	85.00	0.38	0.425	229.30	1.93
0.250	1.10	0.37	0.250	55.20	0.70
0.15	6.60	0.29	0.15	18.20	0.29
0.075	3.60	0.24	0.075	7.40	0.13

Table 5.16 – Particle size analysis results (Villongo sample)

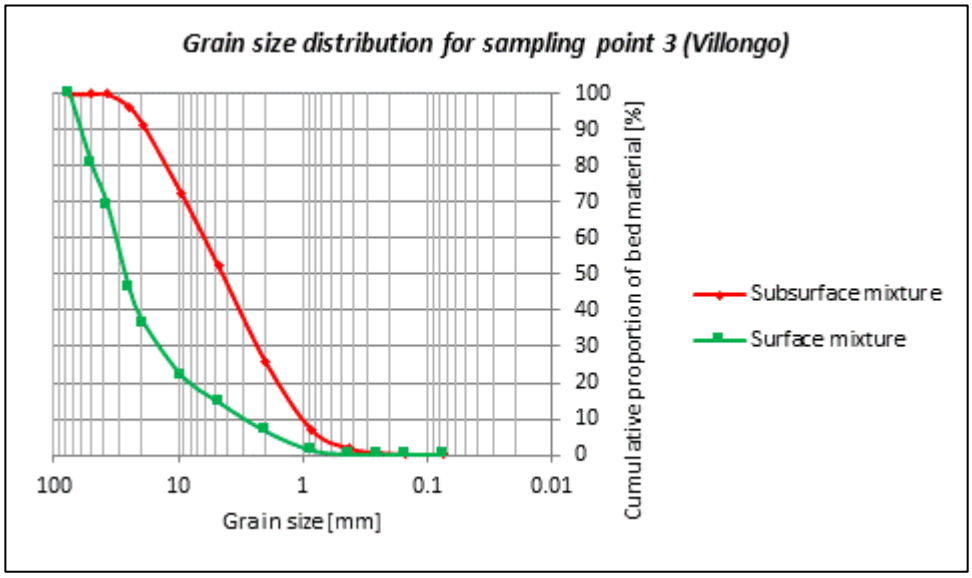

Figure 5.60 – Grain size distribution for sampling point 3 (Villongo)

HEC-RAS **Sediment Control Volume** contains the available erodible sediment (see paragraph 3.5.2 for more details). The width of this volume is limited by main channel bank stations. Its vertical dimension coincides with the grain size corresponding to 98% of the cumulative proportion of bed material (Figure 5.58, Figure 5.59 and Figure 5.60). Therefore, considering surface mixture to define bed gradation, it was assigned a value of 60 mm to reaches that fall within the municipality of Adrara S. Rocco, Adrara S. Martino and a value of 70 mm to reaches that fall within the municipality of Villongo. Similarly, considering subsurface mixture to define bed gradation, it was assigned a value of 25 mm to reaches that fall within the municipality of Adrara S. Rocco, Adrara S. Martino and a value of 30 mm to reaches that fall within the municipality of Villongo.

The bed **Sorting Method** chosen is the "Active Layer". It was decided to use this method because the HEC-RAS manual suggests to use the "Active Layer" algorithm with this transport function. More details can be found in paragraph 3.5.2.

The "Rubey" **Fall Velocity Method** was used. The Guerna Creek is a gravel bed river with a bimodal distribution (gravel and sand) and therefore this fall velocity method is well suited. For more details regarding this fall velocity method, refer to paragraph 3.5.2.

"Sediment Load Series" is the **Boundary Condition** used at the upstream cross section and in correspondence of cross sections characterized by input sediment load. This function is useful when the sediment load cannot be coupled to flow. Input sediment load expresses the mass rate over the defined duration. HEC-RAS requires a rating curve that defines grain size distributions for load rates [*USACE,* 2016 (b)]. The grain size distributions applied (Figure 5.61 and Figure 5.62), are the same that were used in paragraph 5.3 in order to estimate the K factor in the RUSLE model. Two soil samples were taken in the Guerna catchment and therefore two grain size distributions were made: the first one and the second one are associated with, respectively, the upstream and the downstream area of the basin. More details concerning the particle size analysis can be found in paragraph 5.3.
The input sediment loads were assigned to the 7 cross sections, in correspondence of the 7 sub-basins, in the HEC-RAS model. These values are the computed sediment yield reported in paragraph 5.8.2. Therefore, the sediment yield estimated by applying the MUSLE model, were used as input sediment loads in the HEC-RAS model. Finally, to the computed sediment yield of the entire Guerna catchment (which was calculated in paragraph 5.8.1) the contributes of the 7 sub-basins were subtracted. The remainder was divided by the number of other internal cross sections in the Guerna Creek, as input sediment loads.

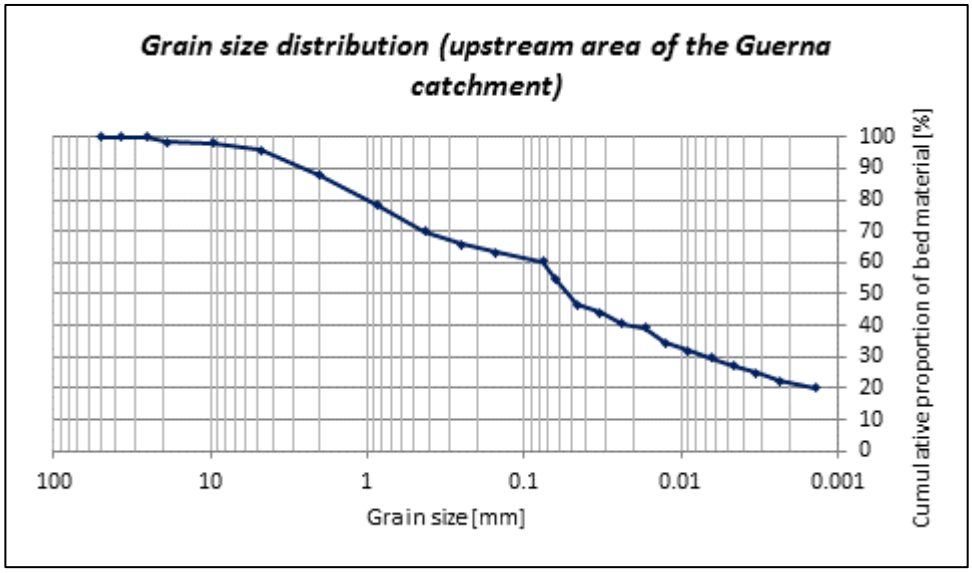

Figure 5.61 – Grain size distribution for the upstream area of the Guerna catchment

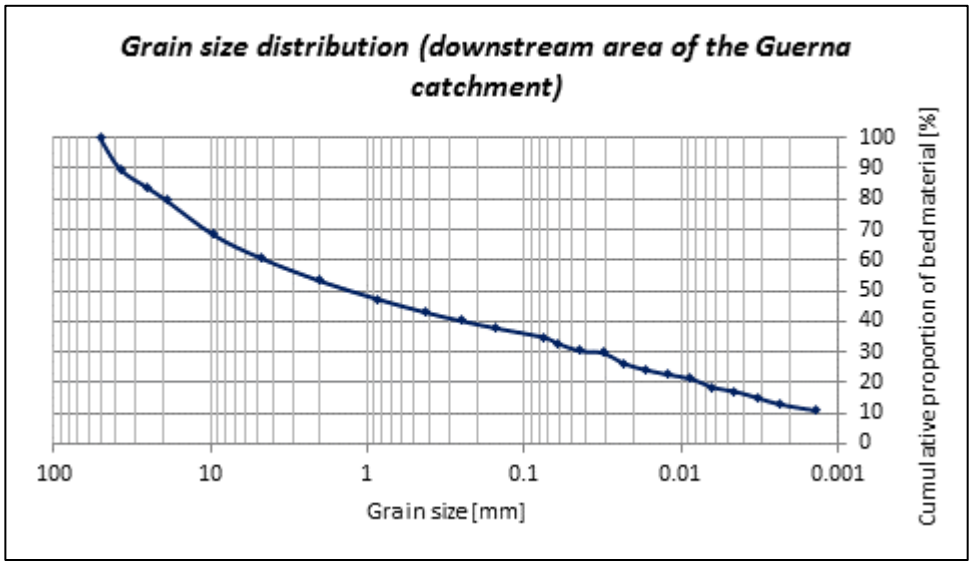

Figure 5.62 – Grain size distribution for the downstream area of the Guerna catchment

5.9.3. Flow data

The **Quasi-Unsteady Flow** approach was used for sediment transport analysis. The hydrograph was approximated with a series of discrete steady flow profiles; each profile lasts 12 minutes in all simulations. More details can be found in paragraph 3.5.3. The boundary condition at the upstream cross section is the hydrograph in correspondence of the outlet of sub-basin 2. Hydrographs in correspondence of the outlet of the other 6 sub-basins were used in the HEC-RAS model as input lateral flow series associated with internal cross sections (see Figure 5.63). Finally, to the volume of runoff calculated at the outlet of the Guerna catchment (see paragraph 5.8.1) the contributes of the 7 sub-basins (see paragraph 5.8.2) were subtracted. The reminder was divided by the number of other internal cross sections as input uniform lateral flows.

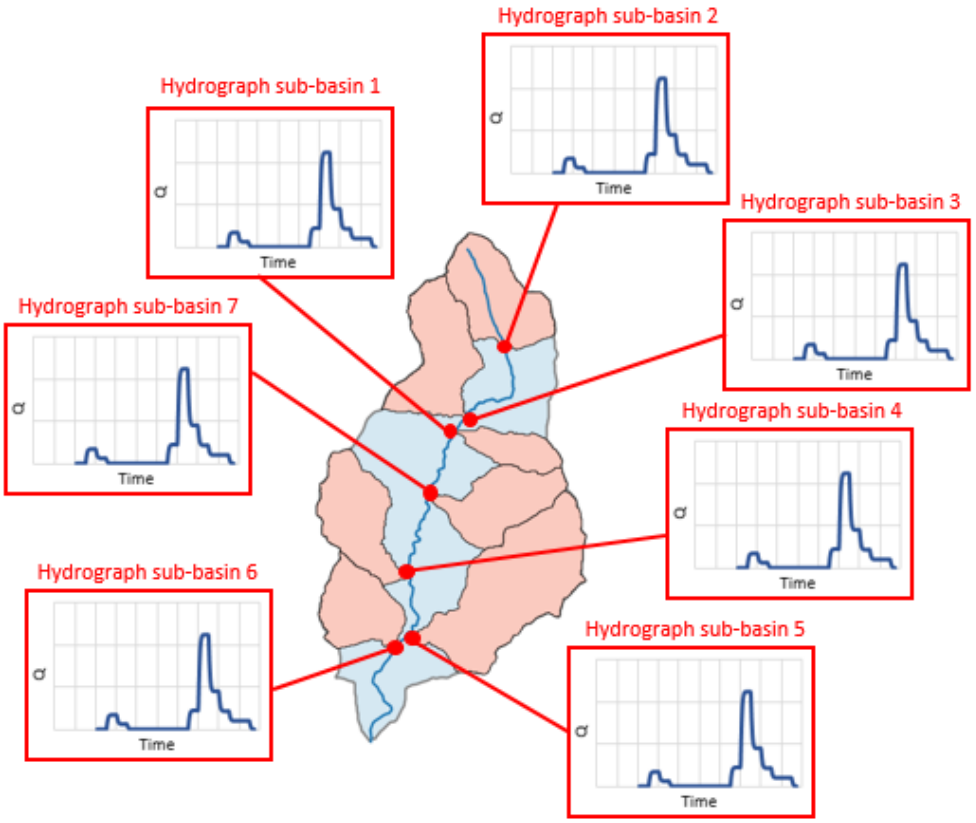

Figure 5.63 – Position of the input flow series in the HEC-RAS model

5.9.4. Simulations and results

Two simulations of sediment transport were conducted using the HEC-RAS for the flood event which was examined (04/09/2011): the first and the second simulation consider, respectively, surface and subsurface mixture to define bed gradation (see Figure 5.58, Figure 5.59 and Figure 5.60). The total time duration of both simulation processes is about 15 hours, in the period from September 4, 2011 at 13:00 to September 5, 2011 at 03:20. The simulation time interval coincides with the duration of the hydrographs built through the concentration time method (see paragraph 5.9.3).

The first simulation, which considers surface mixture to define bed gradation, is more significant for this case study because the Wilcock and Crowe transport function is a surface-based transport model; therefore transport is primarily dependent on the material in direct contact with the flow (see paragraph 2.3.1). However, it was decided to do also the second simulation, which considers subsurface mixture to define bed gradation. This choice makes it possible to evaluate sediment transport and yield in a different situation, in which the surface layer is supposed to be totally removed by the water flow. Therefore, in that situation, the bed gradation consists of finer material and it coincides with the subsurface layer.

The sediment discharge was evaluated in simulation time for 4 different cross sections of the HEC-RAS model. Cross sections analysed are shown in Figure 5.64.

HEC-RAS manual defines the "Sediment discharge" as the total sediment discharge going out of the sediment control volume for a specific cross section, per individual computational time step [*USACE,* 2016 (b)].

The following graphs (Figure 5.65 and Figure 5.66) show the results that were obtained. It is noted that high sediment discharge values are associated with high water discharge values.

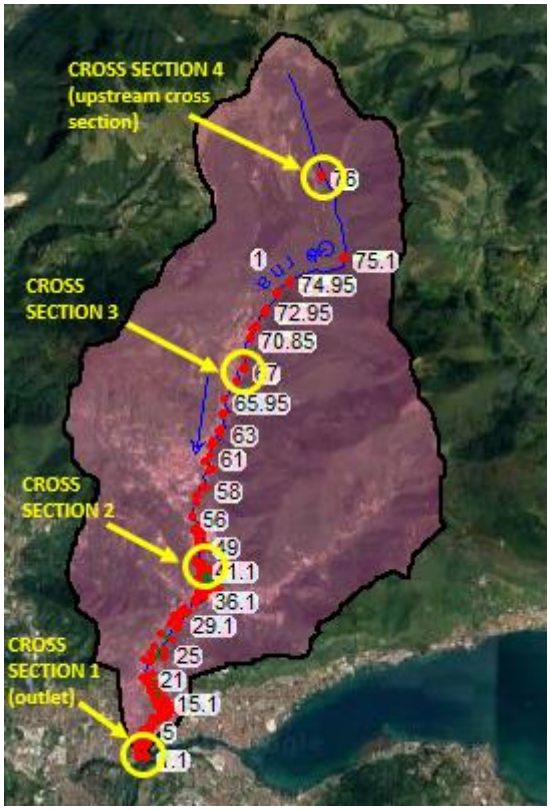

Figure 5.64 – Cross sections analysed in the HEC-RAS model

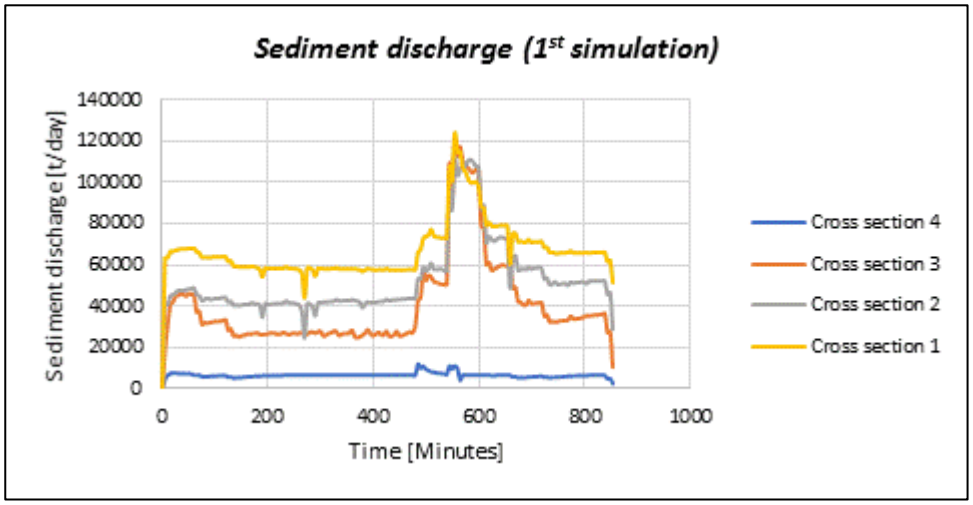

Figure 5.65 – Sediment discharge results considering surface bed gradation in HEC-RAS simulation

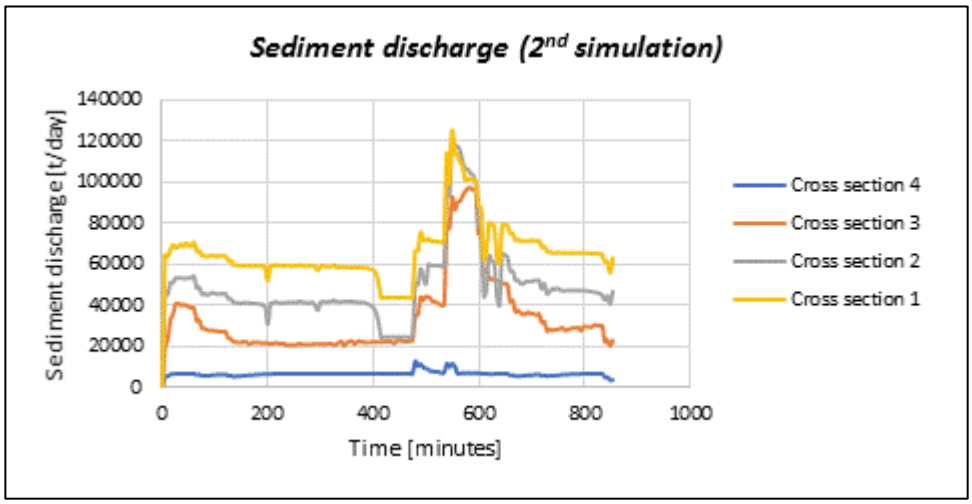

Figure 5.66 – Sediment discharge results considering subsurface bed gradation in HEC-RAS simulation

Table 5.17 shows mean values of sediment discharge at the 4 cross sections which were taken into consideration during the simulation time interval.

Table 5.17 – Mean value of simulation results

	Sediment discharge [t/day]	
	1st simulation	*2nd simulation*
Cross section 1	66810	65654
Cross section 2	52165	49485
Cross section 3	39778	33951
Cross section 4	6632	6583

Notes: 1st simulation = HEC-RAS simulation considering surface mixture to define bed gradation;
2nd simulation = HEC-RAS simulation considering subsurface mixture to define bed gradation.

Mean sediment discharge values in Table 5.17, can be compared to mean bed load intensity recorded at the measuring station in the Rio Cordon catchment for the 14/09/1994 flood event and shown in Table 2.2. Main characteristics of the Rio Cordon basin are reported in paragraph 2.5 and it is a useful comparison with sub-basin 2 (Figure 5.50) of the Guerna watershed because of their similar features shown in Table 5.18. The outlet of the sub-basin 2 is the cross section 4 in Figure 5.64. The sediment discharge recorded in the Rio Cordon catchment during this flood event is 225 m^3/h and this value corresponds to 8040.6 t/day, using 1489 kg/m^3 as density of bed material [*USACE,* 2016 (b)].

Focusing on the first simulation in Table 5.17, the sediment discharge calculated at cross section 1 (the outlet Guerna watershed) has an acceptable order of magnitude, bearing in mind that the basin area is 30.9 km^2.

	Rio Cordon catchment	**Sub-basin 2 of the Guerna catchment**
Geographical location	Alps in northern Italy (Veneto)	Alps in northern Italy (Lombardia)
Area [km²]	5	3
Mean hillslopes gradient [%]	52	62
Mean gradient of the main channel [%]	13.6	14.6
Material of active sediment sources (active layer)	From silt to gravel	From sand to gravel
Peak water discharge [m³/s]	10.4	13.5
Mean sediment discharge [t/day]	*8040.6*	*6632*

Table 5.18 – Comparison between the Rio Cordon catchment and the sub-basin 2 in the Guerna catchment

5.10. Concluding remarks

5.10.1. Water erosion and climate change

The first aim of this research was an estimation of water erosion in the Guerna catchment and a spatial analysis of soil erosion trends in different future climate scenarios.

Previously Bosco et al. (2008) conducted a study to estimate actual erosion over the whole alpine space and a spatial analysis of soil erosion trends in different IPCC scenarios. The main objective was the assessment of soil erosion in relation to climate change. The RUSLE equation was applied to the whole alpine space and it produced, with a spatial resolution of 100 m, the map of actual soil erosion and the maps defining soil erosion rates in IPCC A2 and B2 scenarios 2070-2100. From a comparison between actual and soil losses in A2 and B2 scenarios, it came out that the model did not present relevant raises in erosion rates [*Bosco et al.*, 2008]. Considering the application of RUSLE equation in the Guerna watershed at higher spatial resolution and in the three climate change scenarios analysed, no relevant increases were similarly detected.

In the Guerna catchment, the mean annual amount of precipitation *H* for RCP 2.6 and RCP 8.5 scenarios increased, respectively, by around 6% and 2% compared with *H* = 1100.63 mm/year, which is the value estimated without considering climate change. However, the RCP 4.5 scenario yields a lower value (less than 14%) than the present one. The soil loss calculated using the EPM method for RCP 2.6 and RCP 8.5 scenarios is larger than the value estimated without considering climate change, but it is smaller for the RCP 4.5 scenario, as shown in Table 5.19 and in Table 5.20. Indeed, soil erosion is likely to increase with increased rainfall amount. However, by applying the RUSLE equation, the computed soil loss is higher

than the value estimated without considering climate change only for the RCP 2.6 scenario, as shown in Table 5.19 and in Table 5.20. The reason for this result is the *R* factor value, which increased by around 2.5% compared with the value estimated without considering climate change (R = 2620 MJ·mm·ha^{-1}·h^{-1}·year^{-1}) only for the RCP 2.6 scenario. RCP 4.5 and RCP 8.5 scenarios yield a *R* value which is, respectively, less than 38% and 4% than the present one. Indeed, *R* factor also takes into account the kinetic energy in a single rainfall event and the rainfall intensity that affects soil loss greatly.

Temperature is predicted to rise in all future scenarios considered in the Guerna watershed; the temperature rise is between 0.2°C and 4°C. This is in accordance with both the case studies summarized in Li and Fang (2016) and the undeniable global warming trend, because of higher CO_2 emissions [*Li and Fang*, 2016].

In accordance to Bosco et al. (2008), only rainfall and temperature regimes were considered to account for climate change on water erosion. The future variations of the cover management factor were omitted, especially because analysis revealed that in the last 60 years there have not been significant transformations in land use (except for a small increase in forests and bushes that slightly reduced water erosion).

The aim of the RUSLE methodology is to estimate water erosion in agricultural areas, therefore the approach is not well suitable to erosion assessment in mountain catchments [*Dominici et al.*, 2015]. Some researchers assert that the most common soil erosion models, such as the RUSLE, have to be used on hilly agricultural areas where sheet and rill erosion processes prevail. Nevertheless, Bosco et al. (2008) used the RUSLE model in an alpine environment because this model is one of the most used and it is the only model in which input data can be obtained in different ways (measurement, estimation, interpolation). In addition, it has a more flexible data processing system as well as an acquired experience in the application both on a local and continental scale. Its application in alpine areas could lead to a coarse estimation of water erosion processes, but their objective was the assessment of the soil erosion in relation to climate change. Therefore, their analysis should be considered comparative and not absolute [*Bosco et al.*, 2008]. For these reasons, also considering the Guerna catchment, the RUSLE methodology was useful to evaluate water erosion in order to compare its results with EPM's results and other case studies, also evaluating as well as different climate change scenarios. In paragraph 5.3.1, the RUSLE factors estimated were also compared with those provided by ESDAC (European Soil Data Centre) and the results can be considered satisfactory.

The EPM method accounts for a more complete description of the meteorological forcing, since both precipitation and air temperature are included in the equation. Table 5.19 summarises the results that were obtained:

	Without considering climate change scenario	***Climate change scenario***		
		RCP 2.6	***RCP 4.5***	***RCP 8.5***
RUSLE method	302271 t/year	308890 t/year	186187 t/year	289188 t/year
EPM method	30264 m^3/year	32582 m^3/year	27306 m^3/year	32913 m^3/year

Table 5.19 – Summary of the RUSLE and EPM results

By considering a specific weight of 2.75 t/m^3 [*Efthimiou et al.,* 2016], soil loss computed for the Guerna watershed in the years 2005-2016 by the RUSLE equation is about three times higher than its evaluation according to the EPM method. Table 5.20 shows that they were obtained by using a specific weight of 2.75 t/m^3:

	Without considering climate change scenario	***Climate change scenario***		
		RCP 2.6	***RCP 4.5***	***RCP 8.5***
RUSLE method A_{tot} [t/year]	302271	308890	186187	289188
EPM method W_{g_tot} [t/year]	83225	89600	75091	90512

Table 5.20 – Summary of the RUSLE and EPM results considering a specific weight of 2.75 t/m³

This overestimate is coherent with the results obtained for other case studies (Fiumara Sfalassa, South Italy), with a similar topography [*Dominici et al.*, 2015; *Auddino et al.*, 2015].

The climate change impacts on water erosion may not be negligible even by the middle of this century. According to the EPM method and to RCP 2.6, RCP 4.5 and RCP 8.5 scenario, the annual average soil loss could change by 8-10% on a basin scale.

5.10.2. Sediment yield and transport

The second aim of this research was to evaluate sediment yield for a single rainfall event and to use the sediment load obtained as input material into the HEC-RAS model of the Guerna catchment: the goal was the simulation of sediment transport.

Sediment yield was estimated using MUSLE equation and considering a very high rainfall event. The mean value achieved in the Guerna catchment (32.5 t/ha) is approximately one-third of the mean value obtained by the RUSLE model (97.7 t/(ha·year)). The sediment yield for the rainfall event analysed was also estimated, using MUSLE equation, for the 7 sub-basins identified in the Guerna catchment; it was decided to use these values as input sediment load in the HEC-RAS model. It should be noted that the MUSLE equation provides only an estimate of sediment yield and a suitable calibration should be made to obtain an accurate sediment yield prediction. Indeed, as demonstrated by Sadeghi (2004), this model could overestimate the sediment yield as compared with the measured values.

Bed gradation curves used in the HEC-RAS model were made through particle size analyses, which were carried out in the geotechnical lab at University of Brescia. *Wilcock and Crowe* is the transport function that was chosen to simulate sediment transport, because it is widely used to model sediment transport in heterogeneous sand-gravel mixtures.

Runoff hydrographs in correspondence of the outlet of the 7 sub-basins were used in the HEC-RAS model as input flow series. The "Time-Area method" was adopted to create runoff hydrographs. Therefore, the rainfall excess hyetograph was estimated using SCS-CN method and the time-area curve was built for each sub-basin.

Table 5.21 summarises the simulation results (sediment discharge) that were obtained at the upstream cross section and at the outlet cross section of the Guerna catchment, considering both surface and subsurface mixture to define bed gradation:

	Sediment discharge [t/day]	
	Bed gradation: surface mixture	*Bed gradation: subsurface mixture*
Upstream cross section	6632	6583
Outlet cross section	66810	65654

Table 5.21 – Summary of the solid transport simulation results in the Guerna catchment

Values achieved and reported in Table 5.21 can be considered satisfactory, because they are comparable to the field results obtained for another case study (Rio Cordon catchment, North Italy), with similar characteristics.

6. General conclusion

Erosion, transfer and deposition of soil particles and the impact of climate change at the catchment scale are very important in several fields of the earth sciences, especially in the last decade. Mathematical modelling approaches can be used to assess and quantify sediment production and transport.

The role of sediment transport in river dynamic is essential in order to evaluate the impacts of large magnitude flood events on the environment. The severity of a flood event is often the combinated results of the flow discharge and the consequent sediment discharge. Nevertheless, there is a lack of sediment transport data available for rivers around the world; this lack is mainly due to the conventional methods of collecting data during extreme events, which are often expensive, difficult and dangerous. The evaluation of soil loss due to water erosion and the knowledge of climate change impacts on this phenomenon in a watershed is essential to identify potential hydrogeological risk areas and to ensure a good management of the territory. However, soil loss and sediment yield field data are rare, making the validation of estimated values a hard task. For these reasons, this work could provide a useful contribution to scientific research.

This thesis project was implemented for the first part in Canada (at the University of Waterloo), and for the second part in Italy (at the University of Brescia). Therefore, the first case study is the Mimico Creek, which is situated in Toronto, southern Ontario, Canada; the second case study is the Guerna catchment, which is located in the Province of Bergamo, Italy.

As regards the first case study (Mimico Creek), the objective is to illustrate the development of a sediment transport model of the study reach, where sediment transport investigations were conducted, using HEC-RAS and to compare the simulation results achieved to field observations. The developed model was calibrated to a series of discharge events where in-situ bedload sampling occurred. Results showed that the Wilcock and Crowe transport equation suits better to the study reach than the Meyer-Peter Müller transport model. Calibration curves were developed to estimate sediment discharge in Mimico Creek, using the Wilcock and Crowe transport model and considering both step-wise discharge and unsteady flow simulations. These curves determine bed material transport rates as a function of calibration parameter. The calibration process was conducted implementing and not implementing the BSTEM (Bank Stability and Toe Erosion Model) in HEC-RAS. The sensitivity analysis showed that calibration without the BSTEM looks better than the one which considers the BSTEM. The results of the calibrated model were used to calculate the mean travel distance of bed material. The values achieved showed that the Wilcock and Crowe equation under-predict the transport of the coarsest fractions in the bed load and the absence of the BSTEM overlooks the presence of fine material; for these reasons the travel distances calculated considering the BSTEM are longer. Finally, the travel distances of different grain sizes were estimated using the Wilcock and Crowe calibrated model, neglecting the contribution of the BSTEM and considering the unsteady flow approach. Particle size show a steep reduction in travel distance with increase in particle size. The

findings indicate that transport distance values are higher for the flood event with higher peak discharge, generally in accordance with field measurements. The fractional transport distances of different grain classes estimated using simulation results are lower than tracer surveys because in the field only the mobile particles with a diameter greater than 30 mm were considered, while using simulation results, both mobile and immobile particles were taken into account.

As regards the second case study (the Guerna catchment), the soil loss due to water erosion in the study area was estimated, using the RUSLE and EPM model, and a spatial analysis of soil erosion trends in different IPCC scenarios was conducted. Results show that, considering the application of RUSLE equation, and the different climate change scenarios analysed, the model did not report relevant increases. The soil loss calculated using EPM method for two of the three future scenarios is larger than the value estimated without considering climate change, but it is smaller for the third future scenario. In accordance to other research and to the results of the analysis on the Guerna catchment, only rainfall and temperature regime were considered to evaluate the effects of climate change on water erosion; the future variations of the cover management factor were omitted. Results show that soil loss computed for the Guerna watershed by the RUSLE equation is about three times higher than its evaluation according to the EPM method. This overestimate is coherent with the results obtained for other case studies with a similar topography. Indeed, the aim of the RUSLE methodology is to estimate water erosion in agricultural areas and not in mountain areas. Moreover, the EPM method accounts for a more complete description of the meteorological forcing, since both precipitation and air temperature are included in the equation. Nevertheless, in line with other studies, it was decided to use the RUSLE model in the study area (an alpine environment) because this model is one of the most used, because it is useful the assessment of soil erosion in relation to climate change and because of its comparison to the EPM model and other case studies. According to the EPM method and to the future scenarios, the annual average soil loss could change by 8-10% on a basin scale.
An assessment of the sediment yield, as input material into the HEC-RAS model of the Guerna creek, was conducted: the goal was the simulation of sediment transport. Sediment yield was estimated using the MUSLE equation and the mean value achieved in the study area is approximately one-third of the mean value obtained by the RUSLE model. The sediment yield for the rainfall event analysed was also estimated, using the MUSLE equation, for the 7 sub-basins identified in the Guerna catchment; it was decided to use these values as input sediment load in the HEC-RAS model. Wilcock and Crowe is the transport function that was chosen and the “Time-Area method” was adopted to create runoff hydrographs. Results can be considered satisfactory, because they are comparable to the field values obtained for another case study, with similar characteristics.

The main contributions of this PhD dissertation are listed, considering both case studies investigated.

Contributions to the first case study (the Mimico Creek):

- implementation and calibration of a sediment transport model in HEC-RAS, using field data collected during high magnitude low frequency events in a study area characterised by critical hydraulic aspects. The calibration process is followed by the validation of the appropriate transport equation;
- development of a calibration curve for the Wilcock and Crowe transport function and the trend equation which expresses sediment discharge in terms of flow discharge. These curves can be useful to estimate both sediment discharge and the calibration parameter of the transport function in Mimico Creek for flood events where in-situ bedload sampling are not available;
- sensitivity analysis of the calibrated HEC-RAS model, in order to know the effect of the BSTEM option;
- comparison between two different hydrodynamic approaches in the sediment transport analysis: the "Quasi-Unsteady Flow approach" and the "Unsteady Flow approach";
- comparison of simulated transport distances against available field observations. It provides another mechanism to validate appropriate transport equations; particularly where in-situ bedload sampling may not be available.

Contributions to the second case study (the Guerna catchment):

- estimation of soil loss and sediment yield in a study area exposed to hydrogeological risk and which was affected, in the past, by flooding and erosion events;
- comparison between two different empirical models (RUSLE and EPM) to estimate sediment loss due to water erosion. The identification of the most suitable model for the study area was made possible thanks to the confrontation with other case studies;
- assessment of the effects of climate change on soil loss due to water erosion;
- implementation of a sediment transport model in HEC-RAS in order to evaluate sediment transport in the Guerna Creek and comparison with another case study.

6.1. Limitations and future research lines

The research activity contained in this PhD dissertation has some limitations, which could be overcome by conducting future research for the two case studies analysed.

The first case study: the Mimico Creek

Regarding the sediment transport analysis in the Mimico Creek, an interesting future research line is to find a link between path length distances and channel morphology.

Other future developments concern the structure of the HEC-RAS model that was made. Its geometry can always be improved, by including additional cross section surveys. The comparison of current surveys with new surveys of the cross sections used in the model, can

also be a point of interest in order to know the morphological changes of the bed channel over the years. Furthermore, other sediment functions can be tested and calibrated, to compare them to the Wilcock and Crowe transport function. Finally, the sensitivity analysis can be improved, considering other elements (for example, changing the boundary conditions).

Further transport investigations and bed load samplings may be carried out, considering new competent flood events. This operation can be useful to improve and validate the calibration curve for the Wilcock and Crowe transport function (see paragraph 3.8) and the trend equation which expresses sediment discharge in terms of flow discharge (see paragraph 3.4). Finally, the bed load sampling using Helley-Smith sampler can be improved, using another measurement technique that also pays attention to the finest sediment. Indeed, it was noted that particles smaller than 0.5 mm were not suitable due to sampling biases associated with Helley-Smith.

The second case study: the Guerna catchment

As regards the estimation of sediment loss and sediment yield due to water erosion in the Guerna catchment, future developments concern field measurements of soil loss and sediment yield at basin level to improve, compare and validate the results that were obtained. There are different techniques in order to measure and to monitor erosion and deposition rates at basin level; some of them are listed below [*Bagarello and Ferro*, 2006]:

- erosion pins [*Ferro*, 1999];
- Photo-Electronic-Erosion-Pin (PEEP) system [*Lawler*, 1991; *Lawler*, 1992; *Lawler*, 1993, *Lawler*, 1994; *Lawler*, 2002];
- sedimentation tank and channel to measure flow discharge at the outlet basin. For example, the recording station at the outlet Rio Cordon basin [*Lenzi et al*., 2004];
- techniques of isotope tracers. The isotope Cesium-137 is the most used [*Baker*, 1967; *McHenry*, 1969; *McHenry and Ritchie*, 1977; *Ritchie and McHenry*, 1990; *Ritchie et al*., 1972].

Moreover, the use of these techniques over a long lapse of time (up to 50 years) would provide the assessment of soil loss values estimated considering future scenarios, which are characterised by the impact of climate change.

Future developments of the HEC-RAS model concern the calibration process using field data, in order to improve and validate the results that were achieved.

The first phase is the calibration of the hydraulic HEC-RAS model, without considering sediment input and sediment transport. This phase involved adjustment of Manning's roughness coefficient of the channel and the flood plain, which best fitted the measured water discharge. Therefore, a hydrometric gauge station and a rating curve are needed.

The second phase is the calibration of the sediment transport HEC-RAS model, comparing sediment discharge simulation results with the measured ones and adjusting the calibration

parameter (τ_{rm}^{*} for the Wilcock and Crowe equation) which best fitted the measured sediment discharge. Anyway, the calibration parameter should remain within reasonable ranges. Therefore, measured values of sediment discharge are needed.

The unsteady flow approach was not used due to instability problems related to the complexity of this HEC-RAS model. The attempt to improve the model in order to solve these problems, may be seen as another important future development.

Furthermore, other sediment functions can be tested and calibrated, in order to compare them to the Wilcock and Crowe transport function. The goal is to find which suits this case study best.

Finally, it should be noted that the model geometry can always be improved, by including additional cross section surveys.

Appendix

Ackers-White transport function

Ackers-White (1973) is a total load function developed from flume data for relatively uniform gradations ranging from sand to fine gravels. A range of bed configurations was used during flume experiments (plane, rippled and dune forms). This transport function has the advantages of a dimensional analysis technique. It uses the physical arguments to express the mobility and transport rate of sediment in terms of some dimensionless parameters. The Ackers-White equation was developed in terms of particle size, mobility and transport. The general for a single grain size is the following:

$$G = \gamma_w Q X$$

$$X = \frac{G_{gr} s d_s}{D\left(\frac{u_*}{V}\right)^n}$$

$$G_{gr} = C\left(\frac{F_{gr}}{A} - 1\right)$$

where: G = sediment discharge [kg/s]

Y_w = unit weight of water [kg/m^3]

Q = discharge [m^3/s]

X = sediment concentration, in parts per part

G_{gr} = sediment transport parameter [-]

s = specific gravity of sediments [-]

d_s = mean particle diameter [m]

D = effective depth [m]

u_* = shear velocity [m/s]

V = average channel velocity [m/s]

n = transport exponent, depending on sediment size [-]

C = coefficient [-]

F_{gr} = sediment mobility parameter [-]

A = critical sediment mobility parameter [-]

Engelund-Hansen transport function

Engelund-Hansen (1967) is a total load transport equation developed from flume data, using relatively uniform sand sizes between 0.19 mm and 0.93 mm. Its application should be restricted to sand systems. It has been extensively tested, and found to be fairly consistent with field data. This equation is an explicit function of channel velocity, bed shear and the d50 (median particle size) of the material. The general transport equation for the Engelund-Hansen function is represented by:

$$g_s = 0.05\gamma_s V^2 \sqrt{\frac{d_{50}}{g\left(\frac{\gamma_s}{\gamma}-1\right)}}\left[\frac{\tau_0}{(\gamma_s-\gamma)d_{50}}\right]^{3/2}$$

where: g_s = unit sediment transport [kg/(s·m)]

γ = unit weight of water [kg/m^3]

γ_s = unit weight of solid particles [kg/m^3]

V = average channel velocity [m/s]

τ_o = bed level shear stress [kg/m^2]

d_{50} = particle size of which 50% is smaller [m]

Laursen-Copeland transport function

The Laursen (1958) method is a total load transport function, derived from a combination of qualitative analysis, original experiments, and supplementary data. Transport of sediments is defined based on the hydraulic characteristics of mean channel velocity, depth of flow, energy gradient and on the sediment characteristics of gradation and fall velocity. Laursen parameterized this equation with material that extended slightly into the silt range. Copeland (1989) extended the range of applicability to gravel-sized sediments. The range of applicability is 0.011 to 29 mm, median particle diameter. Recent work demonstrated that the Laursen equation outperforms other transport functions in the very fine sand and very coarse silt range. The general transport equation for the Laursen (Copeland) function for a single grain size is the following:

$$C_m = 0.01\gamma\left(\frac{d_s}{D}\right)^{7/6}\left(\frac{\tau_0}{\tau_c}-1\right)f\left(\frac{u_*}{\omega}\right)$$

where: C_m = sediment discharge concentration, in weight/volume

Υ = unit weight of water [kg/m^3]

d_s = mean particle diameter [m]

D = effective depth of flow [m]

τ_o = bed shear stress due to grain resistance [kg/m^2]

τ_c = critical bed shear stress [kg/m^2]

$f\left(\frac{u_*}{\omega}\right)$ = function of the ratio of shear velocity to fall velocity as defined in Laursen's Figure 14 (Laursen, 1958)

Toffaleti transport function

Toffaleti (1968) is a total load transport function that was developed primarily for sand sized particles, using a set of both flume and field data (the flume experiments used sediment particles with mean diameters ranging from 0.3 to 0.93 mm). It performs particularly poorly for gravel sized particles. Successful applications of this method suggest that mean particle diameters as low as 0.095 mm are acceptable. This equation is usually applied to 'large rivers', since most of the data used to develop it were from large, suspended load systems. This transport function describes the relationship between sediment, hydraulics, and water temperature. The Toffaleti method breaks the suspended load distribution into vertical zones, replicating two-dimensional sediment movement. Four zones are used to define the sediment distribution: the upper zone, the middle zone, the lower zone and the bed zone. Sediment transport is calculated independently for each zone and the summed to arrive at total sediment transport. The general transport equations for the Toffaleti function for a single grain size is represented by:

Lower zone:

$$g_{ssL} = M\frac{\left(\frac{R}{11.24}\right)^{1+n_v-0.756z} - (2d_m)^{1+n_v-0.756z}}{1+n_v-0.756z}$$

Middle zone:

$$g_{ssM} = M\frac{\left(\frac{R}{11.24}\right)^{0.224z}\left[\left(\frac{R}{2.5}\right)^{1+n_v-z} - \left(\frac{R}{11.24}\right)^{1+n_v-z}\right]}{1+n_v-z}$$

Upper zone:

$$g_{ssU} = M\frac{\left(\frac{R}{11.24}\right)^{0.224z}\left(\frac{R}{2.5}\right)^{0.5z}\left[R^{1+n_v-1.5z} - \left(\frac{R}{2.5}\right)^{1+n_v-1.5z}\right]}{1+n_v-1.5z}$$

Bed zone:

$$g_{sb} = M(2d_m)^{1+n_v-0.756z}$$

$$M = 43.2C_L(1+n_v)VR^{0.756z-n_v}$$

$$g_s = g_{ssL} + g_{ssM} + g_{ssU} + g_{sb}$$

where: g_{ssL} = suspended sediment transport in the lower zone [t/(day·m)]

g_{ssM} = suspended sediment transport in the middle zone [t/(day·m)]

g_{ssU} = suspended sediment transport in the upper zone [t/(day·m)]

g_{sb} = Bed load sediment transport [t/(day·m)]

M = sediment concentration parameter [-]

C_L = sediment concentration in the lower zone

H = hydraulic radius [m]

d_m = median particle diameter [m]

z = exponent describing the relationship between the sediment and hydraulic characteristics [-]

n_v = temperature exponent [-]

Yang transport function

Yang (1973, 1984) is a total load transport equation which bases transport on Stream Power (the product of velocity and shear stress). The function was developed and tested over flumes and field data. The equation includes two separate relations for sand and gravel transport. Principally, the sediment size range is between 0.062 and 7.0 mm. Channel widths

range from 0.13 to 532 m, depths from 0.011 to 15.1 m, water temperature from 0° to 34.3°, average channel velocity from 0.23 to 2 m/s, and slopes from 0.000043 to 0.029. The general transport equations for sand and gravel using the Yang function for a single grain size is the following:

$$G = \frac{\gamma_w Q C_t}{1000000}$$

- for sand $d_m < 2$ *mm*:

$$logC_t = 5.435 - 0.286log\frac{\omega d_m}{\nu} - 0.457log\frac{u_*}{\omega} + \left(1.799 - 0.409log\frac{\omega d_m}{\nu} - 0.314log\frac{u_*}{\omega}\right) log\left(\frac{VS}{\omega} - \frac{V_{cr}S}{\omega}\right)$$

- for gravel $d_m \geq 2$*mm*:

$$logC_t = 6.681 - 0.633log\frac{\omega d_m}{\nu} - 4.8161log\frac{u_*}{\omega} + \left(2.784 - 0.305log\frac{\omega d_m}{\nu} - 0.282log\frac{u_*}{\omega}\right) log\left(\frac{VS}{\omega} - \frac{V_{cr}S}{\omega}\right)$$

where: G = sediment discharge [kg/s]

Q = discharge [m^3/s]

γ_w = unit weight of water [kg/m^3]

C_t = total sediment concentration, ppm

ω = particle fall velocity [m/s]

d_m = median particle diameter [m]

ν = kinematic viscosity [m^2/s]

S = energy gradient [-]

V = average channel velocity [m/s]

u_* = shear velocity [m/s]

List of figures

List of tables

References

Scientific papers

Ackers P. and White W.R. (1973). *Sediment transport: new approach and analysis*. Proc. ASCE 99(11), 2041-2060.

Arekhi S., Shabani A. and Rostamizad G. (2011). *Application of the modified universal soil loss equation (MUSLE) in prediction of sediment yield (Case study: Kengir Watershed, Iran)*. Arabian Journal of Geosciences.

Armanini A. and Gregoretti C. (2005). *Incipient sediment motion at high slopes in uniform flow condition*. Water Resources Research, Vol. 41, W12431.

Auddino M., Dominici R. and Viscomi A. (2015). *Evaluation of Yield Sediment in the Sfalassà Fiumara (south-western, Calabria) by using Gavrilovic method in GIS Environment*. Rend. Online Soc. Geol. It., Vol. 33, pp.3-7.

Baker P.S. (1967). *Basic principles and application techniques of isotope tracers*. Transactions of ASAE, Vol. 10, pp.705-710, 714.

Beven K. (1989). *Changing ideas in hydrology – The case of physically-based models*. Journal of Hydrology, Vol. 105, pp.157-172.

Bosco C., De Rigo D., Dewitte O., Poesen J. and Panagos P. (2015). *Modeling soil erosion at European scale: towards harmonization and reproducibility*. Natural Hazards and Heart System Sciences, Vol. 15, pp. 225-245.

Brown L.C. and Foster G.R. (1987). *Storm erosivity using idealized intensity distribution*. Transactions of ASAE, Vol. 30, pp.379-386.

Carling P.A. and Reader N.A. (1982). *Structure, Composition and Bulk Properties of Upland Stream Gravels*. Earth Surface Processes and Landforms, 7, 349-365.

Desmet P.J.J. and Govers G. (1996). *A GIS procedure for automatically calculating the USLE LS factor on topographically complex lanscape units*. Journal of Soil and Water Conservation, 51, pp. 427-433.

Dey S. and Ali S.Z. (2017). *Mechanics of Sediment Transport: Particle Scale of Entrainment to Continuum Scale of Bedload Flux*. J. Eng. Mech (ASCE), 143(11):04017127.

Efthimiou N., Likoudi E., Panagoulia D. and Karavitis C. (2016). *Assessment of soil susceptibility to erosion using the EPM and RUSLE models: the case of Venetikos river catchment*. Global NEST Journal, Vol. 18, N°1, pp. 164-179.

Gaeuman D., Andrews E.D., Krause A. and Smith W. (2009). *Predicting fractional bed load transport rates: Application of the Wilcock-Crowe equations to a regulated gravel bed river*. Water Resources Research, Vol. 45, W06409, pp. 1-15.

Gwapedza D., Hughes D.A. and Slaughter A.R. (2018). *Spatial scale dependency issues in the application of the Modified Universal Soil Loss Equation (MUSLE)*. Hydrological Sciences Journal, 63:13-14, , pp. 1890-1900.

Haschenburger J.K. and Church M. (1998). *Bed Material Transport Estimated from the Virtual Velocity of Sediment*. Earth Surface Processes and Landforms, 23, 791-808.

Hassan M.A., Church M. and Schick A.P. (1991). *Distance of Movement of Coarse Particles in Gravel Bed Streams*. Water Resources Research, 27 n°4, 503-511.

Hassan M.A., Church M. and Ashworth P.J. (1992). *Virtual Rate and Mean Distance of Travel of Individual Clasts in Gravel-Bed Channels*. Earth Surface Processes and Landforms, 17, 617-627.

Houbrechts G., Van Campenhout J., Levecq Y., Hallot E., Peeters A. and Petit F. (2012). *Comparison of methods for quantifying active layer dynamics and bedload discharge in armoured gravel-bed rivers.* Earth Surface Processes and Landforms, 37, pp. 1501-1517.

Huang C., Wells L.K. and Norton L.D. (1999). *Sediment transport capacity and erosion processes: model concepts and reality*. Earth Surface Processes and Landforms 24, 503-516.

Kura R.W., Annable W.K. M.ASCE and Tolson B.A. (2010). *Sensitivity of Field Data Estimates in One-Dimensional Hydraulic Modeling of Channels*. (Tecnnical notes), Journal of Hydraulic Engineering 136(6), 379-384.

Lamarre H., MacVicar B.J. and Roy A.G. (2005). *Using passive integrated transponder (PIT) tags to investigate sediment transport in gravel-bed rivers*. Journal of Sediment Research, 75, 736-741.

Lane L.J., Hernandez M. and Nichols M. (1997). *Processes controlling sediment yield from watersheds as functions of spatial scale*. Environmental Modelling & Software, 12, pp. 355-369.

Laursen M. Emmett (1958). *Total Sediment Load of Streams*. Journal of the Hydraulic Division (ASCE), 84 (HY1), 1530 – 1 to 1530 - 36.

Lawler D.M. (1991). *A new technique for the automatic monitoring of erosion and deposition rates*. Water Resources Research, 27, pp. 2125-2128.

Lawler D.M. (1991). *A new technique for the automatic monitoring of erosion and deposition rates*. Water Resources Research, 27, pp. 2125-2128.

Lawler D.M. (1992). *Design and installation of a novel automatic erosion monitoring system*. Earth Surface Processes and Landforms, 17, pp.455-463.

Lawler D.M. (1993). *The measurement of river bank erosion and lateral channel change: a review*. Earth Surface Processes and Landforms, 18, pp.777-821.

Lenzi M.A. (2004). *Displacement and transport of marked pebbles, cobbles and boulders during floods in a steep mountain stream*. Hydrological Processes, 18, pp. 1899-1914.

Lenzi M.A., Mao L. and Comiti F. (2004). *Magnitude-frequency analysis of bed load data in an Alpine boulder bed stream*. Water Resources Research, Vol. 40, W07201.

Lenzi M.A., Mao L. and Comiti F. (2006). *Effective discharge for sediment transport in a mountain river: Computational approaches and geomorphic effectiveness*. Journal of Hydrology 326, pp. 257-276.

Li Z. and Fang H. (2016). *Impacts of climate change on water erosion: A review*. Earth-Science Reviews, 163, 94-117.

Liébault F. M.A. and Laronne J.B. (2008). *Evaluation of bedload yield in gravel-bed rivers using scour chains and painted tracers: the case of the Esconavette Torrent (southern French Preaslps)*. Geodinamica Acta 21, pp. 23-34. DOI. 10.3166/ga.21.23-34.

Lisle T.E. (1995). *Particle size variations between bed load and bed material in natural gravel bed channels*. Water Resources Research 31(4), pp. 1107-1118. https://doi.org/10.1029/94WR02526

Lu H., Moran C.J. and Prosser I.P. (2006). *Modelling sediment delivery ratio over the Murray Darling Basin*. Environmental Modelling & Software, 21, pp. 1297-1308.

McHenry J.R. (1969). *Use of tracer technique in soil erosion research*. Isotopes and Radiation Technology, 6, pp. 280-287.

McHenry J.R. and Ritchie J.C. (1977). *Estimating field erosion losses from fallout Cesium-137 measurements*. IAHS-AISH, Publ. 122, pp. 26-33.

Milanesi L., Pilotti M., Clerici A. and Gavrilovic Z. (2015). *Application of an improved version of the Erosion Potential Method in alpine areas*. Italian Journal of Engineering Geology and Environment, 1 (2015), Sapienza Università Editrice, pp. 17 - 30.

Mitasova H., Hofierka J., Zlocha M. and Iverson L.R. (1996). *Modeling topographic potential for erosion and deposition using GIS*. Int. Journal of Geographical Information Science, 10(5), pp. 629-641.

Molnar D. and Julien P. (1998). *Estimation of upland erosion using GIS*. Computers & Geosciences, 24, pp. 183-192.

Moore I. and Burch G. (1986). *Physical basis of the length-slope factor in the universal soil loss equation*. Soil Science of America Journal, 50, 1294-1298.

Muzik I. (1996). *Flood modelling with GIS-derived distributed unit hydrographs*. Hydrological Processes, vol. 10, pp. 1401-1409.

Nearing M.A., Foster G.R., Lane L.J. and Finkner S.C. (1989). *A Process-Based Soil Erosion Model for USDA-Water Erosion Prediction Project Technology*. Transactions of the ASAE, Vol. 32, N.5, pp. 1587-1593 (published by the American Society of Agricultural Engineers).

Nearing M.A. (1997). *A single, continuous function for slope steepness influence on soil loss*. Science Society of America Journal, 61(3), 917-919.

Nearing M.A., Jetten V., Baffaut C., Cerdan O., Couturier A., Hernandez M, Le Bissonnais Y., Nichols M.H., Nunes J.P., Renschler C.S., Souchere V. and Van Oost K. (2005). *Modeling response of soil erosion and runoff to changes in precipitation and cover*. Catena, 61(2-3), 131-154.

Nichols M.H. (2004). *A Radio Frequency Identification System for Monitoring Coarse Sediment Particle Displacement*. Applied Engineering in Agriculture, 20(6),783-787.

Nunes J.P., Seixas J. and Keizer J.J. (2013). *Modeling the response of within-storm runoff and erosion dynamics to climate change in two Mediterranean watershed: a multi-model, multi-scale approach to scenario design and analysis*. Catena, 102, 27-39.

Ochiere H.O., Onyando J.O. and Kamau D.N. (2015). *Simulation of Sediment Transport in the canal Using the Hec-Ras (Hydrologic Engineering Centre – River Analysis System) In an Underground Canal in Southwest Kano Irrigation Scheme - Kenya*. International Journal of Engineering Science Invention, Vol. 4, Issue 9, pp. 15-31.

Orlandini S. (2002). *On the spatial variation of resistance to flow in upland channel networks*. Water Resources Research, Vol. 38, N. 10, 1197.

Panagos P., Meusburger K., Ballabio C., Borrelli P.and Alewell C. (2014). *Soil erodibility in Europe: A high-resolution dataset based on LUCAS* . Science of the Total Environment, 479-480 (2014), 189-200.

Panagos P., Borrelli P., Poesen J., Ballobio C., Lugato E., Meusburger K., Montanarella L. and Alewell C. (2015) (a). *The new assessment of soil loss by water erosion in Europe*. Environmental Science & Policy, 54 (2015), 438-447.

Panagos P., Ballabio C., Borrelli P., Meusburger K., Klik A., Rousseva S., Tadic M.P., Michaelides S., Hrabalikova M., Olsen P., Aalto J., Lakatos M., Rymszewicz A., Dumitrescu A., Begueria S. and Alewell C. (2015) (b). *Rainfall erosivity in Europe*. Science of the Total Environment, 511 (2015), 801-814.

Panagos P., Borrelli P., Meusburger K., van der Zanden E.H., Poesen J., and Alewell C. (2015) (c). *Modelling the effect of support practices (P-factor) on the reduction of soil erosion by water at European scale*. Environmental Science & Policy, 51 (2015), 23-34.

Panagos P., Borrelli P., Meusburger K., Alewell C., Lugato E. and Montanarella L. (2015) (d). *Estimating the soil erosion cover-management factor at the European scale*. Land Use Policy, 48 (2015), 38-50.

Panagos P., Borrelli P. and Meusburger K. (2015) (e). *A New European Slope Length and Steepness Factor (LS-Factor) for Modeling Soil Erosion by Water*. Geosciences, 5, 117-126.

Panagos P., Meusburger K., Van Liedekerke, Alewell C., Hiederer R. and Montanarella L. (2014) (f). *Assessing soil erosion in Europe based on data collected through a European network*. Soil Science and Plant Nutrition, Vol. 60, pp. 15-29.

Parsons A.J. and Stromberg S.G.L. (1998). *Experimental analysis of size and distance of travel of unconstrained particles in interrill flow*. Water Resources Research, vol. 34,n°9, pp. 2377-2381.

Plumb B.D., Annable W.K., Thompson P.J. and Hassan M.A. (2017). *The Impact of Urbanization on Temporal Changes in Sediment Transport in a Gravel Bed Channel in Southern Ontario, Canada*. Water Resources Reasearch, 53, 8443-8458.

Ponce V.M. and Hawkins R.H. (1996). *Runoff Curve Number: has it reached maturity?*, Journal of Hydrologic Engineering, (1)1, pp. 11-19.

Pruski F.F. and Nearing M.A. (2002). *Runoff and soil-loss responses to changes in precipitation: a computer simulation study*. Journal of Soil and Water Conservation, 57 (1), 7-16.

Ranzi R., Le T.H., and Rulli M.C. (2012). *A RUSLE approach to model suspended sediment load in the Lo river (Vietnam): Effects of reservoirs and land use changes*, Journal of Hydrology, 422-423, pp. 17-29.

Reid I., Layman J.T. and Frostick L.E. (1980). *The Continuous Measurement of Bedload Discharge*, Journal of Hydrolic Research, 18:3, pp. 243-249.

Renard K.G., Foster G.R., Weesies G.A. and Porter J.P. (1991). *RUSLE Revised universal soil loss equation*, Journal of Soil and Water Conservation, Vol. 46, N° 1, January-February 1991, pp. 30-33.

Ritchie J.C. and McHenry J.R. (1990). *Application of radioactive fallout cesium-137 for measuring soil erosion and sediment accumulation rates and patterns: a review*, Journal of Environmental Quality, Vol. 19, pp. 215-233.

Ritchie J.C., McHenry J.R. and Gill A.C. (1972). *The distribution of cesium-137 in the litter and upper 10 centimeters of soil under different cover types in Northern Mississippi*, Health Physics, Vol. 22, pp. 197-198.

Rubey W.W. (1933). *Settling Velocities of Gravel, Sand, and Silt Particles*, American Journal of Science, 5th Series, Vol. 25, N° 148, 1933, pp. 325-338.

Sadeghi S.H. R., Gholami L., Khaledi Darvishan A. and Saeidi P. (2013). *A review of the application of the MUSLE model worldwide*, Hydrological Sciences Journal, 59, pp. 365-375.

Tfwala S.S. and Wang Y.M. (2016). *A new acoustic sensor for sediment discharge measurement*, Water, 8, 53.

Toth G., Jones A. and Montanarella L. (2013). *The LUCAS topsoil database and derived information on the regional variablity of cropland topsoil properties in the European Union* . Environment Monitoring and Assessment, 185(9):7409-7425.

Vacca C. and Dominici R. (2015). *Preliminary considerations on the application of the Gavrilovic method in GIS environment for the calculation of sediment produced by the catchment area of the Stilaro Fiumara (Calabria south-east)*. Rend. Online Soc. Geol. It., Vol. 33, pp.104-107.

Wilcock P.R. (1997). *Entrainment, displacement and transport of tracer gravels*, Earth Surface Processes and landforms, 22, 1125-1138.

Wilcock P.R. (2001). *Toward a Practical Method for Estimating Sediment-Transport Rates in Gravel-Bed Rivers*, Earth Surface Processes and landforms, 26, 1395-1408.

Wilcock P.R. and Crowe J.C. (2003). *Surface-based Transport Model for Mixed-Size Sediment*, Journal of Hydraulic Engineering (ASCE), 129(2), 120-128.

Whiting P.J. and King J.G. (2003). *Surface particle sizes on armoured gravel streambeds: effects of supply and hydraulics*, Earth Surface Processes and Landforms, 28(13), 1459-1471 https://doi.org/10.1002/esp.1049.

Walling D.E. (1983). *The sediment delivery problem*, Journal of Hydrology, vol. 65, pp. 209-237.

Wong M. and Parker G. (2006). *Reanalysis and Correction of Bed-Load Relation of Meyer-Peter and Müller Using Their Own Database*, Journal of Hydraulic Engineering, 132(11), 1159-1168.

Yang C.T. (1973). *Incipient Motion and Sediment Transport*, Journal of the Hydraulics Division (ASCE), Vol. 99, N° HY10, pp 1679-1704.

Yang C.T. (1984). *Unit Stream Power Equation for Gravel*, Journal of the Hydraulics Division (ASCE), 110 n° 12, 1783-1797.

Yang C.Y. and Julien P.Y. (2018). *The ratio of measured to total sediment discharge*, International Journal of Sediment Reasearch, DOI: https://doi.org/10.1016/j.ijsrc.2018.11.005, In Press, Corrected Proof, Available online: 27 November 2018

Zhang X.C., Nearing M.A. and Norton L.D. (2001). *How WEPP mode responds to different cropping and management systems*, In "Sustaining the Global Farms", Stott D.E., Mohtar R.H. and Steinhardt G.C. eds, pp. 871-876.

Zhang Y., Degroote J., Wolter C. and Sugumaran R. (2009). *Integration of Modified Universal Soil Loss Equation (MUSLE) into a GIS framework to assess soil erosion risk* , Land Degradation & Development, 20, pp. 84-91.

Book/Handbook/Manual/Report/Professional paper

AMEC Environment & Infrastructure (2014). *July 8th, 2013 Extreme Raifall Event*. Summary & Analysis Report, Toronto, Ontario, Canada.

Angeli L. (2004). *Sviluppo di metodologie di analisi per la stima dell'erosione dei suoli con applicazione specifica ad un'area pilota*. LaMMA-CRES, December 2004.

Armanini A. and Scotton P. (1995). *Criteri di dimensionamento e di verifica delle stabilizzazioni di alveo e di sponda con massi sciolti e massi legati*. *Moderni criteri di sistemazione degli alvei fluviali.* Acts of refresher course, 10-14 October 1994, Bios editorial, Cosenza.

Armanini A. (2018). *Principles of River Hydraulics.*

Bagarello V. and Ferro V. (2006). *Erosione e conservazione del suolo*, McGraw-Hill Education.

Bagnold R.A. (1966). *An Approach to the Sediment Transport Problem From General Physics*, Geological Survey Professional Paper 422-I, 1-37, United States Government Printing Office, Washington.

Benestad R., Haensler A., Hennemuth B., Illy T., Jacob D., Keup-Thiel E., Kotlarsky S., Nikulin G., Otto J., Rechid D., Sieck K., Sobolowski S., Szabò P., Szépszò G., Teichmann C., Vautard R., Weber T. and Zsebehàzi G. (2017). *Guidance for EURO-CORDEX climate projections data use*, EURO-CORDEX Guidelines, Version 1.0, August 2017.

Bosco C. and Oliveri S. (2007). *Climate Change, Impacts and Adaptation Strategies in the Alpine Space*, Strategic INTERREG III B Project CLIMCHALP, Natural Hazard Report, Chapter 3, Milano.

Bosco C., Rusco E., Montanarella L. and Oliveri S. (2008). *Soil erosion risk assessment in the alpine area according to the IPCC scenarios*, chapter of JRC Scientific and Technical Reports "Threats to Soil

Quality in Europe" edited by Toth G., Montanarella L. and Rusco E. [http://publications.jrc.ec.europa.eu/repository/handle/JRC46574]

Chow V.T. (1959). *Open-Channel Hydraulics*, McGraw-Hill.

Copeland Ronald R. and Thomas William A. (1989). *Corte Madera Creek Sedimentation Study – Numerical Model Investigation*, US Army Engineer Water Ways Experiment Station, Vicksburg, Mississippi. TR-HL -89-6.

Doe W.W. and Harmon R.S. (2001). *Introduction to soil erosion and landscape evolution modeling*, in "Landscape Erosion and Evolution Modelling".

Emmett W.W. (1980). *A field calibration of the sediment-trapping characteristics of the Helley-Smith bedload sampler*, Geological Survey Professional Paper 1139, 1-44, United States Government Printing Office, Washington.

Engel B. and Mohtar R. (1999), *Estimating soil erosion using RUSLE (Revised Universal Soil Loss Equation) and the Arcview GIS*, Purdue University.

Engelund F. and Hansen E. (1967). *A Monograph on Sediment Transport in Alluvial Stream*, 1-63, Teknisk Forlag, Copenhagen V., Denmark.

Fattorelli S. and Marchi L. (1988). *Metodi deterministici per la valutazione dei deflussi di piena*, Gruppo Nazionale per la Difesa dalle Catastrofi Idrogeologiche, Rapporto 1988, Linea 1.

Ferro V. (2002). *La sistemazione dei bacini idrografici*, McGraw-Hill Education.

Giandotti M. (1934). *Previsione delle piene e delle magre dei corsi d'acqua*, Memorie e studi idrografici, Pubbl. 2 del Servizio Idrografico Italiano, Vol. VIII, 107.

Government of Malaysia, Department of Irrigation and Drainage (2012). *Urban Stormwater Management Manual for Malaysia*, MSMA 2nd Edition, Kuala Lumpur, Malaysia.

Helley E.J. and Smith W. (1971). *Development and Calibration of a Pressure-Difference Bedload Sampler*, United States Department of the Internal Geological Survey, Water Resources Division, Open-File Report 73-108, Menlo Park, California.

Jones A., Panagos P., Barcelo S., Bouraoui F., Bosco C., Dewitte O., Gardi C., Erhard M., Hervás J., Hiederer R., Jeffery S., Lükeville A., Marmo L., Montanarella L., Olazábal C., Petersen J.E., Penizek V., Strassburger T., Tóth G., Van Den Eeckhaut M., Van Liedekerke M., Verheijen F., Viestova E. and Yigini Y. (2012). *The State of Soil in Europe*, Joint Research Centre (JRC) Reference Reports, Luxemburg: Publications Office of the European Union.

Keizer J., Djuma H. and Prasuhn V. (2016). *Soil erosion by water*, In: "Soil threats in Europe: status, methods, drivers and effects on ecosystem services", Joint Research Centre (JRC) Technical Reports.

Merlo C. (1973). *Determinazione mediante il "Metodo Razionale" delle portate massime di piena di data frequenza nei piccoli bacini*, Annali della Facoltà di Scienze Agrarie, Tipografia Vincenzo Bona, Torino.

Meyer-Peter E. and Müller R. (1948), *Report of the Second Meeting, International Association for Hydraulic Structures Research (IAHSR)*, Stockholm, pp. 39-64.

Mezzini E., Ventura F., Vittori Antisari L. and Magnani F. (2015), *A RUSLE model application with GRASS GIS: an evaluation study in the Rio Centonara catchment*, Geomatics Workbooks n.12, "FOSS4G Europe Como 2015", pp. 509-522.

Mitasova H. and Brown W.M. (2002), *Using Soil Erosion Modeling for Improved Conservation Planning: A GIS-based Tutorial Geographic Modeling Systems Lab*, University of Illinois at Urbana-Champaign.

Moisello U. (2003), *Idrologia tecnica*, La Goliardica Pavese s.r.l.

Overton D. E. and M. E. Meadows (1976), *Stormwater Modeling*, New York: AcademicPress.

Pregnolato M. and D'Amico M. (2011), *Water Regime in the Alpine Space: Soil Erosion in a Changing Environment*, Technical Report, ADAPALP project-WP4, April 2011.

Puglisi S. (1986). *Appunti di morfometria.* Acts of "XXIII Corso di Cultura in Ecologia, Sezione Selvicoltura, Ecologia e Pianificazione", 8-13 September, Università degli Studi di Padova, San Vito di Cadore.

Renard K.G., Foster G.R., Weesies G.A., McCool D.K. and Yoder D.C. (1997), *Predicting soil erosion by water: a guide to conservation planning with the revised universal soil loss equation (RUSLE)*, USDA Agriculture Handbook, n.703.

Richards K. (1993), *Sediment delivery and the drainage network*, In: Beven K. and Kirkby M.J. (Eds), "Channel Network Hydrology", Wiley, Chichester, pp. 221-254.

Samuelsson P., Gollvik S., Jansson C., Kupiainen M., Kourzeneva E. and Van De Berg W.J. (2015), *The surface processes of the Rossby Centre regional atmospheric climate model (RCA4)*, Technical Report, SMHI, METEOROLOGI Nr 157.

Shields A. (1936), *Anwendung der Aehnlichkeitsmechanik und der Turbulenzforschung auf die Geschiebebewegung*, Mitteil., PVWES, Berlin.

Soil Conservation Service (SCS) (1972), *National Engineering Handbook*, Section 4, Hydrology.

Sturm T.W. (2001). *Open Channel Hydraulics*, McGraw-Hill Higher Education, International Edition 2001.

Sturm T.W. (2010). *Open Channel Hydraulics*, McGraw-Hill Higher Education, International Edition 2010.

Toffaleti F.B. (1968). Technical Report n°5 *A Procedure for Computation of Total River Sand Discharge and Detailed Distribution, Bed to Surface*, Committee on Channel Stabilization, U.S. Army Corps of Engineers.

USACE (US Army Corps of Engineers, Hydrologic Engineering Center). HEC-RAS USDA-ARS Bank Stability & Toe Erosion Model (BSTEM), *Technical Reference and User's Manual*, (2015).

USACE (US Army Corps of Engineers, Hydrologic Engineering Center). HEC-RAS River Analysis System, *Hydraulic Reference Manual*, Version 5.0 (2016) (a).

USACE (US Army Corps of Engineers, Hydrologic Engineering Center). HEC-RAS River Analysis System, *User's Manual*, Version 5.0 (2016) (b).

Wischmeier W.H. and Smith D.D. (1961), *A Universal Equation for Predicting Rainfall-Erosion Losses. An Aid to Conservation Farming in Humid Regions*, ARS Special Report 22-66, Agricultural Research Service, U.S. Dept. of Agric., Washington DC, p.11.

Wischmeier W.H. and Smith D.D. (1978), *Predicting rainfall-erosion losses – A guide to conservation planning*, U.S. Dept. of Agric., Agr. Handbook, n. 282.

Proceedings Papers/Workshops

Berteni F. and Grossi G. (2017). *Water erosion and climate change in a small alpine catchment*. Geophysical Research Abstracts Vol. 19, EGU General Assembly 2017. Vienna, Austria, April 2017.

Dominici R., Campolo F., Ferrari P. and Modaffari D. (2015). *Tecniche per lo studio dell'analisi dell'erosione costiera con metodologie fotogrammetriche e telerilevate*. Conferenza ASITA. Lecco, Italy.

Berteni F., Plumb B.D., Annable W.K. and Grossi G. (2018). *Using high-resolution bedload transport tracer measurements to investigate the characteristics of bedload transport over a large urban flood event*. 9th International Conference of Fluvial Hydraulics, Lyon-Villeurbanne, France, September 2018.

Ferro V. (1999). *Problematiche inerenti la modellazione e la misura dell'erosione e della produzione di sedimenti*. Seminario su Monitoraggio e Modellazione dei Processi Idrologici, Palermo, 80 pp.

Gavrilovic Z. (1988). *The use of an empirical method (Erosion Potential Method) for calculating sediment production and transportation in unstidied or torrential streams*. International Conference River Regime, 18-20 May 1988, pp. 411-422.

Gibson S. and Piper S. (2007). *Sensitivity and Applicability of Bed Mixing Algorithms*, World Environmental and Water Resources Congress 2007: Restoring Our natural Habitat, ASCE.

Gibson S., Simon A., Langendoen E., Bankhead N. and Shelley J. (2015). *A physically-based channel-modeling framework integrating HEC-RAS sediment transport capabilities and the USDA-ARS bank-stability and toe-erosion model (BSTEM)*, Proc. 3rd Joint Federal Interagency Sedimetation and Hydrologic Modeling Conference, April 19-23, 2015, Reno, NV. 12pp.

Gitas I.Z., Douros K., Minakou C., Silleos G.N. and Karydas C.G. (2009). *Multi-temporal soil erosion risk assessment in N. Chalkidiki using a modified USLE raster model*, EARSeL eProceedings 8, pp. 40-52.

Hossain M. Monowae and Rahman M. Lutfor (1998). *Sediment transport functions and their evaluation using data from large alluvial rivers of Bangladesh. Modelling Soil Erosion, Sediment Transport and Closely Related Hydrological Processes* (Proceedings of a symposium held at Vienna, July 1998). IAHS Publ. n°249, 1998.

Laronne J.B., Outhet D.N. and Duckman J.L. (1992). *Determining event bedload volume for evaluation of potential degradation sites due to gravel extraction, N.S.W., Australia* (In "Erosion and Sediment Transport Monitoring Programmes in River basins": Proceedings of the Oslo Symposium, August 1992). IAHS Publ. n°210. IAHS Press: Wallingford; pp.87-94.

Lawler D.M. (1994). *Temporal variability in streambank response to individual flow events: the River Arrow, Warwickshire, US*. In Olive L. et al. Eds., "Variability in Stream Erosion and Sediment Transport", IAHS Publication n°24, Proceedings of an international symposium held at Canberra, Australia, 12-16 December 1994, pp. 171-180.

Lawler D.M. (2002). *Automated monitoring of bank erosion dynamics: new developments in the Photo-Electronic Erosion Pin (PEEP) system*. Erosion and Sediment Transport Measurement: Technological and Methodological Advances Workshop, June, Oslo.

Le T.H., Rulli M.C. and Ranzi R. (2009). *Surface erosion and sediment transport in the Lo river basin,* Proc. 50th Foundation Anniversary of the Water Resources University, Hanoi, Water Resources University, pp. 13-20.

Miyamoto K., Kurihara J., Sawada T. and Itakura Y. (1992). *A study of field methods for measuring sediment discharge* (In "Erosion and Sediment Transport Monitoring Programmes in River basins": Proceedings of the Oslo Symposium, August 1992). IAHS Publ. n°210, pp. 107-114.

Piest R.F., Kramer L.A. and Heinemann H.G. (1975). *Sediment movement from loessial watersheds,* Present and prospective technology for predicting sediment yields and sources: Proceedings of the Sediment-Yield Workshop (Usda Sedimentation Laboratory, Oxford, Mississippi, November 28-30, 1972), USDA Agr. Res. Serv. Pub. ARS-S-40.

Ricci G.F., Jeong J., De Girolamo A.M. and Gentile F. (2018). *Modelling management practices to reduce soil erosion in an agricultural watershed in Southern Europe*. SWAT Conference. Brussels, Belgium.

Romkens M.J.M., Prased S.N. and Poesen J.W.A. (1986). *Soil erodibility and properties,* Trans. 13th congress of the Int. Soc. Of Soil Sci., Hamburg, Germany 5, pp. 492-504.

Sadeghi S. H. (2004). *Application of MUSLE in prediction of sediment yield in Iranian conditions,* ISCO2004-13th International Soil Conservation Organization Conference-Brisbane, paper 998, pp.1-4.

Taniguchi S., Itakura Y., Miyamoto K. and Kurihara J. (1992). *A review of the application of the MUSLE model worldwide* (In "Erosion and Sediment Transport Monitoring Programmes in River basins": Proceedings of the Oslo Symposium, August 1992). IAHS Publ. n°210, pp. 135-142.

Williams J.S. (1975). *Sediment-yield prediction with universal equation using runoff energy factor,* In: Present and prospective technology for predicting sediment yield and sources, Sediment-Yield Workshop, USDA, ARS.S-40, U.S. Department of Agriculture, Agricultural Research Service, pp. 244-252.

Zemljic M. (1971). *Calcul du debit solide-Evaluation de la vegetation comme un des facteurs antiérosif,* International Symposium Interpraevent, Villaco.

PhD Dissertations/Master Theses

Ajward, M. H. (1996): *A spatially distributed unit hydrograph model using a geographical information system*. Ph.D. Dissertation, Civil Engineering Dept., University of Calgary, Calgary.

Berteni F. (2012): *Sistema combinato di valutazione dell'erosione di versante e del trasporto solido nella rete idrografica*. Master Thesis, Academic year 2010-2011, University of Brescia, Italy.

Bussi G. (2014): *Implementation of a distributed sediment model in different data availability scenarious*. Ph.D. Dissertation, Universidad Politécnica de Valencia, Spain.

Einstein H. A. (1937): *Bedload transport as a probability problem*. Ph.D. Dissertation, translated by W.W. Sayre in Shen, W.W. (Ed.) 1972 "Sedimentation", Colorado State University, App. C.

Kilgore J.L. (1997): *Development and evaluation of a GIS-based spatially distributed unit hydrograph model*. Master thesis, Virginia Polytechnic Institute and State University, Blacksburg, VA.

Plumb B.D. (2017): *Impacts of Hydromodification and Sediment Supply Alterations on Bedload Transport and Bed Morphology in Urbanizing Gravel-bed Rivers*. PhD Dissertation, University of Waterloo, Ontario, Canada.

Webography

https://esdac.jrc.ec.europa.eu/

https://esg-dn1.nsc.liu.se/projects/esgf-liu/

https://grass.osgeo.org/

https://grass.osgeo.org/grass74/manuals/addons/r.traveltime.html

https://oceanservice.noaa.gov/facts/gltides.html

https://open.canada.ca/en

https://portal.enes.org/

http://www.arpalombardia.it/Pages/ARPA_Home_Page.aspx

http://www.cordex.org/

https://www.dpi.nsw.gov.au/__data/assets/pdf_file/0003/255153/fact-sheet-1-types-of-erosion.pdf
http://www.ec-earth.org/
http://www.geoportale.regione.lombardia.it/
http://www.ipcc.ch/publications_and_data/ar4/syr/en/mains1.html
https://www.javacoeapp.lrc.gov.on.ca/geonetwork/srv/en/main.home
http://www.oglioconsorzio.it
https://www.qgis.org/it/site/
https://www.smhi.se/en/
http://www.wmo.int/pages/prog/wcp/ccl/faqs.php
www.marinfo.gc.ca

Reference standards of soil analysis

ASTM (1971): Test designation D 1140, *Standard Method for Amount of Material in Soils Finer than the No. 200 (0.075 mm) Sieve.* Vol. 04.08. ASTM Philadelphia, USA.

ASTM (1972): Test designation D 422, *Standard Method for Particle-Size Analysis of Soils.* Vol. 04.08. ASTM Philadelphia, USA.

ASTM (1981): Test designation E 11, *Standard Specification for Wire-cloth Sieves for Testing Purposes.* Vol. 14.02. ASTM Philadelphia, USA.

ASTM (1986): Test designation E 100, *Standard Specification for ASTM Hydrometers.* Vol. 14.01. ASTM Philadelphia, USA.